Final project report
ChiNorBC

The ChiNorBC final project report

Chinese-Norwegian Project on Emission, Impact, and Control Policy for Black Carbon and its Co-benefits in Northern China

CAEP CICERO CRAES Norwegian Environment Agency NIPH

Chinese-Norwegian Project on Emission, Impact, and Control Policy for Black Carbon and its Co-benefits in Northern China

About this report

This report is final report produced under the Chinese-Norwegian Project on Emission, Impact, and Control Policy for Black Carbon and its Co-benefits in Northern China (ChiNorBC). The project is jointly implemented by the Chinese Research Academy of Environmental Sciences (CRAES) and the Norwegian Environment Agency (NEA), in partnership with the Chinese Academy of Environmental Planning (CAEP), the Norwegian Institute of Public Health (NIPH) and CICERO Center for International Climate Research, with financial support from the Norwegian Ministry of Foreign Affairs.

There is no internationally agreed definition of black carbon (BC) and organic carbon (OC). BC is the light-absorbing component of fine particles and is produced by incomplete combustion of fossil fuel, biofuel and biomass. BC is always co-emitted with OC. Emissions of BC and OC affects the climate and have adverse health effects. Reductions of BC and OC will have co-benefits for climate, air quality and health.
ChiNorBC developed improved emission inventories for BC- and OC- emissions in China using the most recent, best available national statistics and measurements obtained in the project. Based on this, new estimates of effects of BC/OC on climate, air quality, and health was provided. Ultimately the ChiNorBC provided Chinese policy makers with policy solutions for reducing BC/OC emissions in China which maximizes the co-benefits. The project will further raise scientific, governmental, and public awareness and enhance the understanding of the impacts of BC/OC emissions reductions.

The project website can be found at: http://chinorbc.org/

Acknowledgements

In addition to the authors highlighted under each chapter, we would like to acknowledge the guidance and insights of a number of colleagues in the implementing institutions. We would in particular thank professor Meng Fan for his enthusiasm, knowledge and contribution as a project leader on the Chinese side in the first phases of this project. We also would like to add our appreciation to the Norwegian Embassy in Beijing for funding this highly interesting and relevant project.
.

Findings and opinions expressed in this paper are not necessarily shared by those contributing to the work, and any errors and omissions are the responsibility of the authors and partner institutions.

Date: June 2023

Published by the ChiNorBC-project

The cover design is non-figurative and created by Eilif Ursin Reed, Communication Advisor, Cicero, and is inspired by melting glaciers and polluted snow.

About the partner institutions in the ChiNorBC-project

Chinese Research Academy of Environmental Sciences (CRAES)

The Chinese Research Academy of Environmental Sciences (CRAES), founded in 1978, is a leading institute in environment-related studies in China, including studies on short-lived climate pollutants and its impacts. There are more than 1000 employees whose backgrounds cover all important areas of environmental sciences, including atmospheric science. One of the main responsibilities of CRAES is to provide technical and scientific support for decision making of Ministry of Ecology and Environment (MEE).

Norwegian Environment Agency (NEA)

The Norwegian Environment Agency (NEA) is an advisory and executive body under the Ministry of Climate and Environment (MCE), fully funded by the Norwegian Government. It has about 700 employees in Trondheim and Oslo as well as in local offices throughout the country. NEA was established 1st July 2013 after a merge of the former Directorate for Nature Management (est. 1965) and the Climate and Pollution Directorate (est. 1974). The Norwegian Nature Inspectorate (SNO) is organized as a department within NEA. The primary tasks of NEA are to reduce greenhouse gas emissions, manage Norwegian nature, and prevent pollution.

Chinese Academy of Environmental Planning (CAEP) is a public institution with independent legal status founded in 2001. Its missions are: Carrying out strategic research on national ecological civilization, green development and beautiful China, and undertaking technical support for the preparation and implementation of national medium and long-term ecological environment planning, key river basins and regions planning, and environmental planning in key fields, so as to meet the major needs of the country.

The Norwegian Institute of Public Health (NIPH) is a Norwegian government agency and research institute and is Norway's national public health institute. NIPH acts as a national competence institution placed directly under the Ministry of Health and Care Services, with approximately 1400 employees in Oslo and Bergen. It is responsible for knowledge production and systematic reviews for the health sector and provides knowledge about the health status in the population, influencing factors and how it can be improved.

CICERO Center for International Climate Research (CICERO) is a private foundation that for over thirty years has delivered interdisciplinary research of high scientific quality on climate science, economics, and policy. CICERO's mission is to conduct research and provide reports, information and expert advice about issues related to global climate change and international climate policy with the aim of acquiring knowledge that can help mitigate the climate problem and enhance international climate cooperation. CICERO has approximately 80 employees situated in the Oslo Science Park.

Table of Contents

Acronyms and Abbreviations

CAEP	Chinese Academy for Environmental Planning, China
CICERO	Center for International Climate Research, Norway
CRAES	Chinese Research Academy of Environmental Sciences
MEE	Ministry of Ecology and Environment of China
MFA	Ministry of Foreign Affairs, Norway
MOFCOM	Ministry of Commerce of China
NEA	Norwegian Environment Agency
NIPH	Norwegian Institute on Public Health, Norway
UN Environment	The United Nations Environment
WMO	World Meteorological Organization

Definition of Concepts

BC	Black carbon
CO	Carbon monoxide
CTM	Chemical transport model
GTP	Global temperature change potential
GWP	Global warming potential
HFCs	Hydrofluorocarbons
LLGHGs	Long-lived greenhouse gases
nmVOCs	Non-methane volatile organic compounds
NOx	Nitrogen oxides
OC	Organic carbon
$PM_{2.5}$	Fine particles with a diameter of 2.5 micrometers or less
PM_{10}	Inhalable particles with a diameter of 10 micrometers or less
SLCFs	Short-lived climate forcers
SO_2	Sulfur dioxides
Strategies	A careful plan or method
NG	Natural gas
CO_2	Carbon dioxide
GHGs	Greenhouse gases
NDC	Nationally Determined Contribution
NO_2	Nitrogen Dioxide
OA	Organic aerosol
RF	Radiative Forcing

Executive Summary

Black Carbon (BC) and Organic Carbon (OC) are particulate matter formed from incomplete combustion of carbonaceous matter such as fossil fuels, biofuels and biomass. Both are short-lived climate forcers (SLCFs) which have relatively short lifetime in the atmosphere, for particles on the order of days. BC has a warming effect while OC has a cooling effect on the atmosphere. As important components of atmospheric aerosols, BC and OC aerosols have important impacts on ambient air quality, human health, and regional and global climate change.

1. Overview of the ChiNorBC project

According to the memorandum of understanding (MOU) regarding Economic and Technical Cooperation signed by the Government of the people's Republic of China (China) and the Government of the kingdom of Norway (Norway), as well as the memorandum of understanding signed by the Ministry of Ecology and Environment of the People's Republic of China (MEE) and the Norwegian Ministry of Climate and Environment (MCE). The Ministry of Commerce of the People's Republic of China (MOFCOM) and the Norwegian Ministry of Foreign Affair (MFA) have entered into the Agreement (Chinese-Norwegian Project on Emission, Impact and Control Policy for Black Carbon and its Co-benefits in Northern China) dated 29 November 2019. The main implementing agencies for the project are the Chinese Research Academy of Environmental Sciences (CRAES) and the Norwegian Environment Agency (NEA), in partnership with the Chinese Academy of Environmental Planning (CAEP), the Norwegian Institute of Public Health (NIPH) and Center for International Climate Research (CICERO), with financial support from the Norwegian Ministry of Foreign Affairs.

The implementation period of the project was 3.5 years (from October 2019 to June 2023). The aim was to:

- Review Norwegian relevant polices and counter-measures and experiences of BC/OC emissions reduction,
- Develop or update BC/OC emission inventories in northern China,
- Assess the impacts on air quality and climate using global and regional models,
- Assess the impacts of current BC/OC concentrations in the atmosphere on human health,
- Make recommendations for the development of BC/OC abatement measures in China.

2. Key results of the ChiNorBC project

（1）Review of the Chinese path to dealing with air pollution

In order to improve ambient air quality, the Chinese government has since 2013 successively promulgated and implemented a series of important policies, such as the Action Plan on Prevention and Control of Air Pollution and the Three-Year Action Plan to Fight Air Pollution (Table 1). Supporting

policies including elimination of outdated production capacity, in-depth control of pollution in key industrial sectors (e.g. thermal power, iron and steel, cement), control of coal-fired boilers, clean heating, and prevention and control of mobile source pollution have been implemented. The policies involve the industrial, residential, transportation, and many other sectors. During the 14th Five-Year Plan period (2021–2025), China will accelerate the transformation and upgrading of industrial structure and strictly control the construction of high energy-consuming and high-emission projects. At the same time, China will strengthen the collaboration between different ministries. and conduct unified policy planning and standard setting, along with unified monitoring and assessment, unified supervision and enforcement, and unified inspection and accountability, in order to provide support and guarantees for achieving the synergistic effect of pollution and carbon reductions.

Major relevant polices and counter-measures:

Since 2013, China has released a series of air pollution prevention and control policies, significantly reducing the emission of particulate matter (PM), sulfur dioxide (SO_2) and other pollutants, which has achieved synergies with BC emission reduction. The policies included improving legal frameworks, standards and action plans on air quality improvement, upgrading industrial standards and companies, restructuring industry, optimizing energy structure, prevention and control of mobile source pollution and treatment of non-point source pollution. In 2020, China announced carbon peak and carbon neutrality action in China, that included carbon peaking before 2030 and carbon neutrality before 2060.

Table 1 A series of released air pollution prevention and control policies

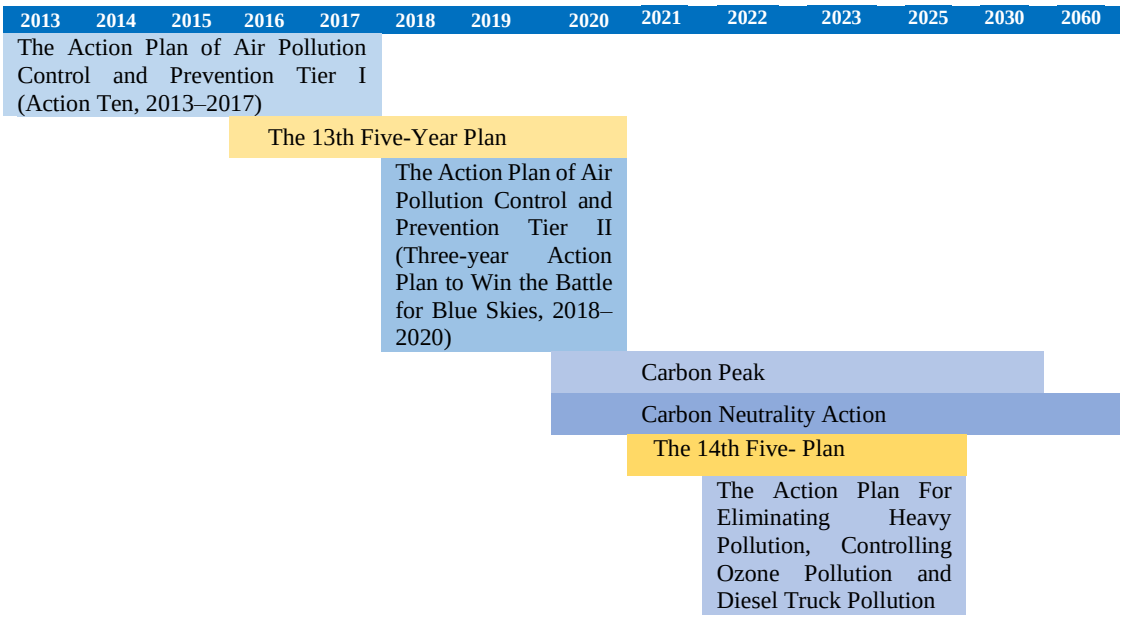

Achievement of air quality improvements:

Since 2013, China has achieved positive results in air pollution prevention and control, with the overall ambient air quality seeing substantial improvement (Figure 1). The annual average measured $PM_{2.5}$ concentration of 337 cities at or above prefecture level (hereinafter referred to as the “337 cities”) in

2020 was 33 μg/m^3, down by 29.1% from 2015. From 2015 to 2020, The annual average measured concentration of $PM_{2.5}$ in Beijing dropped by more than 50%..

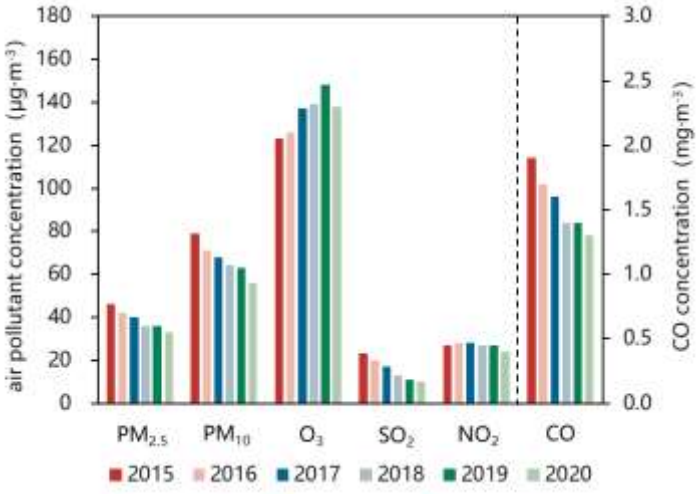

Figure 1 Changes in national annual average measured concentrations of major air pollutants from 2015-2020 in the 337 cities

（2）Development of new emission inventories and scenarios

Existing Black Carbon emission inventories were reviewed and emission factors from literature obtained. Measurements and in-situ investigation were done for mobile and residential sectors to collect activity levels and derive emission factors. Based on a publicly available emission inventory established by Tsinghua University, ChiNorBC-2018 BC/OC and other air pollutants emission database and inventories for Northern China have been established. This was done by updating the information of two key sectors (residential and mobile sectors) and optimizing the others. Total BC emissions of Northern China in the ChiNorBC-2018 inventory and the sector distribution are shown in Figure 2.

The residential sector contributed the most, accounting for more than half of the emissions, followed by industrial sector, accounting for 25%, the mobile (including on-road and off-road mobile sources) sector, accounting for about 13%.The residential sector contributed the most, accounting 56% of the emissions, followed by industrial and mobile (including on-road and off-road mobile sources) accounting for 26% and 13% respectively. In view of the dominance of the residential sector, more focus should be directed towards reducing these emissions in Northern China, not leaving other sectors like industry and mobile unattended.

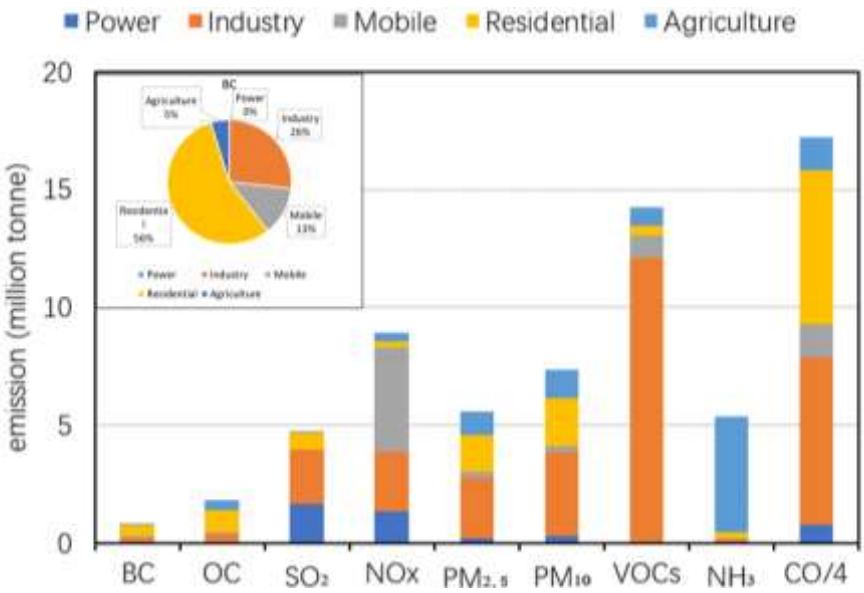

Figure 2 BC emissions of Northern China and the sector distribution in the ChiNorBC-2018 inventory

（3）The co-benefits of mitigating BC/OC emissions in China

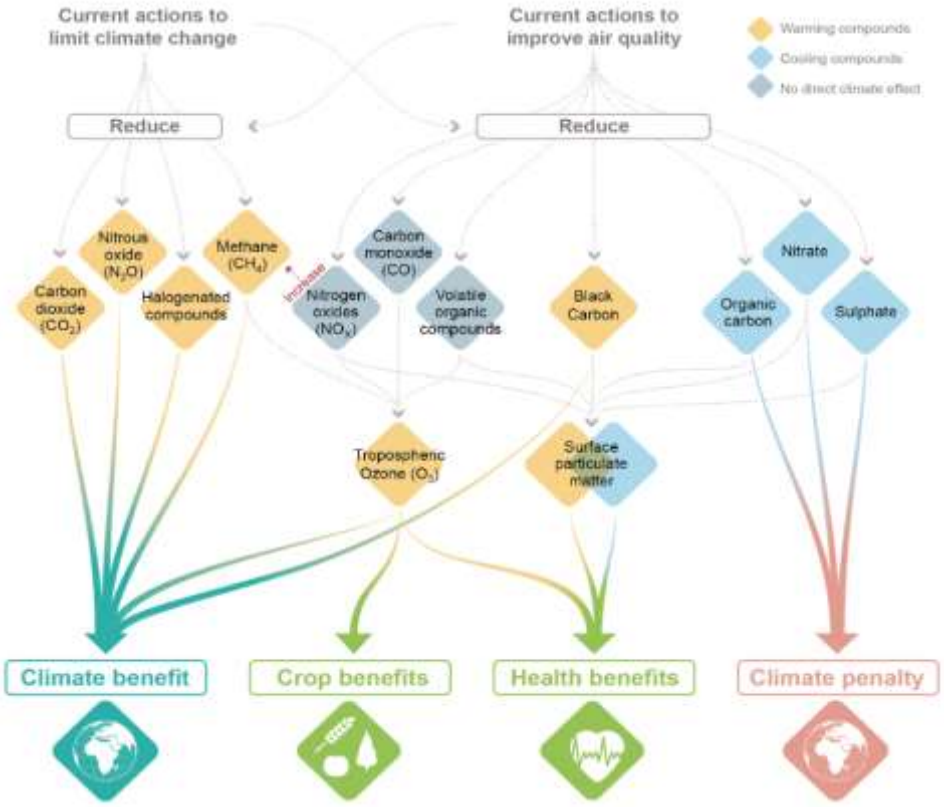

Figure 3 Links between actions aiming to limit climate change and actions to improve air quality (FAQ 6.2 from IPCC, 2021)

BC/OC constitute important parts of atmospheric fine particulate matter ($PM_{2.5}$) and is always co-emitted.

By reducing the emissions, we can obtain air quality, climate and health benefits. Emission control measures will in many cases also mitigate other harmful pollutants, thus many co-benefits can be achieved by optimizing reduction strategies.

1) Emission reduction potential

The ChiNorBC project conducted scenario analyses of BC and OC mitigation pathways using an integrated modeling framework to support policymaking. With the consideration of structural adjustment, end-of-pipe control, and industrial layout optimization, three scenarios with increasing stringency, namely business as usual scenario (BAU), strengthened end of pipe control scenario (EOP) and ambitious control scenario (ABC), are designed. Structural adjustments and strengthened end-of-pipe control measures are effective in reducing BC and OC emissions across Northern China (Figure 4).

The analysis suggests that by 2035, BC and OC emissions in Northern China could decline by 20-43% and 17-35%, respectively, with varying control strictness. The residential, industrial, and mobile sectors have the greatest potential for emission reduction with effective measures implemented.

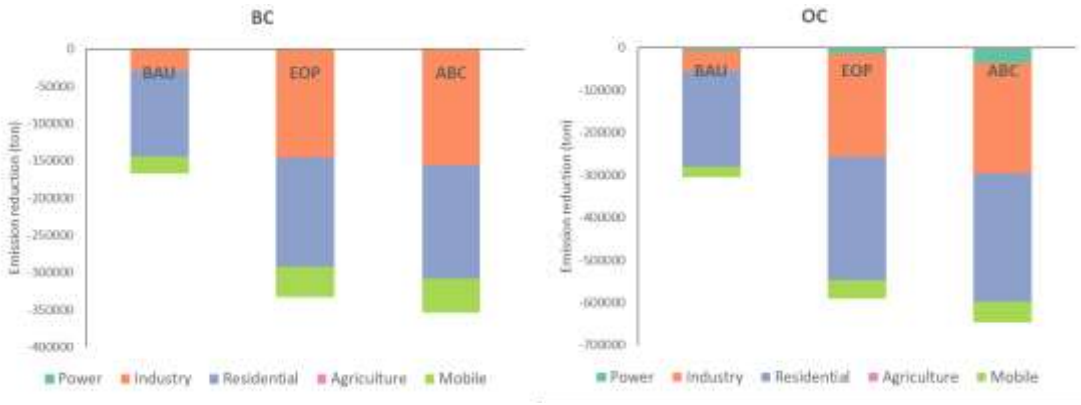

Figure 4 Reductions of BC and OC emissions by 2035 compared with 2018 in the three emission reduction scenarios (Reductions in the agriculture sector is to small to be visible)

2) On air quality

The air quality model simulation performance under the ChiNorBC-2018 emissions inventory has improved considerably compared to the baseline emission inventory. Model results compare much better to the monitoring data, especially for BC/OC.

The air quality modelling results for 2018 show that the concentrations of atmospheric pollutants exhibit clear seasonal variations. The highest pollution mostly occurs during winter, while the summer season generally has the best air quality. The simulated BC/OC concentrations were highest in Beijing, Tianjin, Hebei and surrounding areas and Northeast China. The 2018 concentration of BC and OC during winter is shown in figure 5.

Based on the three scenarios developed in the project, the more pronounced decrease in pollutant

concentrations is seen in the ABC scenario. And the maximum decreases in concentrations simulated in the ABC abatement scenario were 60.0% (9.7μg/m^3) and 54.0% (13.8μg/m^3) for BC and OC, respectively. At the same time, the annual average concentrations of other conventional pollutants simulated in this emission reduction scenario are below the concentration limits of the secondary standards in the national air quality standards in 2035.

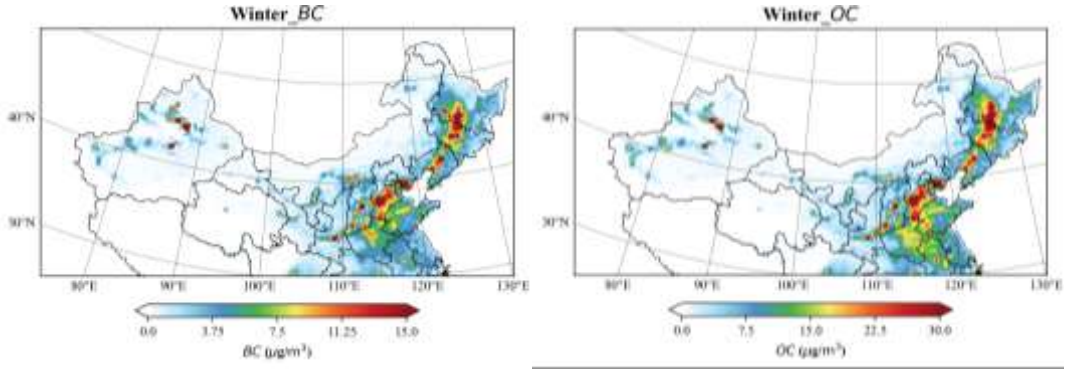

Figure 5 The spatial distribution of the simulated average concentrations of BC/OC in winter (Note that the scales are different for BC and OC)

3) On climate change

Reductions from 2018 to 2035 in the total amount of BC, OC, sulfate, and nitrate aerosols in the atmosphere are simulated for all three scenarios developed in the project. The relative reductions are largest for BC and nitrate (up to 20% for China as a whole in the ABC scenario), and smallest for sulfate (~2-5%). Larger relative reductions in BC and nitrate of up to 40% are found over the regions with the heaviest pollution today.

In the ChiNorBC project, the resulting estimated radiative forcing and impact on global mean temperature is broadly consistent with the current status of scientific knowledge on aerosol-induced climate impacts.

Aerosols can also have important effects on local and regional climate, including on extreme events, through changes in the hydrological cycle and dynamics of the atmosphere. Such effects have not been quantified in the ChiNorBC project, but such quantifications are needed for a more comprehensive understanding of climatic co-benefits or potential trade-offs of BC/OC mitigation.

4) On health

Exposure to $PM_{2.5}$ is a leading environmental risk factor for premature mortality and loss of healthy life years worldwide. BC is the vital component of $PM_{2.5}$, its porous structure is easier to absorb organic compounds, so it has a greater impact on human health. As the sources of $PM_{2.5}$ may vary considerably between regions, knowledge regarding the potential adverse effects of different types of particles is important for implementing effective mitigating measures. The project aimed to perform a health risk assessment of air pollution particles and rank the emissions sectors and sources.

- Our systematic review of the literature showed that long-term exposure to BC was associated with increased total mortality and mortality due to specific diseases. The impact of BC on the respiratory system was higher than on the cardiovascular system.
- Experimental studies in research animals and 2-dimentional (D)/3D cell culture models showed that exposure to BC and $PM_{2.5}$ can cause inflammation, immune cell imbalance, dysregulated gene expression and increased RNA m^6A modification in the lungs, which may reveal the molecular mechanisms underlying the health effects of $PM_{2.5}$ exposure, both in the lung and secondary organs.
- $PM_{2.5}$ sampled in specific cities with representative pollution sources exhibited different inflammatory effects in cell culture models through the release of inflammatory mediators. The results may suggest a higher contribution of industrial emissions and coal burning to PM toxicity than traffic emissions. However, the differences between the samples were small and more experiments and samples must be included to perform an accurate toxicity ranking of the different sources of particles.

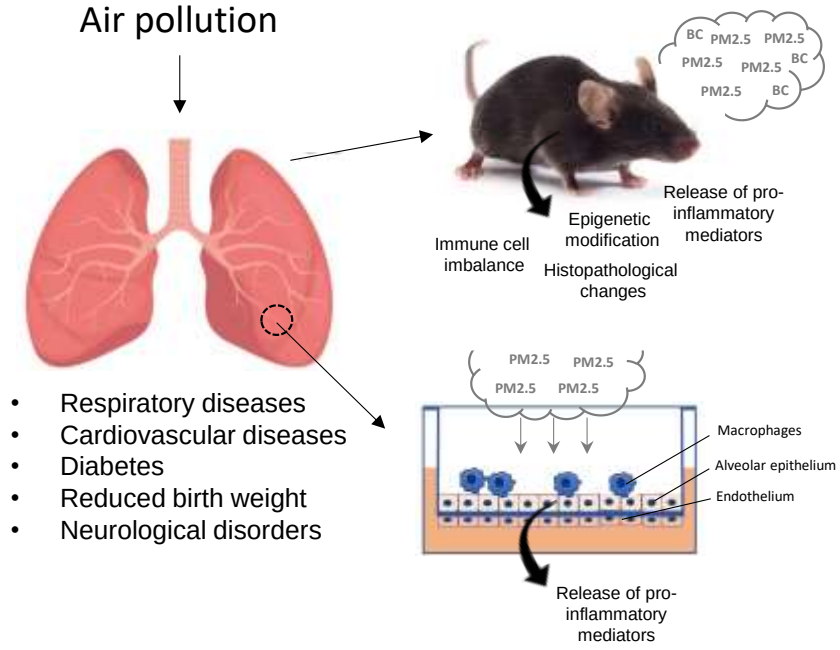

Figure 6 The study of $PM_{2.5}$/BC on health effects. Inhalation of $PM_{2.5}$ can cause a range of diseases. The present study examines the adverse effects of different types of $PM_{2.5}$ using experimental animal models and advanced cell cultures, focusing on the effects on inflammation and epigenetic modifications.

（4）Project dissemination products and outreach

In order to raise awareness and build capacity, the ChiNorBC project has published an extensive number of disseminations products. The publications are aimed at different audiences from policy makers via scientists to the general public.

1) The ChiNorBC web site

All the dissemination products, key results, project history, project participants and contact information can be found at the ChiNorBC web site (http://chinorbc.net/)

2) The final project report

All key results from the project are contained in the final project report. The report has seven chapters and has around 200 pages.

3) Review reports:

Based on the main research content of each of the project outputs, five review reports have been published.

- Review of BC/ OC emissions and control measures in China and Norway.
- Review of BC/ OC emissions inventories.
- Review of impact assessment of BC/OC on air quality and climate change.
- Review of human health effect of BC in air pollution.
- Review of policies of China for the control of BC/OC.

4) Book:

A hard copy book named *A Review of Emissions, Impacts and Policies*(China Environment Publishing Group·Beijing, 2022) has been published based on the review reports:

5) Brochure and Cartoon movie:

A brochure and a cartoon movie for introducing emissions and impacts of BC/OC have been developed.

6) Peer reviewed scientific papers:

Several scientific papers acknowledging the ChiNorBC project have already been published, and we anticipate that there will be more in the coming years. The papers are listed on the ChiNorBC web site.

7) Seminars and workshops

The project was carried out during the covid pandemic, so most of the seminars were digital. The *Final governmental seminar* and an *In-depth seminar* took however physically place in Beijing. The *kick-off meeting*, *two emission workshops* and *a scenario workshop* was carried out. The reports from the meetings are available on http://chinorbc.net/.

3. Uptake of project results in policy making

（1）Fitting BC mitigation programs into China’s atmospheric and socio-economic development policies and national policies

Black Carbon is a major air pollutant and climate forcer in China. Reducing BC emissions would help achieve China's strategic target of carbon peaking and carbon neutrality, as well as the target of constructing a "Beautiful China" characterized by clean air. While China has established a policy framework to improve air quality and cope with climate change, tailored mitigation policies specifically targeting BC emissions could be reinforced to better integrate them into China's atmospheric and socio-economic development policies.

Despite that the importance of reducing BC emissions has been widely studied, specific mitigation

policies have yet rarely been implemented in China. During the past decade, BC was mainly co-abated by measures that focused on reducing primary $PM_{2.5}$ emissions. While the scientific research should be continued, political will and public awareness are likely to be t important for integrating BC control into China's national policies. The Chinese government is now committing to tackle issues that are of most concern by the general public. Therefore, enhancing the public understanding of the impacts of BC emissions on health and the environment would help form a consensus of targeted mitigation among all parties including the policymakers, scientists, and the general public. This wills likely contribute to the political commitments and social actions and there by emission reductions with benefits for climate, air quality and health.

（2）Exploring the future path for mitigating BC/OC emissions in China

The ChiNorBC-2018 inventory shows that the residential, industrial and mobilesectors are the primary contributors to BC emissions in Northern China. This indicates that abatement actions should focus primarily on these sectors. However, different sectors and types of measures should be focused on when implementing BC control due to the varying emission reduction potential of different control measures across provinces. This can be attributed to the varying industrial and energy structures, as well as the stringency of existing control measures across regions.

Therefore, targeted policies should be developed to address the specific needs and challenges of each province to achieve optimal results in reducing BC emissions.

To further reduce BC emissions in Northern China, with the anticipation of maximizing the air quality, climate, and public health co-benefits, it is suggested to promote the adjustment of energy, industry, and transportation structures in Northern China, as well as maximize the potential of end-of-pipe treatment with a specific focus on key sectors such as residential , industrial, and transportation.

It is also necessary to advocate for the whole society to work together and mobilize all sectors of society to participate in atmospheric environment protection and climate change mitigation. The actions to be taken to achieve reductions in BC/OC and obtain substantial co-benefits for air quality, health, and climate are:

- Implement measures underlying the most ambitious control scenario (that is, the ABC scenario) developed in the ChiNorBC project in key regions to further strengthen the environmental policymaking in China.
- Focus on air pollution control policies that reduce emissions from industrial processes as well as coal burning, particularly in the residential sector, to better protect the public health of Chinese citizens.
- Abate BC emissions from the transportation sector.
- Account for differences in what sectors and types of measure that should be targeted when implementing BC control in different provinces in Northern China.
- Consider both structural adjustments, end-of-pipe control measures, and industrial layout adjustments to substantially reduce emissions and achieve co-benefits.

- Promote a shift from fossil fuels to clean renewable energies by increasing access to wind and solar power, as well encourage construction of hydropower bases.
- Accelerate elimination of unabated coal power plants and coal-fired boilers.
- Limit the development of energy-intensive projects and industrial furnaces using highly polluting fuels.
- Reduce residential coal use by facilitate transition to renewable energy, industrial waste heat, cogeneration, electricity, gas and other applicable ways to substitute coal-fired heating boilers and bulk coal.
- Promote the railway and waterway transportation for the medium and long-distance transportation of bulk commodities.
- Enhance implementation of ultra-low emission standards[1] policies by installation of advanced end-of-pipe control devices in key industries.

[1] For example, a coal-fired power plant meets "ultralow emission standards" when its emission levels of major air pollutants are similar to those from gas-fired power plants.

1 Introduction

Authors: Miaomiao Cheng (CRAES), Vigdis Vestreng (NEA)

Short-lived climate forcers (SLCFs) play an important role in air pollution as well as for global and regional climate change. SLCFs are agents that have relatively short lifetime in the atmosphere, ranging from a few days to a few decades. SLCFs like black carbon (BC) and methane have a warming influence on climate, while others like organic carbon (OC) and sulfate contribute to cooling. As one of the critical SLCFs in terms of climate effect, BC is also among the most important atmospheric substances detrimental to human health. BC and OC are important components of particulate matter (PM), and affect climate because of their radiative characteristics (IPCC, 2021). BC and OC are always co-emitted although with very varying relative fractions depending on source.

Main species in this report

Short-lived climate forcers

Short-lived climate forcers (SLCFs) are agents that have relatively short lifetime in the atmosphere - a few days to a few decades - and have a warming or cooling influence on climate. The main warming short lived climate forcers are black carbon, methane, and tropospheric ozone. They contribute to human enhancement of the global greenhouse effect. Black carbon and organic carbon which are the focus of this report, are also dangerous air pollutants, with various detrimental impacts on human health.

Black Carbon

Black carbon is a major component of soot and is produced by incomplete combustion of fossil fuel, biofuel and biomass. It is emitted from various sources including diesel cars and trucks, residential stoves, forest fires, agricultural open burning, and some industrial facilities. It has a warming impact on climate that is about 900 [100 to 1700] times stronger than CO_2 in a hundred-year perspective (IPCC, 2013). The climate impact is considerably larger in the short term. Its lifetime varies from a few days to a few weeks. Black carbon causes both atmospheric warming and when deposited on ice and snow, an increase of the melting rate. It also influences cloud formation and impacts regional circulation and rainfall patterns. In addition, black carbon impacts human health. It is a primary component of particulate matter in air pollution.

Fine particulate matter ($PM_{2.5}$)

Particulate matter that is less than 2.5 μm in aerodynamic diameter is referred to as $PM_{2.5}$. It has an important impact on air quality and visibility. These fine particles have relatively short residence time (days to weeks) in the atmosphere but can still be transported long distances. With small particle size, large surface area and ability to adsorb toxic and harmful substances (such as heavy metals, polycyclic aromatic hydrocarbons (PAHs) and microorganisms), they have harmful impacts on human health and atmospheric environmental quality.

Nitrogen oxides (NO_x)

Nitrogen oxides (NO_x) are a group of gases that are mainly formed during the combustion of fossil fuels. The dominant portion of these gases is nitric oxide (NO). However, NO can react with other gases in the atmosphere to form nitrogen dioxide (NO_2) which is harmful to health. These reactions take place very quickly and are reversible, so the two gases are referred to together as NO_x. NO_x are also precursors for the formation of tropospheric ozone and $PM_{2.5}$.

Tropospheric Ozone

Tropospheric ozone (O_3) is the ozone present in the lowest part of the atmosphere (up to 10-15km above the ground). It is a greenhouse gas and has a lifetime of a few days to a few weeks. It is not directly emitted but formed by sunlight-driven oxidation of other agents, called ozone precursors, in particular methane but also carbon monoxide (CO), non-methane volatile organic compounds (NMVOCs) and nitrogen oxides (NOx). Tropospheric ozone is a harmful pollutant that has detrimental impacts on human health and plants and is responsible for reductions in crop yields.

This report is part of a series of outputs produced under the Chinese-Norwegian Project on Emission, Impact, and Control Policy for Black Carbon and its Co-benefits in Northern China (ChiNorBC). The project is jointly implemented by the Chinese Research Academy of Environmental Sciences (CRAES) and the Norwegian Environment Agency (NEA), in partnership with the Chinese Academy of Environmental Planning (CAEP), the Norwegian Institute of Public Health (NIPH) and CICERO Center for International Climate Research, with financial support from the Norwegian Ministry of Foreign Affairs.

The ChiNorBC project focus on improving the knowledge and capability of China to conduct scientific assessments that co-benefit air pollution control and climate change in Northern China (Figure 1-1) and to provide recommendations and support in policy making for reducing BC and OC emissions from multiple aspects (emissions inventories, air quality, climate change, health, and policies).

Figure 1-1 The Northern China is the main study area in the ChiNorBC project

1.1 Black Carbon and its effects

Black carbon (BC) is formed through the incomplete combustion of fossil fuels, biofuel and biomass. It consists of pure carbon in several linked forms. BC warms the Earth by absorbing sunlight and re-emitting heat to the atmosphere and by reducing albedo (the ability to reflect sunlight) when deposited on snow and ice. BC is always co-emitted with organic carbon (OC) which cools the atmosphere. The BC and OC are crucial components in $PM_{2.5}$ (Wang et al., 2021). More information about the characteristics of BC and OC can be found in Cheng et al., 2022.

Due to the rapid economic development in China in recent decades, the combustion of coal, other fossil fuels, and biofuels has increased considerably. This has resulted in large amounts of BC/OC being emitted into the atmosphere. This situation has not only caused heavy air pollution in megacities of China. BC/OC are also forcers of regional climate change thus air pollution and climate change are closely linked (see Chapter 4 and 5). Northern China experiences severe air pollution, particularly during the winter season due to increased coal and firewood combustion for heating and which also occur during unfavourable weather conditions, such as calm winds and a strong inversion layer. Therefore, BC/OC produces adverse effects on air quality, health, and climate change and has become an important topic in environmental and climatic research because of the physical and chemical characteristics.

BC is an important component of particulate matter, which contributes about 5–15% to the particulate matter concentration in urban air, and a major cause of regional air pollution. Furthermore, BC is one of the most radioactively important aerosol components in the atmosphere. BC plays an important role in shaping regional and global climate including extreme weather events. BC aerosols enhance the occurrence of extreme haze pollution episodes in megacities in China due to induced heating in the aerosol-planetary boundary layer (PBL). The resulting decreased surface heat flux substantially

depresses development of the PBL. In addition, BC has affected human health more than other pollutants because of the ease of adsorption to organic compounds and its porous structure. Accumulating evidence has identified the health risks associated with short-lived climate forcers, particularly BC and secondary organic aerosols. Exposure to BC/OC may lead to decreased lung function, obesity, and effects on neurocognition in human beings. Toxicological and health risk assessment studies conducted in Northern China will help to better understand the relationship between diverse exposure type and the incidence of disease (see Chapter 6). An integrated report jointly published by the UN Environment and WMO has validated the dual role of BC as an air pollutant and a climate forcer (UNEP, 2011). In addition, BC/OC are also important precursors for the formation of secondary organic and inorganic aerosols, that may be valuable when evaluating air quality, climate change, and health risks (Bond et al., 2013; Laskin et al., 2015; Zhang et al., 2020).

1.2 China's status on Black and Organic Carbon control

Since greenhouse gas emissions such as carbon dioxide and air pollutant emissions have many of the same sources, there can be good synergistic effects of emission reductions both for climate and air pollution. In order to improve ambient air quality, the Chinese government has successively promulgated and implemented two important policies, the *Action Plan on Prevention and Control of Air Pollution and the Three-Year Action Plan to Fight Air Pollution* since 2013, and implemented supporting policies including elimination of outdated production capacity, in-depth control of pollution in key industrial sectors (e.g. thermal power, iron and steel, cement), control of coal-fired boilers, clean heating, and prevention and control of mobile source pollution. The policies involve the industrial, residential, transportation, and many other sectors. During the 14th Five-Year Plan period (2021–2025), China will accelerate the transformation and upgrading of industrial structure and strictly control the construction of high energy-consuming and high-emission projects. The fundamental policies are: (1) construction of a clean and low-carbon energy systems, development of non-fossil energy, and reduction of fossil energy consumption; (2) increasing optimization and adjustment of transportation structure, and promoting public to rail, public to water, and multimodal transportation; and (3) selection of typical regions and cities to carry out pilot projects of meeting environmental quality standards and carbon emission peaks. At the same time, China will strengthen work coordination and conduct unified policy planning and standard setting, along with unified monitoring and assessment, unified supervision and enforcement, and unified inspection and accountability, to provide support and guarantees for achieving the synergistic effect of pollution reduction and carbon reduction.

1.2.1 Major relevant polices and counter-measures

Since 2013, China has released a series of air pollution prevention and control policies, significantly reducing the emission of particulate matter, SO_2 and other pollutants, and achieving synergies with BC emission reduction. The policies included improving legal framework, standards, and action plans on air quality improvement, upgrading industrial standards and companies, restructuring industries, optimizing energy structure, prevention and control of mobile source pollution and treatment of non-point source pollution. In 2020, China announced carbon peak and carbon neutrality action in China, that included carbon peaking before 2030 and carbon neutrality before 2060. More details about these countermeasures of air pollution control can be found in Cheng et al., 2022.

1.2.2 Achievement of air quality improvements

Since 2013, with the implementation of the *Action Plan on Prevention and Control of Air Pollution* and the *Three-Year Action Plan to Fight Air Pollution*, China has achieved positive results in air pollution prevention and control, with the overall ambient air quality seeing substantial improvement. The annual

average measured $PM_{2.5}$ concentration of 337 cities at or above prefecture level (hereinafter referred to as the "337 cities") in 2020 was 33 μg/m^3, down by 29.1% from 2015 (Figure 1-2); at the same time, the annual average measured concentrations of sulfur dioxide (SO_2), carbon monoxide (CO), inhalable particulate matter (PM_{10}) and nitrogen dioxide (NO_2) dropped by 10~56%.

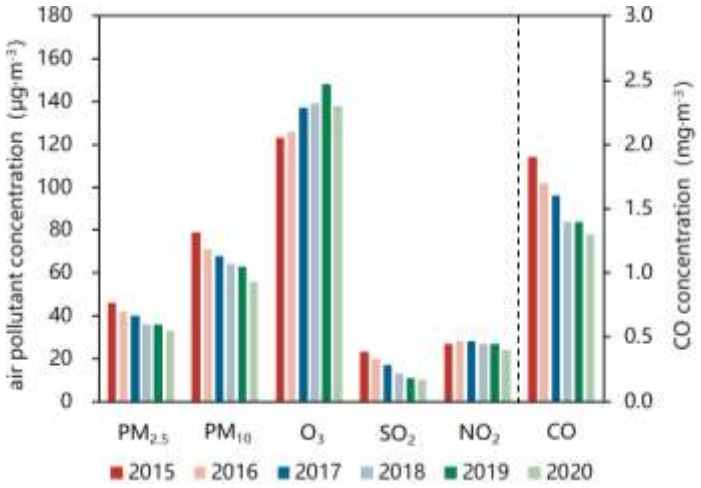

Figure 1-2 Changes in national annual average measured concentrations of major air pollutants from 2015-2020 in the 337 cities (Wang et al., 2022)

From 2015 to 2020, in Beijing-Tianjin-Hebei and the surrounding areas (hereinafter referred to as the "2+26 cities" region), the annual average measured concentrations of various pollutants, except O_3, showed a downward trend. In 2020, the concentrations of SO_2, PM_{10}, $PM_{2.5}$ and CO dropped by 35-70% compared to 2015, and the concentration of $PM_{2.5}$ was down by 35%. The annual average measured concentration of $PM_{2.5}$ in Beijing dropped by more than 50%, a remarkable progress. Starting from 2016, all the 2+26 cities met the national annual standards for SO_2 and CO concentration (that is, 60 μg/m^3 for SO_2, and 4 mg/m^3 for CO; national air quality standard issued by the Ministry of Ecology and Environment (MEE) (GB3095-2012).

The number of days with measured good air quality[2] in the "2+26 cities" region shows a slight increasing trend. The ratio of clean days increased from 53.6% in 2015 to 63.5% in 2020. Based on observation-based statistics, the number of days with heavy pollution shows a decreasing trend. The ratio of days of heavy pollution or above was down from 8.9% in 2015 to 3.5% in 2020.

1.3 Overview of the ChiNorBC project

The overall purpose of the ChiNorBC project is to improve the capacity to control emissions and strengthen the capacity and policies of local decision-makers in Northern China to reduce BC/OC emissions in a way that maximized the co-benefits on climate change, air quality, and health

A key objective of the project has been to understand the BC/OC emissions trends in northern China. The BC/OC emissions inventories in Northern China, which have been published by different institutions, are often inconsistent in total emissions or in specific sectors and trends. This is due to the differences in emission factors chosen, activity levels recognized, and methodologies applied. These inconsistent emissions results have led to scientific uncertainty and add challenges in identifying major emission sources and formulating pertinent policy. For this reason, a more comprehensive, and consistent BC/OC emissions inventory was needed for Northern China. This project provides scientific data support to formulate and implement policies by incorporating new emissions factors derived from new

[2] Days with good air quality refers to days with air quality index (AQI) lower or equal to 100; days with heavy pollution refers to days with AQI greater than 200.

measurements, investigated activity levels, and improved methodology. For more information please see Chapter 2, *Establishment of black and organic carbon emissions inventories for Northern China.*

The project has contributed to narrowing the knowledge gaps regarding the impacts of BC/OC on climate change, air quality, and health in China. Although much attention has been paid to the effects of BC on climate change, the effects of BC/OC on air quality and health in China has received less public focus. With the rapid development in China in recent decades, a large amount of BC/OC has been emitted into the atmosphere. This has not only caused visible decreases in air quality and is harmful to the populations of megacities of China, but the pollutants are complex forcers of global and regional climate change due to their various lifetimes and properties. Therefore, it is important to assess the effects of BC on climate change, air quality and health together using global and regional chemical transport models, investigations, and experiments. For more information, please see Chapter 4, *Evaluation of the air quality*, Chapter 5, *Evaluation of climate effects* and Chapter 6, *Health risk assessment*.

Furthermore, the project has provided recommendations for establishing novel policy design for reducing BC/OC emissions at the regional level in Northern China. A series of clean air actions have been carried out in recent years in China, e.g., the Action Plan on air pollution and prevention, specific to control air pollution and protect human health. $PM_{2.5}$ acts as the core target species of these actions. As BC/OC is a component of $PM_{2.5}$, clean air campaigns can reduce BC/OC emissions. China's climate mitigation policy is primarily focused on energy policy, particularly the restructuring of energy resources and increasing energy efficiency and energy savings, all of which affect the consumption of coal and emissions of BC/OC. By studying and developing policy recommendations for reducing BC/OC, it is possible to recognize the interrelatedness of air quality and climate change effects and incorporate that knowledge to determine optimal pathways for achieving both air quality and climate change policy goals in northern China. Therefore, the effects and co-benefits of reducing BC/OC emissions on climate change, air quality and health were identified in this project. Policy suggestions for reducing the emissions and impacts of BC/OC in Northern China was developed and the results were disseminated/proposed to relevant government agencies/ministries, scientists, and the public to facilitate implementation of policies and actions in accordance with health and climate needs. For more information, please see Chapter 3, *Scenario analysis and Chapter* and Chapter 7, *Policy recommendations*.

ChiNorBC first developed a baseline by analyzing the current emission and concentration levels in Northern China, as well as existing strategies to reduce the impacts of BC/OC (Chapter 1 and Review report 1[3]). The study area contains Beijing-Tianjin-Hebei (BTH) and the surrounding area (Beijing, Tianjin, Hebei, Inner Mongolia, Shanxi, Henan, and Shandong Provinces), Northeast China (Heilongjiang, Jilin, and Liaoning Provinces) and Northwest China (Shaanxi, Ningxia, Gansu, and Xinjiang Provinces). Current practices in Norway and other countries are assessed to gain experience. Five review reports are published on the ChiNorBC website (http://chinorbc.net/). With this background, ChiNorBC has developed improved emission inventories for BC- and OC- emissions in China using the most recent, best available national statistics and measurements obtained in the project (Chapter 2). Based on this, scenarios have been developed (Chapter 3), and results obtained on air quality (Chapter 4), climate change (Chapter 5) and health (Chapter 6). Finally, in Chapter 7, policy recommendations to maximize the co-benefits of reducing BC and OC has been described. The project has also raised scientific, governmental, and public awareness and enhance the understanding of the positive impacts of BC/OC emissions reductions through multiple dissemination products designed for different target groups. A review book including the emissions, impacts and co-benefits of BC/OC reduction in both China and Norway has been published. A brochure and cartoon video have been made to tell people about BC emissions and its impact, and to propose green lifestyle aimed to reduce carbon emissions. These dissemination products can be found on the ChiNorBC website (http://chinorbc.net/)

[3] Output-1-Review of BCOC emissions and control measures in China and Norway .pdf (http://chinorbc.net/)

2 Establishment of Black and Organic Carbon emissions inventories for northern China

Authors: Guorui Zhi, Wenjing Jin, Yanjun Wang, Yuzhe Zhang, Xiaohui Du (CRAES) , Ingeborg Rønning, Scott Randall, Tor Skudal, Vigdis Vestreng (NEA)

2.1 Introduction

Black carbon and organic carbon (BC/OC) emissions data for China have been published by different institutions and are often inconsistent in total or specific sectors due to substantial differences in the emission factors chosen, activity levels recognized, and methodologies applied. These inconsistent results often lead to misunderstandings and confusion and add difficulty to identifying major emissions sources and to formulating policy. For this reason, a more comprehensive, more accurate and reliable BC/OC emissions inventory has been developed for Northern China to provide scientific data support for the formulation and implementation of policies. In addition to BC and OC emission data, the ChiNorBC-2018 inventory also covers $PM_{2.5}$, PM_{10}, SO_2, NO_X, CO, NMVOC and NH_3. The inventories have been developed by incorporating new emissions factors derived from measurements and investigated activity levels obtained in the ChiNorBC-project and improved methodology. According to available literature, residential and mobile source sectors are among the most important sectors in emissions and uncertainty. The focus has therefore been to conduct intensive studies on these two sectors. Existing emission data for national emissions have also been updated with the new activity data and emission factors obtained in the ChiNorBC project.

This chapter responds to the ChiNorBC-project's Output 2 task "Establishment of BC/OC Emissions Inventory for Northern China". Below we document the methodology and process to compile a new emission inventory for Northern China, and a national inventory for modelling purposes.

2.2 Methodology

The new national 2018 and Northern China 2018 inventories, are based on an existing inventory with the base year 2018. The emissions of residential sector and mobile sector in the existing inventory are updated with data obtained in the ChiNorBC-project. The emissions of other sectors are either maintained as is given that no inconsistencies or other problems were found, or partially modified if problems are identified. The methodological framework is shown in Figure 2-1.

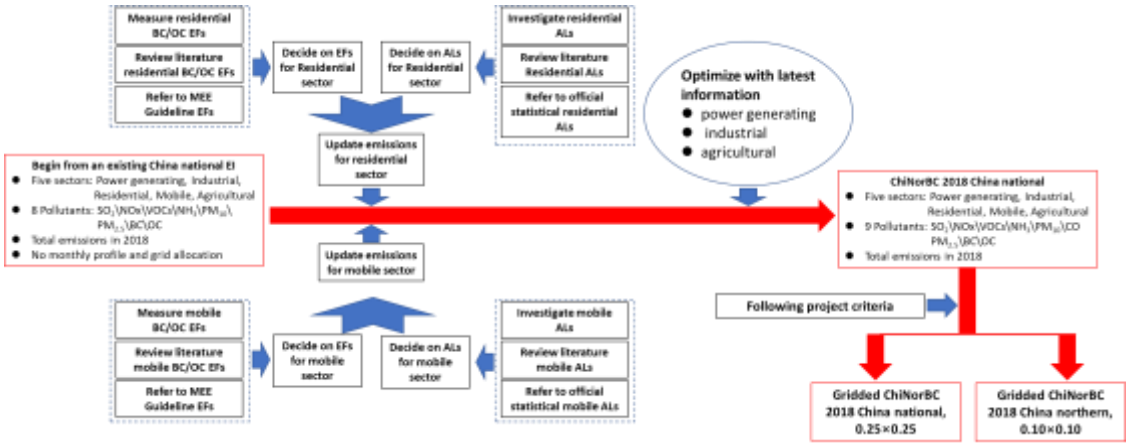

Figure 2-1 Roadmap for establishing the ChiNorBC-2018 inventories. Note: EI for emission inventory; AL for activity level; EF for emission factor

2.3 Measurements of BC/OC emission factors of residential and mobile sectors

The Residential and mobile sectors are defined as the key sectors due to the significant contribution of BC emissions.

In the residential sector, measurements were carried out on different coals used in households for heating and cooking. In the mobile sector, diesel and gasoline engines with different technologies were measured both for on-road passenger cars and trucks and off-road agricultural and construction machinery.

2.3.1 Residential

The residential sector is also known as the domestic or the household sector. This has long been the most important sector in China in terms of BC emissions. Here we have carried out measurements to determine the emission factors of BC and OC for domestic conditions (household heating or cooking). The measured EFs serve as one of three sources for determining the final EFs used for calculation of the BC and OC emissions in the base year 2018.

2.3.1.1 Dilution sampling system

A dilution sampling and on-line measurement system was set up to collect $PM_{2.5}$ samples and monitor real time information. The schematic of the system is shown in Figure 2-2.

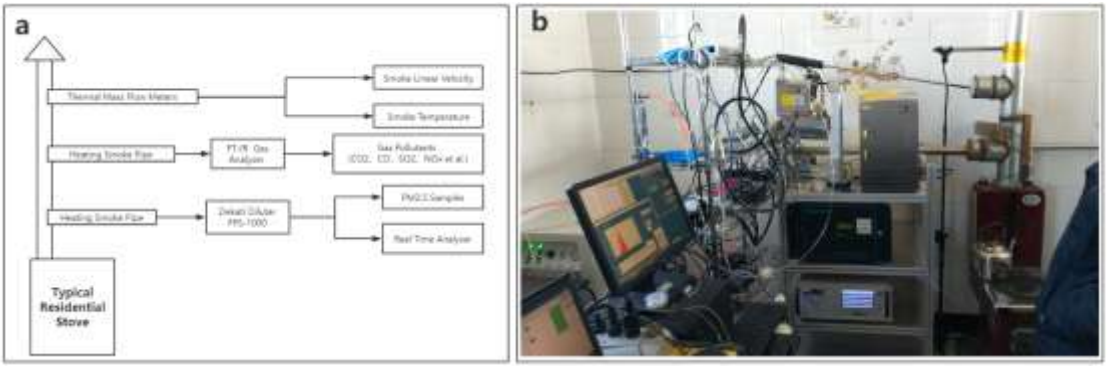

Figure 2-2 The dilution sampling and on-line measurement system.

Left: The schematic of the measurement system; Right: On site photo

2.3.1.2 Coals used in the measurement process

Coals with differed ranks were selected for measuring the EFs of residential coals Table 2-1. Previous studies have demonstrated that coal rank plays a major role in PM emissions, particularly BC and OC emissions. The rank of a coal depends on its geological maturity and is usually represented by the value of volatile matter content in the coal on dry and ash free basis (V_{daf}). In the following table Table 2-1, two coals, Y9 and X1, are anthracitic (high rank) and the others are all bituminous.

Table 2-1 Coals used in this project

No.	V_{daf}%	Ash%	C_{FIX}%	M%
Y1	36.63	12.41	49.42	10.96
Y2	31.26	4.60	64.47	1.69
Y5	40.72	27.13	42.88	0.74
Y9	9.94	11.35	79.5	0.43
X1	4.75	9.07	86.08	0.62
X2	15.18	25.00	63.37	0.27

V_{daf}-volatile matter content in the coal on dry ash free basis; Ash-ash content; C_{FIX}-fixed carbon; M-moisture

2.3.1.3 Analysis of samples and calculation of EFs

Coals in Table 2-1 were burned separately in household stoves. $PM_{2.5}$ emissions were collected on quartz fiber filters. The sampled BC filters were measured with the DRI model 2001A carbon analyzer made by the Desert Research Institute with the thermal/optical reflection (TOR) method. The analyzer reports the results in elemental carbon (EC) and organic carbon (OC). The instrument and the IMPROVE protocol used to analyze the BC components are shown in Figure 2-3.

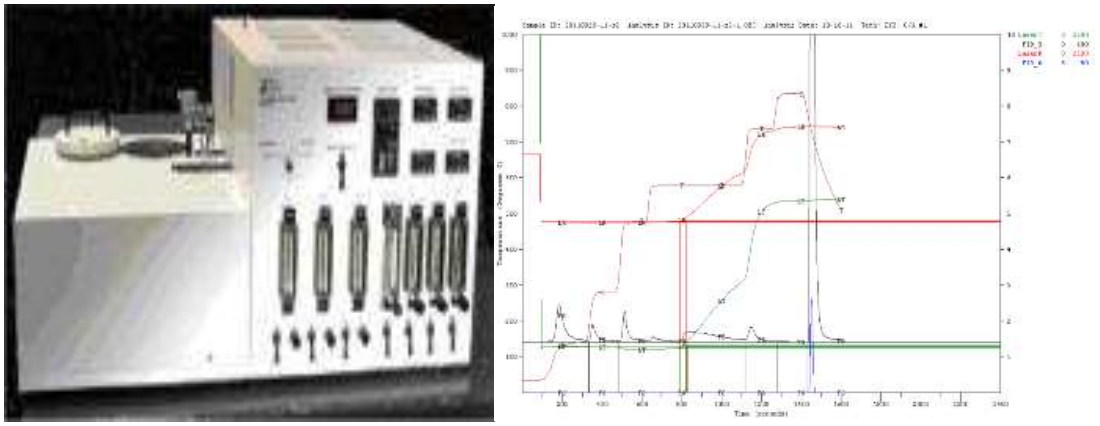

Figure 2-3 OC/EC measurement instrument. (a) DRI Model 2001A (b) IMPROVE protocol

The mass densities of OC and EC on filters were measured. Previous studies show that EC measured by TOR approach is usually higher than that by thermal/optical transmission (TOT) approach (e.g., Zhi et al., 2011). The values of EFx (g/kg, on dry and ash-free basis) were calculated according to the following formula:

$$EFx = \rho \times A \times 10^{-6} / (M1\text{-}M2) \times F/f$$

Where x —OC, EC

ρ—mass of x per unit area of loaded filter (μg/cm^2)

A—the area of loaded filter (cm^2)

M1—the mass of a fuel before combustion (kg)

M2—the mass of a fuel after combustion (kg)

F—the total flow rate of flue gas in the chimney

f—the flow rate of sampled flue gas

EC measured through the TOR approach is usually assumed equal to BC. Hereafter in this chapter, BC will be used in most cases though sometimes EC is used. The EFs calculated are given in Table 2-2. These values formed part of the basis for determining the final EFs for the calculation of emissions from residential sector.

Table 2-2 EFs measured in this study

No.	BC (kg/tonne)		OC (kg/tonne)	
	Chunk	Briquette	Chunk	Chunk
Y1	7.63	-		11.52
Y2	1.08	-		4.28
Y5	2.26	-		10
Y9	0.25	-		1.66
X1	-	0.17		-
X2	-	0.08		-

No.	BC (kg/tonne)		OC (kg/tonne)	
	Chunk	Briquette	Chunk	Chunk
Mean	2.805	0.125		6.865

2.3.2 Mobile

2.3.2.1 Measurement system

For the emission level of Phase IV diesel trucks (China Phase IV diesel standard, as referenced in the Review report 1[4],), BC were sampled with the vehicles running on the chassis dynamometer, as shown by Figure 2-4.

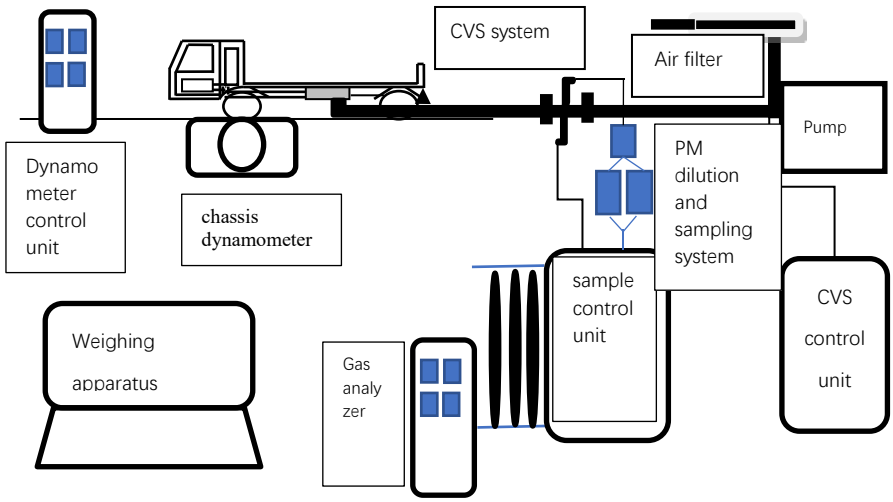

Figure 2-4 Schematic diagram of experiment equipment for vehicle BC sampling (China Phase IV).

For the level V diesel truck used engines (China Phase V), samples with BC were sampled with the engines installed on the engine bench, as shown by Figure 2-5.

Figure 2-5 Test bench for diesel engine of China phase V.

[4] Output-1-Review-of-BCOC-emissions-and-control-measures-in-China-and-Norway-FINAL.pdf (http://chinorbc.net/)

For off-road machinery (Table 2-5), samples with BC were sampled with the portable emission measurement system (PEMS) installed on the machinery, as shown by Figure 2-6.

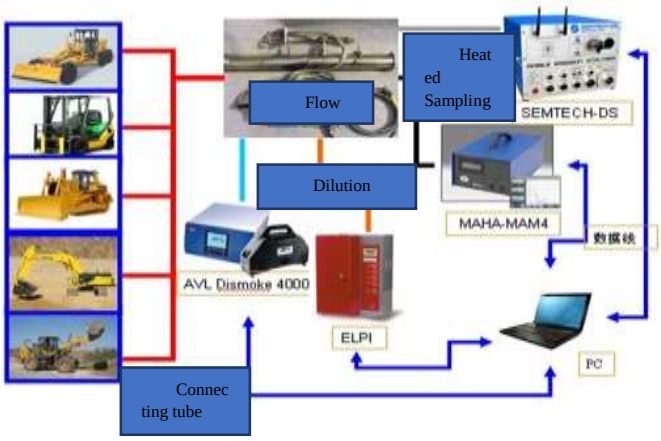

Figure 2-6 Off-road machinery BC sampling with the PEMS.

The sampled BC filters for off-road and on-road mobile sources were also measured with the DRI 2001A carbon analyzer.

2.3.2.2 Vehicles measured

The automobile statistical yearbook presented the annual sale quantities of automobiles from manufacturers and models based on which the test samples were selected. The selection of the test samples was referred to the data of the relevant automobile statistical yearbook. The typical models were chosen with the popular manufactures and models revealed by the yearbook which had a large proportion sale in the market. The information of the four phase IV vehicle samples and the seven phase V engine samples from the different manufactures are shown in Table 2-3 and Table 2-4.

Table 2-3 China phase IV vehicle samples information

No	Manufacturers	Maxweight（kg）	Engine	Displacement (L)	Rate power (KW)	Aftertreatment components
1	Jiangling	4495	JX493ZLQ4	2.771	80	DOC+POC
2	Dayun	4465	YN27CRD2	2.672	60	DOC+POC
3	Dongfeng	24600	YC6J220-46	6.494	162	SCR
4	Jiefang	40000	JP6	12.52	415	SCR

Table 2-4 China phase V engine samples information

No	Engine model	Aftertreatment	Displacement/L	Rate Power/kW
1	ISGe5-430	SCR	11.800	315
2	ISB220 50	SCR	5.900	159
3	HFC4DA1-2D	SCR	2.771	85
4	D10.38-50	SCR	9.726	276

No	Engine model	Aftertreatment	Displacement/L	Rate Power/kW
5	WP2.3Q110E50	SCR	2.29	77
6	WA329597	SCR	3.857	103
7	CA4DC3-12E5	SCR	3	91

The off-road machinery samples information is shown in Table 2-5.

Table 2-5 off-road machinery samples information

No.	Type	Manufactures	Rate Power (kW)	Curbweight (kg)	Emission level
WJ01	Excavator	Lingong	35.5	5800	Phase 2
WJ02		Volve	37	5600	Phase 1
WJ03		Xiaosong	185	/	Phase 3
WJ04		Xiaosong	107	/	Phase 2
WJ05		JCB	212	/	Phase 3
WJ06		Rili	185	/	Phase 3
ZZ01	Loader	Shangong	45	4800	Phase 1
ZZ02		Shangong	47	5360	Phase 2
ZZ03		Futian	92	10100	Phase 3
ZZ04		Xiagong	196	16600	Phase 3
ZZ05		Xutong	162	/	Phase 2
YL01	Roller	Luogong	36.75	2000	Phase 1
YL02		Xugong	73.5	14000	Phase 1
YL03		Xugong	128	18000	Phase 3
YL04		Xugong	128	18000	Phase 2
YL05		Zhongwaijian	132	20000	Phase 1
CC01	Forklift	Longgong	37	4300	Phase 2
CC02		Heli	58	6900	Phase 2
DT01	Tractor	Dongfanghong	70	3100	Phase 1
DT02		Leiwo	66	/	Phase3
DT03		Dongfanghong	66.2	3030	Phase 2
XT01		Shantuo	22	/	Phase 2
XT02		Dongfanghong	29	/	Phase 3
XT03		Dongfanghong	14.7	/	Phase 1
CC01	Combined Harvester	Feixiang	92	4900	Phase 2
CC02		Fugesen	92	7000	Phase 2

Pictures in Figure 2-7 show the on-site test setup.

Figure 2-7 On-site testing pictures.

2.3.2.3 Calculation

The EC, OC, and TC (Total Carbon=EC+OC) could be measured by DRI 2001A. The PM could be weighed by the weighing apparatus. The proportion of EC or OC to the TC could be expressed by $K_{EC/TC}$ and $K_{OC/TC}$, as follows.

$$K_{EC/TC}=\rho(EC)/\rho(TC)*100 \quad (1)$$

$$Koc_{/TC}=\rho(OC)/\rho(TC)*100 \quad (2)$$

The ratio of EC in PM is $K_{EC/PM}$, expressed with the following formula.

$$K_{EC/PM}=\rho(EC)/\rho(PM)*100 \quad (3)$$

The ratio of OC in PM is $K_{OC/PM}$, expressed with the following formula.

$$K_{OC/PM}=\rho(OC)/\rho(PM)*100 \quad (4)$$

The phase IV diesel vehicles were tested under the no-load, half load and full load conditions, as shown in Figure 2-8. The phase IV medium duty truck means the truck has a total weight (including the cargo loaded) is between 4.5 tonnes and 12 tonnes, which meet the China phase IV emission standard. The phase IV heavy duty truck means the truck has a total weight (including the cargo loaded) more than 12 tonnes, which meet the China phase IV emission standard.

In the Figure 2-8, each bar showed the averaged results of the tested models under the same load with 3 times measurement. The figure showed that the average results were slightly different under the different loads and the whiskers (min-max values) overlap sometimes. So, the test results under the half load were used to develop the BC emission factors in the project. The average $K_{EC/TC}$, $K_{OC/TC}$, $K_{EC/PM}$, and $K_{OC/PM}$ were 78, 22, 66, and 18.6.

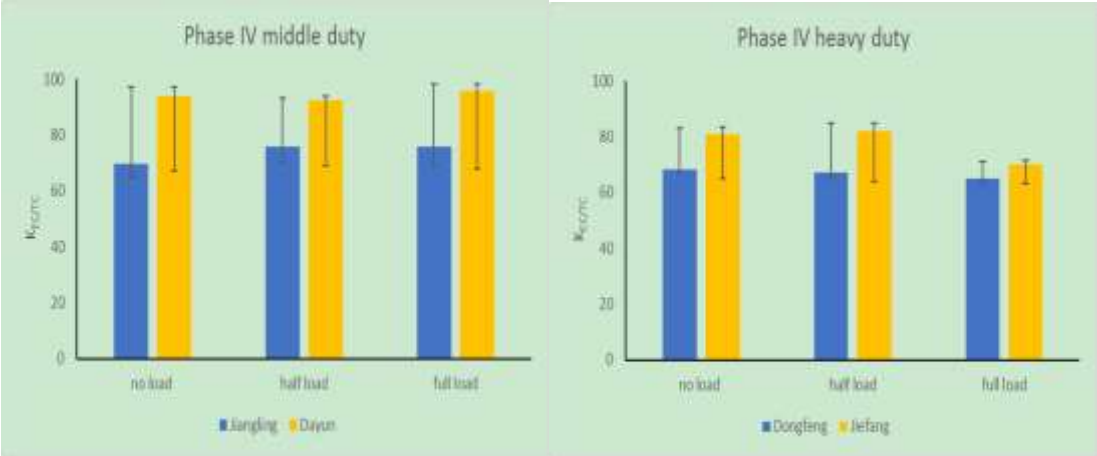

Figure 2-8 Phase IV diesel vehicle test results vehicles. (a) $K_{EC/TC}$ for Phase IV middle duty (b) $K_{EC/TC}$ for Phase IV heavy duty vehicles

The phase V diesel engines were tested under rated operation point. An operation condition on which the engine runs to its maximum power recommended by the manufactures is called rate power point. A max smoke point is where a diesel engine's power reach higher than a rated power. The results of $K_{EC/TC}$ are shown in Figure 2-9. The average $K_{EC/TC}$, $K_{OC/TC}$, $K_{EC/PM}$, and $K_{OC/PM}$ were 82.3, 17.7, 72, and 15.5.

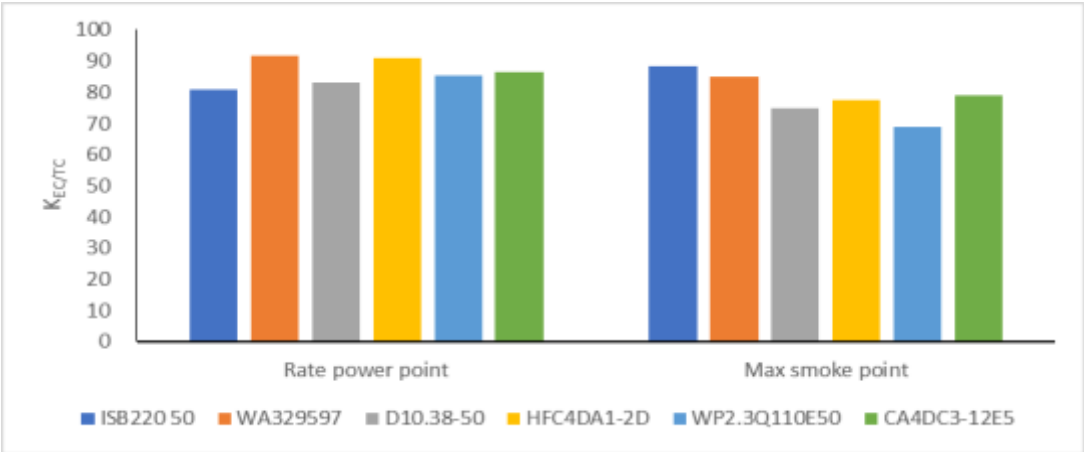

Figure 2-9 Phase V diesel engine test results.

The bars show data from six out of seven tested engines. The engine model "ISGe5-430" had obvious low values compared with the other engines, which not included in the result summary of Figure 2-9. The measurement had been checked with no problem. So, the low value of the engine was probably because the engine has a big deterioration of combustion control technologies or bad production quality.

The different kinds of construction machinery EC testing results are shown in Figure 2-10. The $K_{EC/PM}$ ($K_{EC/PM}$=$K_{BC/PM}$) varied from about 25% to 50% for the different construction machinery types. The meaning of each bar could be referenced to the table 2-5. The result of each bar was the average value of one test with PEMS installed on the machinery in a real world running. The dotted line was the average value of the different machineries.

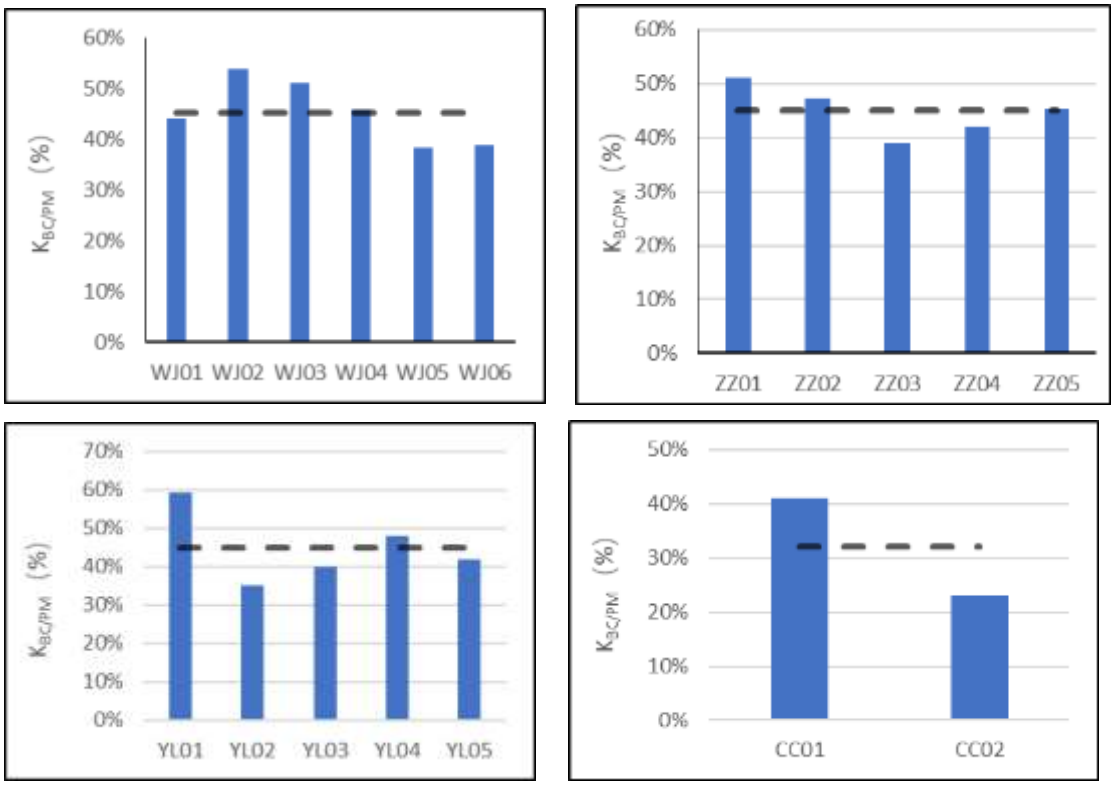

Figure 2-10 Construction machinery EC testing results.

The EC test results for different kinds of agriculture machinery are shown in Figure 2-11. The $K_{EC/PM}$ varied from about 20 to 55 for the different agricultural machinery types. The result of each bar was the average value of one time test with PEMS installed on the machinery in a real world running. The dotted line was the average value of the different machineries.

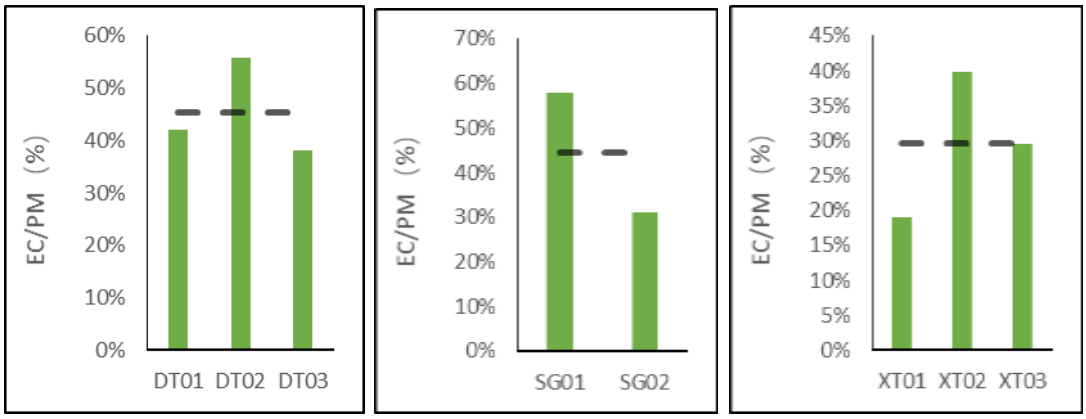

Figure 2-11 The EC test results for different kinds of agriculture machinery types.

The average $K_{EC/PM}$, $K_{OC/PM}$ for phase I/II and phase III were calculated to be 31, 44, 45 and 33, separately.

Table 2-6 $K_{EC/PM}$, $K_{OC/PM}$ Summary for mobile source samples

Mobile Sources	$K_{EC/PM}$	$K_{OC/PM}$
Trucks	66 (medium duty, phase IV) 72 (heavy duty, phase V)	18.6 (medium duty, phase IV) 15.5 (heavy duty, phase V)
Construction machinery	45 (Excavator) 45 (Loader) 45 (Roller) 33 (Forklift)	33 (Excavator) 33 (Loader) 33 (Roller) 45 (Forklift)
Agriculture machinery	31 (phase I/II) 45 (phase III)	44 (phase I/II) 33 (phase III)

2.4 Recommendation of BC/OC emission factors for key sectors

2.4.1 Residential

As described in the roadmap (Figure 2-1), the EFs for emission calculation in our inventories are the result from averaging over up to three data origins: measured by the ChiNorBC- project, extracted from literature (see Output 2 Review Report for details[5]), and recommended in MEE (Ministry of Ecology and Environment) guidelines. If one of the three data origins was missing EF data, the averaging was conducted over the other two data sources. Table 2-7 shows the data used to derive the mean EF value to be applied in calculating the base year 2018 emissions in the ChiNorBC-project. Note that the three

[5] Output-2-Review-Report-Review-of-BC_OC-Emissions-final.pdf (http://chinorbc.net/)

origins weigh equally in deriving the EFs for our inventories as we have no knowledge regarding which origin weighs more than the others.

Table 2-7 EFs (g/kg) for residential sector used in this study

	Data origin	BC	OC	$PM_{2.5}$	NOx	CO	VOCs	NH_3
Chunk	Literature	2.13	4.37	10.40	1.35	159.40	1.64	1.03
	MEE	2.63	3.12	6.25	1.20	118.00	2.13	
	Measurement	2.81	6.87					
	Mean	**2.52**	**4.79**	**8.33**	**1.28**	**138.70**	**1.89**	**1.03**
	sd	0.35	1.91	2.93	0.11	29.27	0.35	
Briquette	Literature	0.17	3.11	4.79	0.26	90.52	1.10	0.70
	MEE	0.17		0.83	1.23	72.00		
	Measurement	0.13	0.62					
	Mean	**0.15**	**1.86**	**2.81**	**0.75**	**81.26**	**1.10**	**0.70**
	sd	0.03	1.76	2.80	0.69	13.10		

In order to estimate the EFs for SO_2 and PM_{10} we applied recommended methodology from the literature. EF of SO_2 for chunk coal is 6.2 times the sulfur content in % and for briquette is 6.8 times the sulfur content in % according to MEE guidelines (MEE, 2016); The EF of PM_{10} can be derived from the relation $PM_{2.5}/PM_{10}$=77.8% (Lei et al., 2011).

2.4.2 Mobile

Tests of the diesel vehicles and machineries confirmed previous findings that the BC/PM ratios are dependent on which Chinese emission standard (China phase I-VI) the vehicle or machine belongs to because different combustion and emission control technologies have been adopted to meet the requirements in corresponding standards. Therefore, in this project, different $K_{EC/PM}$, $K_{OC/PM}$ values were used for the different emission level diesel vehicles and off-road machineries. The test results of $K_{EC/PM}$ and $K_{OC/PM}$ were used for China phase IV and phase V diesel vehicles and China phase I/II and phase III off road machineries. For China phase I/II and phase III diesel vehicles, literature data of BC/PM ratios was used (please see the Output 2 Review of BC/ OC emissions inventories report for details[6]). The ratios of BC/PM and OC/PM used in the ChiNorBC-project is shown in in Table 2-8 below. Again, we note that the EC is assumed equals to BC.[3]

[6] Output-2-Review-Report-Review-of-BC_OC-Emissions-final.pdf (http://chinorbc.net/)

Table 2-8 The ratio of BC and OC to PM (the $K_{BC/PM}$, $K_{OC/PM}$ ratios) used in the ChiNorBC-project

Mobile source category	Fuel type	China II and before		China III		China IV		China V	
		BC	OC	BC	OC			BC	OC
Vehicle	Diesel	0.51	0.32	0.56	0.32	Vehicle	Diesel	0.51	0.32
	Gasoline	0.27	0.58	0.27	0.58		Gasoline	0.27	0.58
Off-road construction machinery	Diesel	0.31	0.44	0.45	0.33	Off-road construction machinery	Diesel	0.31	0.44
Off-road agriculture machinery	Diesel	0.31	0.44	0.45	0.33	Off-road agriculture machinery	Diesel	0.31	0.44

To derive BC and OC emission factors (E_{BC}, E_{OC}) in g/km, we use the BC/OC ratios (**$K_{BC/PM}$, $K_{OC/PM}$** as shown in Table 2-9 to multiply the PM emission factors (E_{PM10}), as shown by the formula below.

$$E_{BC}=E_{PM10}*K_{BC/PM} \quad (5)$$

$$E_{OC}=E_{PM10}*K_{BC/PM} \quad (6)$$

In this project, the E_{PM10} was picked from China "Road Motor Vehicle Air Pollutant Emission Inventory Development Technical Guidelines" (MEE, 2014) (as shown in Table 2-9) and "the Technical Guidelines for the Development of Inventories of Atmospheric Pollutants from Non-road Mobile Sources(MEE, 2014)" (as shown in Table 2-10) issued by MEE of China.

Table 2-9 PM_{10} emission factors of road motor vehicles recommended in the guideline (g/km)

			China 1	China 2	China 3	China 4	China 5
Passenger Vehicle	Light Duty	Gasoline	0.029	0.012	0.008	0.003	0.003
		Diesel	0.070	0.058	0.036	0.034	0.034
	Medium Duty	Gasoline	0.067	0.020	0.012	0.007	0.007
		Diesel	0.516	0.174	0.164	0.118	0.059
	Large Duty	Gasoline	0.177	0.080	0.049	0.049	0.049
		Diesel	1.092	0.980	0.439	0.280	0.140
Truck	Light Duty	Gasoline	0.067	0.020	0.012	0.007	0.007
		Diesel	0.299	0.290	0.114	0.064	0.013
	Medium Duty	Gasoline	0.177	0.080	0.049	0.049	0.049
		Diesel	1.006	0.303	0.190	0.110	0.022
	Heavy Duty	Gasoline	0.177	0.080	0.049	0.049	0.049
		Diesel	0.692	0.558	0.270	0.153	0.030

Table 2-10 PM_{10} emission factors of off-road machinery recommended in the guideline (g/kWh)

Power Range	Fuel Type	Before China 1
Power<37kW	Diesel	1.2
37<Power<56kW	Diesel	1.0
75<Power<130kW	Diesel	0.8
Power>130kW	Diesel	0.7

The BC/OC emission factors we used in this project are listed in Table 2-11 (on-road vehicles) and Table 2-12 (off-road machinery).

Table 2-11 BC and OC emission factors of on road vehicles (g/kWh)

			China 1		China 2		China 3		China 4		China 5	
			BC	OC	BC	OC	BC	OC	BC	OC	BC	OC
Passenger Vehicle	Light Duty	Gasoline	0.00783	0.01682	0.00324	0.00696	0.00216	0.00464	0.00081	0.00174	0.00081	0.00174
		Diesel	0.0357	0.0224	0.02958	0.01856	0.02016	0.01152	0.02244	0.00714	0.02448	0.00714
	Medium Duty	Gasoline	0.01809	0.03886	0.0054	0.0116	0.00324	0.00696	0.00189	0.00406	0.00189	0.00406
		Diesel	0.26316	0.16512	0.08874	0.05568	0.09184	0.05248	0.07788	0.02478	0.04284	0.01239
	Large Duty	Gasoline	0.04779	0.10266	0.0216	0.0464	0.01323	0.02842	0.01323	0.02842	0.01323	0.02842
		Diesel	0.55692	0.34944	0.4998	0.3136	0.24584	0.14048	0.1848	0.0588	0.1008	0.0294
Truck	Light Duty	Gasoline	0.01809	0.03886	0.0054	0.0116	0.00324	0.00696	0.00189	0.00406	0.00189	0.00406
		Diesel	0.15249	0.09568	0.1479	0.0928	0.06384	0.03648	0.04224	0.01344	0.00936	0.00273
	Medium Duty	Gasoline	0.04779	0.10266	0.0216	0.0464	0.01323	0.02842	0.01323	0.02842	0.01323	0.02842
		Diesel	0.51306	0.32192	0.15453	0.09696	0.1064	0.0608	0.0726	0.0231	0.01584	0.00462
	Heavy Duty	Gasoline	0.04779	0.10266	0.0216	0.0464	0.01323	0.02842	0.01323	0.02842	0.01323	0.02842
		Diesel	0.35292	0.22144	0.28458	0.17856	0.1512	0.0864	0.10098	0.03213	0.0216	0.0063

Note： 1 light duty passenger vehicle means the length of the vehicle is below 6 m and a passenger capacity of no more than 9 persons;

2 medium duty passenger vehicle means the length of the vehicle is below 6 m and a passenger capacity of no more than 19 persons;

3 large duty passenger vehicle means the length of the vehicle is more than 6 m and a passenger capacity of more than 20 persons;

4 ligth duty truck means a cargo loaded vehicle whose total length is below 6 m and the total weight is below 4.5 tonnes;

5 medium duty truck means the truck has the length of more than 6m and the total weight is between 4.5 and 12 tonnes;

6 heavy duty truck means the truck’s total weight (cargo and the vehicle) is more than 12 tonnes.

Table 2-12 BC and OC emission factors of off- road machinery (g/kW.h)

Machinery type		Before China 1		China 1		China 2		China 3	
		BC	OC	BC	OC	BC	OC	BC	OC
Construction machinery	Excavators (100kW)	0.248	0.352	0.217	0.308	0.093	0.132	0.1125	0.0825
	Bulldozer (120kW)	0.248	0.352	0.217	0.308	0.093	0.132	0.1125	0.0825
	Loader (135kW)	0.217	0.308	0.1674	0.2376	0.062	0.088	0.081	0.0594
	Forklift (40kW)	0.31	0.44	0.2635	0.374	0.124	0.176	0.1575	0.1155
	Roller (110kW)	0.248	0.352	0.217	0.308	0.093	0.132	0.1125	0.0825
	Pave machinery (80kW)	0.248	0.352	0.217	0.308	0.093	0.132	0.1125	0.0825
	Grader (110kW)	0.248	0.352	0.217	0.308	0.093	0.132	0.1125	0.0825
	Others (Diesel) (30kW)	0.372	0.528	0.31	0.44	0.2945	0.418	0.2475	0.1815
Agriculture machinery	Larger and medium tractor (29.2kW)	0.372	0.528	0.31	0.44	0.2945	0.418	0.2475	0.1815
	Small tractor (9.6kW)	0.372	0.528	0.31	0.44	0.2945	0.418	0.2475	0.1815
	Combine harvester (42.5kW)	0.31	0.44	0.2635	0.374	0.124	0.176	0.1575	0.1155
	Irrigation machinery (14.9kW)	0.372	0.528	0.31	0.44	0.2945	0.418	0.2475	0.1815
	Others (Diesel) (3.0kW)	0.372	0.528	0.31	0.44	0.2945	0.418	0.2475	0.1815

For the BC factors of the inland ships, there were limited publications (Table 2-13

Table). In view of the technical level of Chinese ships lagging behind foreign ships and the high sulfur content in the fuels, the BC factor of China inland ships was chosen as 0.36 g/kg fuel in this project. The OC factor was calculated as 0.162g/kg fuel according to the BC/OC ratio of 40:18.

Table 2-13 BC emission factors of ships from the literature

Literature	BC EF (g/kg fuel)	Method
Lack D.A,, Light absorbing carbon emissions from commercial shipping, Geophys. 25 Res. Lett., 35, 2008	0.36-1	Optical
Agrawal, H., Emission Measurements from a Crude Oil Tanker at Sea, Environmental Science & Technology, 42 (19).2008	0.1	Thermal
Corbett, J.J., Updated emissions from ocean shipping. Journal of Geophysical Research: Atmospheres, 108, 4650,2003	0.37	Not available
Petzold, A., Recommendations for reporting “black carbon” measurements. Atmospheric Chemistry and Physics, 13,2013	Average 0.179±0.018 0.06（85%load） 0.36（10% load）	Thermal
Naya Olmer, Bryan Comer.et al. Greenhouse gas emissions from global shipping,2013-2015 Detailed methodology, ICCT,2017	stroke, 50%laod HFO:0.49 (g/kg fuel) Distillate:0.26(g/kg fuel)	Not available

2.5 Recommendation of activity data for key sectors

Deciding on the activity data for key sectors is also an important step for inventory construction. Here we compiled an activity dataset. These data are collected from publicly available data or from our own field investigation. The publicly available data are either in official releases, internet publications, or in literature published by ourselves or our peers.

2.5.1 Residential

As described in the roadmap, the final activity level for each of the 17 provinces is from either our field investigation, or literature reports or statistics or a balanced consideration of them, with field investigation preferred. For example, China has been promoting clean energy for Northern China’s rural household winter heating- The coal-to-gas or coal-to-electricity activity rates applied are mostly from governmental releases. Furthermore, to cover all energy types related to residential sector, the data of

biomass fuel and gaseous fuel (LPG & LNG) are also compiled. All these activities contribute to building a dataset of activity levels.

Selecting typical household coal heating village needs to meet the following requirements:

- Raw coal heating is the essential way to get warm,
- Neat shape, surrounding flat,
- Have certain independence, away from other villages and large pollution sources,
- Get the cooperation of local governments,
- No plan to change to gas or electricity plan recently,
- Transportation is convenient for personnel round-trip, as close to Beijing as possible.

Based on the above requirements and considering to fully understand the actual situation of winter heating in China, especially in northern China, the research group carried out a series of research activities.

The survey mainly adopts the method of in-situ household investigation to obtain the activity level data of rural heating method, heating area, heating period, coal type, consumption and other energy use. According to data obtained, we analyzed regional heating habits, time distribution, coal type and annual consumption, energy structure and other conditions.

A village cadre field guide a villager to fill in the survey form. Take Yaojiapu Village of Tangshan City as an example, there are 834 villagers in the village, and about 30 long-term vacant houses. This survey actually involved 418 households, accounting for 52% of the residents in Yaojiapu Village, and the survey data is highly representative.

The energy data in 2018 for residential sector of Northern China are presented in Table 2-14 and has been used in calculating emissions of the base year 2018. It should be noted that Anhui and Jiangsu are not included in this table. One of the reasons is that not all cities of these provinces belong to Northern China. The northern part of Anhui Province accounts for only 40% of the population, while the northern part of Jiangsu Province accounts for 35%. The proportion of the total GDP of the northern part is even smaller, around 20% respectively. In addition, the statistical yearbook on which the data are based cannot distinguish between cities within a province, so it is not possible to calculate the energy consumption of the northern part of these two provinces. Therefore, the energy data of the two provinces are not included in this data list.

Huge differences can be seen in energy consumption among provinces, which can be attributed to the differences in population, latitude, altitude, and economic level as well as clean energy penetration.

Table 2-14 Energy data for residential sector in individual provinces of Northern China. Anhui and

Jiangsu are not included because not all areas of Anhui and Jiangsu belong to northern China, so these two provinces are not listed in this table.

Province	Chunk	Briquette	Biomass	LPG	LNG	Electricity
	10^4 tonnes	10^4 tonnes	10^4 tonnes	10^4 tonnes	10^8 m^3	10^8 kWh
Beijing	30	45	25	12	36	47
Gansu	602	32	93	43	0	49
Hebei	1580	83	242	113	450	307
Henan	614	32	344	160	18	321
Heilongjiang	1966	103	129	60	0	70
Jilin	1859	98	98	46	0	42
Liaoning	2025	107	127	59	0	97
Inner Mongolia	2192	115	80	37	0	40
Ningxia	365	19	18	9	0	11
Qinghai	307	16	17	8	0	10
Shandong	1051	55	318	148	46	330
Shanxi	1987	105	134	63	75	82
Shaanxi	634	33	123	57	0	101
Tianjin	3	52	20	9	28	33
Xinjiang	2319	122	78	36	0	41
Total	**17534**	**1017**	**1846**	**860**	**653**	**1581**

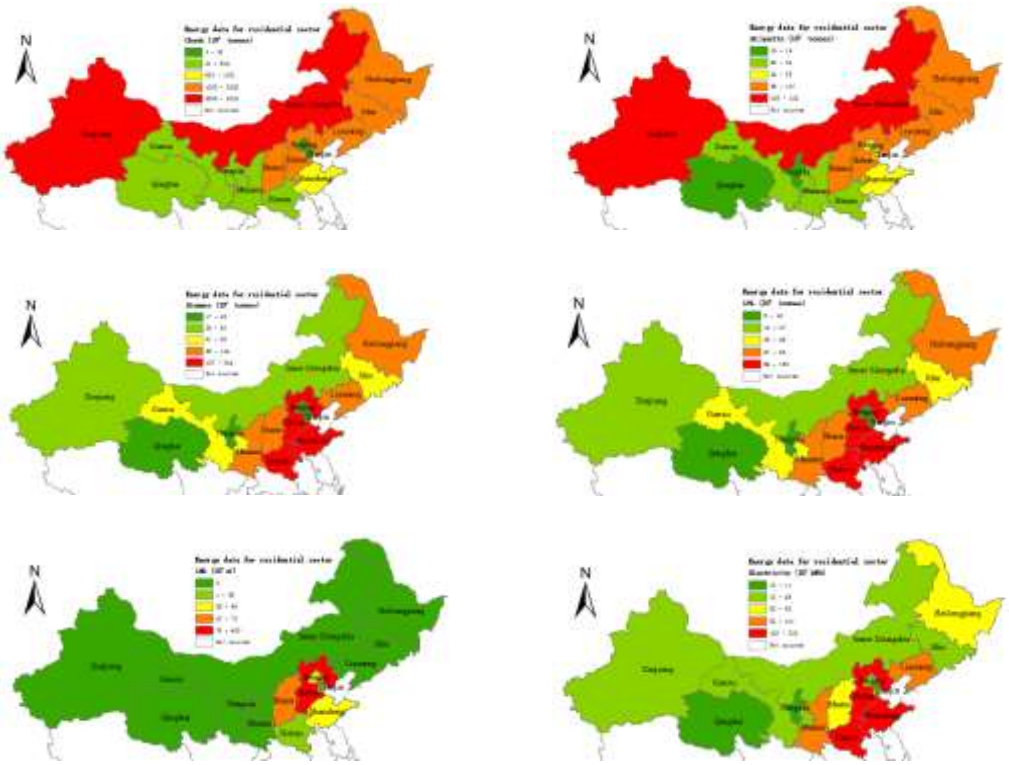

Figure 2-12 The energy structure of each province in Northern China. Anhui and Jiangsu are not included because not all areas of Anhui and Jiangsu belong to northern China, so these two provinces are not included in these figures.

With every energy type represented by standard coal equivalent (SCE, 1 SCE=1 TCE (tons standard coal equivalent) = 29.3GJ), Figure 2-13 shows the energy structure of each province. Since 2018, China has been making strong efforts to replace household raw coal with clean energy sources like electricity and gas in the so called "2+26" cities including Beijing, Tianjin, and 26 other cities in Hebei, Shanxi, Henan, and Shandong Provinces. The clean energy penetration effects can be perceived from this figure. Shift-to-clean-energy campaign continued in not only "2+26" cities, but also other provinces of Northern China. The improvement in air quality and the decrease in ambient BC concentration witnessed these years resulted partly from these actions (see Review report 1 for details[7]. In 2018, the ratios of raw coal replacement by electricity and/or gas for "2+26" cities are listed in Figure 2-14.

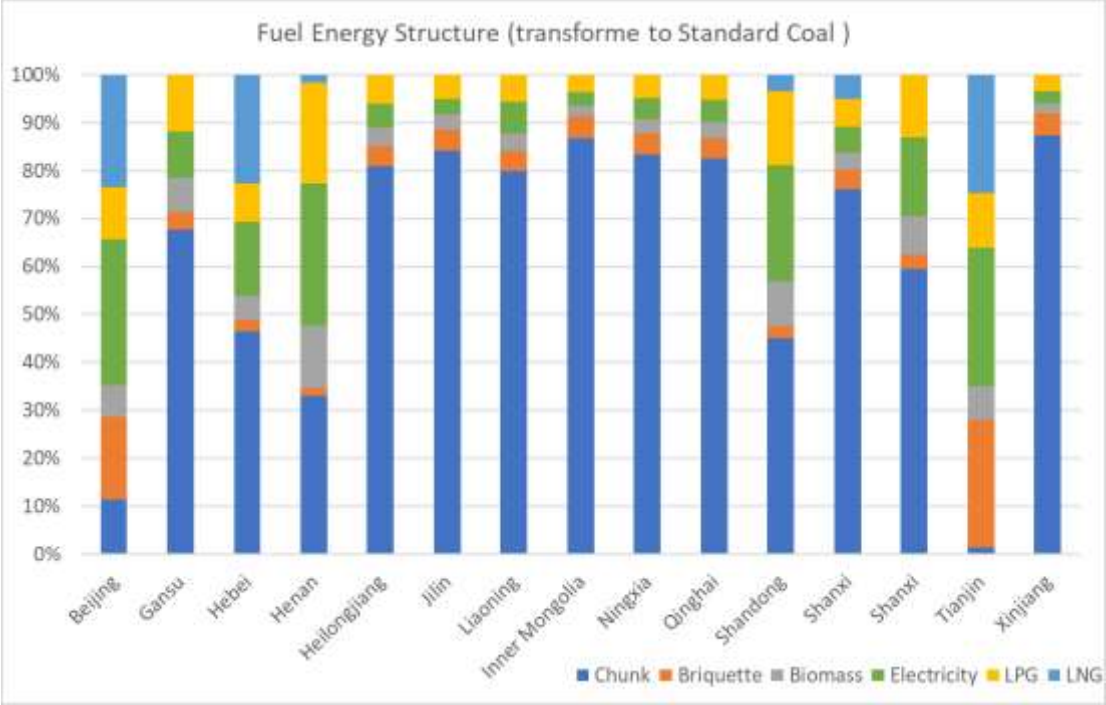

Figure 2-13 Energy structure in Northern China 2018 (by standard coal equivalent).

[7] http://chinorbc.net/wp-content/uploads/2022/09/Output-1-Review-of-BCOC-emissions-and-control-measures-in-China-and-Norway-FINAL.pdf

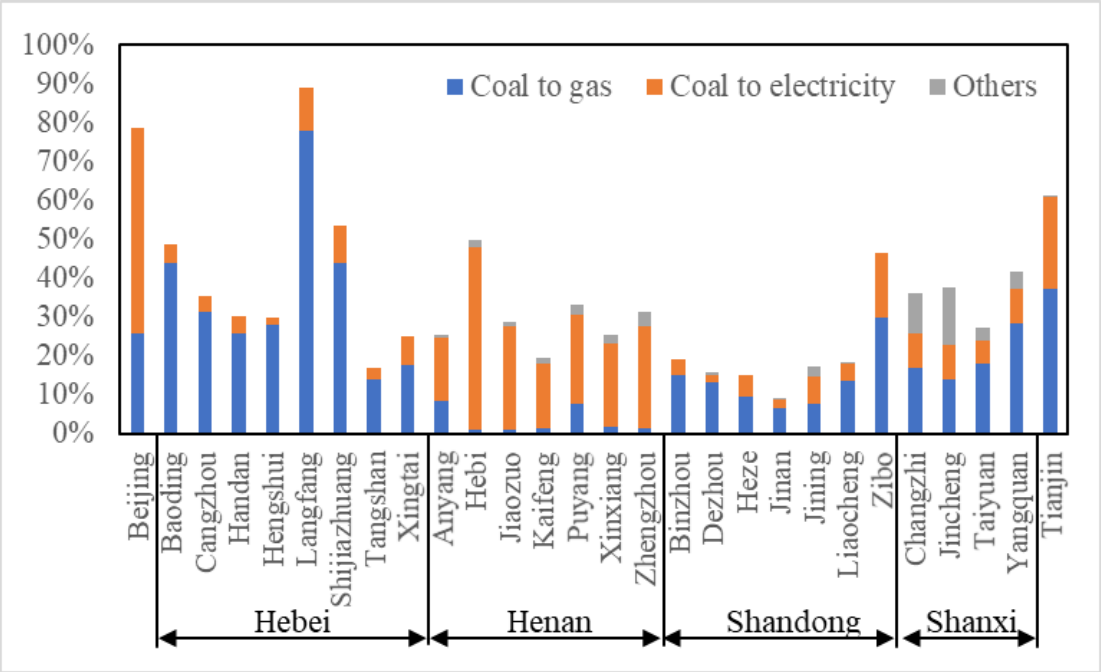

Figure 2-14 Raw coal replacement by electricity and/or gas for “2+26”cities in 2018

The time series of activity levels from 2016 to 2020 are shown in Figure 2-15. Energy consumption was broken down into four types: coal, biomass, gas, and electricity. These data are from our field survey and the algorithm for energy allocation from a journal paper of our own (Zhang et al., 2020).

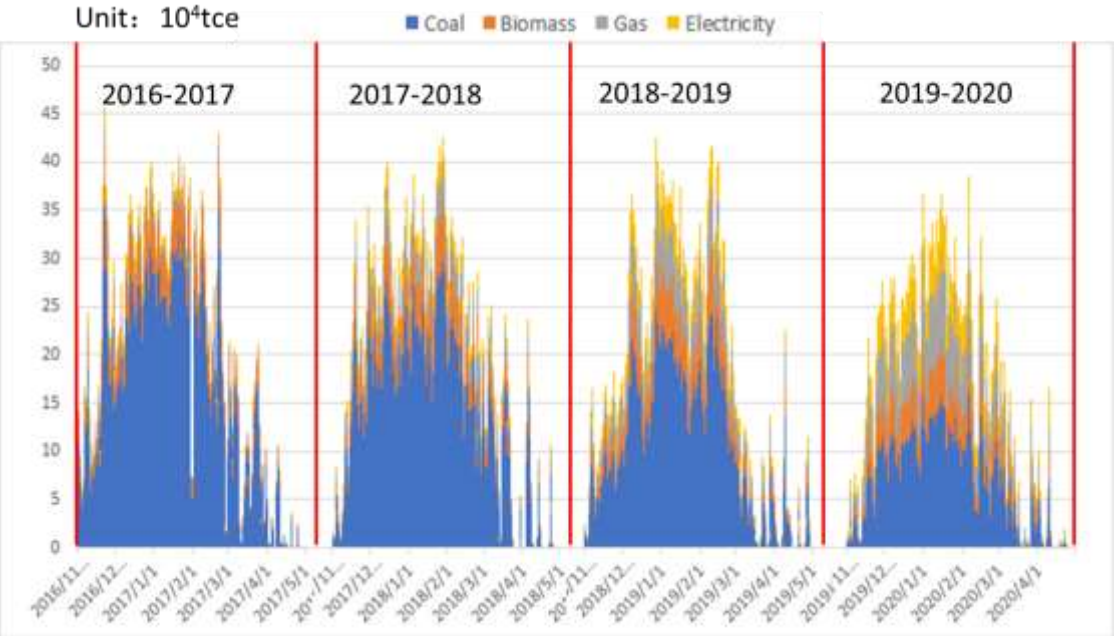

Figure 2-15 The Beijing-Tianjin-Hebei region and its surrounding areas everyday energy consumption.Unit 10^4 tons standard coal equivalent (tce).

2.5.2 Mobile

The vehicle population by types for different provinces was investigated using the China Automotive Industry Yearbooks (China Association of Automobile Manufacutures,2019). Construction Machineries population was investigated using the China Construction Machinery Industry Yearbooks (China Construction Machinery Association,2019). Agricultural machineries population was reviewed with the China Agricultural Machinery Industry Yearbook (China Association of Agricultural Machinery,2019). Survey and analysis were conducted to classify the population by the emission level according to the emission standard implement requirement (MEE,2014). The vehicle population by provinces in 2018 is listed in Table 2-15.

Table 2-15 Number of light duty passenger cars by emission level and province. The provinces in bold are provinces in Northern China. Provinces are listed according to geographical location.

Provinces	China 5	China 4	China 3	China 2	China 1
Beijing	447449	3257699	1419952	0	0
Tianjin	231915	1686732	637918	64944	0
Hebei	1383844	8501583	1255838	1007307	1200004
Shanxi	555546	3466128	956614	833590	150813
Inner Mongolia	368925	2553960	799253	397037	694039
Liaoning	561299	3521438	1036501	595418	1306001
Jilin	298785	2165715	587236	330307	377987
Heilongjiang	358769	2328053	716383	404724	388477
Shanghai	461458	2417809	617133	0	0
Jiangsu	1872303	10682729	2633167	1795305	0
Zhejiang	1509916	7240285	2551891	1959646	1107849
Anhui	972645	4668367	860935	533139	65139
Fujian	622027	3369934	800655	664292	153488
Jiangxi	660391	3030878	601424	340276	57122
Shandong	1638043	10908704	2945890	2170791	1512736
Henan	1587458	8259368	1665634	1074905	421509
Hubei	881973	4527429	805096	533847	206449
Hunan	947773	4611720	879646	391847	228862
Guangdong	2310807	11350716	2812094	2801691	320629
Guangxi	652454	2853336	588345	287847	680327
Hainan	136630	572257	156921	120821	140764

Provinces	China 5	China 4	China 3	China 2	China 1
Chongqing	510769	2695912	471820	0	0
Sichuan	1182321	6539272	1616687	695544	467
Guizhou	632013	2746160	473590	322206	109301
Yunnan	650711	3653039	912322	614489	162071
Tibet	34357	141868	32776	30242	103427
Shaanxi	668639	3591187	912221	443060	0
Gansu	237661	1627504	347293	162085	220935
Qinghai	88465	571522	116450	18973	101363
Ningxia	98133	682245	171177	101132	100163
Xinjiang	312979	1781666	388636	103400	647305
Northern China	11682858	70254600	17451098	10036117	6539166
National	22876458	126005215	30771498	18798865	9809922

There is limited literature that directly give the vehicle travelled mileages of vehicles or working hours per year. So, the authoritative data was used. These data were recommended by "Road Motor Vehicle Air Pollutant Emission Inventory Development Technical Guidelines" issued by the Ministry of Ecology and Environment in 2014 (hereinafter referred to as 'motor vehicle emission inventory preparation guide') (MEE,2014).

For the activity level of various types of non-road mobile machinery in China, recommended values are also given in the technical guidelines for the development of inventories of atmospheric pollutants from non-road Mobile Sources (hereinafter referred to as the guidelines for the development of inventories of emissions from non-road mobile sources) issued by the Ministry of Ecology and Environment in 2014 (MEE, 2014).

As for the inland water and coastal vessels, the fuel consumption was calculated by the passenger and cargo turnover per year from the China Statistical Yearbook or China Traffic Yearbook (Ministry of Transportation of people's republic of China,2019) with the formula below.

$$Y=(0.065*Z_{passenger}+Z_{cargo})*YX \qquad (7)$$

In formula (7), Y is the inland water and coastal vessels' fuel consumption, $Z_{passenger}$ is the passenger-kilometers per year, Z_{cargo} is the tonne-kilometers per year, YX is the coefficient, recommended as 50 by the guideline.

The vehicle kilometers travelled (VKTs) per year used in the vehicle BC emission inventory development are listed in Table 2-16. For the construction machinery and agriculture machinery, the working hours are presented in Table 2-17.

Table 2-16 Annual On-road Vehicle Kilometers Travelled by types

Vehicle Type	VKT（km）	Vehicle Type
Small, micro passenger cars	18000	Small, micro passenger cars
Medium passenger cars	31300	Medium passenger cars
large passenger cars/Coach	58000	large passenger cars/Coach
light-duty, micro size truck	30000	light-duty, micro size truck
Medium duty truck	35000	Medium duty truck
Heavy duty truck	75000	Heavy duty truck

Table 2-17 Recommend working hours of non-road machinery per year

Types		Working hours per year
Construction machinery	Excavators	770
	Bulldozers	770
	Loaders	770
	Forklifts	770
	Road rollers	770
	Pavers	770
	Graders	770
	Others	770
Agricultural machinery	Large and medium tractors	500
	Small tractors	500
	Combine Harvester	150
	Drainage and irrigation machinery	380
	Others	380

The inland water and coastal vessels passenger and cargo turnover of 2018 for different provinces are shown in Table 2-18.

Table 2-18 Inland water and costal vessels passenger kilometers and cargo tonne kilometers by province in 2018. The provinces in bold are provinces in Northern China.

Provinces	Cargo turnover 10^8 tonnes*km	Passenger turnover 10^8 person*km
Beijing	0	0
Tianjin	1326.6	0.21
Hebei	490.88	0.19
Shanxi	0.13	0.08
Inner Mongolia	0	0

Provinces	Cargo turnover 10^8 tonnes*km	Passenger turnover 10^8 person*km
Liaoning	6317.59	6.05
Jilin	0.2	0.18
Heilongjiang	6.08	0.36
Shanghai	27990.8	0.79
Jiangsu	6121.94	3.47
Zhejiang	9352.5	6.3
Anhui	5630.88	0.39
Fujian	6209.37	2.75
Jiangxi	238.11	0.34
Shandong	1835.52	12.76
Henan	1021.75	0.61
Hubei	2850	4.74
Hunan	458.96	3.63
Guangdong	24177.41	11.13
Guangxi	1590.64	3.29
Hainan	774.27	4.10
Chongqing	2238.53	5.59
Sichuan	270.13	1.91
Guizhou	45.07	6.77
Yunnan	17.33	3.02
Tibet	0	0
Shaanxi	0.52	0.62
Gansu	0.05	0.13
Qinghai	0	0.1
Ningxia	0	0.07
Xinjiang	0	0
Northern China	**22752.14**	**25.22**
National	**98965.26**	**79.58**

2.6 Building emission inventories based on an existing inventory

2.6.1 Description of the base inventories

For China, there are various BC/OC inventories. They address different base years or geographical scopes or sectors, but few of them address all sectors or whole China. This can be seen in a review report specifically prepared for this project[8]..

As described in the roadmap in section 2.2, the Methodology section, the new inventories in the ChiNorBC-project are developed from an existing inventory. he Emissions from the residential and mobile sectors are replaced by data obtained in the ChiNorBC-project in order to establish the ChiNorBC-2018 inventories. Professor XING Jia, who worked in Tsinghua University and was a guest expert attending our emission workshop, back to back with the ChiNorBC-project kick-off meeting in December 2020, agreed to share with us the national 2018 emission inventory of his team. In XING inventory (unpublished), there are more than 10 sectors. We regrouped them into 5 sector-packages in line with the MEIC inventory (Lu et al., 2011). The MEIC inventory shows monthly/gridded emission information by 5 sector-packages: power generating, industrial, residential, mobile, and agricultural. The methodology of regrouping is shown in Table 2-19.

In this way we could allocate our emissions into monthly and gridded formats by making use of the temporal/spatial distribution of emissions in the MEIC inventory

Table 2-19 Regrouping of the XING sectors into 5 sector-packages.

Regrouped into sector-packages	Original sectors in XING2018
Power generating	Power plant
Industrial	Industry combustion; Industrial process (Cement, steel, cement, other industrial process),
Residential	Domestic fossil fuel; domestic biofuel;
Mobile	Road transport; non-road transport
Agricultural	Open burning; livestock; fertilizer application

The emissions of each pollutant in XING inventory 2018 are shown in Figure 2-16. On BC emissions alone (upper right insert of this figure), residential sector contributes the most (41%), followed by industrial sector (35%) and mobile sector (14%), while the other two sectors contribute the least.

[8] Output-2-Review-Report-Review-of-BC-OC-Emissions-final.pdf (http://chinorbc.net/)

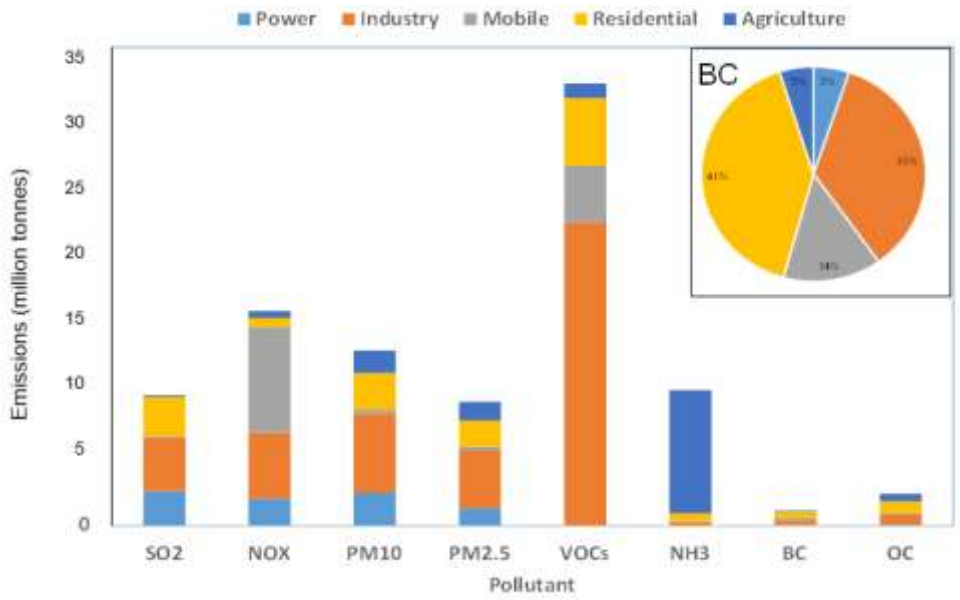

Figure 2-16 The 2018 national emissions by sector of each pollutant in the XING inventory

2.6.2 Construction of inventories for ChiNorBC- project

The next effort is to construct ChiNorBC-2018 inventories based on XING2018. Pollutants included in ChiNorBC-2018 inventories are BC, OC, $PM_{2.5}$, PM_{10}, SO_2, NO_X, CO, NMVOC and NH_3. Thesteps needed to develop the ChiNorBC-2018 inventories are described below.

Step I: replace XING2018 emissions from residential sector with new data. With the emission factors (EFs) and activity levels (ALs) obtained and recommended in this report, we calculated the emissions from residential sector for whole China and Northern China (e.g., Figure 2-17 left for Northern China BC and OC).

Step II: replace XING2018 emissions from mobile sector with new data. With the EFs and Als recommended in this report, we calculated the emissions from the mobile sector (e.g., Figure 2-17 right for Northern China BC and OC).

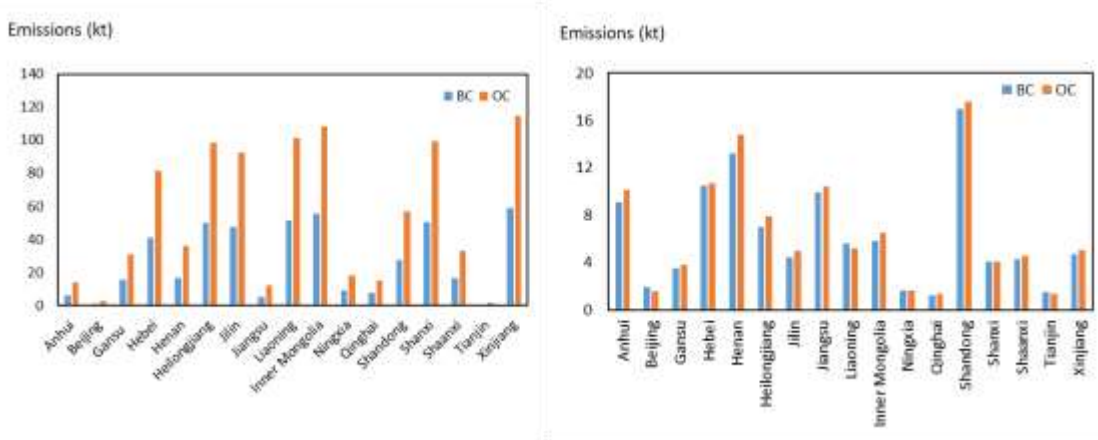

Figure 2-17 BC/OC emissions from Northern China by province. Left: residential; right: mobile.

Step III: For power generating sector, we referred to China National Yearbook of Energy for thermal power generation in 2018. In view of the overwhelming domination of coal in thermal power in China, we derived the power coal consumption (2140 million tons) from power generation and then calculated the emissions by coal consumption in accordance with MEE's inventory construction handbook for PM_{10}, $PM_{2.5}$, VOCs, CO, NH_3, BC, and OC. For SO_2 and NOx, we retained the values in XING2018 inventory.

Step IV: For industrial and agricultural sectors, we made no changes but retained the values in XING inventory.

With above 4 steps, our own inventories, for China national and China northern ranges, were established.

2.7 Description of the 2018 emission inventories developed

2.7.1 Description of ChiNorBC-2018

The Output 2 team in the ChiNorBC project constructed the 2018 emission inventories, national and Northern China, sectoral and monthly, provincial and gridded for application by the air quality, climate and health modelling teams. The inventory results, particularly for Northern China, are be depicted below.

In the ChiNorBC project the geographical scope of "Northern China" includes 17 out of 31 provinces in China.

The Northern emissions of China are shown in Figure 2-18.

To set these numbers in perspective, we have calculated the emissions of black carbon per capita for Northern China and Norway. The BC-emissions per capita are about 1.2 kg in China and 0.6 kg BC in Norway based on the UN statistics yearbook[9] and emission data referred to in this project.

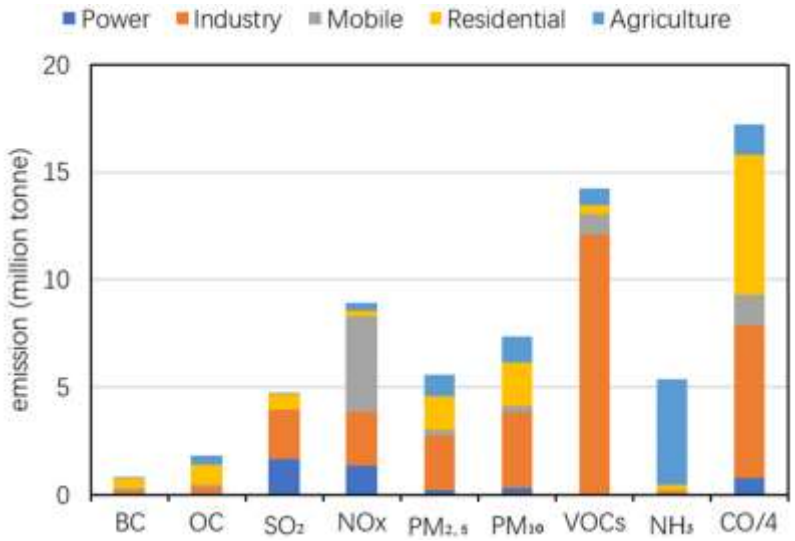

Figure 2-18 Total emissions of China in the ChiNorBC-2018 inventory

[9] https://unstats.un.org/unsd/demographic-social/products/dyb/dyb_2018/

In Table 2-20 the emissions of individual provinces of Northern China are shown.

Table 2-20 Emissions of individual provinces of Northern China

Provincial region	BC	OC	$PM_{2.5}$	PM_{10}	SO_2	NO_X	VOCs	CO	NH_3
Anhui	43.49	158.30	416.16	541.06	325.48	790.98	963.83	3,673.19	390.50
Beijing	3.03	5.61	15.57	19.78	8.71	129.01	478.57	507.05	18.87
Gansu	21.64	46.87	128.53	171.56	152.94	283.95	262.02	1,708.77	179.74
Hebei	89.44	177.68	814.20	1,107.63	526.47	965.13	1,375.30	9,969.70	509.63
Henan	60.87	140.44	456.68	596.57	252.21	913.38	1,314.38	5,707.52	833.36
Helongjiang	71.99	177.04	368.82	466.08	206.44	453.62	584.15	4,597.38	341.37
Jilin	61.44	135.27	294.29	376.02	182.98	332.24	525.20	3,985.43	276.34
Jiangsu	44.36	139.43	464.64	598.98	288.23	859.68	2,337.75	5,040.61	441.34
Liaoning	74.78	151.85	447.56	590.37	424.76	597.33	1,116.18	5,925.48	308.03
Inner Mongolia	74.03	152.42	374.00	488.61	357.82	601.39	532.44	5,022.57	389.79
Ningxia	12.37	24.84	65.99	89.11	521.83	165.90	127.37	1,081.61	63.44
Qinghai	9.50	18.04	43.13	58.18	40.66	89.66	69.74	672.98	84.95
Shandong	72.50	164.18	654.57	845.85	477.91	1,315.19	2,338.55	7,275.23	704.11
Shanxi	76.37	138.53	484.24	633.39	488.99	458.45	623.78	5,889.11	172.62
Shaanxi	35.13	64.22	176.68	242.72	184.33	397.75	602.13	2,584.25	261.68
Tianjin	4.27	9.26	54.29	73.00	30.64	125.45	428.99	743.77	34.61

Provincial region	BC	OC	$PM_{2.5}$	PM_{10}	SO_2	NO_X	VOCs	CO	NH_3
Xinjiang	71.98	147.31	338.31	442.47	264.20	449.03	494.99	4,607.37	370.11
Total	**827.20**	**1,851.28**	**5,597.66**	**7,341.36**	**4,734.61**	**8,928.16**	**14,175.36**	**68,992.01**	**5,380.47**

Table 2-21 gives the monthly emissions for Northern China. As described above, the monthly shares are allocated in line with the MEIC inventory.

Table 2-21 Monthly emissions for Northern China

Month	BC	OC	$PM_{2.5}$	PM_{10}	SO_2	NOx	VOCs	CO	NH_3
1	100.57	286.98	636.05	641.72	480.16	779.66	1226.44	8095.89	327.45
2	91.86	254.47	578.32	586.41	435.73	719.57	1155.21	7379.68	320.14
3	80.90	196.80	528.82	644.33	440.41	770.74	1212.63	6673.12	343.80
4	55.01	100.78	388.56	571.55	339.92	704.19	1087.77	4729.03	449.35
5	52.03	89.26	376.50	574.29	334.97	703.69	1094.33	4494.42	522.77
6	52.94	89.20	382.23	590.21	349.85	728.56	1172.38	4548.74	600.56
7	51.65	88.73	374.62	572.75	335.62	708.32	1082.57	4465.33	568.66
8	51.95	89.13	379.17	583.31	343.43	717.30	1094.14	4501.03	622.75
9	52.44	88.58	379.19	581.81	341.36	711.16	1139.22	4512.60	454.37
10	56.80	104.45	401.31	594.07	351.24	724.46	1159.58	4842.51	365.65
11	81.91	195.99	538.92	683.28	460.83	813.85	1327.64	6724.93	421.19
12	99.15	266.90	633.97	717.64	521.10	846.68	1423.46	8024.73	383.79
Annual	**827.20**	**1851.28**	**5597.66**	**7341.36**	**4734.61**	**8928.16**	**14175.36**	**68992.01**	**5380.47**

The spatial distributions for emissions of Northern ($0.10^{o} \times 0.10^{o}$) China are presented in Figure 2-19. Each grid has emissions that are the sum of the five sectors: power, industrial, residential, mobile and agricultural.

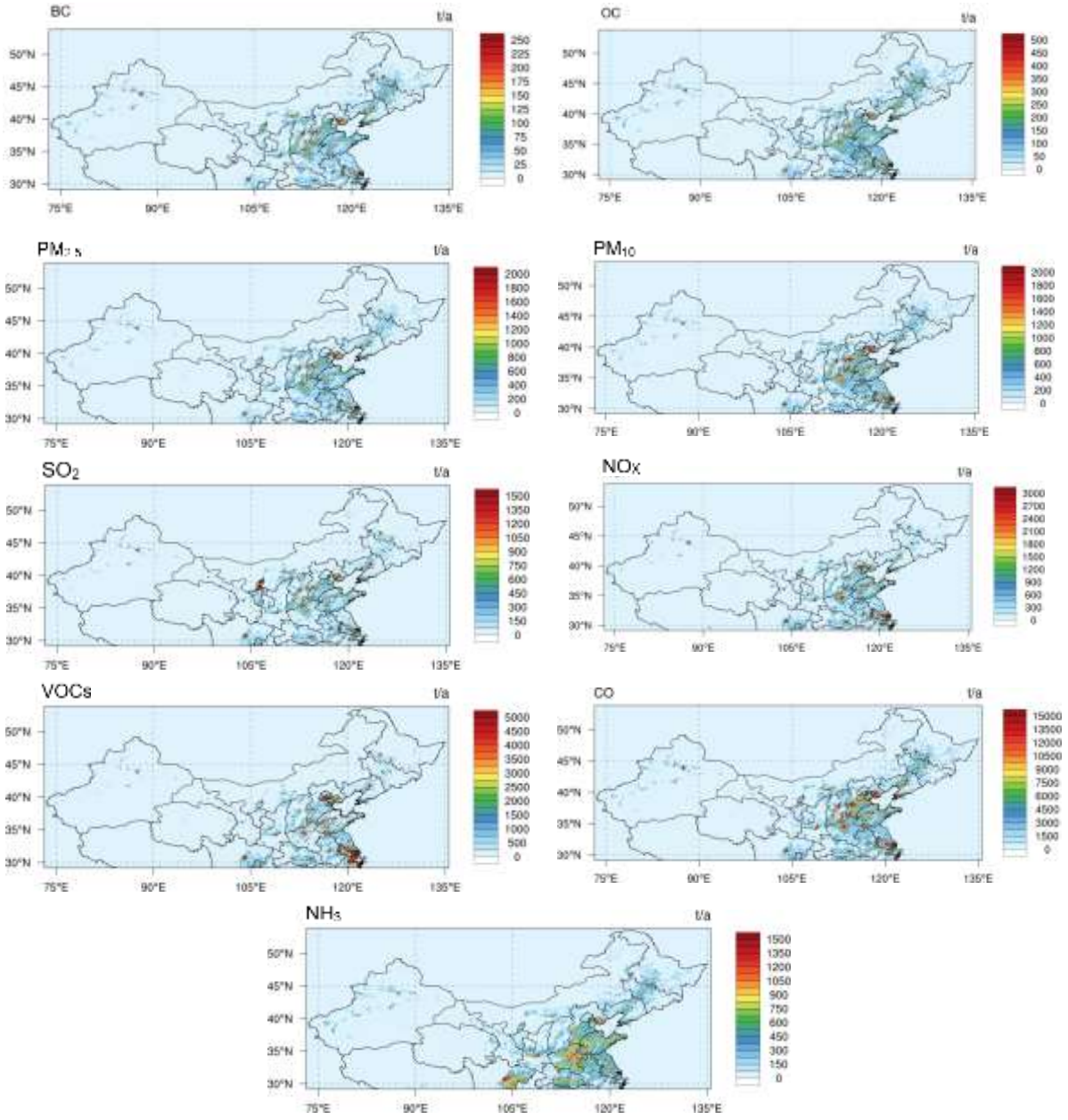

Figure 2-19 2019 Northern China emissions geographical distribution ($0.10^{o} \times 0.10^{o}$ grid resolution) of nine pollutants. Unit: tonnes per year

For sectoral contributions of BC emissions in Northern China, The residential sector contributed the most, accounting for more than half of the emissions, followed by industrial sector, accounting for about a quarter. The mobile (including on-road and off-road mobile sources) and agricultural sectors represented about 13% and 5%, respectively. Emissions from the power generation sector were negligible (Figure 2-20).

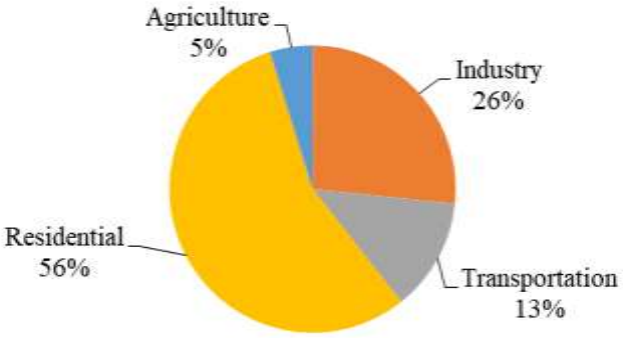

Figure 2-20 Sources of BC emissions in Northern China in 2018

The characteristics of the emission structure in Northern China suggests that the heavy use of fossil fuels and biomass fuels in winter heating is the key reason for the prominent emissions in the residential sector, reflecting the importance of promoting clean heating. As the power industry has basically completed the ultra-low emission transformation, BC emissions therefrom are extremely low; For industrial and mobile sector, there is still large potential to reduce black carbon emissions.

Our inventory takes into account many of the latest and specific situations. In review report 2[10], we compared available inventories about the contributions of BC emissions by sector. In 2018, residential sector accounted for a very important position (36.9%), which ranks the second among all sectors (see figure 4 in review report for more details).

2.7.2 Comparison of ChiNorBC-2018 inventory with other inventories

We have compared the ChiNorBC-2018 inventories for Northern China with MEIC inventory. After 2018, quite a few papers on BC/OC emissions of China were published, yet few of them were for the year of or later than 2018. Figure 2-21 compares the Northern China total emissions of BC and OC between the two inventories, ChiNorBC-2018 and MEIC2019[11]. Among these 5 sectors, residential, industrial and agricultural sectors in ChiNor-2018 have higher emissions than those in MEIC, mobile sector ChiNor-2018 have less emissions than in MEIC and these two inventories are basically equal in power sector. The reason why there are differences between the two inventories is complicated and individually characteristic. For example, residential sector in ChiNor-2018 is based on field investigation which might be different from others. For agricultural sector, MEIC covers no BC emission, which is different from ChiNor-2018 that covers biomass open burning in this sector.

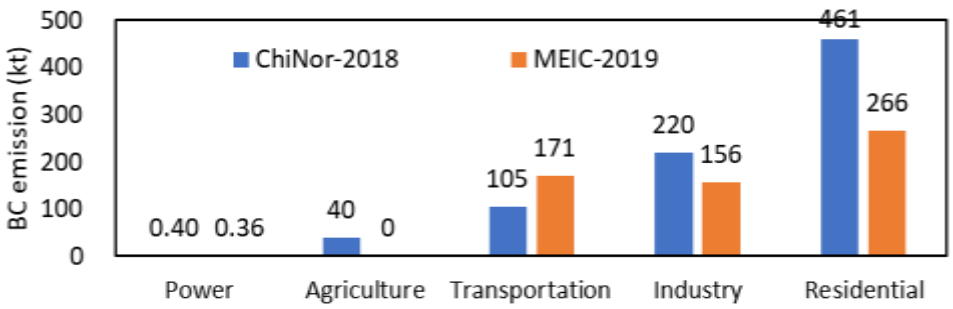

Figure 2-21 Northern China BC emissions compared between the two different inventories.

[2-10] Output 2 - Review Report : Guorui Zhi, Yanjun Wang, Yuzhe Zhang, Wenjing Jin. 2022. Review of BC/ OC emissions inventories.

[11-2] http://meicmodel.org (MEIC website)

3 Scenario analysis

Authors: Xuying Wang, Yixuan Zheng, Wenxin Cao (CAEP)

This study projects future air pollutant emissions in Northern China based on an integrated modeling framework that integrates an energy projection model, a database of emission control measures, scenarios projection, and an emission projection model. The analysis projects air pollution emission levels in varying policy strictness based on three scenarios that are designed based on China's strategic target of carbon peaking and carbon neutrality, as well as the construction of a "Beautiful China"[1].

3.1 Emission control scenario design

3.1.1 Forecast of social development and energy consumption

The framework sketch for black carbon (BC) and organic carbon (OC) emission control scenario analysis is shown in figure 3-1. In the ChiNorBC project, we have projected energy consumption and activity rates of different sectors in China during 2018-2035 by developing long-term economic-social-energy development projections. The projected key parameters for social development, energy consumption level and production of some typical industrial sectors in China is shown in figure 3-2 to 3-6.

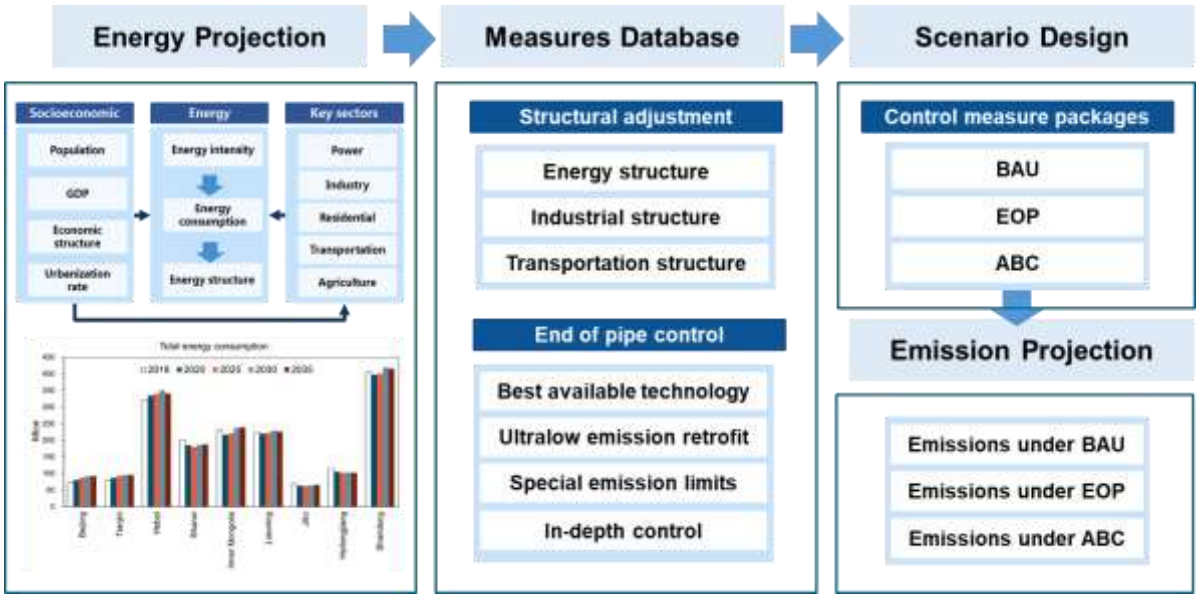

Figure 3-1 Framework sketch of emission control scenario analysis

Note: BAU represents the business as usual scenario, EOP represents the strengthened end-of-pipe control, ABC represents the ambitious control by strengthening both end of pipe control and structural adjustment scenario

3.1.1.1 Social development

Based on the economic-social-energy development scenario, the population of China in 2035 will be 1.47 billion, increased by 4.7% compared with 2018; while the urbanization rate will reach 71.0%, with an increase of 11 percentage points from 2018 to 2035[2]. The output of some important industrial products in China, such as thermal power, crude steel, cement and flat glass will gradually decrease mainly due to expansion of renewable energy, reduced material demand, and material recycle. The population of motor vehicle would however increase by about 149%.

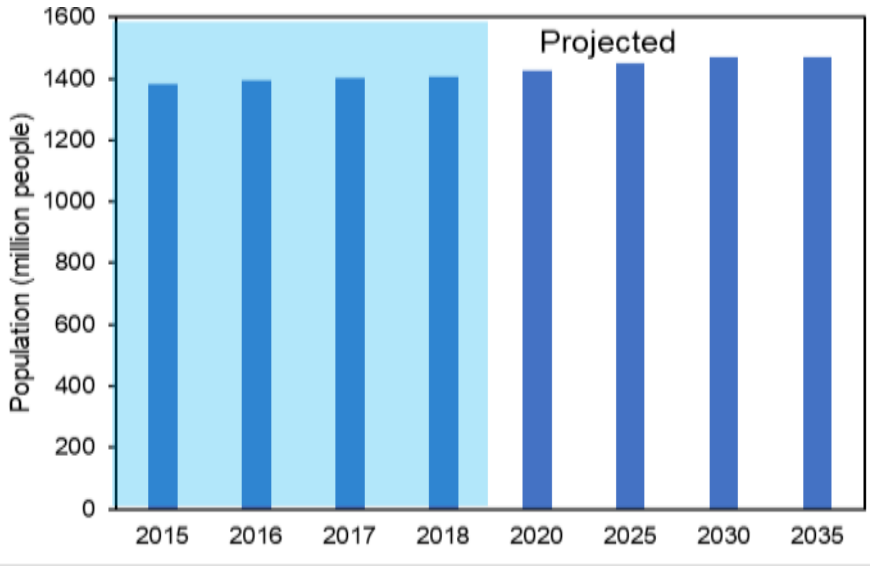

Figure 3-2 Prediction result on the population in the whole of China

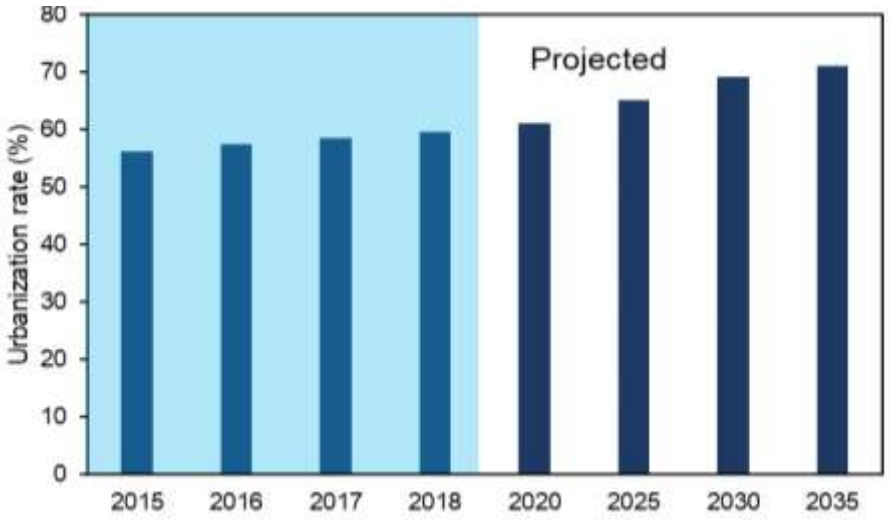

Figure 3-3 Prediction result on the urbanization rate in the whole of China

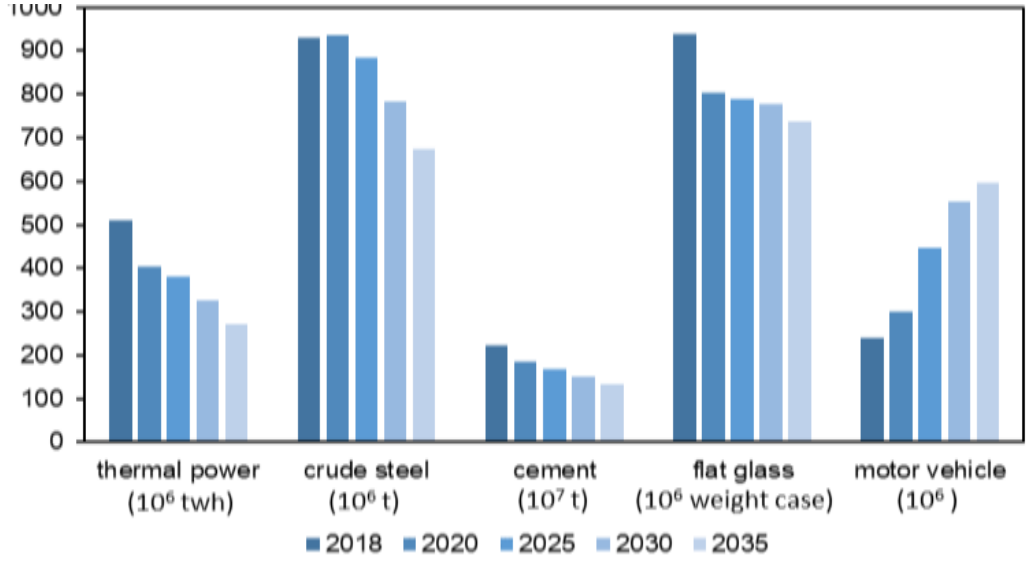

Figure 3-4 Projection result on activity rate of some typical sectors for BC/OC and air pollution control in the whole of China

3.1.1.2 Energy consumption

Based on the energy projection results, national primary energy consumption in 2035 in China would reach 5454 Mtce (million ton coal equivalent). This is an increase of 15.6% over 2018[3]. The projected coal consumption in China is expected to decrease from 2020 onwards while other energy such as renewable energy increase. In 2035, the contribution of coal would decrease to 33%, compared with 59% in 2018[3]. The contribution of primary electricity and other energy would reach around 39% in 2035. Petroleum and natural gas (NG) consumption would together stay rather constant towards 2035.

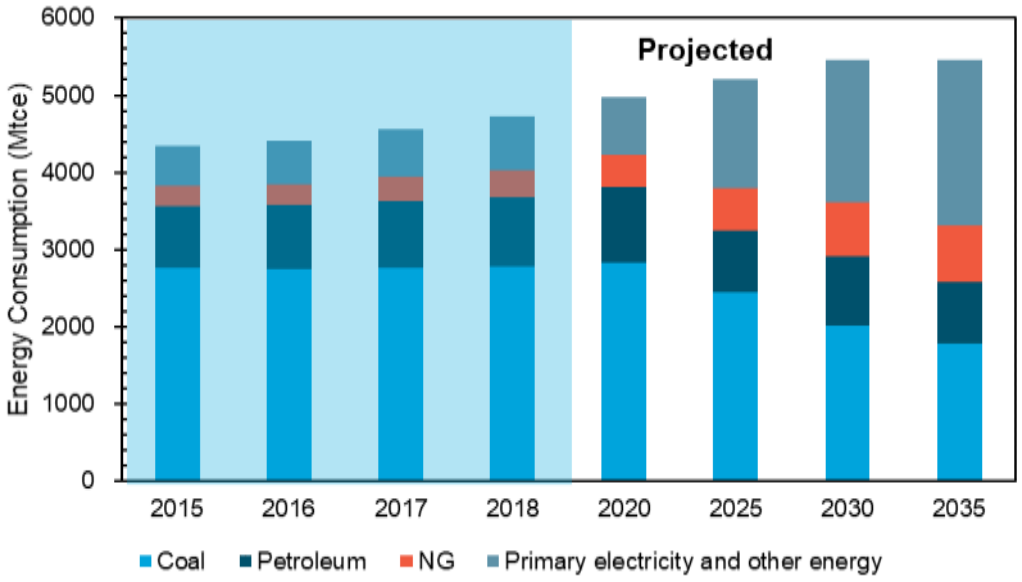

Figure 3-5 Projection result on primary energy consumption in China

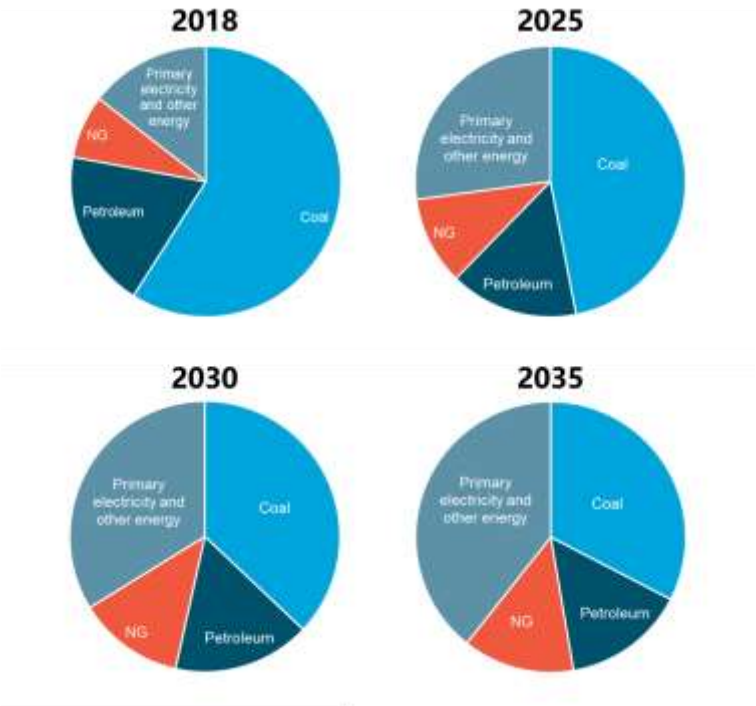

Figure 3-6 Projected composition of national primary energy consumption in China

3.1.2 Collection of relevant control measures

In order to identify the key sectors for implementing BC/OC emission control measures in China during the period 2020-2035, this project explores the emission mitigation potential of BC/OC in China from two types of control strategies: a) structural adjustment and b) end of pipe control. Structural adjustments measures and end of pipe control measures for major sectors are listed in Table 3-1 .The trends in energy, industrial and transportation structure are mainly determined based on the prediction of economic, social and energy development scenario for period 2020-2035 which has been described in 3.1.1. The selection of end of pipe control measures is mainly determined based on the current situation of air pollution emission control in key sectors of China. This includes consideration of factors such as problems existing in end of pipe treatment in various industries, the best feasible control technology type, technical maturity, economic feasibility and so on[4]. For example, for the power industry, steel industry, cement industry, flat glass industry and coal-fired boilers, the future end treatment measures adopted in this project are mainly determined by taking into account the requirements for ultra-low emission technology transformation that have been issued by the state or local authorities. For example, a coal-fired power plant meets "ultralow emission" standards when its emission levels of major air pollutants are similar to those from gas-fired power plants. For sectors that have not yet defined the technical route of ultra-low emission transformation, it has been determined according to the special emission limit requirements in the existing emission standards and in combination with the maturity and economic feasibility of the existing governance technology. The pollutant emission factors after the end treatment of each industry are mainly calculated based on the pollutant emission level after the implementation of corresponding control measures. The emission concentration level of air pollutants after the completion of ultra-low emission transformation or in-depth treatment in various industries is determined according to the existing national emission standard requirements (such as thermal power industry, iron and steel industry, etc.), local emission standard requirements (such as cement industry, flat glass industry, boilers, etc.) or the corresponding parameters of the relevant best available control technology (such as low nitrogen oxides combustion technology, etc.). More information about ultra-low emission technology is included in the report Review of BC/ OC emissions and control measures in China and Norway issued by this project [12].

Table 3-1 Major emission control measures

Sector	Source	Structural adjustment measure	End of pipe control measure
Power	Power plants	Power generation structure adjustment Improving power generation efficiency	Ultra-low emission standard
Industry	Iron and steel	Improving the ratio of EAF (electric arc furnace)	Ultra-low emission standard
	Coking	/	Ultra-low emission standard
	Cement	/	Ultra-low emission standard
	Flat glass	/	Ultra-low emission standard
	Aluminium	/	Special emission limits
Boilers	Coal fired boilers	Phasing out small coal fired boilers	Ultra-low emission standard
	Gas fired boilers	/	Low-NOx combustion retrofits
Transportation	On-road mobile	Phasing out high emission vehicles Strengthening vehicle and oil standard Improving the ratio of new energy vehicles Road to Rail	Intensive supervision
	Off-road mobile	Strengthening emission standard	Intensive supervision

[12] Output-1-Review-of-BC/OC-emissions-and-control-measures-in-China-and-Norway pdf (http://chinorbc.net/)

Sector	Source	Structural adjustment measure	End of pipe control measure
Residential	Raw coal	Coal to electricity Coal to gas	/

3.1.3 Design of different BC/OC control scenarios

This project designs three BC/OC control scenarios for Northern China. Please refer to Chapter 2 for the definition of Northern China. The scenarios included are business as usual scenario (BAU), strengthened end of pipe control scenario (EOP) and ambitious control scenario (ABC). By projecting air pollutant emissions under different control scenarios, we've identified the emission reduction of BC/OC by province and by time under different scenarios. The design principles for the three control scenarios are as follow.

3.1.3.1 BAU

- Principle for BAU:
  Developed on the basis of the predicted economic-social and energy development scenario as described in 3.1.1, in which the structural adjustments have already been implemented, and assuming that the control level of air pollutants for each sector and thereby the emission factors remain at the level of the 2018 base year.

Table 3-2 Major control measures included in BAU

Sector	Source	Control measures	Measure type
Power	**Power plants**	Power generation structure adjustment Improving power generation efficiency	Structural adjustment
Industry	**Iron and steel**	Improving the ratio of EAF	Structural adjustment
		Phasing out small coal fired boilers	Structural adjustment
Boilers	**Coal fired boilers**	Phasing out small coal fired boilers	Structural adjustment
Transportation	**On-road mobile**	Strengthening vehicle and oil standard Improving the ratio of new energy vehicles Phasing out old vehicles Road to rail	Structural adjustment
	Off-road mobile	Strengthening standard Phasing out old off-road vehicles	Structural adjustment
Residential	**Raw coal**	Coal to electricity Coal to gas	Structural adjustment

3.1.3.2 EOP

- Principle for EOP:
  On the basis of BAU scenario, comprehensively strengthening end of pipe control for all sectors in northern China by implementing best available control technology with consideration of various factors such as technical maturity, economic feasibility and so on.

Table 3-3 Major control measures included in EOP. Measures in addition to BAU is marked in grey.

Sector	Source	Control measures	Measure type
Power	**Power plants**	Power generation structure adjustment Improving power generation efficiency	Structural adjustment
		Ultra-low emission standard	End of pipe control
Industry	**Iron and steel**	Improving the ratio of EAF	Structural adjustment
	Coking	Ultra-low emission standard	End of pipe control
	Cement	Ultra-low emission standard	End of pipe control
	Flat glass	Ultra-low emission standard	End of pipe control
	Aluminium	Special emission limits	End of pipe control
Boilers	**Coal fired boilers**	Phasing out small coal fired boilers	Structural adjustment
		Ultra-low emission standard	End of pipe control
	Gas fired boilers	Low-NOx combustion retrofits	End of pipe control
Transportation	**On-road mobile**	Strengthening vehicle and oil standard Improving the ratio of new energy vehicles Phasing out old vehicles Road to rail	Structural adjustment
	Off-road mobile	Strengthening standard Phasing out old off-road vehicles	Structural adjustment
Residential	**Raw coal**	Coal to electricity Coal to gas	Structural adjustment

3.1.3.3 ABC

- Principle for ABC:
  Considering, that the problem of emissions from heavy industry in the Beijing-Tianjin-Hebei (BTH) region and its surrounding areas, is relatively prominent, the capacity and activity rate of some heavy polluting industries (e.g., iron and steel, cement, coal-fired boilers, and raw coal) has been reduced under ABC, compared with EOP. For example, the crude steel production of Hebei for year 2035 in ABC was declined by around 70% compared with EOP.

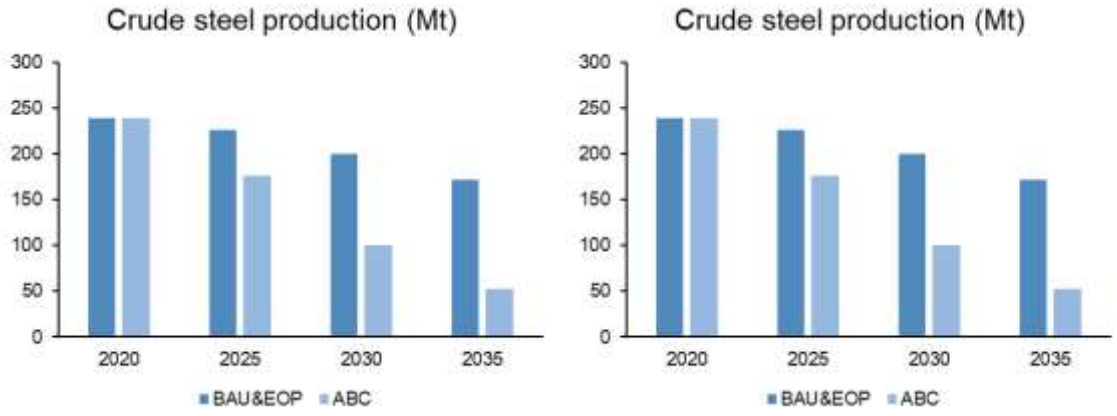

Figure 3-7 Layout adjustment of steel and cement sectors of Hebei under ABC

Note: layout adjustment means adjusting the distribution of production capacity. Cap of production capacity will be set by authorities to facilitate the layout adjustment.

3.2 Result for emission prediction under different scenarios

3.2.1 Emission assessment method

The emissions of air pollutants under different scenarios in northern China were calculated based on the equation shown below.

$$Emi_s = \sum_s Ef_s \times A_s$$

(3-1)

Where s represents sector, Ef_s represents the abated emission factor for sector *s*, A_s represents the activity rate of sector s, and Emi_s represents the assessed emission of specific pollutant for sector *s*.

The emissions of BC, OC and major air pollutants such as SO_2, NO_X and $PM_{2.5}$ in northern China under BAU, EOP and ABC have been calculated and assessed according to the scenario assumptions on fuel mix, activity rates and emission control levels as described in 3.1.

3.2.2 Predicted emission trends during 2018-2035 for Northern China

3.2.2.1 Changes by time

The projected emissions of BC/OC and major air pollutants such as SO_2, NO_X and $PM_{2.5}$ (including BC, OC, and other particles) for Northern China under different scenarios during the period 2018-2035 is shown in Figure 3-8. Based on the assessment, emissions of all the assessed air pollutants will rise in 2020 and decrease afterwards under BAU. The decrease is driven by the projected reduction in activity rates due to the structural adjustments (Table 3-2). Under EOP and ABC emissions of all the assessed air pollutants keep decreasing from 2018 to 2035 due to end of pipe measures and reduced activity rates and capacity (Table 3-2 and section 3.1.3.3.). For all major pollutants during 2018-2035, ABC scenario shows the highest emission reduction percentage while BAU shows the least. The absolute emission levels of BC and OC is shown in Figure 3-9.

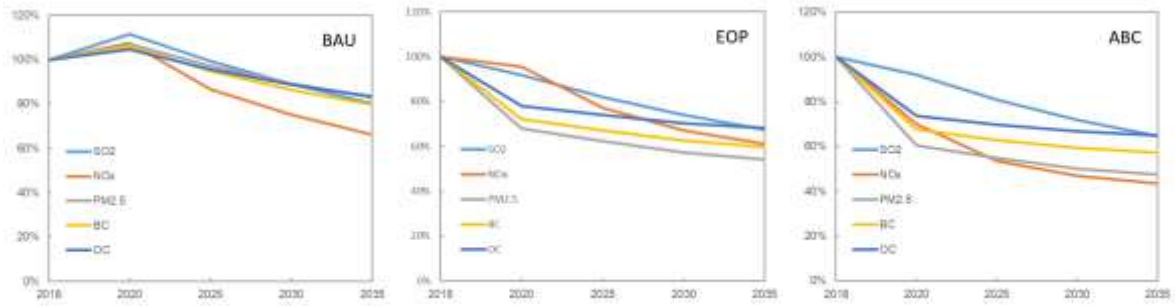

Figure 3-8 Normalized emission changes of air pollutants from 2018 to 2035 for different scenarios in Northern China

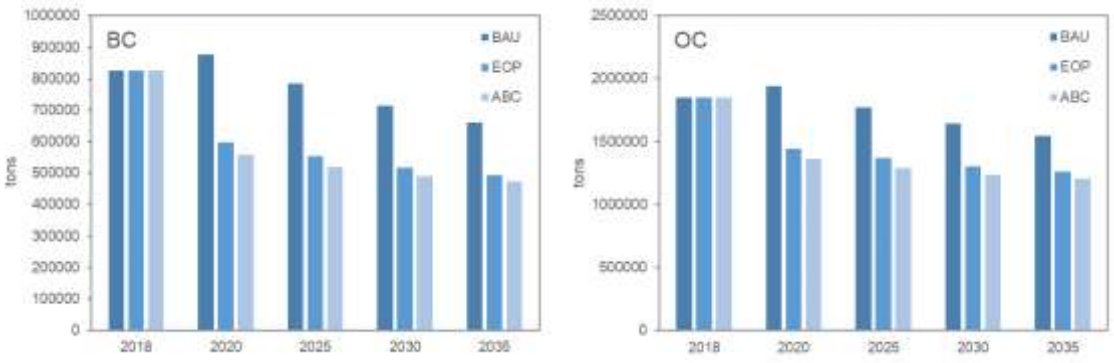

Figure 3-9 BC/OC emission changes from 2018 to 2035 under different scenarios for Northern China

3.2.2.2 Reduction by 2035

Figure 3-10 shows that between 2018 and 2035, the total emissions of SO_2, NO_x, $PM_{2.5}$, BC, OC in Northern China will show a reduction of around 20%, 34%,17%, 20% and 17%, respectively under BAU scenario. This indicates that activity changes and energy structure adjustment would have positive emission mitigation effect on BC/OC and other air pollutants. NOx is experiencing the largest reduction due to structural changes in the transportation sector (Table 3-1), while BC/OC is reduced by about 20%. Similarly, in the EOP scenario, reduction percentages of SO_2, NO_x, $PM_{2.5}$, BC and OC emission in northern China during 2018-2035 would be 33%, 39%, 46%, 40% and 32%, respectively, which are significantly higher than those in BAU, indicating that strengthened end of pipe control measures have considerable emission reduction effect. The percentage reduction of BC has for instance doubled compared to the BAU. Under ABC scenario, emission of SO_2, NO_x, $PM_{2.5}$, BC and OC in Northern China shows further reduction compared with EOP, with reduction percentages of 35%, 57%, 53%, 43% and 35%, respectively, indicating that strengthened layout adjustment could contribute to further emission reductions. The varying emission reduction rates in different sectors contributes to the different reduction rates of primary $PM_{2.5}$ and BC/OC emissions.

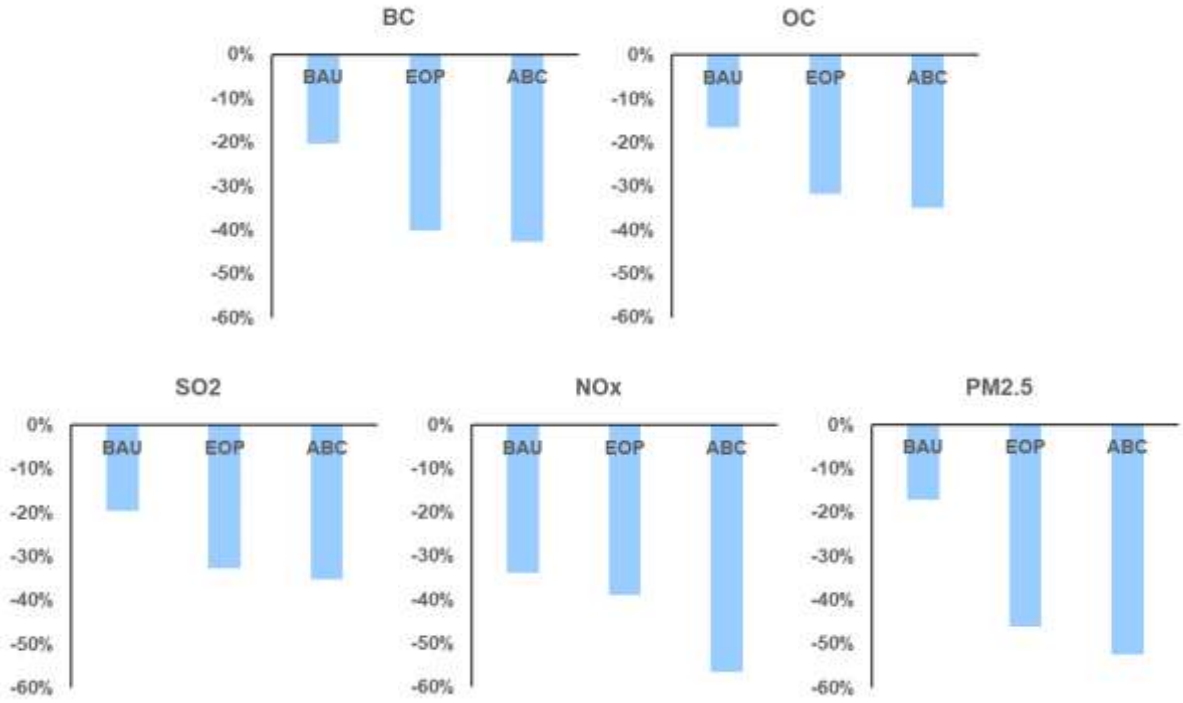

Figure 3-10 Emission reduction percentages by 2035 compared with 2018 for the major air pollutants under different scenarios for Northern China

3.2.2.3 Changes by province

Based on the emission assessment, the provinces in northern China showed different BC/OC emission mitigation potential. Figure 3-11 shows the projected BC emission changes during 2018-2035 under different scenarios by province. Generally speaking, the largest emission reduction happened under ABC scenario for all the provinces in Northern China. The BC emission reduction percentage during the period 2018-2035 under the ABC scenario varies for different provinces, where Shanxi has the largest relative reduction percentage potential (60% of 2018 emissions) and Ningxia has the lowest potential (23% of 2018 emissions).

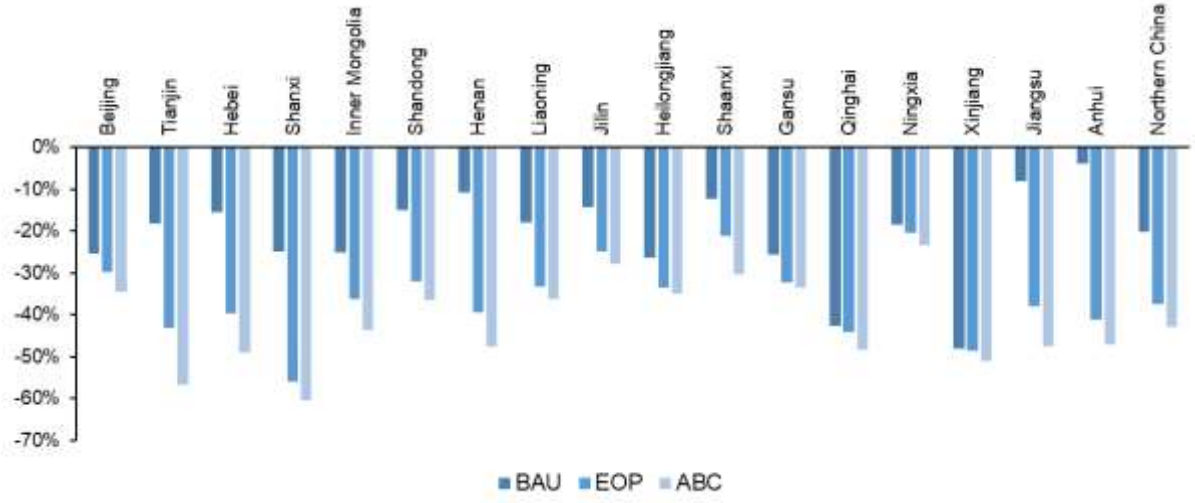

Figure 3-11 Emission reduction percentages of BC by 2035 compared with 2018 of the three scenarios for different provinces and for the whole of Northern China

3.2.2.4 Contributions by sector

The following figure shows the contributions of different sector to BC/OC emission reduction in Northern China for the period 2018-2035 under different scenarios. It shows that the residential sector would be the most important sector for both BC and OC reduction of Northern China under BAU, with the contribution of around 69% and 74% for the total emission reduction of BC and OC during 2018-2035 respectively. In addition to the reductions in the residential sector, emission decreases in the industry sector become important for BC and OC reduction under EOP and ABC. Under EOP, the contribution of residential sector to the total emission reduction of BC and OC during 2018-2035 is 44% and 49%, respectively. Corresponding figures for the industrial sector is 44% and 41%, respectively. Under ABC, the contribution of residential sector to the total emission reduction of BC and OC during 2018-2035 is 43% and 46%, respectively, and that of industrial sector is 44% and 40%, respectively. This indicates that residential sector and industry, with fuel substitution and advanced end-of-pipe control devices implemented, would contribute to major BC/OC emission reduction potential during 2018-2035 in Northern China. The BC-reductions projected for the transport sector is less pronounced but increases as we move from the BAU- to EOP- and further to ABC-scenario. The reductions in the power sector are marginal.

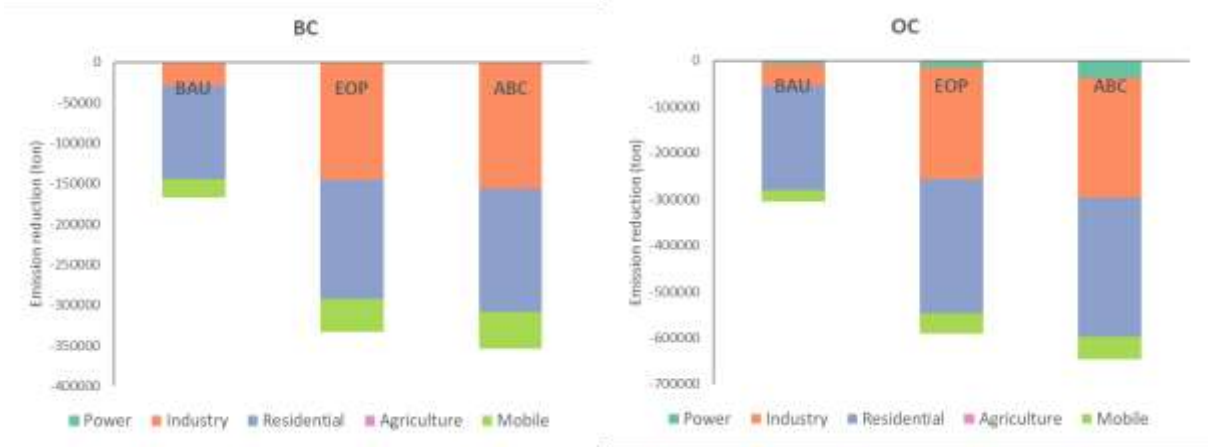

Figure 3-12 BC/OC emission reduction by sector for Northern China during 2018-2035 under different scenarios

3.2.2.5 Contributions by province and sector

Due to the variations in energy, industry, and transportation structures as well as the reference year (i.e., 2018) emission control levels, contribution of emission reduction by sector varies for different provinces. This indicates that different sectors and types of measure should be focused on when implementing BC/OC control in Northern China. For example, as shown in figure 3-13 below, for Beijing, the mobile sources followed by the residential sector play the most important role in reducing BC emission during 2018-2035, while for Hebei, the industrial sector followed by the residential sector are key sectors for BC emission control during 2018-2035.

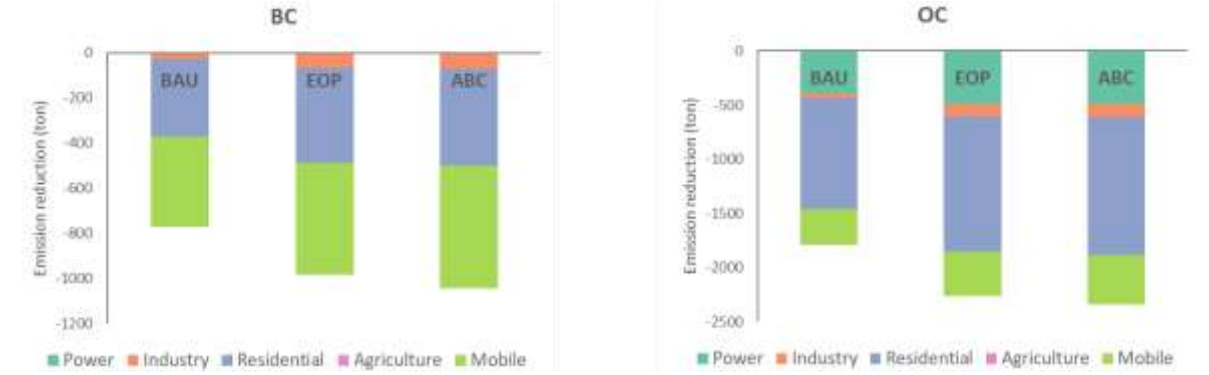

Figure 3-13 Contributions of BC/OC emission reduction by sector for Beijing during 2018-2035

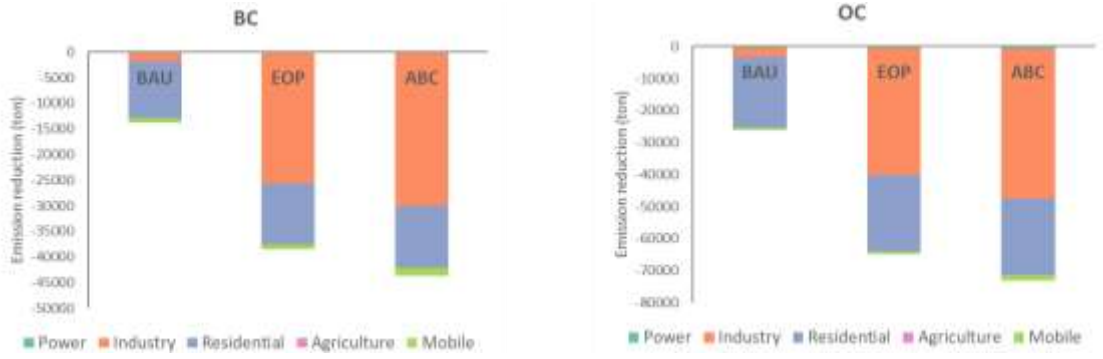

Figure 3-14 Contributions of BC/OC emission reduction by sector for Hebei during 2018-2035

3.3 Summary

Energy consumption and activity level of different sectors for 2018-2035 in China has been projected and described in this project. Three control scenarios (BAU, EOP, ABC) have been designed for Northern China. Based on the design of different control scenarios, emissions of BC/OC under each scenario for 2018-2035 has been estimated. Based on the emission projection results, compared with 2018, the reduction percentage in emissions of BC/OC in 2035 for Northern China under BAU, EOP and ABC increases gradually, with significant decline in all three scenarios. This shows that BC/OC emission reduction potentials of end of pipe control and structural adjustment are both important. The BC and OC emissions in Northern China could be reduced by about 40% by implementing the most ambitions scenario. The BC/OC emission reductions in the residential sector are prominent in all three scenarios. Emission reductions in the industrial sector becomes significant in the end of pipe and most ambitions scenarios. To be noted, due to the differences in energy, industry, and transportation structure as well as the emission control levels, BC/OC emission reduction by sector varies for different provinces. Thus, different sectors and types of measures should be focused on when implementing BC/OC control in Northern China.

4 Evaluation of the air quality

Authors: Xiaohui Du (CRAES), Marianne Tronstad Lund (CICERO)

4.1 Background

With the rapid economic development in China in recent years, the emission of SO_2, NO_x, VOC, PM, and other conventional pollutants caused by human activities has increased sharply. In particular, black carbon (BC) and organic carbon (OC) for the key components of $PM_{2.5}$, has attracted increasing attention from the Chinese scientific community and the public because significant air pollution from BC/OC has been observed in the rapidly developing areas of Northern China. Numerical simulation is a method developed rapidly in recent decades to evaluate the impact of air pollutant emissions on atmospheric concentrations. Such concentrations can be very useful to look further at health and ecosystem impacts. Models represent the many comprehensive chemical and physical processes that shapes the atmospheric composition, providing detailed spatial and temporal distribution of the amount of trace gases and particles in the air. Such models therefore play an important role in understanding the mechanism of atmospheric chemical processes and air pollution levels and their environmental and climatic effects, and can be used to study the relative contributions of sources and long-range transportation of atmospheric pollution. However, due to the differences in research methods and underlying input data used there are still large deviations and controversies in the results from quantitative assessment of BC/OC of air pollutants in China.

This project is significant in that it will provide a highly accurate simulation of BC/OC atmospheric composition. Inaccurate emission inventory is one of the main uncertainties in atmospheric composition simulation. Highly accurate emission inventories on BC/OC in Northern China for recent years have not been established or updated. Therefore, it is necessary to carry out numerical simulation studies on the levels and transport of atmospheric pollutants in Northern China based on transparent, consistent, comparable, complete and accurate emission inventories, and to improve the accuracy of the simulation results by integrating various modelling techniques and methods. The new emission inventories provided by Output 2 of the project is crucial for modelling atmospheric composition in Northern China, especially in heavily polluted areas. It is also useful for policy makers to obtain air quality information caused by BC/OC under different future emission scenarios.

In the ChiNorBC project, simulations with the two atmospheric chemical transport models with different spatial resolutions, the CMAQ-CRAES and OsloCTM3, have been performed with the three-fold objectives:

i) To quantify air pollution levels over China using the most up-to-date emission statistics available and evaluate the model performance against observations and results using other emission inventories,
ii) to quantify effects of the projected emission reductions in 2035 on the air pollution levels in China, and to
iii) quantify the climate effects of differences in present-day emissions between inventories and of the projected reductions until 2035

This chapter presents and discusses findings related to the first two objectives, while the climate effects are presented in Chapter 5.

4.2 Introduction of observation data

4.2.1 Conventional atmospheric pollutants

Conventional air pollution (SO_2, NO_2, O_3, CO, $PM_{2.5}$, and PM_{10}) monitoring data were obtained from the China National Environmental Monitoring Centre (CNEMC, https://air.cnemc.cn:18007/) for January 2018 to December 2018 and included 1,485 air quality monitoring stations in 367 cities (**Fig. 4-1a**). The installation and acceptance of the monitoring system at the state-controlled monitoring stations shall be carried out in accordance with the technical requirements stipulated in The Technical Specification for Installation and Acceptance of The

Continuous Automatic Monitoring System for Gaseous Pollutants in the Ambient Air of China Environmental Protection Standard (HJ 193-2013), and the quality control of the monitoring data shall be carried out in accordance with the Environmental Air Quality Standard (GB 3095-2012). The accuracy and continuity of monitoring data are guaranteed. In order to better evaluate the simulation performance of the model, we selected the hourly and daily (or daily maximum 8-hours) mass concentration (unit: μg/m^3) data of conventional air pollutants nationwide and the subsequent model number simulation data for comparison and evaluation (**Table 4-1**).

4.2.2 BC/OC

Compared with the conventional pollutant data of national control stations, the amount of BC/OC monitoring data collected in China is relatively small. The observed concentrations of BC and OC are mainly from the manual monitoring network (**Fig. 4-1b**). Monitoring data sources are mainly divided into manual and automatic sampling (**Table 4-1**). Due to the complexity and uncertainty of manual sampling, manual sampling data is the daily mean of the city, and concentration data for most of the base year (2018) are missing. Data during the heating season (October to March of the next year) are relatively complete and continuous. Automated online sampling data are site and city hour values, and the time span is also longer than manual sampling, covering the whole year of 2018. In the subsequent model performance evaluation, we selected monitoring data with continuous time and relatively small amount of data as far as possible for comparison, and the date of missing monitoring data would also be eliminated in the comparison of simulation data.

Table 4-1 List of collected air pollutant monitoring data

Data source	Species	Time ranges	Data type
Component Network	BC, OC	Heating season in autumn and winter of 2018	daily average
Online BC/OC data	BC, OC	The whole year of 2018	hourly value
Manual monitoring data of component network	BC, OC	February 2018 to December 2018	daily average
China National Environmental Monitoring Centre	SO_2, NO_2, O_3, CO, $PM_{2.5}$, PM_{10}	The whole year of 2018	Hourly value of air pollution national control quality monitoring sites in China

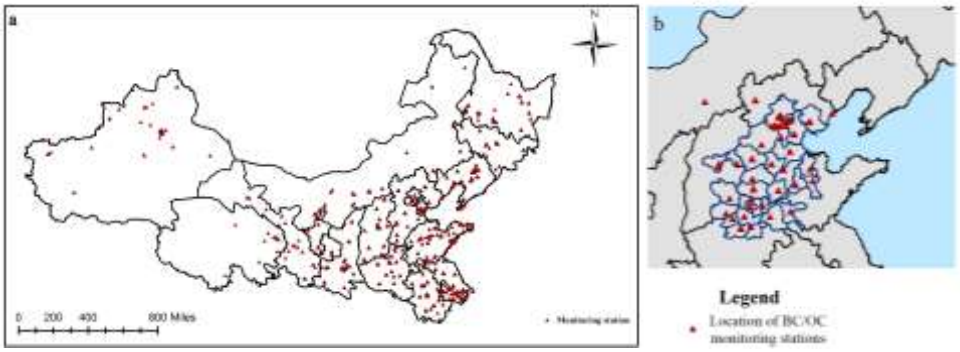

Figure 4-1 Spatial distribution of (a) Conventional atmospheric pollutants and (b) BC/OC monitoring stations

4.3 Chemical transport model (CTMs) and emission inventories applied in the project

This section presents the technical details of the regional (CMAQ-CRAES) and global (OsloCTM3) chemical transport model used, emission inventories, as well as the experimental design.

4.3.1 Introduction to the CMAQ-CRAES

In the study of air pollution, chemical transport models have been widely used because it can make up for the limitations of temporal and spatial resolution, cost and timeliness of monitoring methods. In recent years, China, the United States, Europe and other countries and regions have developed atmospheric numerical models and applied them to air quality simulation. Commonly used three-dimensional gridded air quality models include Community Multiscale Air Quality (CMAQ), Comprehensive Air Quality Model with Extensions (CAMx), Nested Air Quality Prediction Modeling System (NAQPMS), etc. Most of these models include relatively complex gas-liquid-aerosol chemistry and simple heterogeneous chemistry processes, and have good simulation ability for secondary air pollutants (O_3, $PM_{2.5}$ and PM_{10}). This kind of model system can be used for simulation, evaluation and decision-making of multi-scale and multi-pollutant air quality.

CMAQ model system is the core part of the third-generation air quality forecast and assessment system (Models-3) developed by the US National Environmental Protection Agency. Therefore, it is also called Models-3/CMAQ model. Its basic design concept is to put a variety of pollutants together in the framework of an atmospheric model, instead of only focusing on single species and single-phase species. It comprehensively considers pollution problems such as particulate matter, photochemical oxidation, and acid deposition. Its multi-scale characteristics make it suitable for different time periods and different times.

The meteorological background field provided by the mesoscale meteorological model WRF is required in the Models-3/CMAQ model, and then the meteorological field output by the WRF model is processed by using the meteorological chemistry interface processor MCIP (Meteorology-Chemistry Interface Processor) and provided to the CMAQ model and the Sparse Matrix Operator Kernel Emissions (SMOKE) emission source treatment model. Meteorological input data are simulated for the year 2018. The gridded hourly source emission data generated by SMOKE is used as the pollution source input data of CMAQ.

Before running the CMAQ, the initial field conditions, boundary field conditions and photolysis rate constants should be provided. Among them, the initial field conditions are generated by The ICON (The Initial Conditions Processor) module, and the content of this file is the initial time concentration of all pollutants in the first hour of all grids in the simulation area. Boundary field conditions are generated by the BCON (The Boundary Conditions Processor) module, which contains the content of the chemical conditions that simulate the boundaries of the region, which can be divided into static and dynamic. Photolysis rate information is generated by the JPROC (The Photolysis Rate Processor) module, which uses quantum yield and molecular absorption cross-sections to calculate the constants of the rate of photolysis of clean atmospheres in fixed altitudes, solar hours, and latitude zones, which can be used to calculate gaseous chemical conversion and pollutant concentrations.

The CCTM (CMAQ Chemistry-Transport Model) module is the chemical transfer module of the CMAQ model and the core part of the CMAQ, and its main function is to integrate the output results of all the above pretreatment modules for air quality simulation calculations. The output file of the CCTM module is a gridded binary file with temporal resolution, including the concentrations of each gaseous and aerosol contaminant, the hourly dry and wet sedimentation values, visibility, and the integral average concentration values. The main module components of the CMAQ mode and the relationship between each module are shown in **Fig. 4-2**.

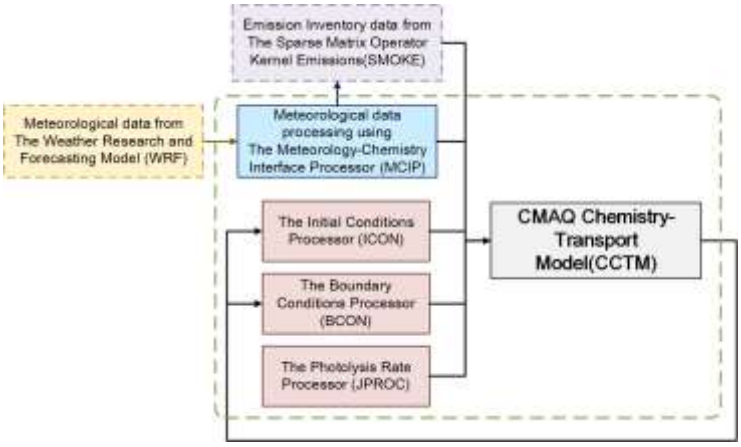

Figure 4-2 CMAQ-CRAES model structural framework diagram

The main CMAQ simulation process options are shown in **Table 4-2**.

Table 4-2 The main processes and simulation options in the CMAQ model

Process	The physical model	Calculation method
Horizontal transmission	Euler continuity equation	Boot/PPM
Horizontal diffusion	K theory	Two-dimensional equation
Vertical transportation	Euler continuity equation	Implicit backward Euler center countercurrent solution
The vertical diffusion	K theory/non-local mixing	Implicit backward Euler/Asymmetric convective diffusion
The gas phase chemical	CB05/CB06/SAPRC99	EBI/IEH/LSODE
Aerosol chemistry	Aqueous inorganic chemistry/organic and inorganic thermodynamics/static bi-modal or multi-modal	RADM-AQ/ISORROPIA/SOAP/CMU
Dry deposition	Gas and aerosol resistance models	The deposition rate is calculated by vertical diffusion
Wet deposition	Gas and aerosol removal models	Eliminate by exponential removal coefficient

4.3.2 Introduction to the OsloCTM3

The OsloCTM3 (Søvde et al. 2012) is a global 3-dimensional chemical transport model. The model, like other offline CTMs, is driven by input of fields of meteorological variables (e.g., temperature, wind, clouds) and emissions of air pollutants and their precursors. The 3-hourly meteorological data used to drive the OsloCTM3 comes from the European Center for Medium Range Weather Forecast (ECMWF) Open Integrated Forecast System (OpenIFS) model, which produces data daily with 12 hours spin-up starting from an analysis at noon on the previous day. These are then pieced together to give a uniform dataset for a whole year. The model can use any emission inventory – see Sect. 3.3 for data used in the simulations for the ChiNorBC project. The standard horizonal resolution of the model, and the one used for the simulations presented here, is a Gaussian grid of 2.25 °x2.25 °. In the vertical, the model has 60 levels with irregular spacing from the surface to 0.1 hPa altitude.

OsloCTM3 treats full tropospheric and stratospheric chemistry and includes modules for the climate and air quality relevant aerosol species; carbonaceous, secondary organic, sulfate, ammonium-nitrate, sea salt and dust aerosols. Details on chemistry and aerosol modules can be found in the scientific literature (Gauss et al. 2003; Lund et al. 2018, Søvde et al. 2012, 2008); here we present brief overviews.

The module for carbonaceous aerosol (BC, OC) was first introduced by Berntsen et al. (2006). The module is a bulk scheme, with aerosols characterized by total mass only and no size distribution. OsloCTM3 treats organic aerosols (OA) instead of OC. If emissions are given as OC, a factor of 1.6 for anthropogenic emissions and 2.6 for biomass burning sources is used for the OC-to-OA conversion, following suggestions from observational studies

(Aiken et al., 2008; Turpin and Lim, 2001). Upon emission, 20% of BC is assumed to be hydrophilic (water soluble) and 80% hydrophobic (insoluble), while a 50:50 split is assumed for OA. Chemical aging, i.e. the process where the initially hydrophobic particles become hydrophilic and hence available for removal by precipitation, is represented by constant transfer rates from hydrophobic to hydrophilic mode, with a seasonal and latitudinal variation. The formation, transport and deposition of secondary organic aerosols (SOA) are parameterized using a two-product model used to represent the oxidation products of the precursor hydrocarbons and their aerosol forming properties (Hoyle et al. 2007, Hoffmann et al., 1997). Precursor hydrocarbons which are oxidized to form condensable species include both biogenic species such as terpenes and isoprene, as well as species emitted predominantly by anthropogenic activities. The chemical equilibrium between inorganic species (including ammonium nitrate) is simulated with the Equilibrium Simplified Aerosol model (EQSAM) [Metzger et al., 2002a; Metzger et al., 2002b]. The sulfur cycle chemistry involves SO_2, as well as dimethyl sulfide (DMS), hydrogen sulfide (H_2S), methanesulfonic acid (MSA) and is connected to model oxidant chemistry. Sulfate aerosols are produced by aqueous phase oxidation of SO_2 (Berglen et al. 2004). Production of sea salt is parameterized using expressions from Monahan et al. (1986) and Smith et al. (1993) with updates following recommendations by Witek et al., (2016). For mineral dust aerosols, the Dust Entrainment and Deposition (DEAD) model v1.3 is used (.

Upon emission, gases and aerosols are subject to chemical processing, transport (advective and convective), and wet and dry removal. Wet scavenging is the primary loss process for aerosols and is calculated based on ECMWF data for convective activity, cloud fraction and rain fall, and on the solubility of individual species. The solubility of aerosols is given by constant fractions, given for each species and type of precipitation (large-scale rain, large-scale ice, and convective). Large-scale precipitation follows Neu and Prather (2012) and convective scavenging is based on the Tiedtke mass flux scheme (Tiedtke 1989).

The model code is openly available from GitHub (https://github.com/NordicESMhub/OsloCTM3). For thi s project, the OsloCTM3 is run with year 2018 emissions using first the default baseline inventory and then with anthropogenic emissions in China replaced by the new estimates from Output 2 of this projec t (see Sect. 4.3.3.3). Additionally, the model is run with the three scenarios for year 2035 emissions, k eeping meteorology fixed at the present-day conditions.

4.3.3 Emission inventories of pollution sources

4.3.3.1 The MEIC emission inventory

In the baseline simulation, the anthropogenic source emission inventories used in the CMAQ-CRAES simulation in the master grid (36 km×36 km) is based on the Multi-resolution Emission Inventory for China (MEIC 2016, http://www.meicmodel.org/; Li et al. 2017) from Tsinghua University and the Regional Emission inventory in Asia (REAS 2.1, https://www.nies.go.jp/REAS/; Kurokawa et al. 2013) compiled by the National Institute of Environmental Research of Japan. Natural source emission inventories were obtained using the Model of Emissions of Gases and Aerosols from Nature (MEGAN3.1; Guenther et al., 2019). Emissions of dust was not included.

The emission inventories in baseline simulation used in the nested grids (12 km x 12 km) were built based on MEIC 2016 and adjusted using locally measured emission inventories based on the emission reduction measures of China's Air Pollution Prevention and Control Action Plan, as well as energy economic and environmental statistics. The nested grid covers an area including 17 provinces, autonomous regions and municipalities in East China (Beijing, Tianjin, Shanghai, Hebei, Henan, Shandong, Shanxi, Anhui, Fujian, Heilongjiang, Jilin, Jiangsu, Jiangxi, Hubei, Hunan, Liaoning, Inner Mongolia, Shaanxi and Zhejiang), including five sectors: power, industry, transport, residential and agriculture, and nine pollutants: SO_2, NO_x, CO, PM_{10}, $PM_{2.5}$, BC, OC, VOCs, NH_3.

A more refined pre-processing system for air pollution emission inventories has also been developed in this study. The system is based on the SMOKE model and uses geographic information related to source emissions to assign source emission inventories spatially, temporal contours, and species assignments for VOCs and particulate matter. The pre-processing process is carried out separately for point sources, surface sources, mobile sources, and natural

sources, so that the source emission inventories in the baseline scenario are processed, converted, and meet the input requirements of the regional air quality model.

Based on the geographical characteristics of various pollutant sources, the spatial distribution of emissions was used to assign the MEIC2016 anthropogenic source emission inventory to the simulation grid. The overall regional distribution of emissions of various pollutants in China in 2016 is shown in the **Figure 4-6**, with pollutant emissions from different cities generally showing a characteristic of "high in the central and eastern parts and low in the west", with large differences in emissions across the region, which is mainly related to the distribution of human activities. The spatial distribution of emissions differs significantly between pollutants. For example, the regulation of the energy mix and improvements to the technology for the treatment of exhaust gases from chimneys have led to the disappearance of CO and SO_2 pollution from large areas. The distribution of these two pollutants is in a centralized distribution, and the areas with high emissions are mainly concentrated in the urban center.. The emission distribution of NO_x from different provinces shows a linear pollution characteristic, closely related to the road network, . The intensity and range of NH_3 emissions are relatively more dispersed in space.

For the 17 provinces in Northern China, the cities with the largest annual emissions of pollutants are mainly in the Shandong Province, which has the largest annual emissions of NO_x, BC, OC, $PM_{2.5}$, PM_{10} and VOCs among the cities in northern China, with 1785 kt/year, 141 kt/ year, 360 kt/ year, 919 kt/ year, 1140 kt/ year, 2913 kt/ year respectively. The largest annual emission of NH_3 is in Henan Province with 970 kt/ year. The largest annual emission of CO is in Hebei Province with 18,468kt/ year.

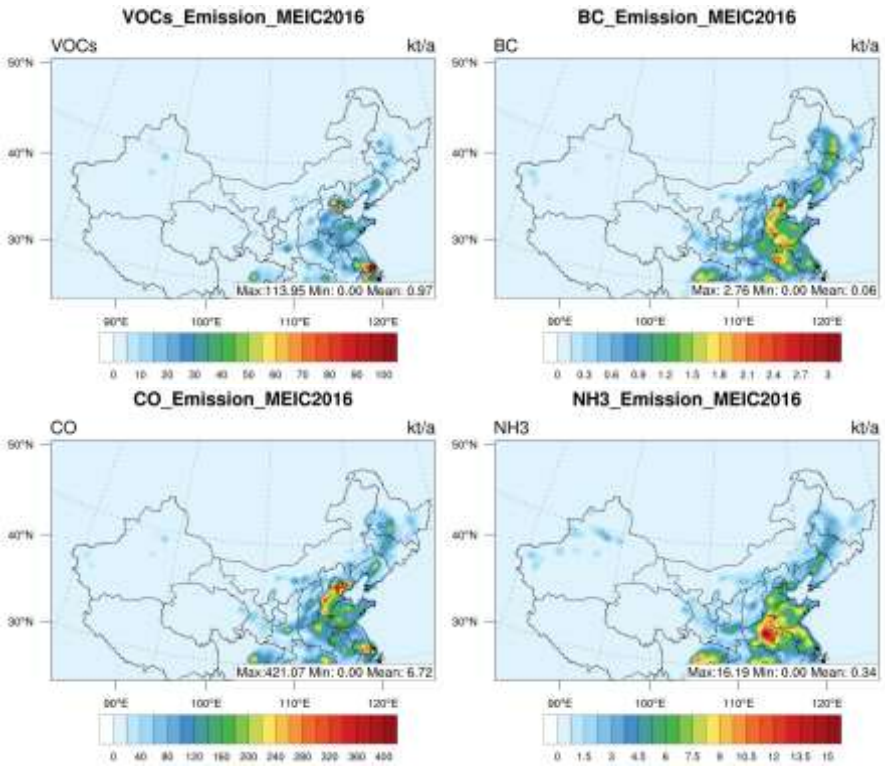

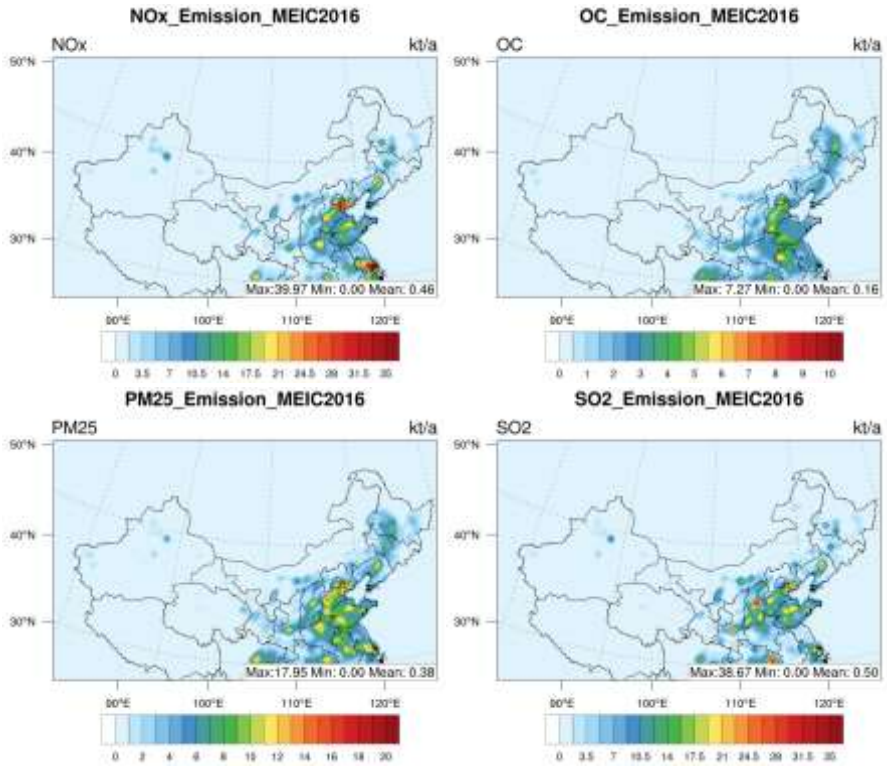

Figure 4-6 Spatial distribution of MEIC2016 emissions used in the CMAQ-CRAES baseline simulation

4.3.3.2 The CEDS emission inventory

The anthropogenic source emission inventories used in the baseline OsloCTM3 simulation is the Community Emission Data System version 2021 (CEDSv21) (Hosely et al. 2018; Feng et al. 2020; O'Rourke et al. 2021). The CEDS is developed to produce consistent estimates of global emissions of chemically reactive gases (CO, CH4, NH3, NOx, SO2, NMVOCs) and carbonaceous aerosols (BC, OC) over the industrial era (1750 - present). The inventory uses existing emission inventories, emission factors, and activity/driver data to estimate annual country-, sector-, and fuel-specific emissions over time. Emissions are provided on an annual basis at the level of country and sector and gridded with monthly seasonality. In the final gridded product, emissions are available for seven aggregate sectors, agriculture, energy, industrial, transportation, residential (including commercial, other), solvents (production and application), waste management, and international shipping.

More recently, it became clear that there were biases in the initial CEDS 2016/2017 release, most notably an underestimation of the decreasing trend of SO_2 and NO_x emissions in China over the past couple of decades. In the 2021 release, these issues were largely addressed and has been found to improve the OsloCTM3 ability to reproduce observed trends over the East Asia region (Lund et al. 2022). The CEDS emissions have been widely used in the studies of the atmosphere and climate, and the initial release of the inventory formed the basis for the sixth phase of the Coupled Model Intercomparison Project (CMIP6) and hence for the assessments of the sixth report by the Intergovernmental Panel on Climate Change (IPCC). Hence, using it as a baseline here enables comparison with the broader scientific literature and provides added relevance for the project results.

Figure 4-7 show the year 2018 emissions of selected precursor gases and BC and OC. The overall features of the spatial distribution are like the MEIC2016 emissions described above, with the largest emission hotspots towards the East. For China as a whole, CEDSv2021 gives annual total emissions of 150 Mt CO, 12 Mt NH_3, 23 Mt NOx, 13 Mt SO_2, 1.2 Mt BC, and 1.9 Mt OC. BC, OC, and CO emissions exhibit a clear seasonal cycle (not shown) with higher emissions during the winter season. This seasonal cycle is driven by residential emissions and presumably reflects the need for more heating during winter times. The seasonal variation can also be seen for SO_2 emissions, whereas NOx emissions are relatively flat throughout the year and has a much smaller relative contribution from

the residential sector to the total. As can be expected, NH_3, which is primarily emitted from agricultural activities, peaks during spring, with a secondary peak in September.

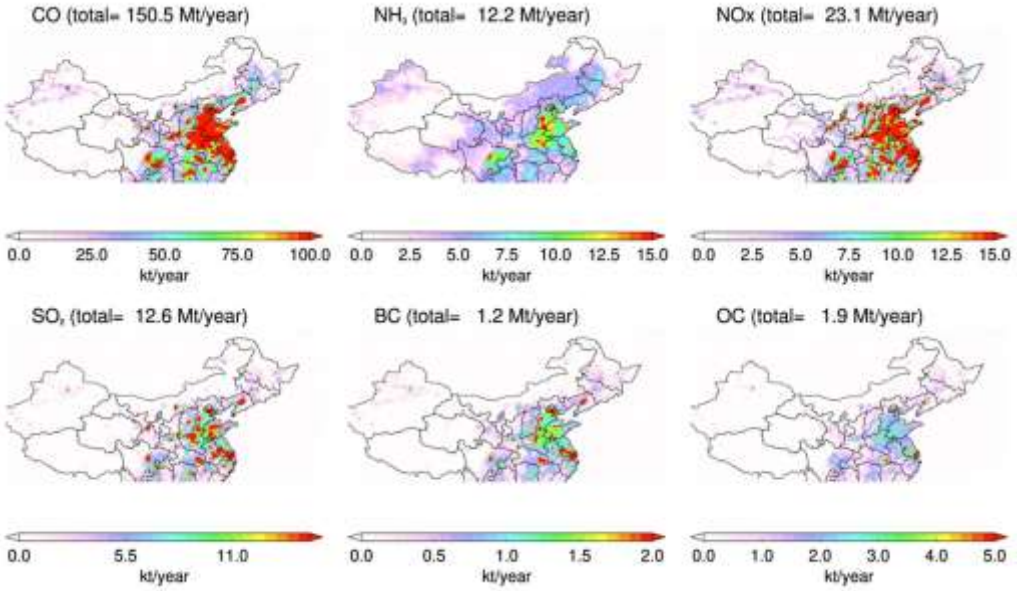

Figure 4-7 Spatial distribution of annual (year 2018) total emissions of CO, NH_3, NOx, SO_2, BC and OC from the CEDS emission inventory used in the OsloCTM3 baseline simulation (note the different color scales)

4.3.3.3 ChiNorBC-2018 emission inventories

The anthropogenic source emission inventories (NO_x, CO, VOCs, BC, OC, $PM_{2.5}$, PM_{10}, SO_2 and NH_3) were updated using the emission inventory information provided in Output 2 for each province in the Northern China. **Figure 4-8** illustrates the differences between the modeled ChiNorBC-2018 emission inventories and the baseline MEIC2016 emission inventories for each pollutant. The differences in the variation of each pollutant emissions are obvious. Except for the Beijing-Tianjin-Hebei and Yangtze River Delta regions, most Chinese regions show an increase in NO_x emissions after updating the emission inventory, with the maximum increase in emissions being about 41kt/a in the Tiannjin. The emissions of CO, SO_2, VOCs decrease most significantly in the central and eastern regions, with the maximum decrease in emissions being -697 kt/a (Shandong), -85 kt/a (Shanxi) and -161 kt/a (Shandong) respectively. Differences in emissions of NH_3 were more subdued and dispersed, with emissions declining mainly in central China. The spatial distribution of the differences in emissions of $PM_{2.5}$, BC and OC associated with particulate matter is relatively similar. Emissions in most of Northern China is higher (e.g., Shanxi Province) while emissions in Beijing, Tianjin and Hebei and surrounding cities are lower. For China as a whole, the ChiNorBC -2018 emissions are lower than MEIC by 30% for BC, 41% for OC, 29% for NOx, 47% for CO, 21% for PM2.5, 43% for SO_2 and 10% for NH_3. The only species for which the ChiNorBC -2018 emissions are higher is OC, by 35%. Emissions are described in more detail in Chapter 2 of this projects.

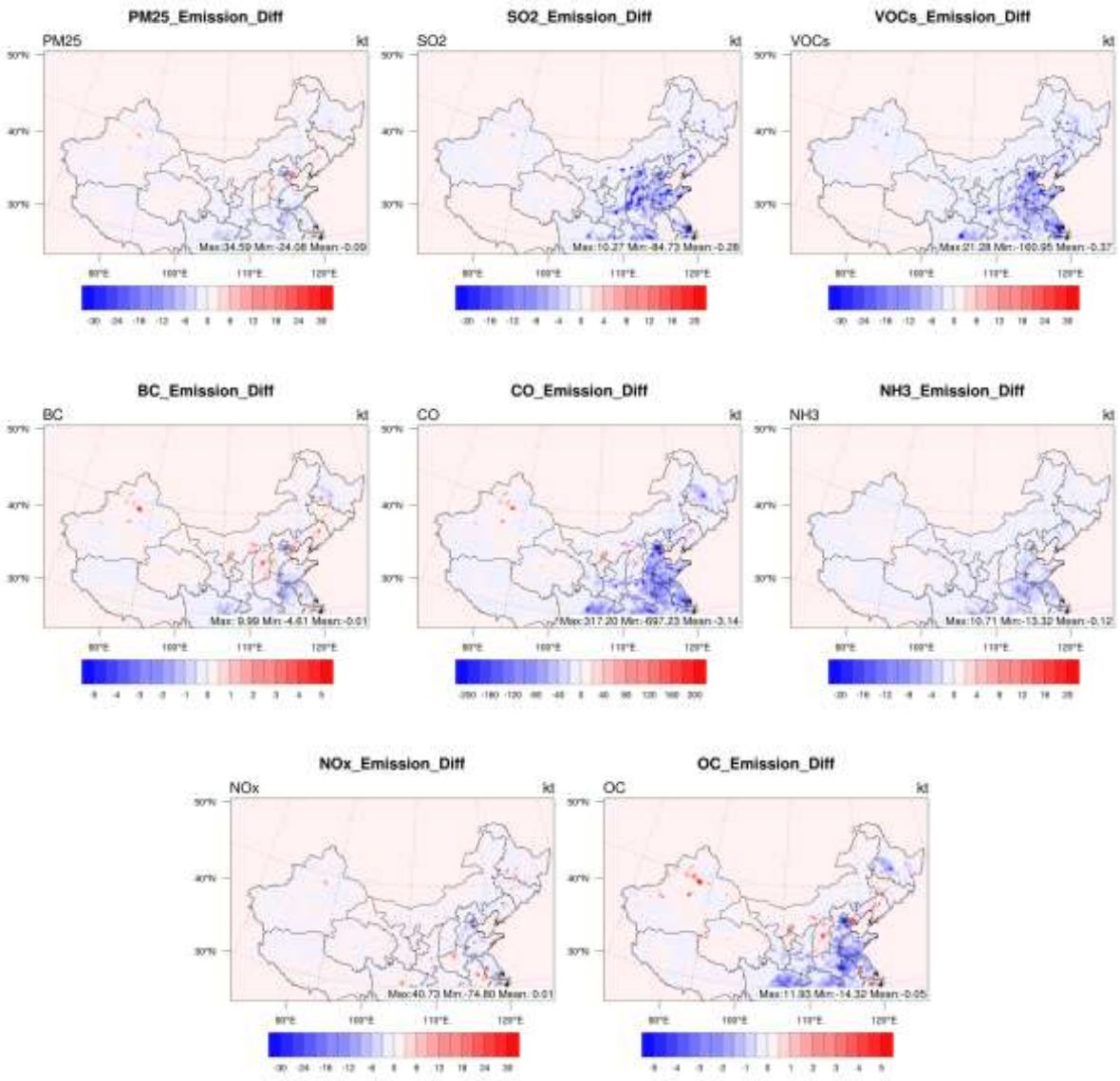

Figure 4-8 Spatial distribution of differences in emissions changes between the ChiNorBC -2018 and MEIC2016 emission inventory for each pollutant

Table 4-5 Ratio between the ChiNorBC-2018 and MEIC2016 emission inventory for each pollutant

	SO_2	NO_x	BC	OC	$PM_{2.5}$	PM_{10}	VOCs	NH_3	CO
Xinjiang	0.84	0.91	2.47	1.97	1.59	1.63	0.84	1.09	1.32
Qinghai	1.00	0.97	1.11	0.82	0.68	0.73	0.54	1.12	0.71
Gansu	0.73	0.87	0.51	0.42	0.57	0.63	0.62	0.86	0.43
Ningxia	4.24	1.10	1.69	1.34	1.13	1.17	0.78	1.05	1.21
Shananxi	0.39	0.90	0.61	0.40	0.52	0.59	0.76	0.91	0.45
Shanxi	0.38	0.62	1.09	0.77	0.90	0.92	0.78	0.86	0.65
Neimenggu	0.42	0.76	0.88	0.69	0.80	0.83	0.63	0.88	0.55
Henan	0.47	0.83	0.59	0.51	0.70	0.73	0.86	0.86	0.49
Anhui	1.45	0.94	0.38	0.46	0.65	0.70	0.75	0.83	0.36
Jiangsu	0.73	0.68	0.54	0.64	0.90	0.95	1.01	0.81	0.49
Shandong	0.38	0.74	0.52	0.44	0.71	0.74	0.81	0.96	0.45
Hebei	0.50	0.59	0.67	0.52	0.98	1.05	0.73	0.90	0.54

Beijing	0.14	0.54	0.18	0.11	0.17	0.17	0.95	0.51	0.23
Liaoning	0.71	0.58	0.98	0.77	0.95	1.01	0.86	0.87	0.69
Jilin	0.62	0.62	0.84	0.70	0.79	0.83	0.66	1.02	0.59
Heilongjiang	0.46	0.61	0.59	0.52	0.64	0.69	0.54	0.98	0.42
Tianjin	0.26	0.44	0.35	0.27	0.69	0.73	0.90	0.96	0.38

Figure 4-9 show the difference between the ChiNorBC -2018 emissions and the CEDSv21 inventory. Overall, the ChiNorBC -2018 emissions are lower than the CEDSv21. There are, however, geographical differences. For instance, OC emissions are mostly lower than CEDSv21 in the southern part of China but higher in the north, whereas there is an east-west pattern of higher and lower emissions for NH_3. For China as a whole, the ChiNorBC -2018 emissions are lower than CEDSv21 by 10% for BC, 35% for NOx and CO, 40% for SO_2 and 23% for NH_3. The only species for which the ChiNorBC -2018 emissions are higher is OC, by 35%. There are also differences between the ChiNorBC -2018 and CEDSv21 emissions in terms of seasonal cycle. Most notably, the seasonal cycle is more pronounced for BC and OC in the ChiNorBC -2018 emissions and flatter for SO_2 and NH_3.

Since the OsloCTM3 is a global model and requires input of global emission fields, some homogenization is required when replacing the CEDSv21 emissions in China with the ChiNorBC -2018 emissions. Firstly, emissions are re-gridded from 0.25 °x 0.25 °to 1 °x 1 °horizontal resolution. Secondly, we assume the same relative speciation of bulk NMVOC emissions to individual VOC compounds as in CEDSv21. Finally, the OsloCTM3 distinguishes between BC and OC emitted from biofuel and fossil fuel combustion. To split the total anthropogenic ChiNorBC -2018 emissions of BC and OC, we scale by the relative distribution from the CEDSv21 for each relevant sector. Emissions from international aviation and shipping is included in the simulations and are from CEDSv21. Biomass burning emissions, including agricultural waste burning, are from the Global Fire Emissions Database version 4 (GFED4, Randerson et al. 2018) and biogenic emissions of VOCs are from the inventory developed with the Model of Emissions of Gases and Aerosols from Nature under the Monitoring Atmospheric Composition and Climate project (MEGAN–MACC) (Sindelarova et al., 2014).

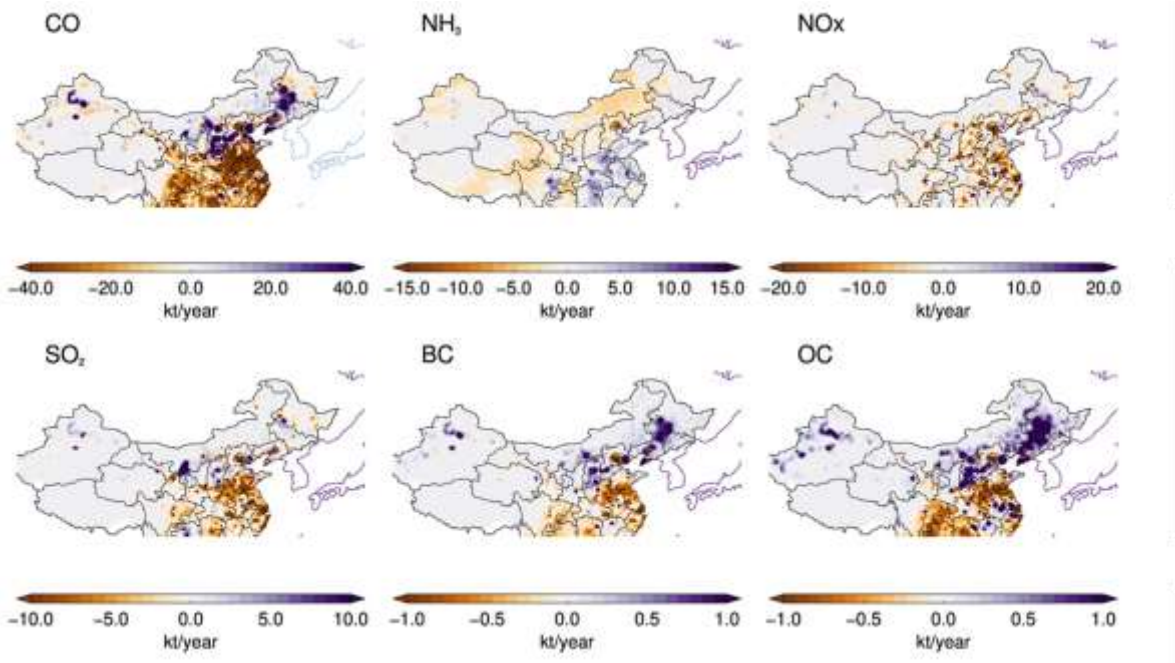

Figure 4-9 Spatial distribution of differences in emissions changes between the ChiNorBC -2018 and CEDSv21 emission inventory for each pollutant (note the different color scales)

4.4 Results from regional CTM simulations

4.4.1 Model performance evaluation

Based on the MEIC2016 and ChiNorBC -2018 emission inventory, the CRAES-CMAQ model simulates air pollutant concentrations (BC, OC, O_3, SO_2, NO_2, $PM_{2.5}$, PM_{10} and CO, etc.) in the Chinese region from January 1, 2018 to December 31, 2018. The simulated air pollutant concentrations (SO_2, NO_2, $PM_{2.5}$, PM_{10}, O_3, CO, BC, OC) were evaluated temporally and spatially based on the available observation station data in China for MEIC2016 and ChiNorBC -2018 emission inventories. The 90th percentile of the maximum daily 8 h (MDA8) average O_3, annual average of NO_2, SO_2, NO_2, $PM_{2.5}$, PM_{10}, CO for each station's observations and the simulation grid where the station during 2018 was located was screened and calculated according to the technical regulation for ambient air quality assessment (on trial; HJ 663-2013).

Three specific statistical indicators—the normalized mean bias (NMB), normalized mean error (NME), and correlation coefficient (*r*)—were determined to evaluate the simulated and observed results. The NMB, NME, and *r* values of the simulated and observed concentrations at each monitoring site were compared according to the criteria and goal levels for chemical transport model performance statistics suggested by Emery et al. (2017). The capital cities of Northern China (Urumqi, Xining, Lanzhou, Yinchuan, Taiyuan, Xi'an, Hohhot, Zhengzhou, Hefei, Nanjing, Jinan, Shijiazhuang, Beijing, Shenyang, Changchun, Harbin) were selected as a typical city.

The calculation formulas of relevant statistical parameters are as follows:

$$\mathbf{NMB} = \frac{\sum_{1}^{n}(M-O)}{\sum_{1}^{n}(O)} \quad (1)$$

$$\mathbf{NME} = \frac{\sum_{1}^{n}|M-O|}{\sum_{1}^{n}(O)} \quad (2)$$

$$\mathbf{r} = \frac{1}{(n-1)}\sum_{1}^{n}\left(\left(\frac{O-\overline{O}}{\sigma_o}\right)*\left(\frac{M-\overline{M}}{\sigma_m}\right)\right) \quad (3)$$

where ***M*** and ***O*** are the simulated and observed site MDA8 O_3 concentrations, respectively, and ***n*** is the number of days that ***M*** and ***O*** are at different sites, ***σ*** is the standard deviation.

4.4.1.1 Model performance results with MEIC emission inventory

Figure 4-10 shows the spatial distribution of the simulated and observed 90th percentile of the MDA8 O_3, annual average of NO_2, SO_2, NO_2, $PM_{2.5}$, PM_{10} and CO during 2018 for MEIC emission inventory. For conventional pollutants, the simulation system used in this study under the MEIC emission inventory performed well for most of the monitoring stations during the 2018 base year, with the spatial distribution trend of simulated air pollutant concentration levels being relatively consistent with that of observed concentrations, especially in the Beijing-Tianjin-Hebei and surrounding areas, and the Yangtze River Delta and the Pearl River Delta.

The simulated concentrations of SO_2 were severely overestimated, with the highest NMB of 665% (Tianjin) and a correlation coefficient r between 0.35-0.72, except for the two northwestern provinces of Qinghai and Gansu, all other Northern Chinese provinces were in a state of simulated overestimation. In addition, the simulated concentrations of $PM_{2.5}$, NO_2 and CO are underestimated in the northwest and overestimated in the east-central region, with the minimum NMB values for these pollutants in the Northern provinces of China being about -68%, -40% and -77% respectively; the maximum values are about 92%, 116% and 83%, and the provinces with poor correlations are also concentrated in the northwest, probably due to the following reasons: Northwest China is vast

and sparsely populated, with underestimation in total emissions and a sparser spatial distribution. In addition, the spatial distribution trends may differ significantly from reality, resulting in large differences between the simulated and observed concentrations in the grids where the air quality monitoring stations are located., Simulated PM_{10} concentrations for most cities in Northern China are also underestimated, with a minimum value of about -86% for NMB, and the underestimation may be due to the absence of a dust source emission inventory in the model. The modelled 90th percentile of the MDA8 O_3 concentrations were the best of all pollutants modelled, with r above 0.65 for northern Chinese cities, between -8% and 20% for NMB and between 13% and 22% for NME. The average *r* values within each region were well within the range of the benchmark (> 0.5 for O_3) suggested by Emery et al. (2017). The NMB and NME values in some regions were slightly above the criteria range (±15%, < 25%, respectively). Due to the absence of monitoring concentrations, the ChiNorBC project only assessed the modelled performance of BC/OC simulated concentrations in some cities in and around Beijing, Tianjin, and Hebei. As seen in **Figure 4-11**, the modelled concentrations of BC/OC show a significant overestimation in Beijing, Tianjin, Hebei and surrounding areas. The differences in the modelled BC/OC concentrations between the ChiNorBC 2018 and MEIC 2016 emission inventories will be presented in Section 4.4.1.2.

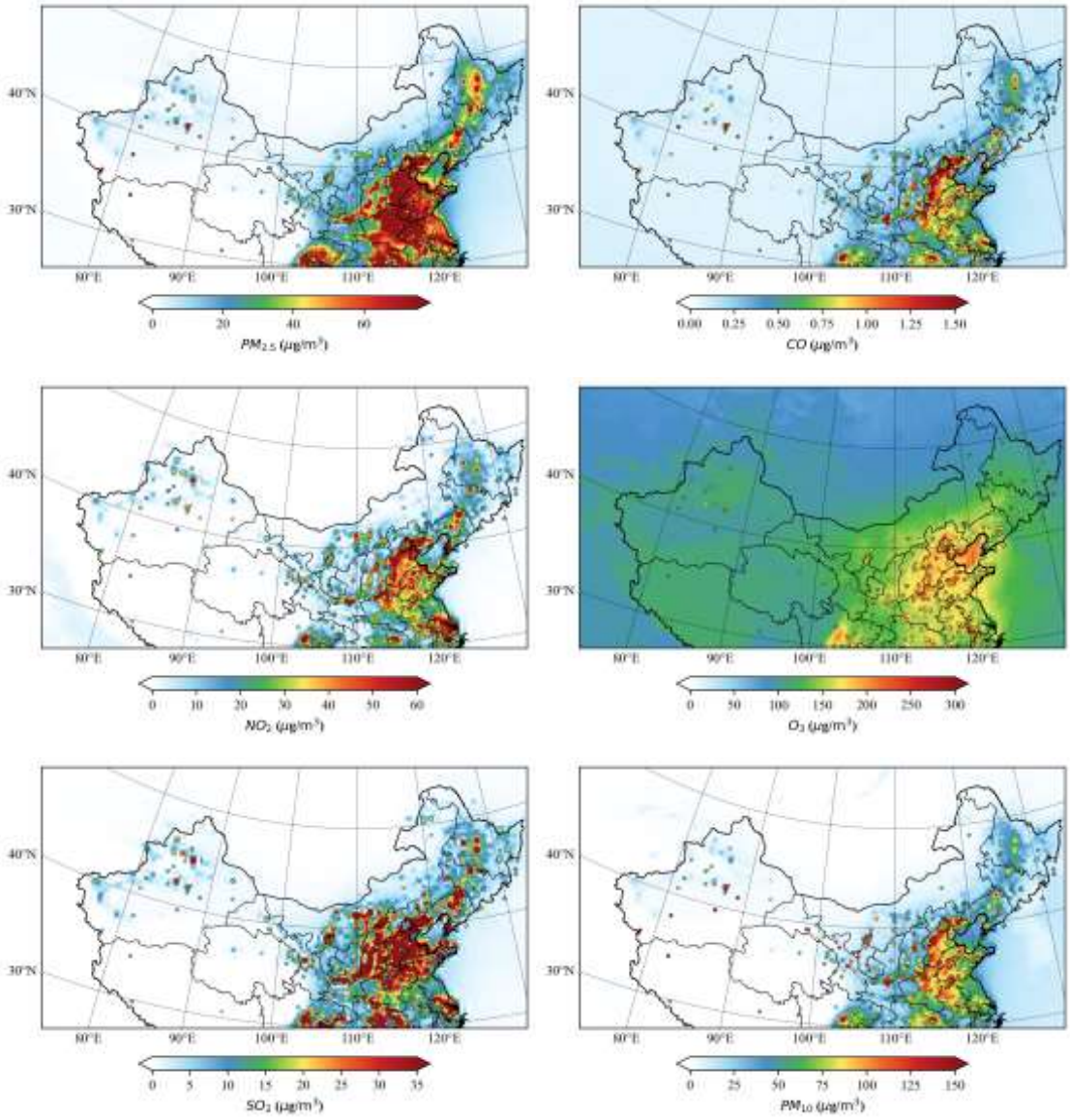

Figure 4-10 Comparison of the spatial distribution of observed and modelled concentrations of conventional pollutants for the MEIC 2016 inventories. The colored circle indicates the air pollutant concentration at the monitoring station; the colored matrix grid indicates the simulated air pollutant concentrations.

Table 4-6 Model performance statistics for simulated 90th percentile of the MDA8 O_3 against observations over Northern China during 2018

Province	NMB	NME	R	Province	NMB	NME	R
Xinjiang	6%	16%	0.86	Jiangsu	2%	18%	0.85
Qinghai	20%	22%	0.65	Shandong	3%	15%	0.90
Gansu	5%	14%	0.79	Hebei	-5%	16%	0.92
Ningxia	10%	16%	0.82	Beijing	-1%	21%	0.88
Shanxi	10%	19%	0.86	Liaoning	-8%	19%	0.86
Shaanxi	6%	16%	0.90	Jilin	-5%	19%	0.83
Inner Mongolia	1%	13%	0.89	Heilongjiang	-4%	17%	0.83
Henan	7%	15%	0.91	Tianjin	13%	24%	0.89
Anhui	2%	17%	0.83				

Table 4-7 Model performance statistics for simulated annual average $PM_{2.5}$ against observations over northern China during 2018

Province	NMB	NME	R	Province	NMB	NME	R
Xinjiang	-68%	68%	0.65	Jiangsu	62%	68%	0.83
Qinghai	-40%	46%	0.15	Shandong	74%	77%	0.76
Gansu	-55%	55%	0.43	Hebei	65%	73%	0.65
Ningxia	-40%	46%	0.33	Beijing	80%	93%	0.63
Shanxi	14%	43%	0.61	Liaoning	46%	55%	0.66
Shaanxi	18%	41%	0.58	Jilin	30%	52%	0.59
Inner Mongolia	-23%	33%	0.58	Heilongjiang	30%	53%	0.66
Henan	51%	60%	0.74	Tianjin	92%	97%	0.68
Anhui	79%	85%	0.77				

Table 4-8 Model performance statistics for simulated annual average PM_{10} against observations over Northern China during 2018

Province	NMB	NME	R	Province	NMB	NME	R
Xinjiang	-86%	86%	0.37	Jiangsu	10%	32%	0.80
Qinghai	-71%	71%	0.04	Shandong	-5%	33%	0.67
Gansu	-82%	82%	0.18	Hebei	-5%	36%	0.54
Ningxia	-75%	75%	0.15	Beijing	29%	68%	0.33
Shanxi	-37%	45%	0.40	Liaoning	-7%	34%	0.52
Shaanxi	-37%	43%	0.44	Jilin	-21%	43%	0.44
Inner Mongolia	-67%	67%	0.31	Heilongjiang	-20%	37%	0.57
Henan	-8%	34%	0.56	Tianjin	25%	53%	0.48
Anhui	25%	45%	0.71				

Table 4-9 Model performance statistics for simulated annual average SO_2 against observations over Northern China during 2018

Province	NMB	NME	R	Province	NMB	NME	R
Xinjiang	106%	106%	0.72	Jiangsu	186%	187%	0.57
Qinghai	-28%	36%	0.47	Shandong	289%	289%	0.53
Gansu	-12%	28%	0.69	Hebei	296%	296%	0.56
Ningxia	67%	85%	0.35	Beijing	615%	615%	0.59
Shanxi	360%	360%	0.62	Liaoning	120%	124%	0.47
Shaanxi	209%	209%	0.54	Jilin	90%	100%	0.50
Inner Mongolia	121%	122%	0.63	Heilongjiang	116%	120%	0.62
Henan	226%	226%	0.60	Tianjin	665%	665%	0.61
Anhui	79%	85%	0.48				

Table 4-10 Model performance statistics for simulated annual average NO_2 against observations over Northern China during 2018

Province	NMB	NME	R	Province	NMB	NME	R
Xinjiang	-21%	25%	0.80	Jiangsu	56%	56%	0.79
Qinghai	-12%	22%	0.61	Shandong	38%	39%	0.85

Gansu	-40%	40%	0.75	Hebei	39%	40%	0.83
Ningxia	4%	23%	0.69	Beijing	62%	63%	0.78
Shanxi	-20%	26%	0.71	Liaoning	43%	45%	0.64
Shaanxi	8%	18%	0.78	Jilin	0%	18%	0.78
Inner Mongolia	-3%	15%	0.82	Heilongjiang	7%	18%	0.82
Henan	29%	30%	0.82	Tianjin	116%	116%	0.65
Anhui	16%	22%	0.81				

Table 4-11 Model performance statistics for simulated annual average CO against observations over Northern China during 2018

Province	NMB	NME	R	Province	NMB	NME	R
Xinjiang	-77%	77%	0.84	Jiangsu	16%	31%	0.76
Qinghai	-65%	65%	0.35	Shandong	2%	26%	0.67
Gansu	-59%	59%	0.57	Hebei	31%	40%	0.64
Ningxia	-57%	57%	0.52	Beijing	83%	87%	0.61
Shanxi	-22%	27%	0.65	Liaoning	-20%	29%	0.58
Shaanxi	-32%	34%	0.66	Jilin	-31%	35%	0.62
InnerMongolia	-46%	47%	0.61	Heilongjiang	-5%	23%	0.71
Henan	-1%	22%	0.66	Tianjin	46%	51%	0.59
Anhui	12%	28%	0.73				

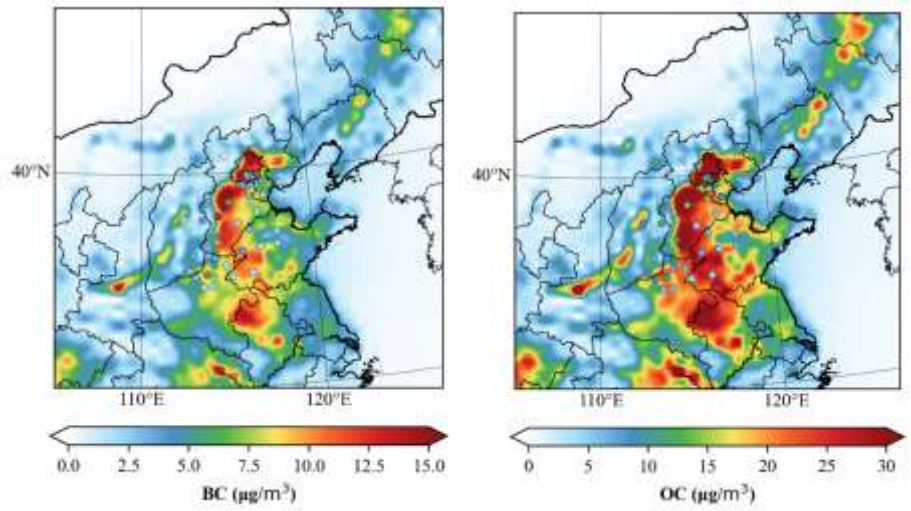

Figure 4-11 Comparison of the spatial distribution of observed and modelled BC/OC concentrations in Beijing, Tianjin, Hebei and surrounding areas. The colored circle indicates the air pollutant concentration at the monitoring station; the colored matrix grid indicates the simulated air pollutant concentrations.

4.4.1.2 Model performance results with the ChiNorBC-2018 emissions inventory

The simulated concentrations of conventional pollutants based on the latest emission inventories provided by Chapter 2 show a significant decrease across the entire Chinese region, as can be seen from the spatial distribution of simulated and observed pollutant concentrations in **Figure 4-12**, which shows that the simulated concentrations of conventional pollutants in economically developed and densely populated regions such as Beijing, Tianjin, Hebei and surrounding areas, Yangtze River Delta and Pearl River Delta in China have decreased particularly significantly. Except for the simulated annual average concentrations of $PM_{2.5}$, the simulated concentrations of all conventional pollutants are underestimated.

The simulated overestimation of SO_2 has improved considerably, with most cities in Northern China changing from simulated overestimation to simulated underestimation, with the minimum value of NMB being around -59% (Inner Mongolia) and the maximum value being around 36% (Xinjiang Uyghur Autonomous Region) as shown in Table 4-12. The correlation coefficient R also improved considerably compared to the simulations with the

MEIC2016 inventory, with R mostly above 0.6. The modelled annual mean CO and NO_2 concentrations also change from being in an overestimated state to an underestimated state in the central and eastern parts of the China, with minimum NMB values of -75% and -64% respectively. Although the modelled concentrations are underestimated, R has been improved to some extent, with most of the R for the simulated annual average CO and NO_2 concentrations above 0.7. On the other hand, the modelled performance of annual mean $PM_{2.5}$ concentrations in the central-eastern region has improved and the overestimation has improved considerably, for example, the NMB in Shandong Province has decreased from 74% to 6%, and the NMB in Heilongjiang Province has decreased from an overestimation of 30% to nearly 0%. However, due to the decrease in particulate emissions, the underestimation of simulated PM_{10} concentrations is more severe, for example, the NMB in Beijing has decreased from an overestimate of 29% to an underestimate of -52%.

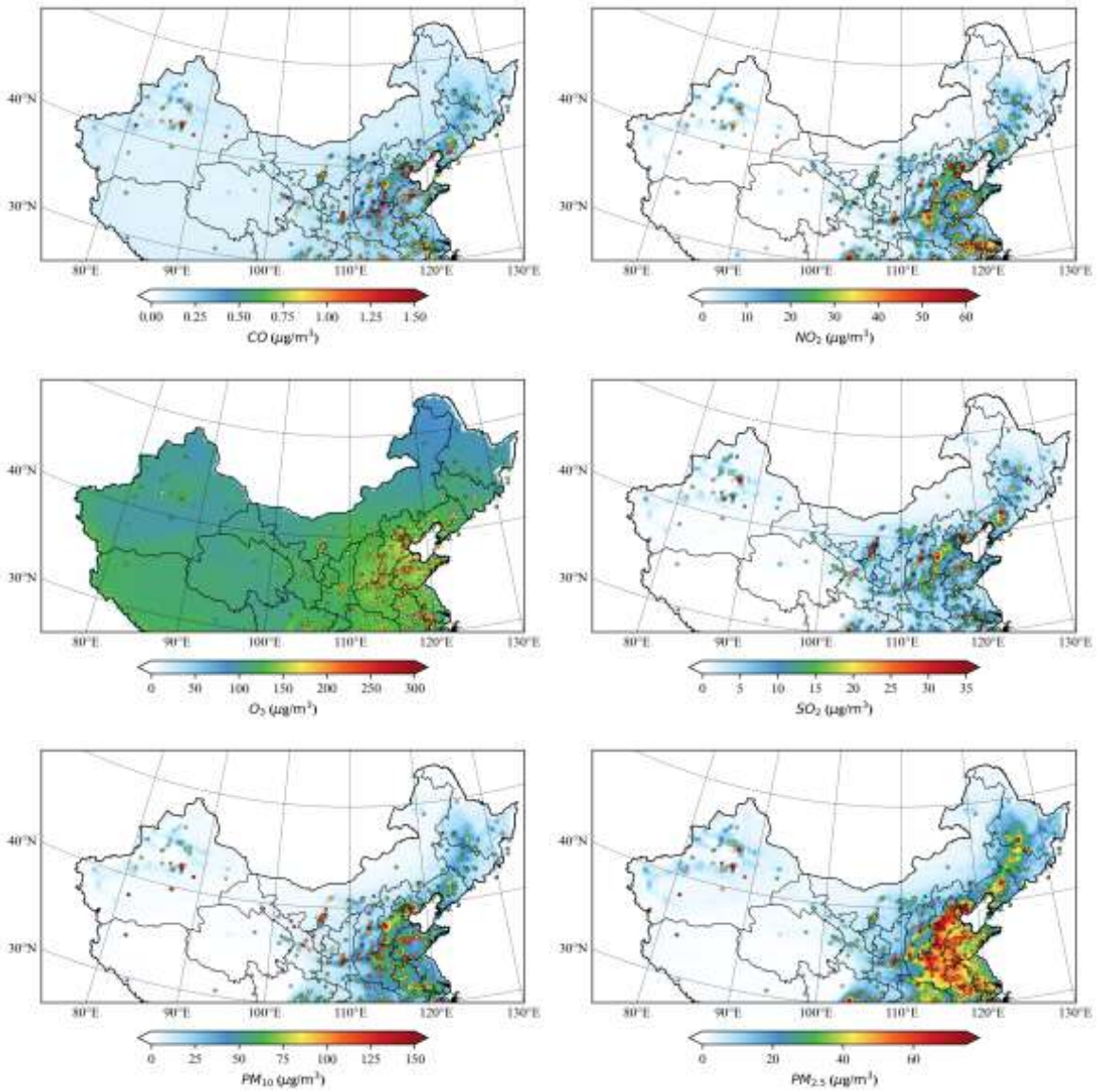

Figure 4-12 Comparison of the spatial distribution of observed and modelled concentrations of conventional pollutants. The colored circle indicates the air pollutant concentration at the monitoring station; the colored matrix grid indicates the simulated air pollutant concentrations.

Table 4-12 Model performance statistics for simulated 90th percentile of the MDA8 O_3 against observations over Northern China during 2018

Province	NMB	NME	R	Province	NMB	NME	R
Xinjiang	6%	18%	0.84	Jiangsu	-4%	20%	0.85
Qinghai	14%	19%	0.62	Shandong	-8%	16%	0.91

Gansu	0%	15%	0.80	Hebei	-15%	21%	0.94
Ningxia	3%	16%	0.82	Beijing	-13%	24%	0.89
Shanxi	-5%	21%	0.86	Liaoning	-13%	20%	0.87
Shaanxi	-4%	19%	0.91	Jilin	-11%	21%	0.83
Inner Mongolia	-3%	15%	0.88	Heilongjiang	-8%	18%	0.81
Henan	-9%	17%	0.92	Tianjin	11%	23%	0.90
Anhui	-15%	20%	0.87				

Table 4-13 Model performance statistics for simulated annual average $PM_{2.5}$ against observations over Northern China during 2018

Province	NMB	NME	R	Province	NMB	NME	R
Xinjiang	-47%	50%	0.73	Jiangsu	22%	34%	0.85
Qinghai	-56%	58%	0.37	Shandong	6%	29%	0.84
Gansu	-69%	69%	0.56	Hebei	17%	39%	0.71
Ningxia	-47%	51%	0.46	Beijing	-32%	49%	0.65
Shanxi	-37%	42%	0.72	Liaoning	15%	32%	0.78
Shaanxi	-20%	33%	0.73	Jilin	-2%	40%	0.69
Inner Mongolia	-52%	52%	0.63	Heilongjiang	0%	41%	0.73
Henan	-12%	29%	0.82	Tianjin	11%	41%	0.71
Anhui	16%	36%	0.81				

Table 4-14 Model performance statistics for simulated annual average PM_{10} against observations over Northern China during 2018

Province	NMB	NME	R	Province	NMB	NME	R
Xinjiang	-77%	77%	0.44	Jiangsu	-16%	27%	0.81
Qinghai	-78%	78%	0.20	Shandong	-41%	42%	0.71
Gansu	-87%	87%	0.26	Hebei	-32%	40%	0.57
Ningxia	-78%	78%	0.18	Beijing	-52%	63%	0.32
Shanxi	-64%	65%	0.49	Liaoning	-26%	34%	0.64
Shaanxi	-57%	57%	0.54	Jilin	-40%	49%	0.53
Inner Mongolia	-79%	79%	0.36	Heilongjiang	-37%	49%	0.60
Henan	-47%	49%	0.61	Tianjin	-27%	42%	0.51
Anhui	-19%	34%	0.71				

Table 4-15 Model performance statistics for simulated annual average SO_2 against observations over Northern China during 2018

Province	NMB	NME	R	Province	NMB	NME	R
Xinjiang	36%	65%	0.80	Jiangsu	-15%	32%	0.62
Qinghai	-40%	49%	0.54	Shandong	-39%	42%	0.72
Gansu	-55%	55%	0.73	Hebei	0%	31%	0.70
Ningxia	-5%	44%	0.50	Beijing	14%	50%	0.69
Shanxi	-12%	32%	0.75	Liaoning	-24%	34%	0.71
Shaanxi	-48%	51%	0.77	Jilin	-29%	40%	0.75
Inner Mongolia	-59%	59%	0.84	Heilongjiang	-33%	38%	0.84
Henan	-31%	42%	0.60	Tianjin	5%	30%	0.77
Anhui	10%	40%	0.43				

Table 4-16 Model performance statistics for simulated annual average NO_2 against observations over Northern China during 2018

Province	NMB	NME	R	Province	NMB	NME	R
Xinjiang	-40%	41%	0.79	Jiangsu	-14%	22%	0.81
Qinghai	-29%	32%	0.70	Shandong	-24%	28%	0.84
Gansu	-64%	64%	0.72	Hebei	-30%	31%	0.81
Ningxia	-35%	38%	0.68	Beijing	-14%	30%	0.71
Shanxi	-44%	45%	0.69	Liaoning	-20%	25%	0.78
Shaanxi	-48%	49%	0.74	Jilin	-44%	44%	0.75

Inner Mongolia	-57%	57%	0.82	Heilongjiang	-43%	43%	0.83
Henan	-25%	30%	0.77	Tianjin	-15%	25%	0.74
Anhui	-12%	22%	0.80				

Table 4-17 Model performance statistics for simulated annual average CO against observations over Northern China during 2018

Province	NMB	NME	R	Province	NMB	NME	R
Xinjiang	-58%	59%	0.90	Jiangsu	-51%	51%	0.83
Qinghai	-71%	71%	0.67	Shandong	-61%	61%	0.85
Gansu	-75%	75%	0.84	Hebei	-47%	48%	0.77
Ningxia	-60%	60%	0.76	Beijing	-58%	59%	0.66
Shanxi	-65%	65%	0.77	Liaoning	-51%	52%	0.79
Shaanxi	-62%	62%	0.82	Jilin	-57%	58%	0.80
InnerMongolia	-73%	73%	0.87	Heilongjiang	-48%	49%	0.80
Henan	-63%	63%	0.77	Tianjin	-54%	54%	0.73
Anhui	-57%	57%	0.81				

The spatial distribution of simulated and observed annual mean BC/OC concentrations during 2018 in key cities in Northern China shows (**Figure 4-13**) that the simulation results with the ChiNorBC -2018 emission inventory could well simulate the BC/OC concentration in Northern China, and the overestimation of the MEIC emission inventory and the simulated pollutant concentration could be significantly improved. Under the MEIC emission inventory, the modelled BC concentrations in Beijing, Tianjin, Hebei and surrounding areas are basically in the range of 10 μg/m^3 -15μg/m^3, the modelled OC concentrations basically in the range of 25 μg/m^3-35 μg/m^3 in Beijing, Tianjin, Hebei and surrounding areas, while under the ChiNorBC -2018 emission inventory, most of the modelled areas in and around Beijing, Tianjin and Hebei modelled BC concentrations below 10μg/m^3, and modelled OC concentrations below 20μg/m^3. In Baoding and Taiyuan, the observed and modelled BC concentrations largely remained between 2.5-7.5 μg/m^3 and the observed and modelled OC concentrations largely ranged from 5-10 μg/m^3.

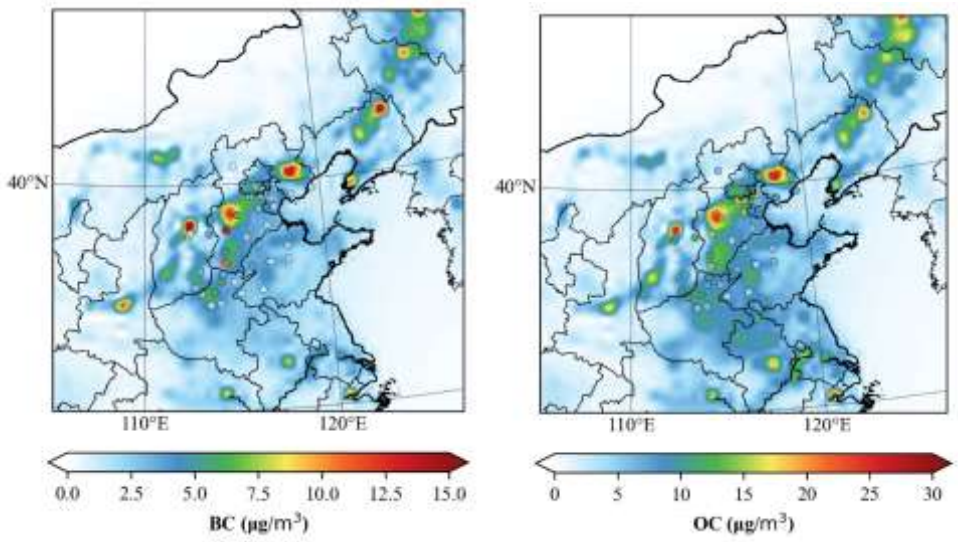

Figure 4-13 Comparison of the spatial distribution of observed and modelled BC/OC annual concentrations for 2018 in Beijing, Tianjin, Hebei and surrounding areas. The colored circle indicates the air pollutant concentration at the monitoring station; the colored matrix grid indicates the simulated air pollutant concentrations.

The simulated and observed monthly average concentrations of all pollutants at each monitoring station in 2018 were extracted, and the difference between the simulated and observed concentrations of the MEIC emission inventory and the ChiNorBC -2018 emission inventory was compared (**Figure 4-14**). The modelled results for SO_2, NO_2, CO and $PM_{2.5}$ deviate more from the line of y=x and most modelled concentrations were overestimated

with the MEIC 2016 inventories, while the modelled results for the ChiNorBC -2018 emission inventory are closer to the observed data. The modelled monthly average concentrations of CO are more concentrated, but the modelled results of the ChiNorBC -2018 emission inventory are generally underestimated. The modelled monthly average PM_{10} concentrations in the ChiNorBC -2018 emission inventory are largely converted from overestimated to underestimated compared to the MEIC emission inventory, with the concentration's distribution remaining deviated from the line of y=x .

Similarly comparing the modelled performance statistics for the baseline and ChiNorBC -2018 emission inventories (**Table 4-17**), the correlation coefficients r has improved for all pollutants, with r increasing from 0.44, 0.56 and 0.63 to 0.5, 0.69 and 0.79 for PM_{10}, SO_2 and CO respectively. The NMB for SO_2 in the modelled performance statistics decreased from 206% to -19% under the baseline emission inventory, and the modelled concentrations of all other conventional pollutants changed from overestimates to underestimates. In addition, the modelled performance statistics for simulated BC/OC concentrations also demonstrate that the NMB for BC and OC decreases from 161% and 169 to 2% and 49%, and NME decreases from 173% and 190% to 50% and 78% from the baseline to the ChiNorBC -2018 emission inventory, with good improvement and enhancement of the modelled simulation performance for BC and OC.

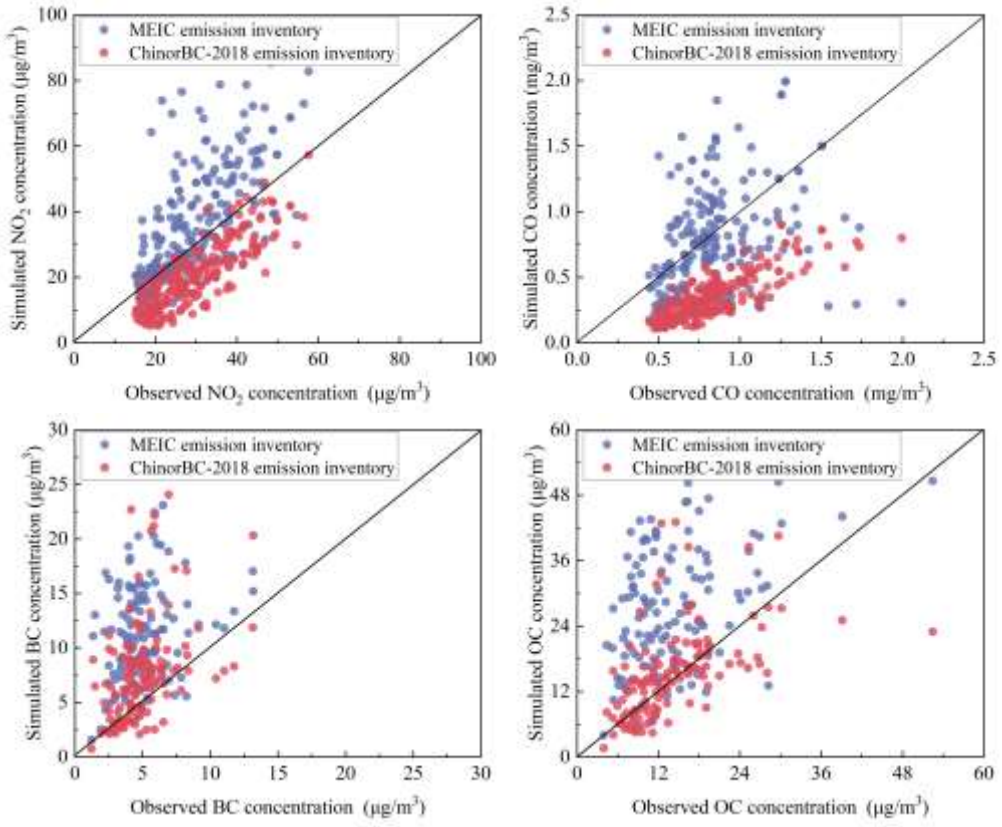

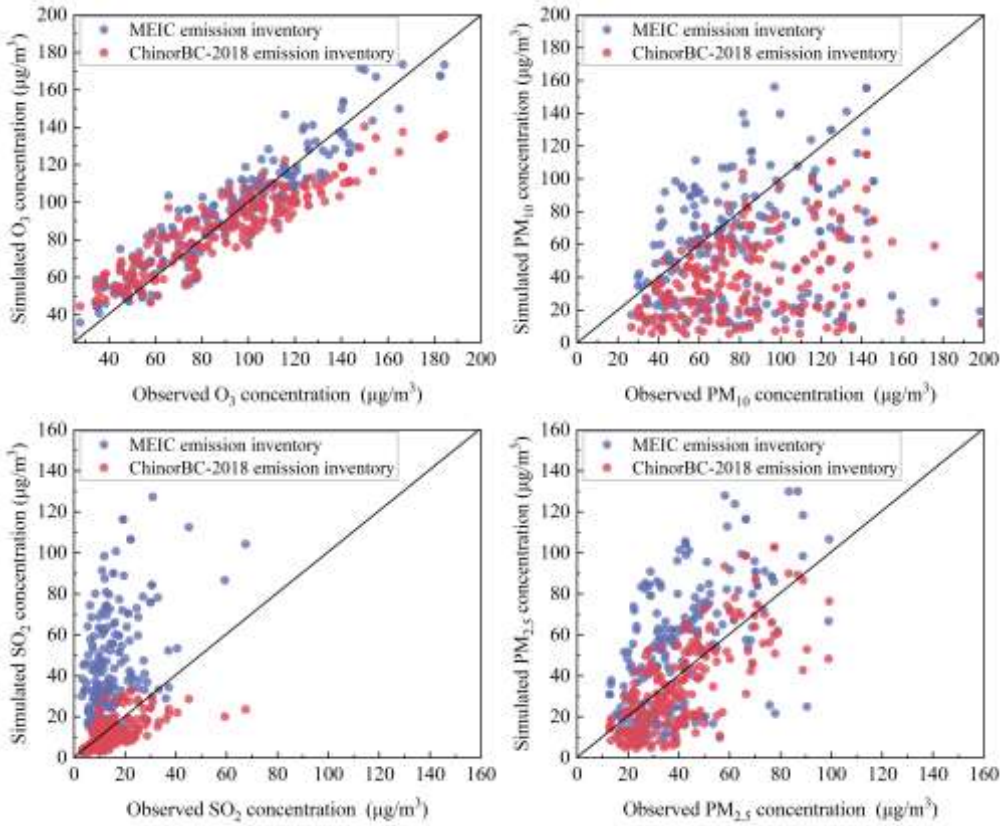

Figure 4-14 Change in monthly average simulated and observed BC/OC concentrations in 2018 for two emission inventories

Table 4-18 Model performance comparison of modelled and observed air pollutants over Northern China in 2018 for ChiNorBC 2018 and MEIC 2016 inventories

MEIC emission inventories				ChiNorBC -2018 emission inventory			
Species	NMB	NME	R	Species	NMB	NME	R
O_3	4%	18%	0.85	O_3	-4%	19%	0.85
$PM_{2.5}$	24%	62%	0.61	$PM_{2.5}$	-17%	43%	0.69
PM_{10}	-25%	52%	0.44	PM_{10}	-50%	56%	0.5
SO_2	206%	215%	0.56	SO_2	-19%	43%	0.69
NO_2	19%	36%	0.76	NO_2	-33%	37%	0.76
CO	-13%	43%	0.63	CO	-60%	60%	0.79
OC	161%	173%	0.59	OC	2%	50%	0.6
BC	169%	190%	0.53	BC	49%	78%	0.53

4.4.2 Simulated pollutant concentration situation

4.4.2.1 Seasonal variations for conventional pollutants

The simulated seasonal trends and spatial distribution of the conventional air pollutants (O_3, NO_2, SO_2, $PM_{2.5}$, PM_{10}) in 2018, based on the ChiNorBC -2018 emission inventory, are shown in **Figure 4-15-19**. For the simulated seasonal variation of SO_2 concentration (**Figure 4-15**). The results of the spatial distribution of the seasonal variation show that the distribution is approximately the same in winter and autumn, and similar in summer and spring. The areas with higher SO_2 concentrations are mainly concentrated in the more densely populated areas of

the city centres of the cities, with a more concentrated distribution than for the other pollutants. The increase in SO_2 concentrations is mainly due to emissions from thermal heating in residents, with the highest SO_2 concentrations occurring in winter, with a maximum concentration of approximately 96.8 μg/m^3 (Xinjiang). SO_2 concentrations in different seasons basically follow the order of spring < summer < autumn < winter, with maximum SO_2 concentrations of 43.8 μg/m^3, 47.6 μg/m^3, 68.8 μg/m^3 and 96.8 μg/m^3 in that order. The seasonal variation of SO_2 concentration in cities such as Ningxia and Tianjin are not significant, with the maximum seasonal SO_2 concentrations in Tianjin and Ningxia ranging from 14.4 μg/m^3-21.4 μg/m^3 and 23.9 μg/m^3-37.3 μg/m^3 respectively.

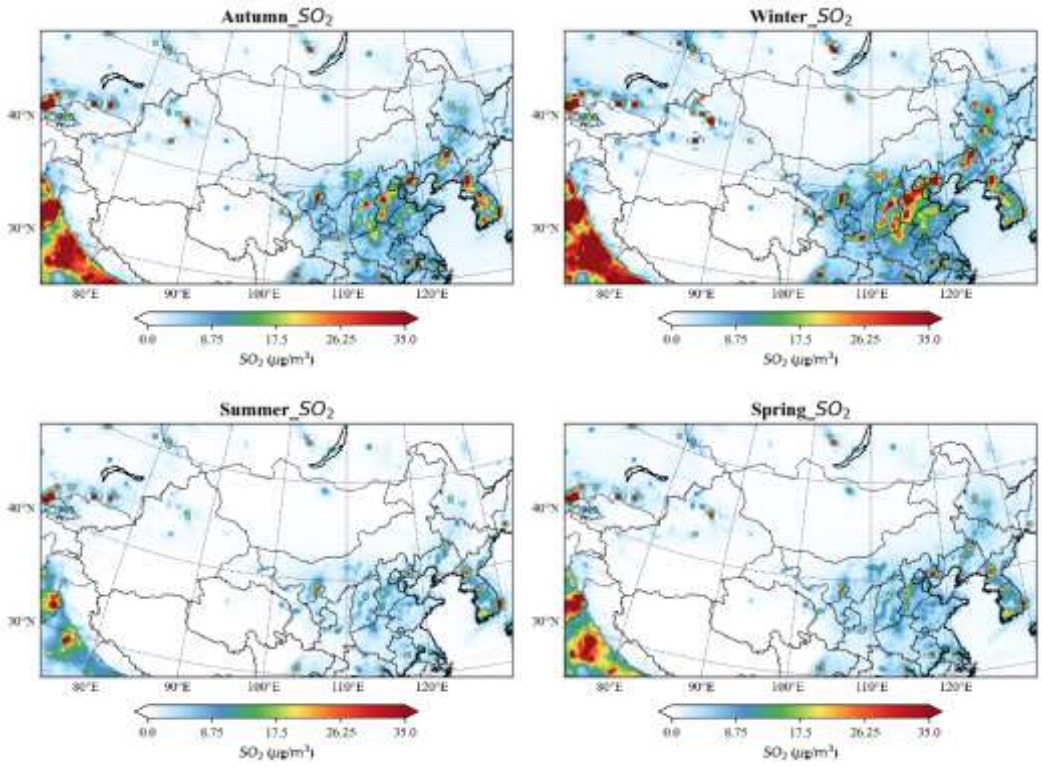

Figure 4-15 The spatial distribution of the simulated seasonal average concentrations of SO_2.

The seasonal variation of simulated NO_2 concentrations is shown in **Figure 4-16**. The results of the spatial distribution of seasonal variations show that the modelled NO_2 concentrations are approximately the same in winter and autumn, and similar in summer and spring, with higher NO_2 concentrations concentrated in Beijing, Tianjin, Hebei and the surrounding areas and the Yangtze River Delta, where the distribution is more concentrated in the main urban areas with high economic development and population than for other pollutants. Therefore, seasonal variations can vary between cities. Thus, the highest NO_2 concentrations occur in summer, with a maximum concentration of approximately 99.1 μg/m^3 (Liaoning). Seasonal variation in NO_2 concentrations varies between provinces, except for cities such as Liaoning, Tianjin, Ningxia, Jiangsu and Anhui; most cities have NO_2 concentrations in the order of summer < spring < autumn < winter. In general, the differences between the simulated NO_2 concentrations in autumn and winter are not significant in Northern China, for example, the maximum NO_2 concentrations in Beijing, Shandong and Henan are between 61.4 μg/m^3-63.5 μg/m^3, 52.8 μg/m^3-53.9 μg/m^3 and 55.4 μg/m^3-56.7 μg/m^3, respectively.

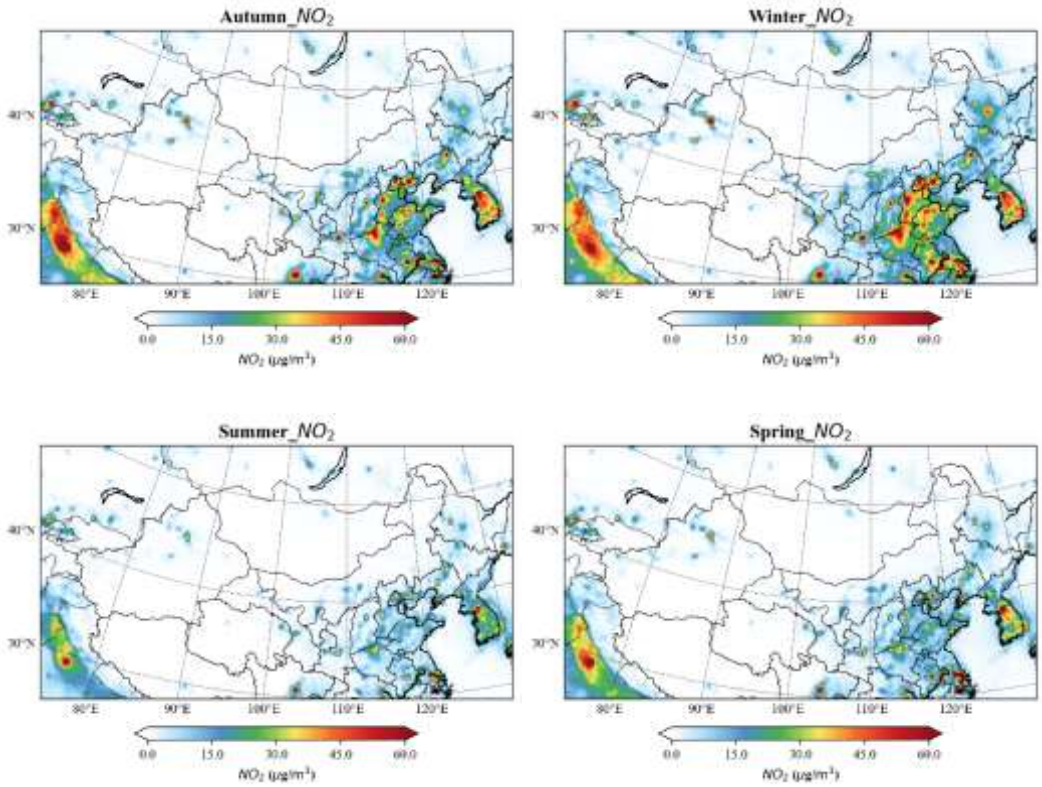

Figure 4-16 The spatial distribution of the simulated seasonal average concentrations of NO_2.

As shown in **Figure 4-17**, the seasonal variation of $PM_{2.5}$ concentrations in Northern China in 2018 shows that the spatial distribution of simulated $PM_{2.5}$ concentrations is similar in all seasons, with higher concentrations mainly concentrated in Beijing, Tianjin, Hebei and surrounding areas, and compared to the eastern regions, the simulated $PM_{2.5}$ concentrations are basically below 30 μg/m^3 in the northwestern regions due to the sparse population and smaller emissions, and even in winter, $PM_{2.5}$ simulated concentrations are also relatively small, with only concentrated higher concentrations occurring in some cities in central Xinjiang, with a maximum of around 167.4μg/m^3. Regional $PM_{2.5}$ simulated concentrations are typically highest in winter due to the use of fuel combustion for central heating in most northern regions and unfavorable meteorological conditions, such as low mixed boundary layer heights, and similarly, lower $PM_{2.5}$ concentrations in summer across China are mainly due to reduced anthropogenic emissions and favorable dispersion conditions for airborne pollutants. The seasonal ranking of $PM_{2.5}$ concentrations is: summer < spring < autumn < winter, with maximum $PM_{2.5}$ concentrations of 115.9 μg/m^3, 120.9 μg/m^3,192.4 μg/m^3 and 205.6 μg/m^3 for each season, respectively. The seasonal characteristics of $PM_{2.5}$ concentrations in each province also show some regional differences, unlike the seasonal variation in concentrations in other provinces, the simulated $PM_{2.5}$ concentrations in Jiangsu and Tianjin are the highest in spring, at 120.9μg/m^3 and 94.6μg/m^3 respectively. Hebei province is the province with higher $PM_{2.5}$ concentrations in all seasons throughout the northern region, with concentrations ranging from 102.9μg/m^3 to 205.6μg/m^3.

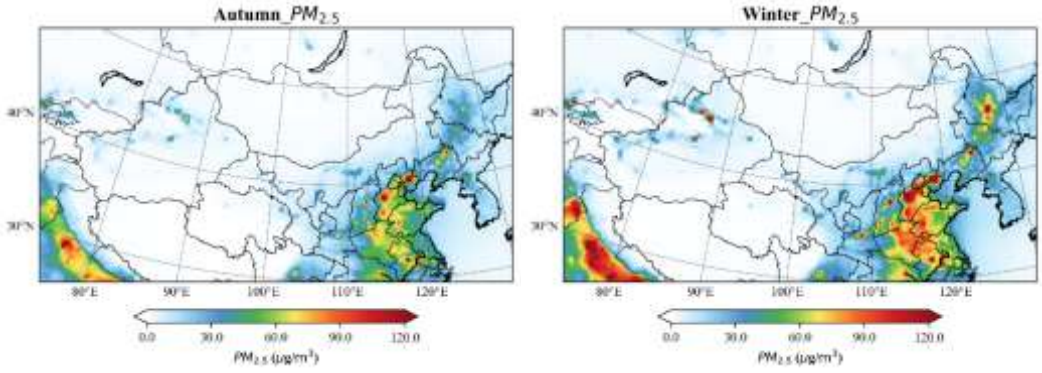

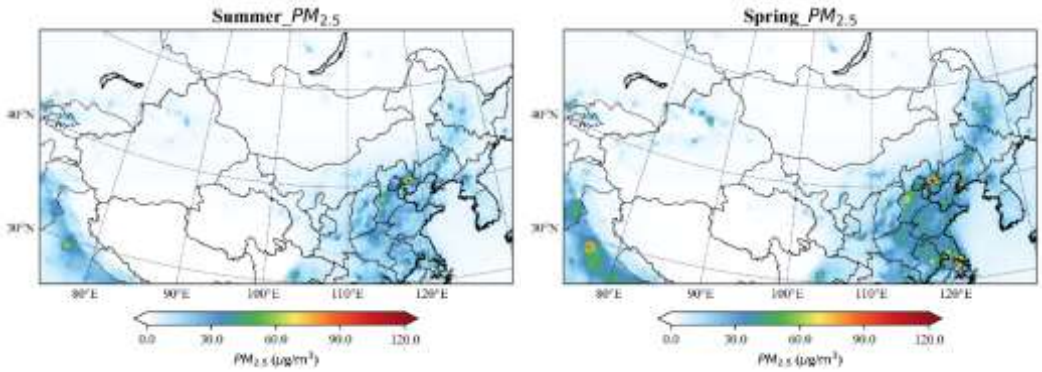

Figure 4-17 The spatial distribution of the simulated seasonal average concentrations of $PM_{2.5}$.

Like the seasonal variation of $PM_{2.5}$, the seasonal variation of the modelled PM_{10} concentration is also in the following order: summer < spring < autumn < winter, with the maximum PM_{10} concentration in each season being 141.2 μg/m^3, 144.9 μg/m^3, 226.7 μg/m^3 and 241.1 μg/m^3 respectively. Tianjin is at a high average concentration in all seasons, with average concentrations ranging from 41.2 μg/m^3 to 67.6 μg/m^3. Due to the lack of an emission inventory of dust and sand sources, the modelled PM_{10} concentrations in the north-western provinces of the country are at a low level, and although the maximum PM_{10} concentration in Xinjiang can reach 196.5 μg/m^3 in winter, there may be a certain degree of underestimation in spring, at 61.2 μg/m^3.

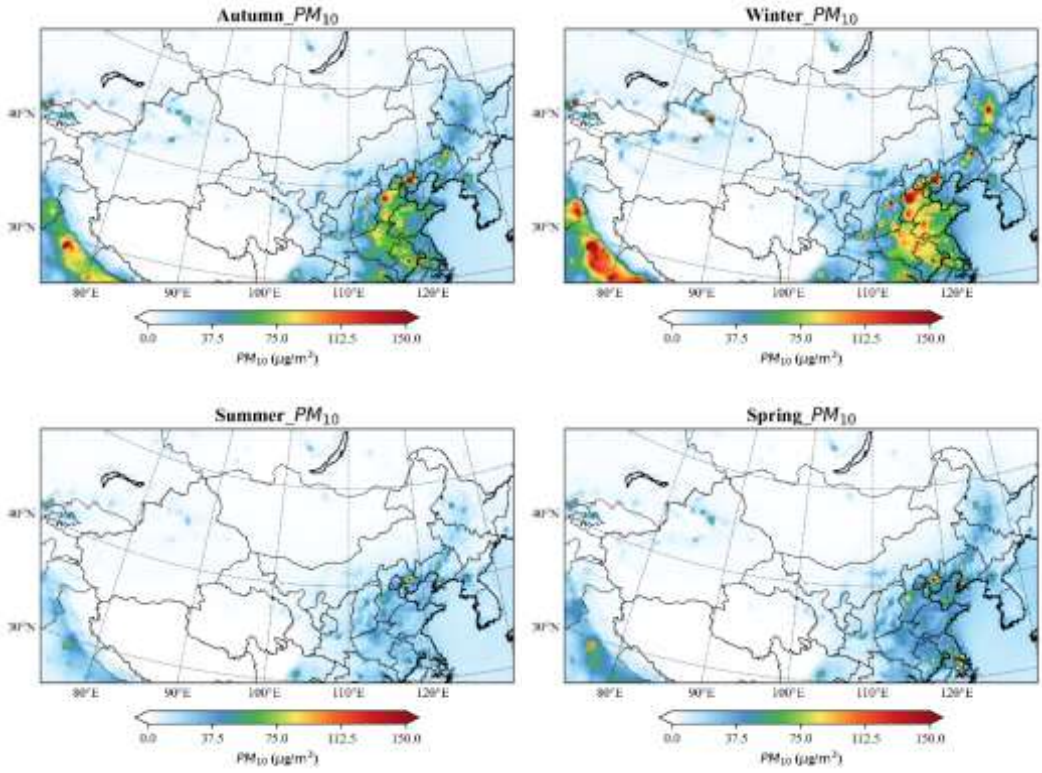

Figure 4-18 The spatial distribution of the simulated seasonal average concentrations of PM_{10}.

As shown in **Figure 4-19**, seasonal variations in ozone pollution are evident, with the highest seasonal mean O_3 occurring in the northern regions during the summer months, when high temperatures, low humidity and low wind speeds are favorable for near-surface O_3 formation, with high summer O_3 concentrations in eastern China, with a maximum concentration of approximately 137.6 μg/m^3 (Shanxi). In contrast to the other seasons, O_3 is higher in autumn and winter mainly in the northwest, with maximum concentrations of about 111.9 μg/m^3 and 112.9 μg/m^3 respectively (Xinjiang), and maximum O_3 concentrations do not vary significantly between regions in spring, with maximum O_3 concentrations ranging from 99.4 μg/m^3 to 119.7 μg/m^3, with higher O_3 concentrations mainly in suburban or remote northwestern areas. O_3 concentrations in the different seasons basically follow the order of

winter < autumn < spring < summer, with maximum O_3 concentrations of 111.9 μg/m^3, 112.9 μg/m^3, 119.7 μg/m^3, 137.6 μg/m^3 in that order.

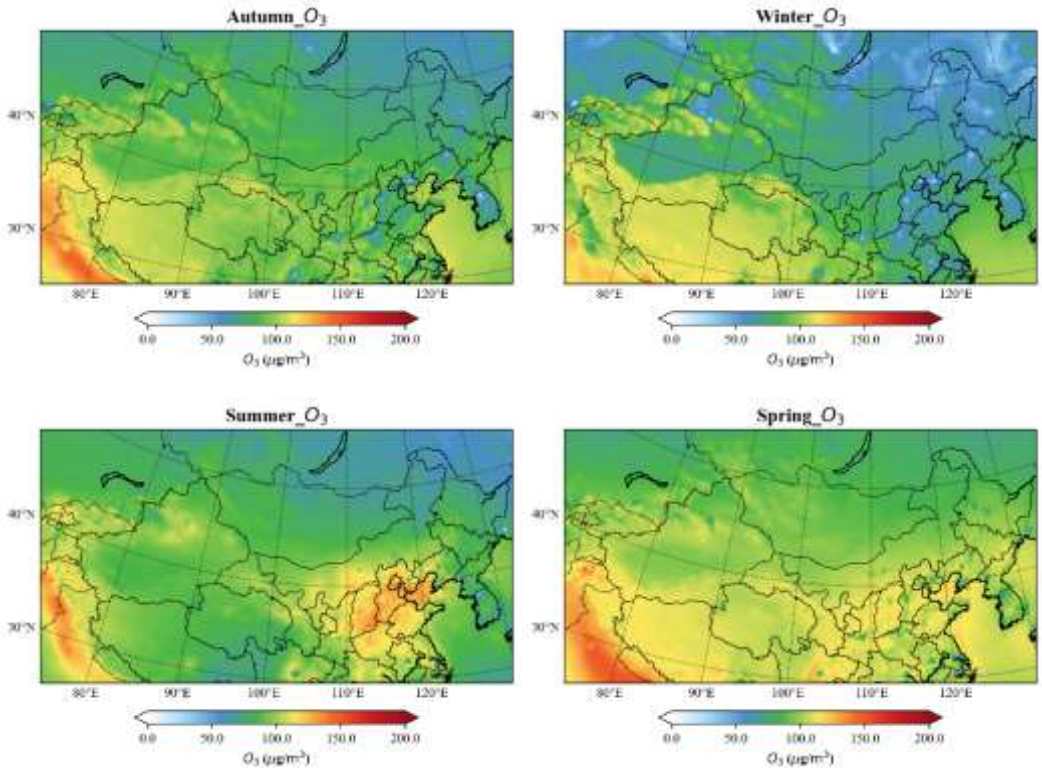

Figure 4-19 The spatial distribution of the simulated seasonal average concentrations of O_3.

4.4.2.2 BC and OC

Figure 4-20-21 shows the spatial distribution of the seasonal variation of BC, OC simulated by the model in 2018. Due to the similarity of carbon source emissions from fossil fuel and biomass combustion, the seasonal variation of simulated BC/OC concentrations is relatively similar, with simulated BC/OC concentrations showing a trend of high in autumn and winter and low in spring and summer, rising in the dry winter months and decreasing in the summer monsoon season. The highest simulated concentration of BC occurs in winter with a maximum of approximately 44.8 μg/m^3 (Xinjiang), and the highest modelled concentration of OC was also in winter, with a value of approximately 58.7 μg/m^3 (Xinjiang). The seasonal variations of simulated BC/OC concentrations were also in the same order: summer < spring < autumn < winter, with maximum BC concentrations of 13.0 μg/m^3, 13.2 μg/m^3, 16.4 μg/m^3, 44.8 μg/m^3 and maximum OC concentrations of 19.5 μg/m^3, 19.5 μg/m^3 and 44.8 μg/m^3 respectively.

The areas with higher BC/OC concentrations were mainly in areas with higher particulate matter emissions from anthropogenic sources. From the simulated spatial distribution trend of BC/OC, the BC/OC concentrations were higher in Beijing, Tianjin and Hebei and its surrounding areas, the eastern provinces and some cities in the northwest region, and the BC/OC concentrations were more widely distributed regionally. The seasonal characteristics of BC/OC concentrations in each province also show some regional differences, unlike the seasonal variation of concentrations in other provinces, the simulated BC/OC seasonal concentration values in Xinjiang, Heilongjiang and Shanxi vary significantly, with the maximum BC simulated seasonal concentrations ranging from 4.1 μg/m^3 - 44.8 μg/m^3, 7.3 μg/m^3 -34.2 μg/m^3 and 5.3 μg/m^3 - 33.0 μg/m^3, respectively, and the maximum OC simulated seasonal concentrations ranging The seasonal variation of BC/OC concentrations in Jiangsu and Anhui cities did not vary significantly, with BC modelled seasonal maximum concentrations ranging from 4.7 μg/m^3 - 7.4 μg/m^3 and 4.2 μg/m^3 - 10.9 μg/m^3, and OC modelled seasonal maximum concentrations ranging from 12.2 μg/m^3 - 20.7 μg/m^3 and 10.6 μg/m^3 - 25.0 μg/m^3, respectively.

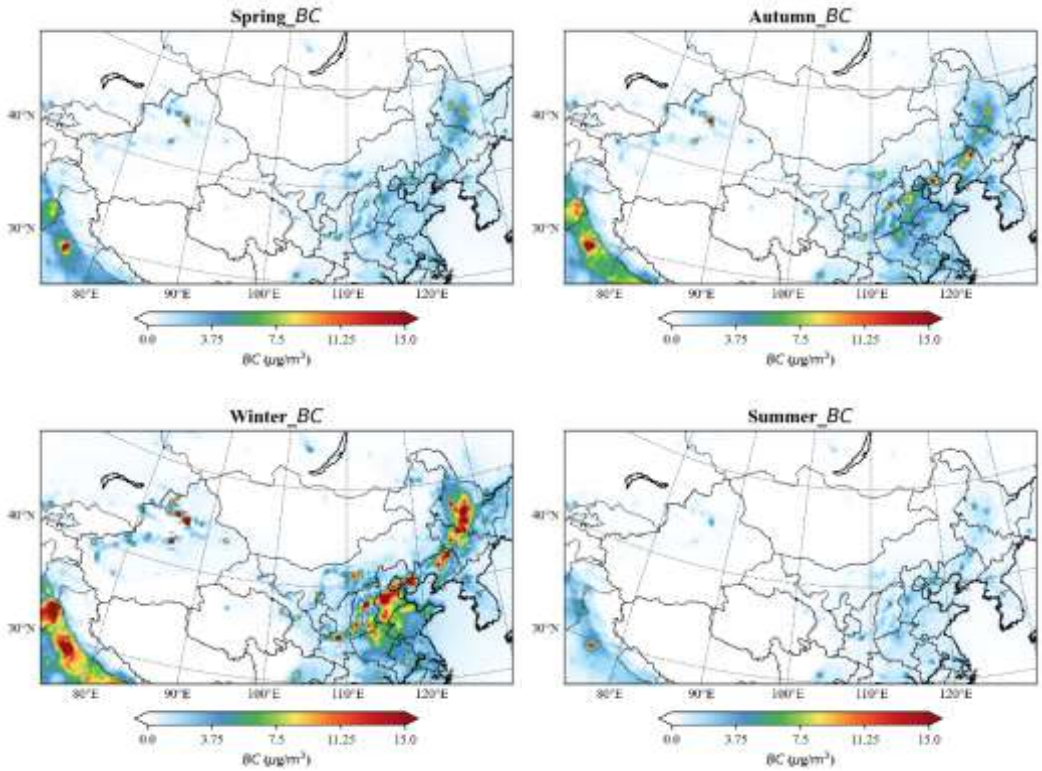

Figure 4-20 The spatial distribution of the simulated seasonal average concentrations of BC.

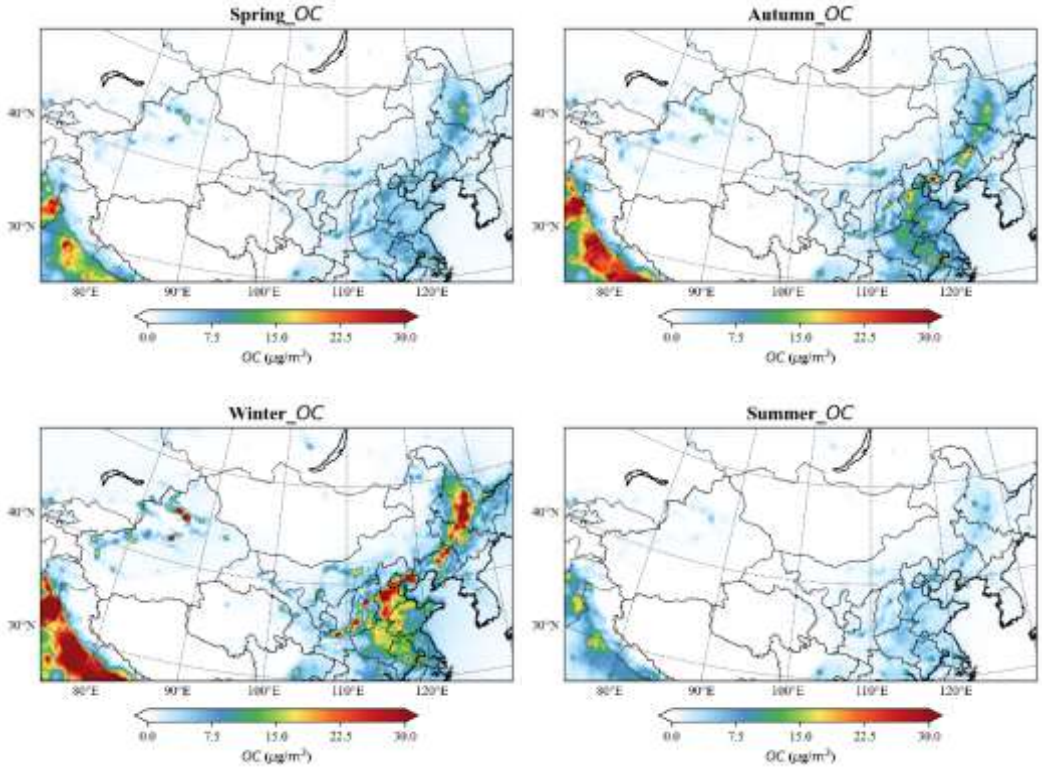

Figure 4-21 The spatial distribution of the simulated seasonal average concentrations of OC.

4.4.3 Simulation results under future emission scenarios

The emission reduction scenarios are divided into: business as usual scenario (BAU), strengthened end of pipe control scenario (EOP) and ambitious control scenario (ABC). Based on the changes in emissions of the five

pollutants SO_2, NO_x, $PM_{2.5}$, BC, and OC from 2018 to 2035 in the northern provinces of China provided in Output 5, we reduced the emissions of these pollutants based on the ChiNorBC-2018 anthropogenic source emission inventories provided in Output 2 to obtain emission inventories for the three scenarios, and conduct air quality simulations for the whole year using the 2018 meteorology as input conditions. **Figures 4-22-24** show the percentage change in modelled concentrations of different pollutants in Northern China for the three emission reduction scenarios. The decrease in the average concentration of each pollutant in 2035 compared to 2018 for the entire China and BTH region is shown in **Table A3**.

For the BAU emission reduction scenario, the regions with high reductions in simulated concentrations of BC, OC and $PM_{2.5}$ are mainly concentrated in the north-western regions, such as Xinjiang, Qinghai and Ningxia. The largest percentage decreases in pollutant concentrations were observed in Xinjiang, where the largest percentage decreases in annual average concentrations of BC, OC and $PM_{2.5}$ were approximately -49%, -44% and -43% compared to the baseline scenario. Most of the decreases in pollutant concentrations are regional, with higher decreases in SO_2 concentrations concentrated in areas such as Qinghai and Ningxia, and a slight increase in concentrations in Beijing, Tianjin and Hebei, mainly due to higher primary SO_2 emissions, with the largest decrease in concentrations in Qinghai province at -56%, and the largest increase in SO_2 concentrations in Jiangsu province, with a maximum increase of 8%. The modelled concentrations of NO_2 have decreased to some extent throughout Northern China, with the largest decreases occurring in the northwest (Qinghai and Ningxia provinces) and in eastern China in Shandong and Henan provinces, with the largest percentage decrease occurring in Gansu province, where the percentage decrease can reach -63%. The modelled concentrations of O_3 did not change much.

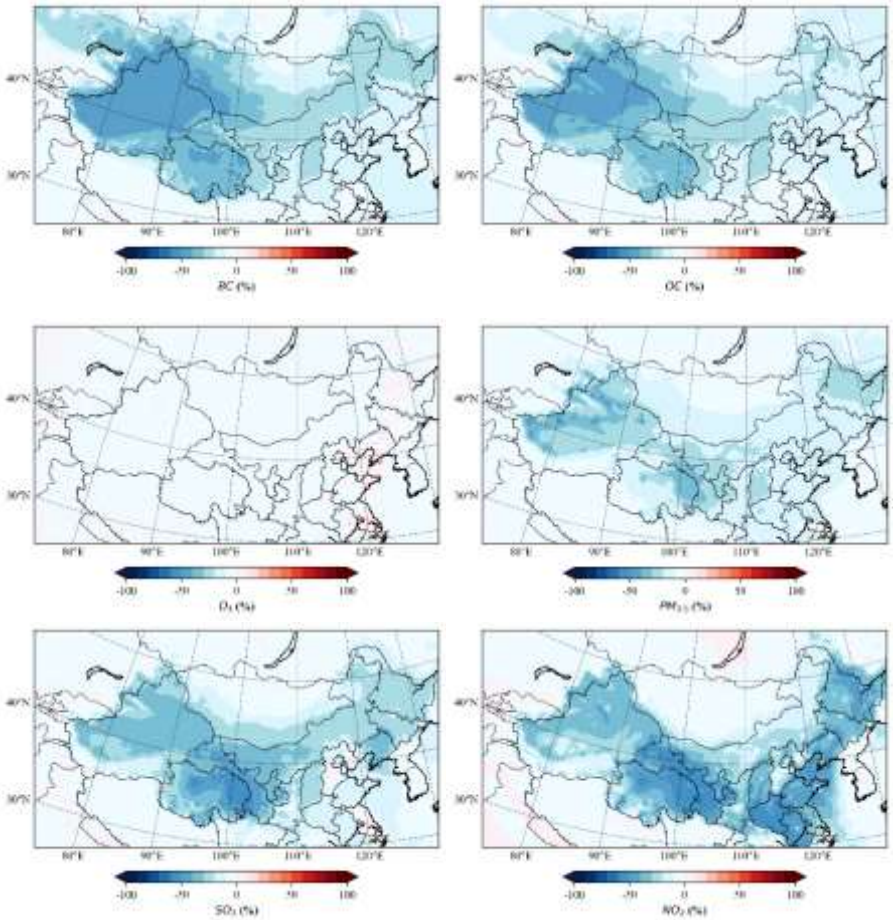

Figure 4-22 Spatial distribution of percentage change in air pollutant concentrations under BAU emission scenario.

For the EOP emission reduction scenario, except for O_3, the simulated concentrations of all pollutants show a decreasing trend in the overall region, with the regions with higher percentage decreases like the BAU reduction scenario. The largest percentage decreases in annual average concentrations of pollutants such as BC, OC and

$PM_{2.5}$ were observed in Shanxi, with the largest percentage decreases of -58%, -52% and -54%, while NO_2 concentrations showed a large decreasing trend throughout Northern China. The largest decreases in concentrations were mainly in the northwest of China (Qinghai and Ningxia provinces) and in the eastern provinces of Shandong, Henan, and Qinghai, with the largest percentage decrease occurring in Henan Province, where the percentage decrease could reach -64%; in most areas the percentage decrease was below -40%, with a smaller decrease in Ningxia, where the largest decrease was -29%. The simulated concentrations of O_3 did not change much, but increased in the east-central regions of Anhui, Liaoning, Tianjin, and Jiangsu, with O_3 concentrations in Anhui and Jiangsu increasing by 26%.

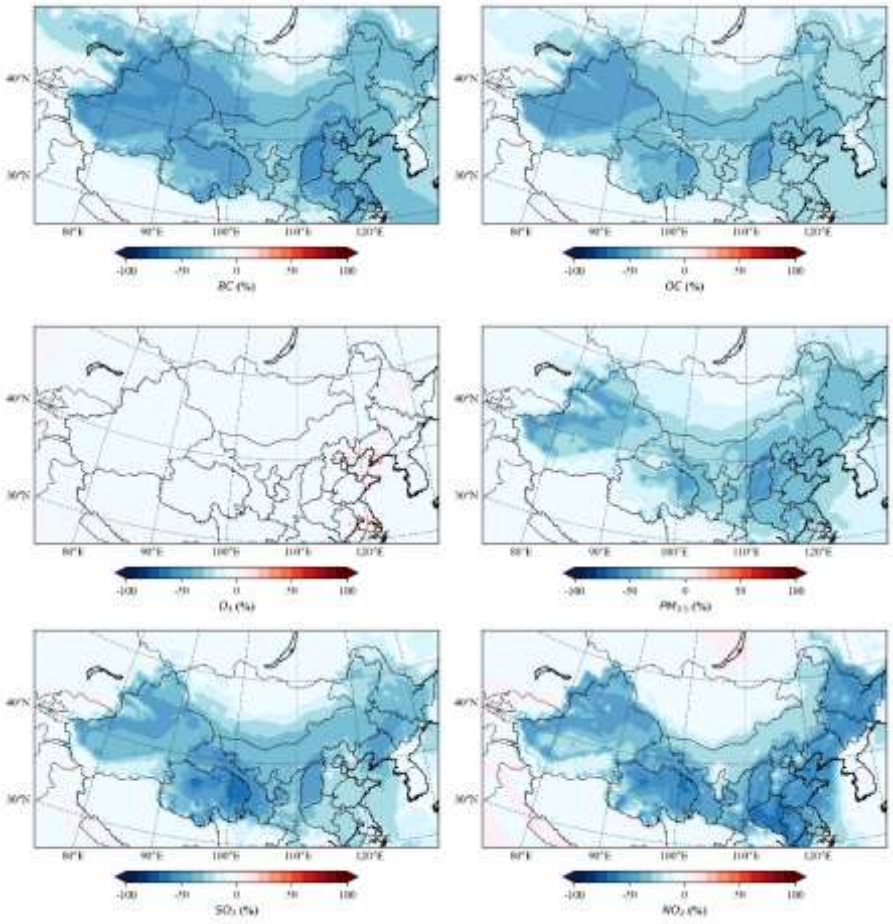

Figure 4-23 Spatial distribution of percentage change in air pollutant concentrations under EOP emission scenario.

The ABC emission reduction scenario shows the largest decrease in pollutant concentrations among the three reduction scenarios. The simulated concentrations of all pollutants, except O_3, show a decreasing trend in the overall region, and the average percentage decrease for each pollutant is below -20% than baseline scenario (ChiNorBC-2018). The increase in O_3 concentrations may be due to the reduction of NO_x emissions in the VOC-limited, which would cause O_3 concentrations to increase rather than decrease. The largest decrease in the modelled concentrations of $PM_{2.5}$ is also in Shanxi, with the largest percentage decrease of about -54%. The minimum value is about -37%, which is the largest percentage decrease in the concentration of all pollutants, where the largest decrease in concentration is mainly in the provinces of Shanxi, Jilin and Henan in eastern and northeastern China, with the largest percentage decrease in concentration occurring in Jilin, where the percentage decrease can reach -78%; the maximum percentage decrease in concentration in most areas is above -50%, and the area with a smaller percentage decrease is Ningxia, where the regional maximum The highest percentage decrease in SO_2 concentrations is concentrated in Qinghai and Ningxia, with the largest decrease of -66% in Qinghai Province, while the simulated O_3 concentrations also did not decrease much, but instead increased in central-eastern areas such as Anhui, Liaoning, Tianjin and Jiangsu, with a maximum increase of 39% in Jiangsu Province.

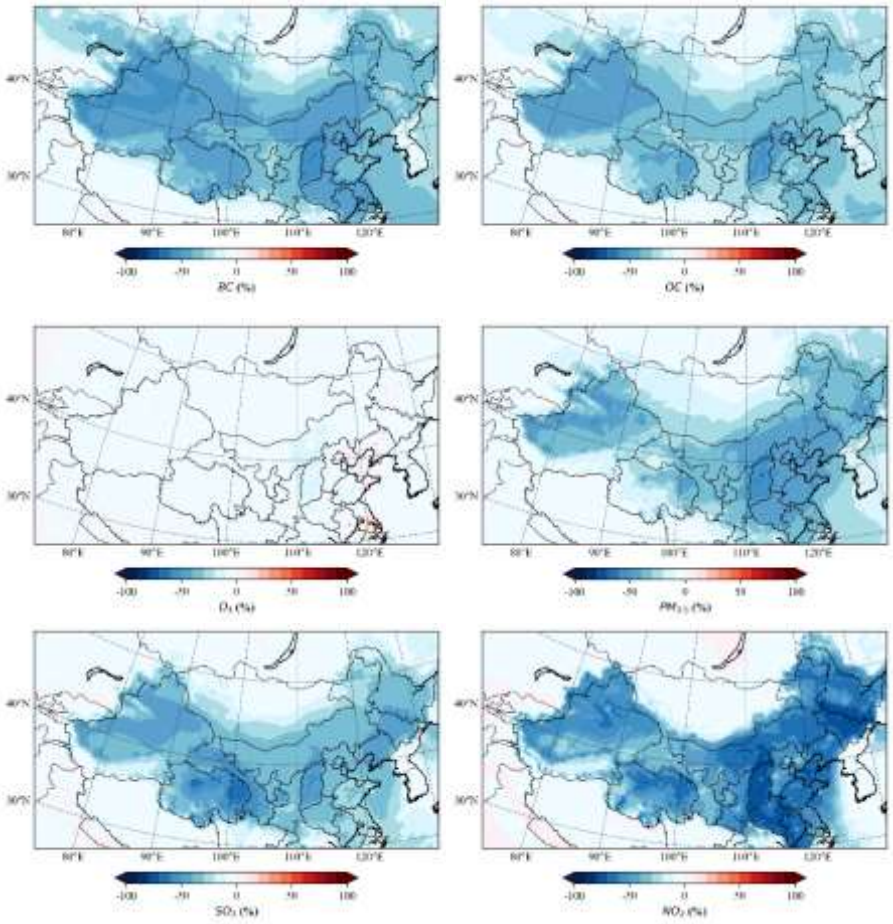

Figure 4-24 Spatial distribution of percentage change in air pollutant concentrations under ABC emission scenario.

4.4.4 Simulation results of future emissions scenarios for specific sectors

Considering the computational cost and time consumption of the simulation, we were not able to simulate the results of concentration changes under each emission reduction for the three emission scenarios simultaneously in a short period of time. In studying the simulated concentration changes of different pollutants in the specific sectors of emission reduction scenarios, only the BAU emission reduction scenario with the smallest percentage reduction of each pollutant among the three scenarios was simulated, so that we could obtain the simulation results as the "minimum" change in the simulated concentration of pollutants after the specific sectors of emission reduction. This also allows us to infer the approximate range of simulated pollutant concentration changes in the other two scenarios when the specific sectors pollutants are reduced.

For the BAU emission reduction scenario, Output 5 provides emission reduction percentages for BC and OC emissions from industrial, transportation and residential sources for three sectors in the northern provinces of China. These BC/OC emissions were reduced by sector based on the ChiNorBC -2018 anthropogenic source emission inventories provided in Output 2 to obtain emission inventories for the three sectoral emission reduction scenarios under the BAU emission reduction scenario, and air quality simulations were conducted for the whole year using the 2018 meteorology as input conditions. **Figures 4-25-27** show the percentage change in BC/OC pollutant concentrations for each sector under the BC/OC pollutant reduction ratio. Also shown is the maximum percentage reduction in BC/OC pollutant concentrations for each province in Northern China under the BC/OC pollutant emission reduction scenarios for different sectors (**Table 4-18**).

The spatial distribution of the percentage change in simulated concentrations for the abatement scenarios for each sector shows that the abatement scenarios for different sectors result in large variations in BC/OC concentrations. This is related to the differences in BC/OC emissions from primary particulate matter emissions in each sector.

The most significant decreases in simulated BC/OC concentrations are for the residential sector. The areas with large percentage decreases in concentrations are mainly in the northwestern regions of Xinjiang, Qinghai and Ningxia in the northwest, and Shanxi and Inner Mongolia in the central part of the country. According to the results in **Table 4-18**, the largest decrease in simulated BC concentrations for the residential source reduction scenario is in Xinjiang, with a maximum decrease of -47.7%, and the smallest decrease is in Anhui Province, with a maximum decrease of -4.5%. The smallest decrease was also in Anhui Province, with a maximum decrease of about -3.4%. The average percentage decrease in simulated BC/OC concentrations for the residential emission reduction scenario in Northern China was approximately -15.4% and -14.3% respectively.

The decrease in simulated BC/OC concentrations under the emission reduction scenario for industrial sources is smaller, with the larger percentage decrease in concentrations mainly in parts of Shanxi and Shandong in central-eastern China and Heilongjiang in northeastern China. According to **Table 4-18**, the largest decrease in simulated BC concentrations under the industrial source scenario is in Heilongjiang, with a maximum percentage decrease of approximately -10.9%; the smallest decrease is in Anhui, with a maximum percentage decrease of approximately -2.7%; the largest decrease in simulated OC concentrations is also in Heilongjiang, with a maximum percentage decrease of approximately -14.0%; the smallest decrease is also in Anhui, with a maximum percentage decrease of approximately -2.1%. The smallest decrease was also in Anhui Province, with a maximum decrease of about -2.1%. The average percentage decrease in simulated BC/OC concentrations for the industrial source reduction scenario in Northern China was approximately -2.7% and -1.9% respectively.

Like the industrial sources, the simulated BC/OC concentrations in the emission reduction scenarios for transport sources also decreased very little, with the larger percentage decreases occurring mainly in western China in areas such as Qinghai and Ningxia. According to the results in **Table 4-18**, the largest decrease in simulated BC concentrations under the transport source emission reduction scenario is in Qinghai, with a maximum percentage decrease of approximately -13.0%; the smallest decrease is in Jilin, with a maximum percentage decrease of approximately -2.4%. In Northern China, the percentage decrease in simulated OC concentrations under the transport source emission reduction scenario does not exceed -10%, with the largest decrease occurring in Qinghai, with a maximum decrease of -7.6%. The average percentage decrease in simulated BC/OC concentrations for the transport source emission reduction scenarios in Northern China is approximately -2.4% and -1.1% respectively.

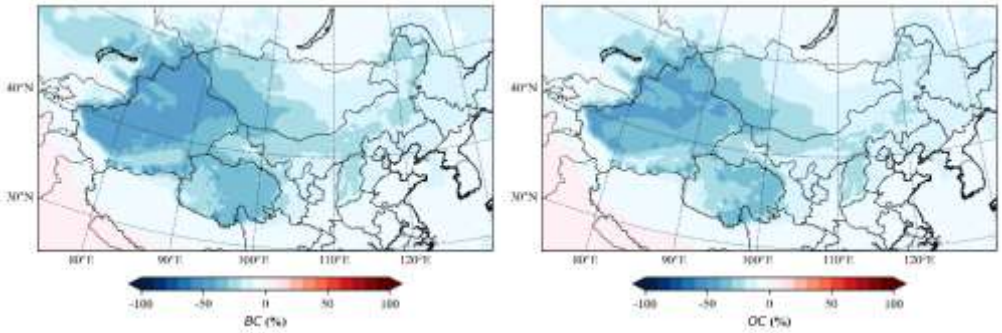

Figure 4-25 Spatial distribution of percentage change in BC/OC concentrations under residential emission reduction scenario.

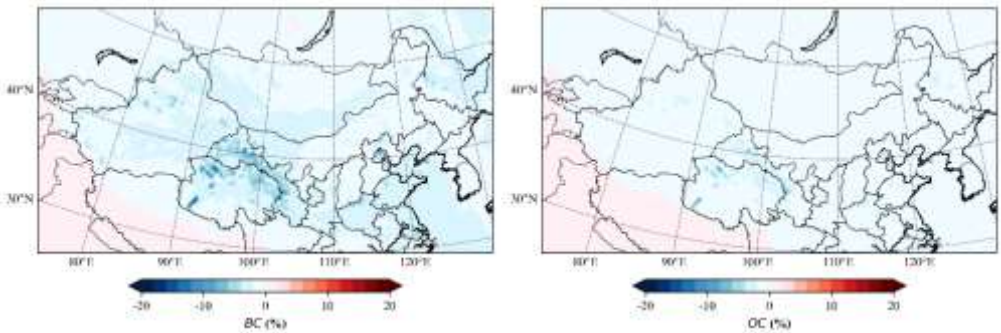

Figure 4-26 Spatial distribution of percentage change in BC/OC concentrations under transportation emission reduction scenario.

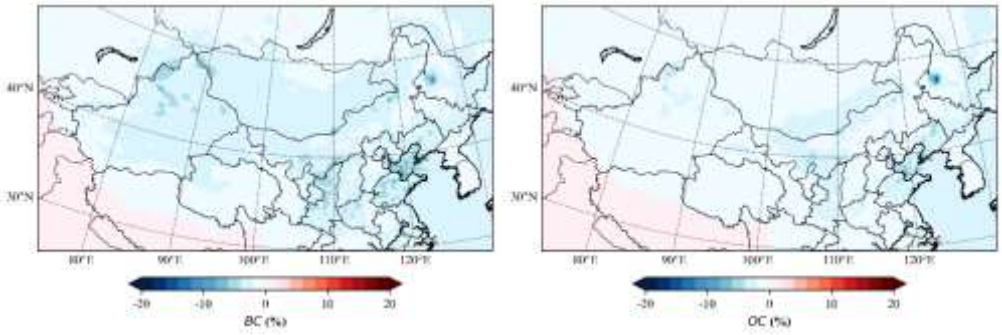

Figure 4-27 Spatial distribution of percentage change in BC/OC concentrations under industrial emission reduction scenario.

Table 4-19 Maximum percentage reduction in BC/OC concentrations for different sectors BAU emission reduction scenarios by province in Northern China

Province	BC			OC		
	Residential	Industry	Transportation	Residential	Industry	Transportation
Hebei	-22.4	-4.5	-2.6	-21.5	-3.5	-1.3
Heilongjiang	-21.3	-10.9	-5.3	-18.9	-14.0	-3.6
Inner Mongolia	-37.5	-7.4	-3.4	-34.2	-5.9	-2.2
Xinjiang	-47.7	-7.1	-6.0	-45.0	-4.5	-3.2
Jilin	-17.6	-3.4	-2.4	-15.8	-4.2	-1.4
Liaoning	-16.2	-4.9	-3.5	-15.3	-6.2	-2.1
Gansu	-38.2	-4.4	-9.9	-34.8	-2.8	-6.0
Beijing	-18.1	-3.4	-8.3	-18.8	-2.4	-4.0
Shanxi	-26.1	-3.8	-2.3	-26.0	-2.6	-1.2
Tianjin	-12.8	-7.8	-4.7	-11.9	-6.9	-2.3
Shaanxi	-15.1	-5.5	-2.6	-14.7	-4.1	-1.6
Ningxia	-18.0	-5.0	-2.3	-16.6	-5.6	-1.1
Qinghai	-43.3	-3.4	-13.0	-43.1	-2.0	-7.6
Shandong	-10.7	-9.6	-6.2	-9.5	-7.7	-3.3
Henan	-15.0	-4.8	-5.6	-14.8	-3.5	-3.2
Jiangsu	-6.7	-3.4	-5.3	-5.0	-3.2	-2.2
Anhui	-4.5	-2.7	-2.7	-3.4	-2.1	-1.1

4.5 Results from OsloCTM3 simulations

4.5.1 Simulated air pollution levels over China

Table 4.19 summarizes the annual, regional mean surface concentrations of the main aerosol species contributing to air pollution as simulated by the OsloCTM3 with year 2018 ChiNorBC2018 anthropogenic emissions. We note that these numbers also include contributions from open burning and natural biogenic emissions. Regional averages are calculated for two box regions, a broader China region (region A) and the Beijing-Tianjin-Hebei and surrounding areas (region B) as shown in **Figure 4-28.** The latter is chosen to cover the most populous and polluted areas.

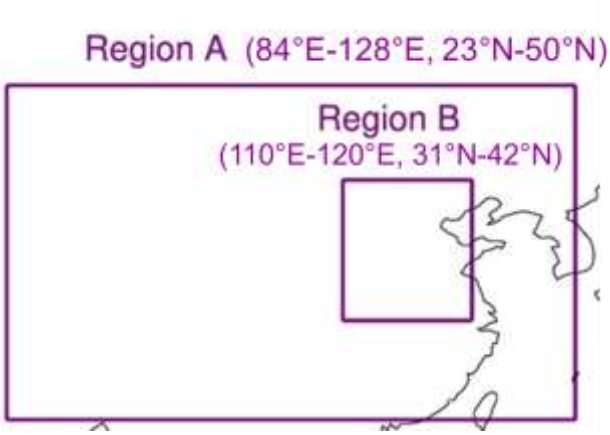

Figure 4-28 Geographical definition of the focus regions over which the pollution concentrations are averaged.

Table 4-20 Annual 2018 mean surface concentrations [μg/m^3] of aerosols from all sources, averaged over region A and region B

	BC	POA	SOA	SO_4	NO_3	NH_4	$PM_{2.5}$	$PM_{2.5\_anthro}$
Region A	1.1	4.1	0.6	1.3	1.1	0.8	27.8	8.9
Region B	3.0	9.0	0.9	2.0	3.6	1.8	39.3	20.5

Over region A, the OsloCTM3 simulates 1.1 μg/m^3 of BC and 4.1 μg/m^3 of organic aerosols, of which the primary emissions contribute 90%. For sulfate, nitrate, and ammonium aerosol we estimate annual mean concentrations of 1.3 μg/m^3, 1.1 μg/m^3, and 0.8 μg/m^3, respectively. In the more polluted region B region, average surface concentrations up to 9.0 μg/m^3 are found for POA. The ranking of the individual species in terms of magnitude is the same here as for the country-wide average, except for nitrate which is relatively more abundant than sulfate.

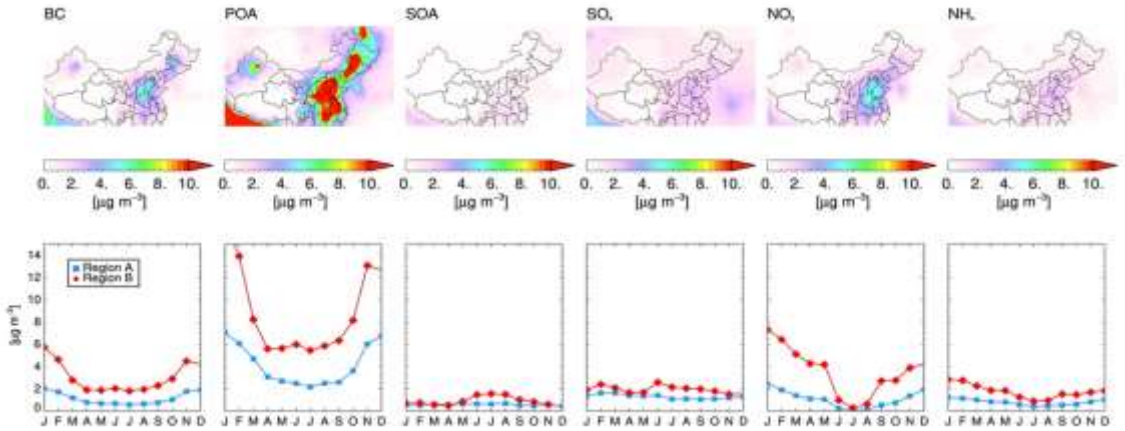

Figure 4-29 (top) Annual mean (2018) surface concentrations [μg/m3] of BC, primary organic aerosol, secondary organic aerosol, sulfate, nitrate and ammonium aerosol. (bottom) Corresponding monthly mean surface concentrations averaged over regions A and B.

The underlying spatial and seasonal distribution of the surface concentrations of individual aerosol species are shown in **Fig. 4-29**. The pollution hotspots, in particular to the northeast, are clearly reflected in the resulting concentrations. In these areas, concentrations reach more than 10 μg/m^3 for primary organic aerosols. However, in most of region A, concentrations between 1 and 5 μg/m^3 are seen. We note that concentrations can be influenced by long-range transport – in the case of China, primarily from India. However, previous studies have found local emissions to be the main contributor to pollution (Stjern et al. 2016).

For several species there are also clear seasonal variations, reflecting both seasonality in the underlying emissions but also in the chemistry, meteorology, and removal processes. In line with the emission seasonality, BC and POA concentrations are higher during winter. Additionally, this time of year often sees less removal by precipitation in many regions. SOA, which is mainly a result of VOC emissions from vegetation, is naturally higher in the summer. The formation of ammonium nitrate is a complex interplay between chemistry, emissions of NOx and NH_3, and competition with available SO_2. In particular, higher sulfate production during summer decreases the nitrate formation and hence contributes to the summertime minimum.

For air quality and health impacts, the exposure to the total amount of fine mode particles ($PM_{2.5}$) is important. In contrast to the CMAQ-CRAES, the OsloCTM3 does not simulate $PM_{2.5}$ directly. However, it can be quantified as the sum of the fine mode aerosol species, as shown in **Fig.4.30** and given in **Table 4.19**. Because $PM_{2.5}$ is heavily influenced by natural emissions of dust and, at least along the coast, sea salt, we also show $PM_{2.5}$_anthro, where these two species are excluded. While the total is what matters for health impacts, dust and sea salt are not easily mitigated and the latter is hence a useful indication of the fraction of the pollution at which policies can be targeted. We estimate regional, annual mean surface concentrations of 28 and 39 µg/m^3 over region A as a whole and region B, respectively, with the OsloCTM3 and the ChiNorBC2018 inventory. Here, the concentrations are highest over North Central China, showing the contribution from mineral dust to the atmospheric abundance of $PM_{2.5}$ (**Fig. 4.30**). Looking at $PM_{2.5}$_anthro, the regional, annual mean concentrations are 9 and 20 µg/m^3 over region A and B, respectively, with higher values during winter and lower during summer.

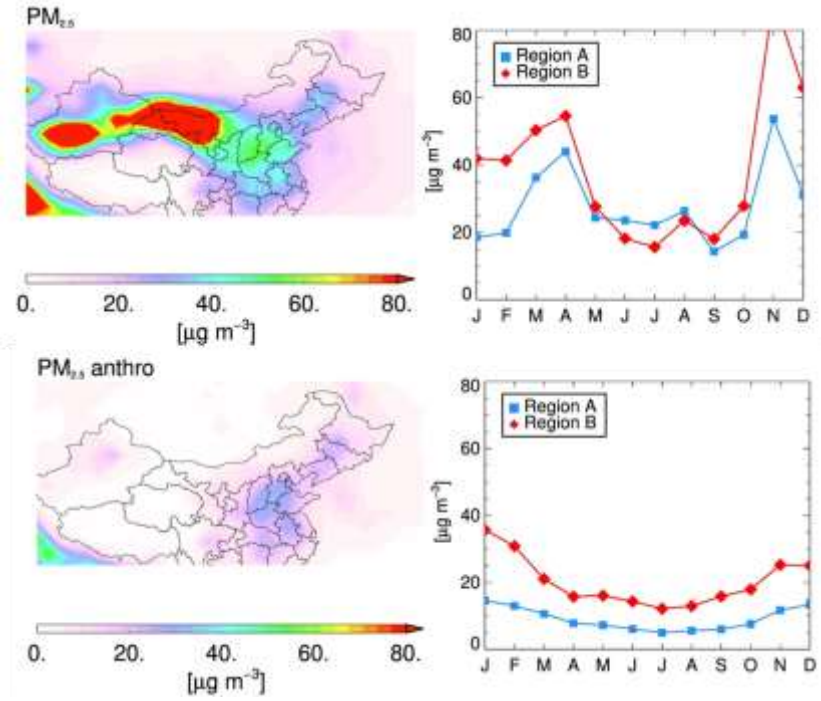

Figure 4-30 Annual and monthly mean concentrations [µg/m^3] of total $PM_{2.5}$ concentration (top) and anthropogenic $PM_{2.5}$ (bottom)

4.5.2 Comparison of results using ChiNorBC -2018 and CEDSv21 emissions

Here we compare the simulated aerosol concentrations obtained with the ChiNorBC -2018 emissions in China to corresponding results with year 2018 emissions from the CEDSv21 emission inventory. As described in **Sect. 4.3.3.3**, the ChiNorBC -2018 are generally lower than CEDSv21 in the region, and this is reflected in the resulting air pollution surface concentrations **(Fig 4-31)**. The differences in 2018 emissions are largest for NO_x, NH_3, and SO_2, and we find up to 30% lower regional mean surface concentrations of sulfate, nitrate, and ammonium aerosols. Smaller differences of around ±5% are found for BC concentrations, while differences in OC emissions result in approximately 10% more primary organic aerosol. For BC and OC, these smaller regional mean numbers are

influenced by spatially cancelling changes, i.e., concentrations are higher to the north and west with ChiNorBC -2018 than with CEDSv21, but lower to the south. Difference can be seen year-round, but for BC, POA, and nitrate are more pronounced during winter, showing the effect of the stronger seasonality in the ChiNorBC -2018 emissions than in CEDSv21. This comparison demonstrates the substantial differences that can arise from uncertainties and spread in underlying emission inventories. In Chapter 5 of this report, we explore whether these differences also influence estimates of radiative forcing.

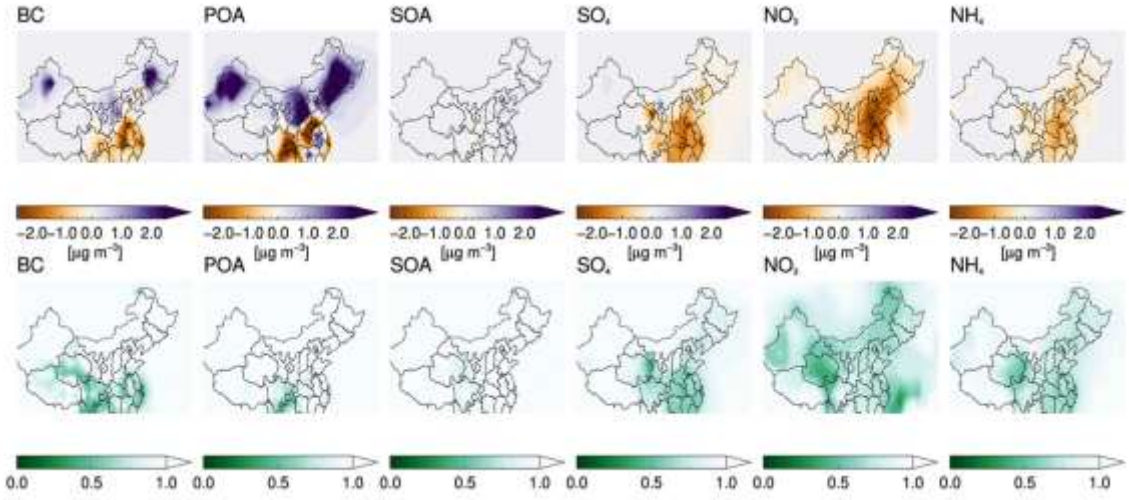

Figure 4-31 Difference in simulated annual mean aerosol concentrations between using ChiNorBC-2018 and CEDSv2021 emissions: (top) absolute difference [μg/m3], (bottom) ratio ChiNorBC-2018/CEDSv21

4.5.3 Comparison of model results with observations

Surface concentrations simulated with the OsloCTM3 are also compared with the corresponding observed concentrations (see Sect. 4.2 and 4.4.1 for details on measurements and statistics used). **Figure 4.32** shows scatter plots of the comparison for BC, OC and $PM_{2.5}$ for all stations, as simulated with the original and ChiNorBC -2018 emission inventories. **Table 4.20** summarizes the bias and correlation between modeled and observed concentrations. The model-measurement comparison shows that when using the using the CEDSv21, the OsloCTM3 overestimates the observed BC surface concentrations, in the lower range of the observations, with an NMB of more than 100% when considering all stations (**Table 4.20**). In contrast, both OC and $PM_{2.5}$ concentrations are underestimated, with a NMB of approximately -50%. Although the model continues to overestimate BC and underestimate OC, replacing CEDSv21 emissions with the ChiNorBC -2018 inventory significantly reduces the bias for both aerosol types. The correlation coefficient is also markedly higher with the ChiNorBC -2018 emissions. In addition to emission magnitude, some of the biases could be caused by issues with the spatial allocation of emission hot spots or challenges arising from the spatial coverage of measurement stations versus the quite coarse resolution of the model, a well-known problem (e.g. Schutgens et al. 2017; Wang et al. 2018). In contrast to BC and OC, switching to ChiNorBC -2018 exacerbates the underestimation of $PM_{2.5}$ concentrations. A similar finding was made by Lund et al. (2022) when switching from the first release of the CEDS emissions, known to be too high in East Asia, to the CEDSv21. A likely reason contributing to this is issues related to dust emissions or other natural sources. Specifically, so-called anthropogenic dust, from urban and agricultural areas, can contribute to $PM_{2.5}$, but are currently not represented in the OsloCTM3. We note that also for $PM_{2.5}$ the linear correlation is improved. Biases in sulfate and nitrate aerosols could also contribute to the biases in $PM_{2.5}$. While concurrent measurements are not available for these species, a previous study did suggest an underestimation of nitrate and sulfate in China, although for year 2010 emissions. We also show the comparison of the precursor gases SO_2 and NO_2. Again, the model underestimates observed concentrations, with both inventories. While an improvement is found for NO_2 with the ChiNorBC -2018 inventory, the underestimation of SO_2 is higher (although the correlation is higher). In the case of SO_2, this may seem somewhat surprising given that emissions are known to be too high in the CEDSv21. However, biases could also be affected by chemical and physical processes, such as formation and subsequent removal of sulfate aerosols from its precursor gas. Further observational data would be required to explore SO_2 and NO_2 biases in more detail.

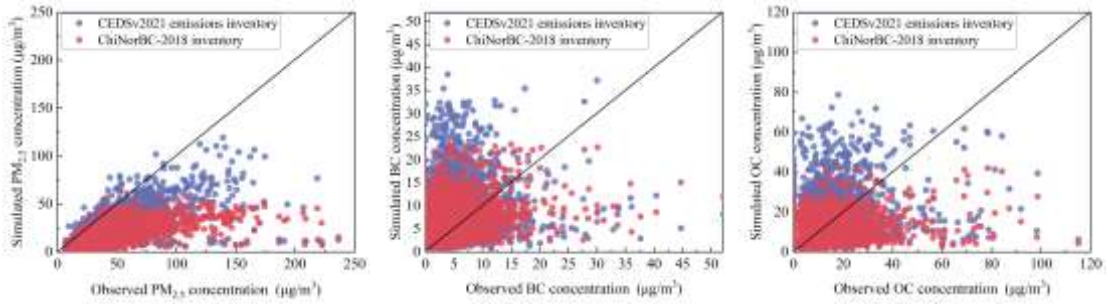

Figure 4-32 Scatter plots of modeled versus observed surface concentrations of BC, OC and $PM_{2.5}$ for the OsloCTM3.

Table 4-21 Statistics for model comparison with measured surface concentrations

CEDSv21 year 2018 emissions				ChiNorBC -2018 inventory			
Species	NMB	NME	R	Species	NMB	NME	R
BC	118%	141%	0.36	BC	30%	7%	0.71
OC	-49%	56%	0.52	OC	-22%	9%	0.51
$PM_{2.5}$	-47%	58%	0.29	$PM_{2.5}$	-63%	65%	0.53
SO_2	-12%	68%	0.23	SO_2	-33%	63%	0.44
NO_2	-42%	57%	0.25	NO_2	-21%	48%	0.46

4.5.4 Projected changes in air pollution

Figure 4-33 shows the result of the reductions in BC, OC, SO_2 and NO_2 emissions projected in year 2035 on annual mean surface concentrations in each of the three scenarios – Business as Usual (BAU), End of Pipe (EOP) and Ambitious Control scenario Ambitious Pollution Control (ABC) – produced in the project. For all species, under all three scenarios, the resulting surface concentrations are lower than the present-day, particularly to the north and east of the region. As expected, reductions are smallest in the BAU scenario and strongest in the ABC, with the largest change occurring between the BAU and EOP scenarios. In the latter, absolute reductions in annual mean surface concentrations of POA up to -0.8 μg/m^3 for region A and -3.6 μg/m^3 for region B are found (**Table 4-21**). These values correspond to 20% and 40% lower concentrations for regions A and B, respectively, in 2035 than in 2018 (**Table 4-22**). For BC, 30% and 45% reductions are estimated for both focus regions. Further strengthening of the mitigation measures in the ABC scenarios results in small additional reductions. There is also a small reduction in SOA: while there is no change in VOC emissions in these simulations, the formation of SOA forms through condensation of oxidation products on POA and is hence indirectly influenced by the reductions in anthropogenic OC emissions.

The changes in sulfate aerosols are relatively small in all three scenarios and mainly located around region B, where a 10% reduction in average surface concentration in 2035, relative to 2018, is estimated in EOP and ABC. By comparison, the difference between emissions scenarios resulted in a 30% lower mean concentration. Studies suggest that SO_2 emissions, the precursor for sulfate aerosols, have already been declining rapidly in China in recent years and the weaker projected changes for SO2 than for other species may indicate that there is limited potential for further reductions. Simulated changes in nitrate and ammonium aerosols on the order of 20-50% in region B, depending on scenario. NH_3 emissions are kept at the 2018 levels and results here are hence due only to declines in NO_x and SO_2 emissions.

We note that while the emission changes in the BAU scenario have little or no effect on global mean surface concentrations, reductions in Chinese emissions under the EOP and ABC scenarios are large enough to also give a notable global mean reduction of approximately 10% in BC and nitrate concentrations compared to year 2018 levels (not shown here).

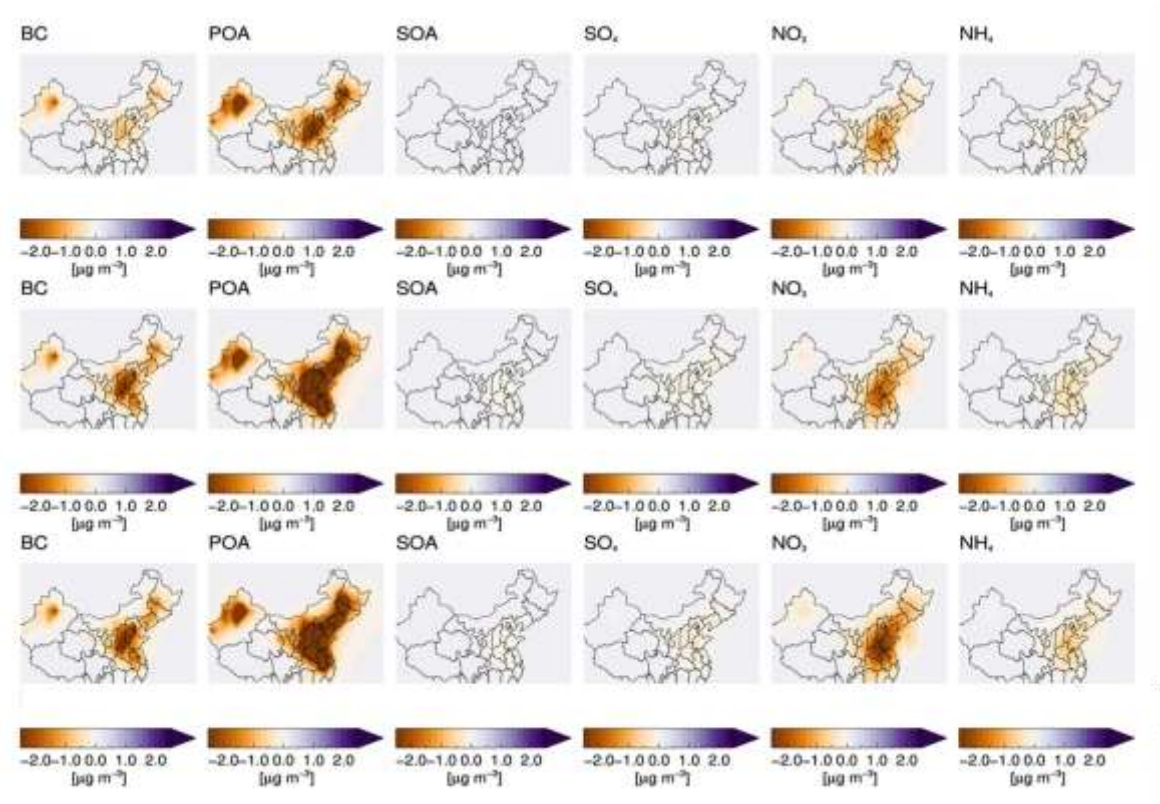

Figure 4-33 Absolute change in annual mean surface concentrations [μg/m3] of BC, POA, SOA, sulfate, nitrate and ammonium aerosols from 2018 to 2035 for each of the three scenarios (top: BAU, middle: EOP, bottom: ABC).

Table 4-22 Absolute difference in annual, regional mean surface concentrations [μg/m^3] of aerosols in 2035 compared to 2018 under each of the three emission scenarios developed in the project

	Region A			Region B		
	BAU	**EOP**	**ABC**	**BAU**	**EOP**	**ABC**
BC	-0.16	-0.31	-0.32	-0.54	-1.37	-1.48
POA	-0.46	-0.84	-0.88	-1.49	-3.64	-3.90
SOA	-0.01	-0.02	-0.03	-0.01	-0.1	-0.1
SO_4	-0.04	-0.07	-0.08	-0.1	-0.22	-0.26
NO_3	-0.24	-0.29	-0.39	-0.99	-1.25	-1.69
NH_4	-0.08	-0.11	-0.14	-0.32	-0.44	-0.58
$PM_{2.5}$	-0.9	-1.5	-1.7	-3.8	-7.4	-8.4
$PM_{2.5\ anthro}$	-1.0	-1.6	-1.8	-3.5	-7.0	-8.0

Table 4-23 Ratio of 2035 and 2018 annual, regional mean surface concentrations of aerosols under each of the three emission scenarios developed in the project

	Region A			Region B		
	BAU	**EOP**	**ABC**	**BAU**	**EOP**	**ABC**
BC	0.9	0.7	0.7	0.8	0.5	0.5
POA	0.9	0.8	0.8	0.8	0.6	0.6
SOA	1	1	1	1	0.9	0.9
SO_4	0.97	0.95	0.9	0.95	0.9	0.9
NO_3	0.8	0.7	0.6	0.7	0.6	0.5

NH_4	0.9	0.9	0.8	0.8	0.7	0.7
$PM_{2.5}$	0.97	0.94	0.94	0.9	0.8	0.8
$PM_{2.5\ anthro}$	0.9	0.8	0.8	0.8	0.7	0.6

The combined effect of reduction in individual aerosol species is a 6% lower $PM_{2.5}$ surface concentration over China as a whole and 20% lower in region B region under the EOP and ABC scenarios (**Table 4-22**), corresponding to approximately -1.5 μg/m^3 and -7 μg/m^3, respectively (**Table 4-21**). As seen from **Fig. 4-34**, this reduction also primarily occurs in region B, with additional peaks in reductions to the northeast and northwest.

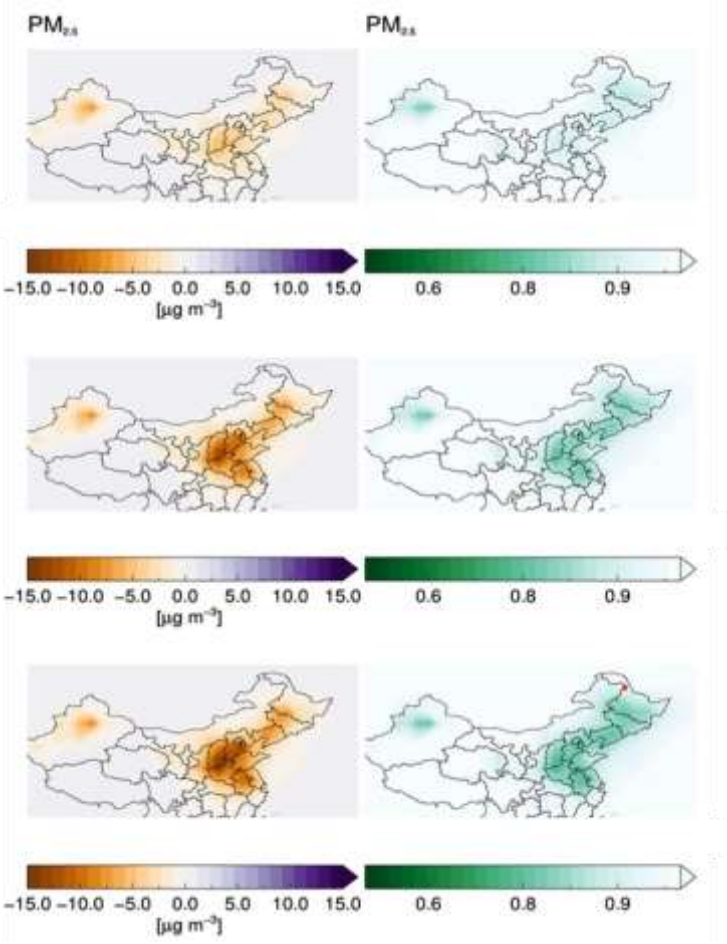

Figure 4-34 Absolute change in annual mean surface concentrations [μg/m^3] of $PM_{2.5}$ from 2018 to 2035 for each of the three scenarios (top: BAU, middle: EOP, bottom: ABC). Right column shows corresponding ratio between 2035 and 2018 concentrations.

Interactions between climate and atmospheric chemistry exist that can influence the change in pollution concentrations, for instance through changes in temperature, stability of the atmosphere or transport and precipitation patterns. As the meteorology is kept constant in all simulations, such effects are not captured here and would require additional investigations using other models than offline CTMs.

4.6 Summary

We applied the 3D air quality model CMAQ and the global OsloCTM3 to simulate the air pollution conditions in the Northern region of China throughout 2018 with three different emission inventories. Model performance, seasonal variations, and trends in air pollutant concentrations for a wide range of air pollutants were assessed. In

addition, we estimated the changes in air quality concentrations between 2018 and 2035 for three scenarios developed in the ChiNorBC project.

Our results with the CMAQ model confirm that the air quality model simulation performance under the ChiNorBC -2018 emissions has improved considerably, especially for BC/OC, with model performance statistics decreasing from 161% and 173% to 2% and 50% for NMB and NME, respectively, for OC; and from 169% and 190% to 49% and 78% for NMB and NME, respectively, for BC, compared to monitoring data. In addition, the overestimation of modelling results for other pollutants has been well improved, for example, the NMB for SO_2 has decreased from 206% to -19% of the baseline inventory. An improved model performance in terms of surface concentrations of BC and OC in most polluted region is also found for the OsloCTM3 when switching from CEDSv21 emissions to ChiNorBC-2018. However, lower ChiNorBC ChiNorBC -2018 emissions exacerbate the underestimation of simulated $PM_{2.5}$ surface concentration. A likely contributing reason is that too high anthropogenic emissions in CEDSv21 has masked an underestimation of dust or other natural aerosol and precursor emissions.

The results of the seasonal variation of air quality in Northern China in 2018, simulated using the ChiNorBC-2018 emission inventory, show that the concentrations of atmospheric pollutants exhibit clear seasonal variations. The highest pollution mostly occurs during winter and the best air quality in summer, except for O_3. The seasonal variations can be attributed to climate and human activities. The stable vertical structure of the atmosphere weakens the turbulent exchange of the atmosphere and hinders the vertical dispersion and dilution of air pollutants, which favors the accumulation of pollutants in localized areas with low wind speeds in winter. Elevated particulate matter may be due to increased plant burning in winter. The main contribution of organic and elemental carbon associated with motor vehicles is also likely to be larger during winter.

For the different emission reduction scenarios (BAU, EOP, ABC), the more pronounced decrease in pollutant concentrations is seen in the ABC emission reduction scenario, which is related to the amount of decrease in pollutant emissions, e.g., the BAU emission reduction scenario causes some increase in simulated SO_2 concentrations due to the increase in SO_2 emissions in some areas. The reduction scenarios for each sector also show the same modelling findings, with the simulated BC/OC concentrations from residential sources decreasing the most (-47.7% and -45.0% decrease) in the simulated BC/OC reduction scenarios for each sector, due to the high proportion of BC/OC emissions from residential sources. Although there may be uncertainties in our modelling results, particularly from emission inventories, the findings of this work are still relevant both in air quality modelling air quality impacts and in assessment.

5 Evaluation of the climate effects

Authors: Marianne Tronstad Lund (CICERO) (Rev.Ed. Jan S. Fuglestvedt, Bjørn H. Samset (CICERO))

5.1 Background and scope

Aerosols play a key role in shaping regional climate, as well as for anthropogenic climate change, due to their perturbations to the Earth's energy budget and hydrological cycle. Globally, the combined effect of aerosols is a negative effective radiative forcing (ERF[13]) estimated to be -1.3 W m^{-2} over the industrial era (year 1750-2014 (Forster et al. 2021). Although the uncertainty surrounding this estimate is significant (ranging from -2.0 to -0.6 W m^{-2}), aerosol cooling has thus masked a significant fraction of the greenhouse gas induced warming to date.

The climate effects arise through several mechanisms. Firstly, aerosols scatter and absorb incoming solar radiation, perturbing the Earth's energy balance and causing a cooling and warming of the surface and atmosphere, respectively. This effect is referred to as the direct radiative forcing (RF) or aerosol-radiation RF (RFari). In high latitude or mountainous regions, the deposition of aerosols on snow and ice can additionally result in increased absorption of sunlight at the surface, and hence increased warming. Scattering aerosols include sulfate (SO_4), nitrate (NO_3), sea salt and organic aerosols (OA, including primary organic carbon - OC). Black carbon (BC) is the most strongly absorbing aerosol, with secondary contributions from dust and the absorbing fraction of OA (so-called brown carbon). Secondly, aerosols change the characteristics of clouds: the particles act as additional nuclei for formation of cloud droplet, leading to more but smaller droplets. This in turn results in a higher cloud albedo, i.e. more sunlight reflected back to space and hence a cooling climate effect. Further to this, more and smaller droplets can also result in clouds that last longer without precipitating, adding an additional cooling contribution. Absorbing aerosols can, under the right conditions, contribute to fewer clouds by heating the atmosphere. On a global scale, this indirect RF, or aerosol-cloud RF (RFaci), contributes most to the total aerosol ERF (approximately 75% according to the most recent assessment by the Intergovernmental Panel on Climate Change (IPCC) (Forster et al. 2021).

Aerosols can affect the hydrological cycle both directly through changes in the atmospheric energy budget and clouds, and indirectly through changes in the surface temperature and subsequent evaporation. Due to their short atmospheric residence time, the aerosol-induced heating and cooling is spatially heterogeneous. This uneven distribution can further drive dynamical changes in atmosphere and ocean, and hence regional shifts in precipitation. For instance, scientific studies suggest that anthropogenic aerosol has weakened the summer monsoon over South and East Asia. Aerosols can also influence land and ocean ecosystems, as well as the carbon cycle, directly through changing the fraction of so-called diffuse radiation and through deposition of nutrients, and indirectly through changes to meteorology and climate. The overall effects on the global carbon cycle are, however, highly uncertain (Szopa et al. 2021).

In the ChiNorBC project, the quantification of the effects of BC, OA and other relevant aerosol species on climate is primarily focused on radiative forcing. Here we include both RFari and RFaci, but not the forcing due to deposition of absorbing aerosols on snow and ice. Furthermore, RFaci accounts only for the cloud-albedo effect, not the cloud-lifetime change. Additionally, we provide first-order estimates of the impacts of emissions in China on global-mean temperature and provide a set of emission metrics for potential further assessment beyond the project. Hydrological or ecosystems impacts are not assessed, and we note that we do not account for possible feedbacks due to underlying climate change on the aerosol distributions and their impact. While such effects can be important for a comprehensive understanding of the implications of emission changes, they require further studies using different modeling tools.

[13] Radiative forcing is a measure of the change in the net energy flux at the top of the atmosphere due to an imposed perturbation, such as changes in greenhouse gas or aerosol concentrations and is measured in watts per meter squared. The *effective* radiative forcing additionally includes the rapid adjustments in e.g. cloud and vertical temperature gradient that results from the initial energy balance disturbance (Forster et al. 2021).

5.2 Quantifying aerosol climate effects

5.2.1 AOD and radiative forcing

While local air quality concerns are primarily related to the abundance of aerosols and other pollutants closest to the surface, the vertical distribution and total amount of particles through the atmosphere (also referred to as atmospheric burden) matter for their impact on the energy budget. The three dimensional, three-hourly concentrations from the OsloCTM3 (see Ch.4, Sect.4.3.2) are input to radiative transfer calculations. Radiative transfer is the quantification of the distribution of energy in the atmosphere and how extinction, absorption, and scattering by aerosols influence the energy propagation. The resulting radiative effect depends on numerous factors, including aerosol optical properties, clouds, surface properties, solar angle, and meteorological conditions.

From these calculations, we derive the (all-sky) total aerosol optical depth (AOD)[14] and the radiative forcing due to changes in anthropogenic aerosols. More specifically, we calculate the instantaneous top-of-the-atmosphere radiative forcing due to aerosol–radiation interactions (RFari) with a multistream model using the discrete ordinate method (Stamnes et al., 1988; Myhre et al. 2013). This model has been used in several studies of anthropogenic emission changes, with recent examples including Lund et al. (2018; 2022), Myhre et al. (2017), and Samset et al. (2019). We refer to the literature for details on assumptions about optical properties for different aerosol species. The same radiative transfer model is used to provide an estimate of the radiative forcing of aerosol–cloud interactions (RFaci). To account for the key process, the change in cloud droplet concentration resulting from anthropogenic aerosols, a formulation developed based on satellite measurements and model fitting by Quaas et al. (2006) is used.

5.2.2 Emission metrics and global mean temperature response

Emission metrics are used to quantify and compare contributions to climate change caused by emissions of different gases. The two most commonly used emission metrics are the Global Warming Potential (GWP) (Houghton et al., 1990) and Global Temperature change Potential (GTP) (Shine et al. 2005). Metrics can be given in absolute terms or normalized by a reference gas, most commonly CO_2. In this normalized form, metrics are used to place the effects of different species on a common CO_2-equivalent scale, by multiplying the chosen metric with the respective emission.

In contrast to the well-mixed greenhouse gases, the climate impact of equal emissions of short-lived climate forcers, such as aerosols, can be different depending on where the emission occurs. Therefore, region-specific GWP and GTP values are sometimes calculated (Aamaas et al. 2016, Lund et al. 2020; 2017), i.e. the global mean climate effects of regional emissions. In the ChiNorBC project, we present updated GWP and GTP values that are specific to emissions of aerosols and precursors that occur in China. We also use the absolute form of the GTP to quantify the global mean temperature response to over time to Chinese emissions of BC and OC, as well as NOx and SO_2. The methods to calculate absolute and normalized metrics are well established and described in detail in the literature (Aamaas et al., 2013; Fuglestvedt et al., 2010; Shine et al., 2005; Myhre et al. 2013). Here we give a brief overview:

The absolute GWP (AGWP) is defined as the time-integrated RF following an emission pulse, i.e., an instantaneous one-off emission. For species i, the AGWP and GWP are given by:

$$AGWP_i(H) = \int_{t=0}^{H} F_i(t)dt \quad (1)$$

[14] Aerosol optical depth (AOD) measures the extinction of a ray of sunlight as it passes through the atmosphere and is hence a quantitative of the amount of aerosol present in the atmosphere, taking into account their different optical properties.

$$GWP_i(H) = AGWP_i(H)/AGWP_{CO2}(H)$$

(2)

where F is the radiative efficiency (W m^{-2} kg^{-1}) and H is the time horizon over which the effect is evaluated.

The AGTP gives the global mean surface temperature response per kg emitted as a function of time following an emission pulse. At time H after the emission, the AGTP and GTP for species i is given by:

$$AGTP_i(H) = \int_{t=0}^{H} F_i(t) IRF_T(H-t)dt \quad (3)$$

where F is the radiative efficiency and IRF is the impulse response function used to estimate the temperature response to a given radiative forcing:

$$IRF(t) = \lambda \sum_{j=1}^{J} \frac{c_j}{d_j} \exp\left(-\frac{t}{d_j}\right) \quad (4)$$

Here, c_j and d_j are constants and timescales, respectively, representing the response of the climate system over time, and lambda is the equilibrium climate sensitivity (ECS)[15]. Here we use values of c_j, d_j and lambda from Geoffroy et al. (2013), consistent with recent literature (Lund et al. 2020, Szopa et al. 2021). This yields an ECS of 0.885 K $(Wm^{-2})^{-1}$), or approximately 3 ℃ warming following a doubling of atmospheric CO_2 concentrations. This is similar to the best estimate ECS from the AR6 (Forster et al. 2021).

In its absolute form, the AGTP can be considered an emission metric-based emulator of the global mean temperature effect of emissions, or in other words a simplified climate model. More complex, coupled climate models are needed to study local-to-regional scale climate effects, as well as impacts beyond temperature change. However, the strong natural variability of the climate system typically makes it challenging to detect a temperature change signal from smaller emissions sources, such as individual regions, in these models (or very long and costly model integrations would be required). More simplified models such as the AGTP provide an alternative that enables us to calculate and compare the human-induced global temperature impacts of sources and scenarios in a transparent and, in terms of computer resources, cost-effective manner. This approach allows us to isolate a clearer signal from natural variability.

Moreover, the AGTP framework can be readily extended from pulse-based emissions to any emission scenario. In this case, the temperature response ΔT at time t for species i is given by:

$$\Delta T_i(t) = \int_0^t E_i(t') AGTP_i(t-t')dt' \quad (5)$$

Using this method, we calculate the global-temperature response to Chinese emissions of pollutants from 2018 to 2035, comparing the three scenarios produced in the ChiNorBC project.

The key input to Eq. 1 and 3 is the radiative efficiency F, i.e. the RF per kilogram species emitted. As mentioned, for short-lived climate forcers such as aerosols, this efficiency can depend on the location of the emission. To capture this, we use radiative efficiencies calculated specifically for emissions in China (using the results of the OsloCTM3 and RTM simulations) and calculate updated region-specific AGTPs and AGWPs for BC, OC, SO_2, and the ozone precursors NOx, CO, and VOC. For the aerosols, we include an estimate of the RFaci derived from the RTM calculations. For BC, studies have shown that the rapid adjustments that arise (see footnote 1) act to offset part of the direct RF (RFari) of the aerosol. To account for this effect, we scale the radiative efficiency of BC by -15% (based on Stjern et al. (2017)). As initially mentioned, the RF due to aerosol deposition on snow and

[15] I.e. the long-term (equilibrium) global mean surface air temperature change resulting from a doubling of the amount of CO_2 in the atmosphere (over pre-industrial levels).

ice is not included in our estimates. For the well-mixed greenhouse gases, the emission location does not matter in the same way. We use globally averaged radiative efficiencies, calculated using the analytical expressions from Etminan et al. (2016) and updated to year 2018 background concentrations, to derive the AGTPs and AGWPs for these gases.

5.3 Aerosols abundances over China in 2018

In this chapter we first discuss the spatiotemporal distribution of BC, OA, and other aerosol species over China and then the total aerosol optical depth, as simulated for year 2018 emissions. We focus on two illustrative regions, a broader covering larger parts of China (region A) and the Beijing-Tianjin-Hebei plus surrounding area (region B), one of the most polluted regions in China (see Fig. 5.1 for region definitions).

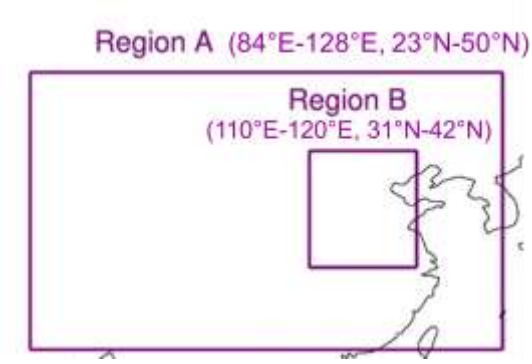

Figure 5-1 Geographical extent of the two regions for which area-average burdens and radiative forcing in this chapter is given

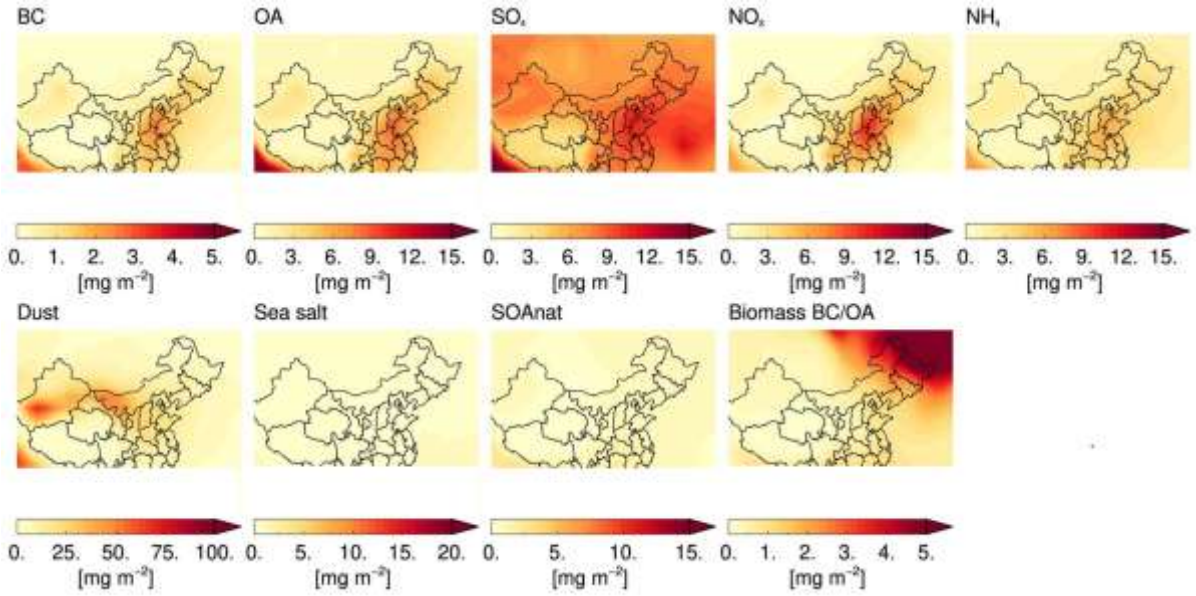

Figure 5-2 Column burdens of anthropogenic (top row) and natural (bottom row) aerosols over China as simulated by the OsloCTM3 with year 2018 emissions from the ChiNorBC project. Note the different scales on the color bars

Figure 5-2 shows the total abundance of individual aerosol species over China (specifically, the burden integrated from the surface to the top of the atmosphere, in mg m^{-2}). Of the anthropogenic pollutants (top row), sulfate and organic aerosol (OA) are most abundant followed by nitrate. Anthropogenic pollution levels peak in eastern China where emissions are highest (see also Chapter 4, e.g. Figure 4.7), with a secondary peak to the northwest. Averaged

over region A, we estimate annual mean burdens of 0.7 mg m^{-2} BC, 2.5 mg m^{-2} OA, 7 mg m^{-2} sulfate, 2 mg m^{-2} nitrate and 2 mg m^{-2} ammonium (Table 5-1) for year 2018 emissions. Over the smaller region B, the average concentrations are higher, as expected given the high anthropogenic emissions in this area. Overall, BC and OA contribute 20-25% of the total amount of anthropogenic aerosols in these regions in our model, with a somewhat smaller relative contributions when considering total aerosol abundances, including natural sources.

Natural sources can also play an important role in determining the regional aerosol abundance and hence for the radiative effects. The bottom row of Figure 5-2 shows the burden of dust, sea salt, secondary OA from natural emissions (SOAnat) and carbonaceous aerosols from biomass burning. Over China, we see that the burden of dust aerosols is high to the north following emissions in the arid zones, while burdens of SOAnat and biomass BC and OA are relatively low, at least on annual mean. Both these sources have a strong seasonal component, with higher emissions during spring and summer and low emissions in winter. On annual mean, however, anthropogenic sources are important for the total aerosol abundances over much of China.

Table 5-1 Area-averaged, annual mean burdens of anthropogenic aerosols over regions A and B.

mg m^{-2}	BC	OA	Sulfate	Nitrate	Ammonium
Region A	0.7	2.5	7.0	2.4	2.4
Region B	1.6	4.5	8.9	6.5	4.3

Figure 5-3 shows the total aerosol optical (AOD), i.e. taking into account the different optical properties of individual aerosol species, as simulated by the OsloCTM3 and Oslo-RTM. AOD is plotted on a unitless scale where low values (below 0.1) indicate clear sky with good visibility, while values closer to 1 indicated very hazy conditions. On annual mean, the spatial patterns follow the pattern of high dust and anthropogenic aerosol loadings (Figure 5-3a). There are also seasonal variations, with peak regional AOD during spring, with a secondary peak during in November (Figure 5-3b). The temporal pattern results from the combined influence of natural and anthropogenic aerosol emissions, chemistry, surface properties and meteorological conditions, including natural variability. For instance, anthropogenic emissions are higher during winter than summer, driving up the aerosol burdens and hence AOD. During summer, the anthropogenic emissions are lower and higher precipitation rates enhance removal of aerosols from the atmosphere, hence lowering the anthropogenic pollution levels and thus AOD. The springtime AOD seems to be a combination of industrial emissions in the east and dust in the north (Fig. 5.3d). Dust emissions increase during spring and because these aerosols are so abundant (see Fig. 5.2), they have a strong contribution to total AOD. Dust is also important during summer in northeastern China (Fig. 5.3e). This suggests that even if anthropogenic aerosol sources are reduced, periods of high AOD and poorer air quality may occur due to the influence of natural aerosols. In November, anthropogenic emissions are again higher compared to preceding months.

Exact attribution of the seasonal differences to individual factors is challenging, as AOD is further influenced by seasonality in atmospheric chemistry (the processes involved in the formation of sulfate and nitrate aerosols require solar radiation) and differences in the reflectivity of the underlying surface, for instance due to the presence of snow or greening of vegetation. We also note that there can be substantial interannual variability in meteorology and hence in the magnitude of AOD (e.g. Liu et al. 2013). Here we run only one year of model integration and additional simulations would be required to disentangle season patterns more clearly from natural variability.

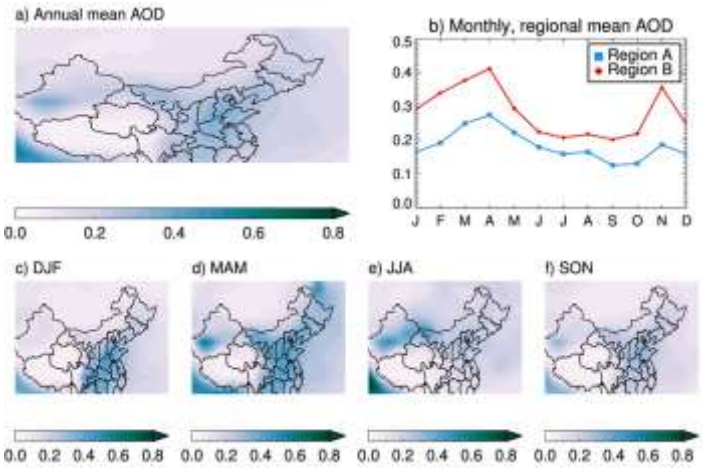

Figure 5-3 a) Annual, b) monthly, and c-f) seasonal mean total aerosol optical depth over regions A and B as simulated by the OsloCTM3 with the ChiNorBC-2018 emissions

When compared with AOD retrieved from remote sensing, the AOD simulated based on OsloCTM3 runs has been found to agree reasonably well in terms of overall spatial pattern (Lund et al. 2018; 2022). The simulated AOD is also similar in pattern and magnitude to that estimated by comparable models. However, the magnitude of annual mean simulated AOD is underestimated, both globally and in several regions, compared to satellite retrievals. This is also the case over China in the present simulations with the new ChiNorBC-2018 emissions. Compared to the AOD retrieved from MODIS (mean of Aqua and Terra instruments) (MOD08, 2018), the simulated annual, regional mean AOD is around 50% lower over both region A and B. However, the general features of higher AOD in west and northeast of China is captured. Additionally, we note that there is a large spread in magnitude of observed AOD from different instruments, where MODIS is in the upper range (Vogel et al. 2022). Similarly, the model also shows an underestimation compared to AOD from ground-based measurements from AERONET (the Aerosol Robotic NETwork, version 3 Level 113 2.0 retrievals at 500 nm) (Holben et al., 1998; Lund et al. 2022). However, the number of stations within the regions of interest here is limited.

5.4 Effects of differences in present-day emission inventories

As described in Chapter 4 of this report, a key objective of the ChiNorBC project has been to implement updated emissions, the ChiNorBC-2018 inventory, of air pollutants in China based on the best available national statistics. Chapter 4 explored the influence of emission inventory differences on surface concentrations of pollutants, showing markedly lower air pollution levels and generally better model-observation agreement with the new emissions. Here we quantify the resulting difference in aerosol burden and the consequent effect on the energy budget in terms of regional radiative forcing.

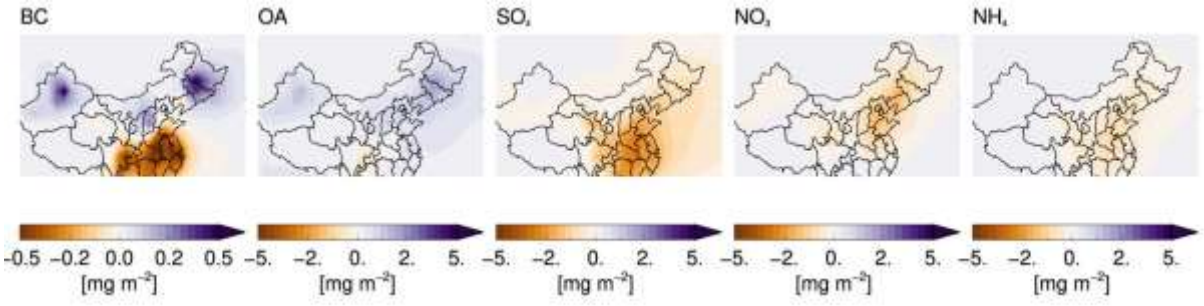

Figure 5-4 Absolute difference in annual mean burden of individual anthropogenic aerosol species between simulations with the ChiNorBC-2018 and CEDSv21 emissions. Note the different scale on the color bar for BC

Figure 5-4 shows the spatially distributed absolute differences in the burdens of anthropogenic aerosols between the simulation with ChiNorBC-2018 and CEDSv21 emissions (see Ch. 4 of this report for a detailed description and comparison of the applied emission inventories). Overall, the ChiNorBC-2018 emissions are lower than other recent global inventories, including CEDSv21, for most species, except for OC. This is reflected in the resulting aerosol abundances. Lower burdens of sulfate, nitrate and ammonium are seen mainly across western China. The BC burden is lower to the southwest, but higher in the north. Organic aerosols exhibit a similar pattern of differences.

Fig. 5-5 shows the corresponding area-averaged burden differences in our two focus regions. The burden difference is +8% for OA and -7% for BC in region A with the ChiNorBC-2018 than with CEDSv21. The burdens of sulfate, nitrate, and ammonium is about 12% lower. For the three latter species, the corresponding difference over the more polluted region B is approximately 17%, while the difference in OA and BC burdens are similar to that for region A, i.e. +8% and -6%, respectively. For sulfate, nitrate, and ammonium, differences between simulations are somewhat smaller than the corresponding surface concentration differences (Chapter 4), reflecting the chemical and physical processing the aerosols undergo as they are transport away from the sources, as well as the potentially larger contribution from long-range transport when considering the total burden rather than the surface concentrations.

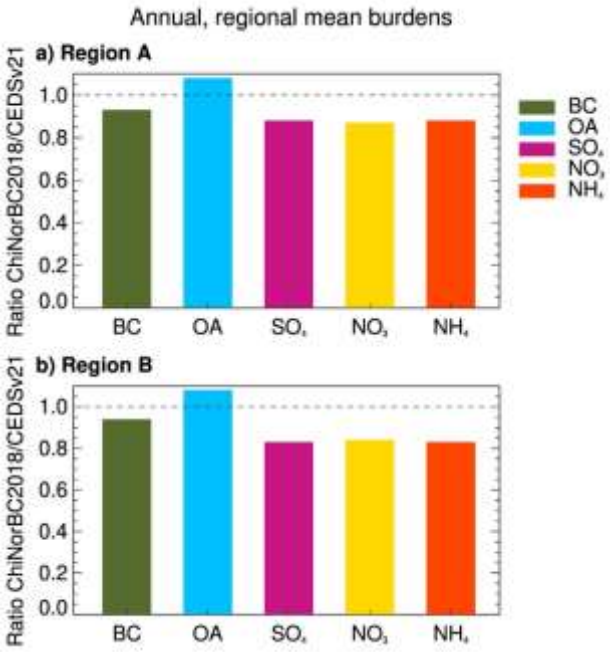

Figure 5-5 Ratio of the burden of individual aerosol species between simulations with the ChiNorBC-2018 and CEDSv21 emissions, averaged over a) region A and b) region B

These individual differences are nevertheless large enough to give a marked effect on simulated total AOD, as seen in Figure 5-6. While the spatial distribution of aerosols is similar between simulations with the two emission inventories (Figure 5-6a and b), reductions up to 0.06 are seen over parts of China (Figure 5-6c), corresponding to up to 25% lower AOD. The largest absolute and relative difference are seen in southeastern and central China. In the southeast, this difference is primarily driven by differences in BC and sulfate (Figure 5-4). The peak difference in central China, as well as the smaller differences to the north, arise mainly from nitrate aerosols and corresponds spatially to difference in NH_3 emissions between the two inventories (Chapter 4, Figure 4.9). For both region A and region B, using the ChiNorBC-2018 inventory reduces the AOD by around 10%.

As discussed above, the AOD simulated with the OsloCTM3 and the ChiNorBC-2018 emissions is lower than that retrieved from satellites. In other words, we do not find an improvement compared to remotely sensed AOD when switching from CEDSv21 emissions to ChiNorBC-2018 (similar results were also found for older emission inventories by Lund et al. 2018). This contrasts with the improved model-measurement comparison found for surface concentrations of individual species in Ch. 4. The poorer AOD agreement with lower emissions may point

to other missing or incorrectly captured emission sources, such as urban or agricultural dust, but requires further investigation to quantify.

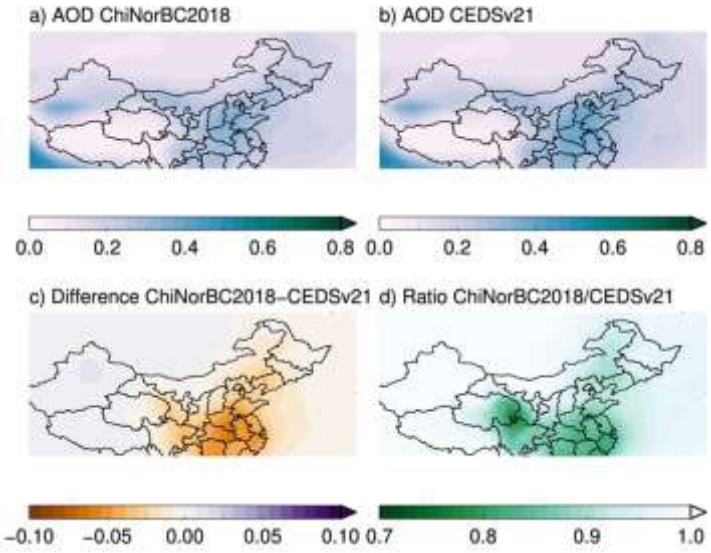

Figure 5-6 Total aerosol optical depth (AOD) simulated by the OsloCTM3 with a) the ChiNorBC-2018 emission inventory and b) CEDSv21 emissions. Panels c) and d) show the difference and ratio between the two inventories, respectively

While we have seen that different emission inventories can result in non-negligible changes in simulated AOD, a further question is how these changes influence the Earth's energy balance and climate. Figure 5-7 shows the radiative forcing, the net effect and split by the direct and indirect effects, that corresponds to the difference in aerosol abundances when switching from CEDSv21 to the ChiNorBC-2018 emissions in China. This change is primarily a reduction, and the difference is larger for scattering aerosols than for aerosols with an absorbing effect. Hence, the resulting RF is positive, i.e. a warming due to the loss of aerosol-induced cooling. We find area average radiative forcing due to differences in the emission inventories of 0.3 W m^{-2} and 0.5 W m^{-2} for region A and B, respectively. These are large numbers when contrasted against e.g. the global mean anthropogenic aerosol-induced RF since 1750 reported by the IPCC. However, we stress that these are not comparable estimates since we here consider the difference in a single year due to underlying model input assumptions and averages over smaller regions. We find that RF from aerosol-cloud interactions dominates difference, with a regional pattern that extends further from the main emission regions than the aerosol-radiation interactions. This is as expected from aerosol transport and the downwind co-location of Chinese emitted aerosol with clouds.

Overall, these results reiterate that uncertainties in emissions can be important for subsequent estimates of aerosol-induced radiative forcing and climate impacts.

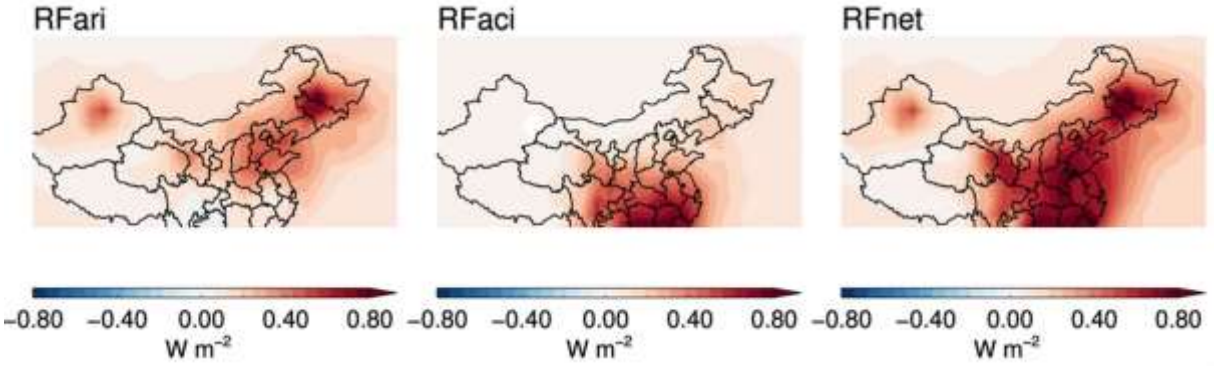

Figure 5-7 The radiative forcing corresponding to the difference in aerosol abundances between simulations with the CEDSv21 and the ChiNorBC-2018 emission inventory

5.5 Effects of changes in emissions from 2018 to 2035

Next, we explore the change in abundances of BC, OA and other anthropogenic aerosols, and the resulting radiative forcing, from present-day to 2035 using emissions from the three scenarios developed in the ChiNorBC project. These are termed business as usual (BAU), end of pipe (EOP), and ambitious control (ABC) – see Chapter 3 of this report for details.

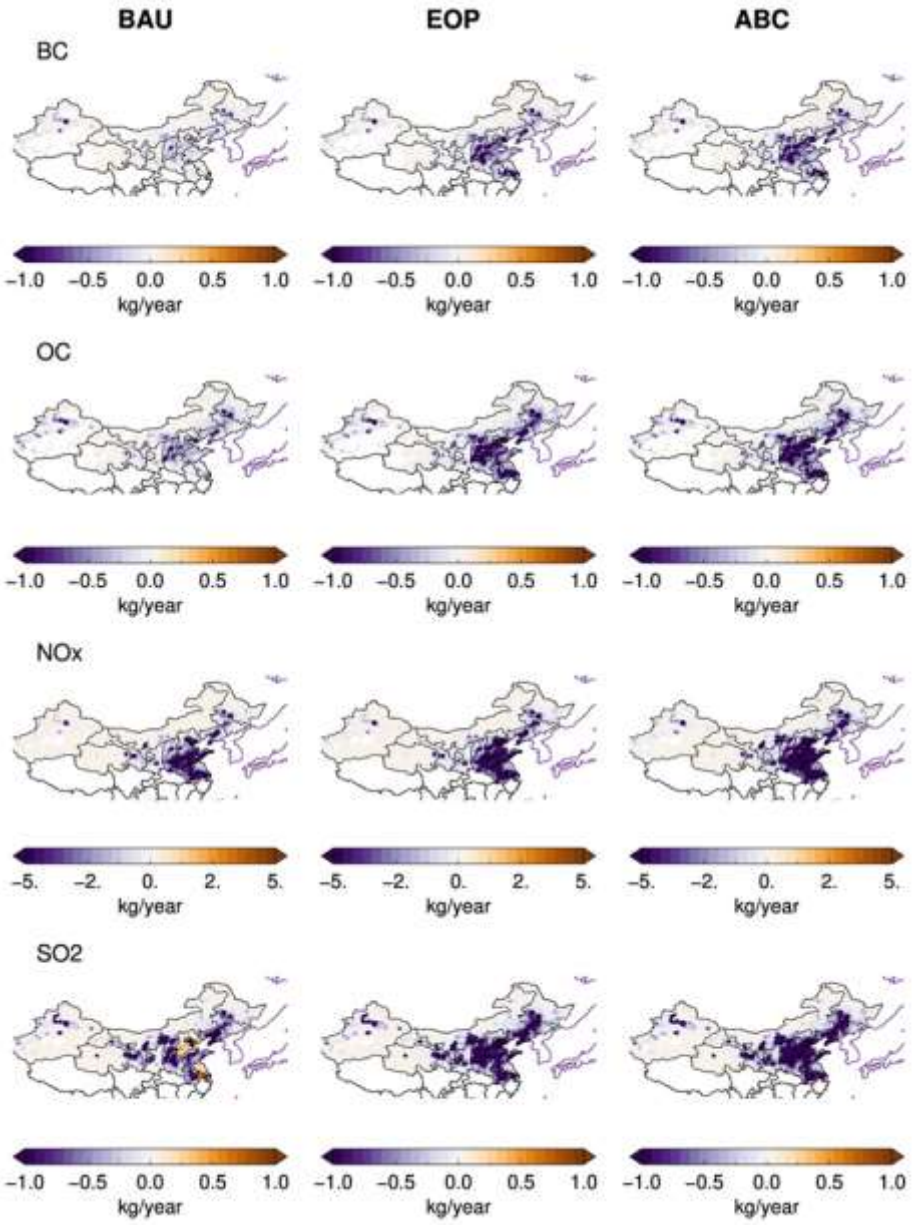

Figure 5-8 Absolute change in emissions of BC, OC, NOx, and SO_2 from 2018 to 2035 under the three scenarios. Note the different scales of the color bars

The original format of the projected emissions is percentage changes by province in China. To produce the gridded future emissions required for the OsloCTM3 simulations, these are mapped onto and subtracted from the year 2018 emissions using a provided shapefile. Emission projections are available for NOx, SO_2, BC and OC, while emissions of CO, VOC, and NH_3 are kept at the 2018 level in these model simulations (due to lack of available projections for these species – see also Chapter 3 for details on the emission scenarios developed in the project). For BC and OC, emission changes are further available by sector, for industry, residential, and mobile. In the absence of similar information for SO_2 and NOx, we distribute the total percentage reduction for each province

equally across these three sectors. While this is an approximation, we expect the impact through transport and chemistry to be minimal given the coarse resolution of the OsloCTM3 relative to the original emission files. Furthermore, the radiative transfer calculations involve different assumptions on optical properties for BC and OC from biofuel and fossil fuel sources, hence depending on sector-specific emission information, however, such distinctions are not included for sulfate and nitrate radiative effects. Figure 5-8 shows how the total changes in NOx, SO_2, BC, and OC emissions from 2018 to 2035 are distributed across China in the input to OsloCTM3. Although absolute magnitudes differ, the geographical pattern of reductions is similar between both scenarios and emitted species, and reductions are consistently strongest in the eastern part of China.

Figure 5-9 is similar to Figure 5-4, but showing the ratio between area-averaged burdens of BC, OA, and other anthropogenic aerosols in 2035 compared to 2018, for each scenario. All anthropogenic aerosol species decline from 2018 to 2035 in all three scenarios, and the reductions are consistently most pronounced for BC, OA, and nitrate. For region A (Figure 5-9a), reductions up to 20% in area average BC and OA burden are estimated in the most stringent scenarios. Over region B, the average burden reductions are even stronger (Figure 5-9b), as expected given that the largest emission reductions are projected here (Figure 5-8). For BC, the area average burden is 16% lower in 2035 in the BAU scenario relative to the simulation with 2018 emissions. With the additional measures in the EOP and ABC scenarios, the reduction increases to around 40%. Similar changes are found for OA. For nitrate, the reduction is similar in magnitude to BC in the BAU case, but the further reduction to EOP and ABC is not quite as strong. We note that emissions of NH_3, which is important for the nitrate burden, are unchanged from the 2018 level in the scenarios. The sulfate burden declines relatively little in all three scenarios. Chinese SO_2 emissions have been declining strongly in recent years (Lund et al. 2022 and references therein), which may affect the potential for achieving further effective controls. We also note that for all species and both regions, the largest reductions in aerosol abundances are found between the BAU and EOP scenarios, with mostly smaller further relative reductions from EOP to ABC.

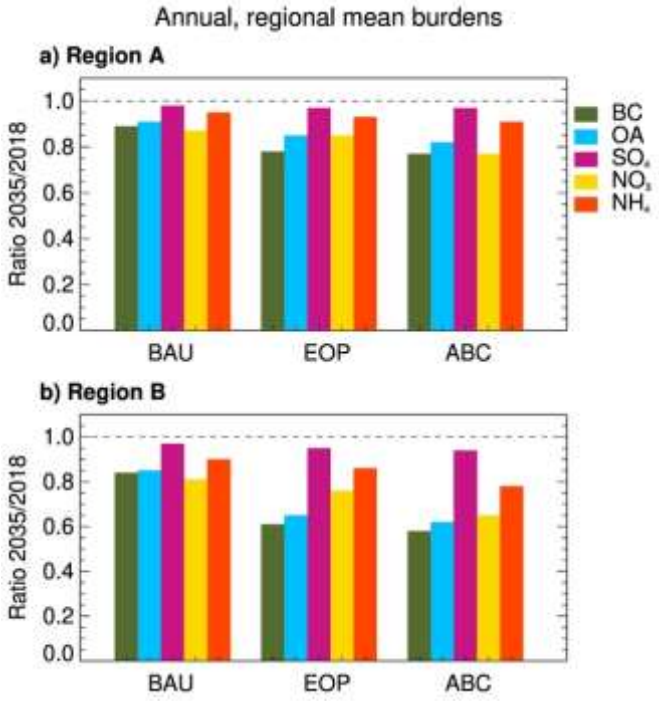

Figure 5-9 Ratio of the burden of individual aerosol species in 2035 relative to 2018 with the three scenarios, averaged over a) China as a whole and b) the BTH region

Figure 5-10 shows the resulting simulated AOD in 2035 in each scenario, and the absolute and relative difference from 2018. The pattern of AOD remains the same and all three scenarios see a notable decline in total AOD following reductions in NOx, SO_2, BC, and OC emissions, with a clear strengthening with stringency of mitigation measures. The main reductions occur in the east, as expected from the locations of the emission changes. Maximum

reductions up 20% in total AOD compared to 2018 are found in the ABC scenario. Averaged over region A, the mean AOD reductions is 4% in the BAU scenario, 6% in EOP, and 7% in ABC. This is consistent with the reduction across aerosol burdens (Fig. 5.9). However, relative numbers are smaller for total AOD than for individual burdens, since different aerosol species contribute differently to the extinction of solar radiation and AOD also includes a significant contribution from natural aerosols which are not changed from the 2018 simulation. For region B, the corresponding numbers are higher, at 8% for BAU, 14% for EOP, and 17% for ABC.

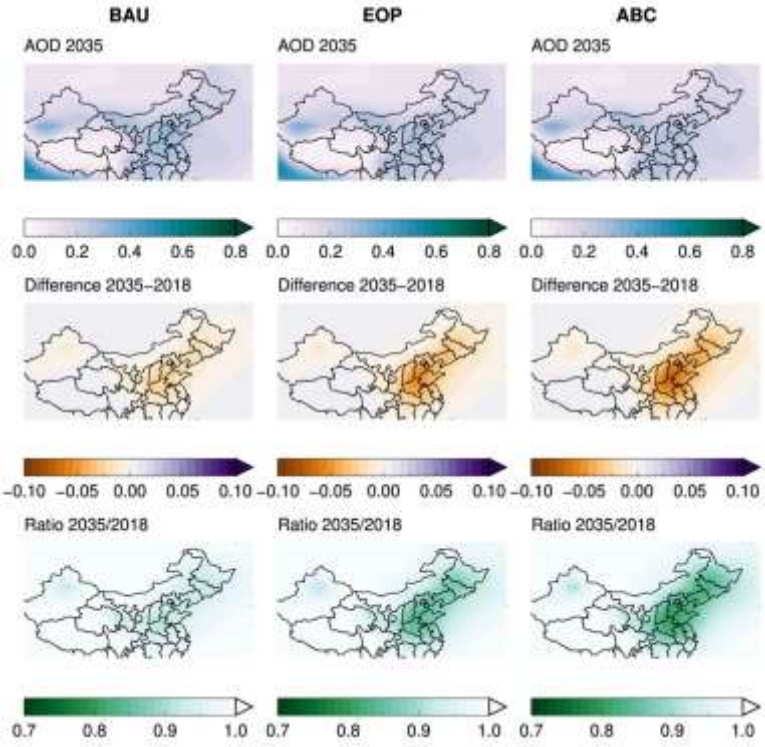

Figure 5-10 Total aerosol optical depth (AOD) simulated by the OsloCTM3 for year 2035 emissions under the three scenarios BAU, EOP and ABC. (top) Year 2035 AOD, (middle) difference between 2035 and 2018, and (bottom) ratio between 2035 and 2018 AOD

Figures 5.11 and 5.12 shows the radiative forcing following the combined reductions in BC, OA, and other anthropogenic aerosol in these scenarios. Figure 5-11 shows the full spatial distribution of the net RF, i.e. the combined effect of aerosol-radiation and aerosol-cloud interactions, while Figure 5-12 shows regionally averaged RF, net and split by the contribution from RFari and RFaci.

In terms of global mean forcing, the emission changes in China result in relatively weak aerosol-induced RF of less than 0.001 W m^{-2} over the 2018 to 2035 period in all three scenarios. When averaged over region A, this RF is 0.02 W m^{-2} in 2035 relative to 2018 under the BAU scenario, strengthening with increasing ambition 0.047 W m^{-2} under ABC. When averaged over region B, which is near to the main emission reductions, a net positive RF of up to 0.3 W m^{-2} in 2035 relative to 2014 is estimated for the most stringent ABC scenario. In all three scenarios, there are geographical differences within China (Fig. 5.11), where the RF is negative to the north but positive in the east. This difference in sign is determined by the relative magnitude of changes in the scattering aerosols and in the absorbing BC (and partly OA). The characteristics of the surface and clouds in different regions also contribute. In this work, we can only quantify the net effect of the combined changes in BC, OC, NOx, and SO_2 emissions. We note, however, that reductions in BC emissions are expected to give a negative RF, that is, a reduced warming effect.

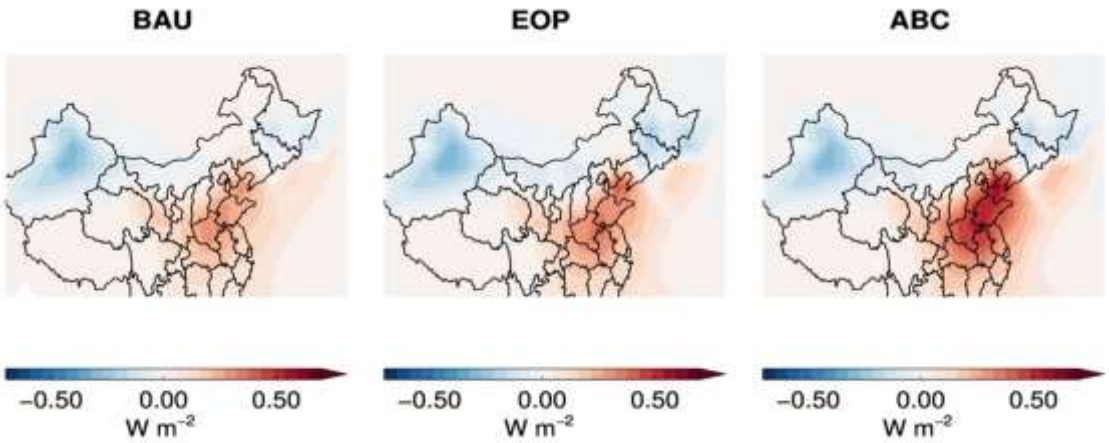

Figure 5-11 Net aerosol-induced radiative forcing in 2035 relative to 2018 in each of the three scenarios

As seen from Figure 5-12 there are also regional differences in the relative role of aerosol-clouds and aerosol-radiation interactions. Over region A, the RFaci gives the dominant contribution to the net RF, while over region B, RFari is relatively more important. One likely reason is that region B is so small that local effects, i.e. RFari, are most important here. Downwind, where the presence of clouds is more important, the RFaci plays a stronger role. An additional factor that can influence the roles of RFaci and RFari is the relative changes in different aerosol species in the regions as they have different influences on radiation and clouds. We also note that RFari is negative (although quite small) for region A in the EOP scenario but becomes weakly positive in the ABC scenario. This is due to the balance, in terms of both magnitude and spatial location, of reductions in scattering and absorbing aerosols. Under EOP, the reductions in absorbing aerosols are strong enough that the resulting negative RFari offsets the positive forcing due to concurrent reductions in scattering aerosols.

In addition to the direct radiative effects, aerosol removal can influence regional dynamics and hydrology, and the result could hence be notable local climate impacts. This is not investigated in the SinoBC project, but in general such effects need further quantification and improved understanding to assess the trade-offs and synergies between improved air quality and climate mitigation. Such an assessment is also important climate risk adaptation in the near-term as aerosol emissions are projected to decline rapidly in concurrence with changing CO_2 and other greenhouse gas emissions.

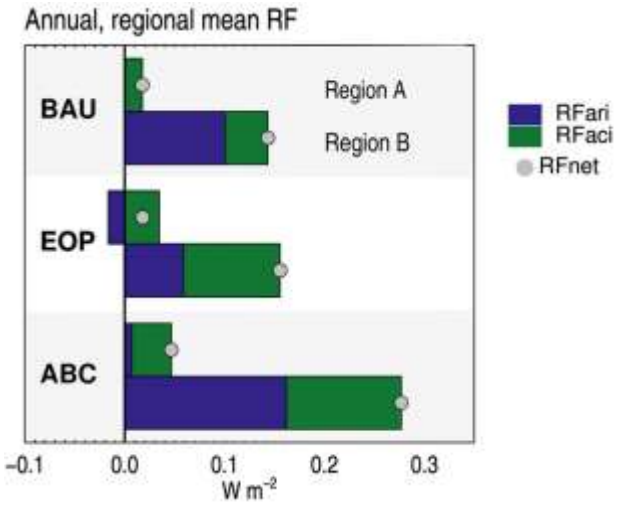

Figure 5-12 Regional mean net aerosol-induced radiative forcing, and the contributions from RFari and RFaci, in 2035 relative to 2018 in each scenario

5.6 Emission metrics and global temperature response

There are several ways to quantify the climate impact of emission reductions. As described in section 5.2, we apply a simplified, analytical climate model, the AGTP, to assess effects on global mean temperature of emissions in China in this project. This approach is well-established and allow us to quantify the human-induced global temperature signal. It does not, however, allow us to quantify local climate effects. Hence, the following figures and analysis all show the effect of emissions in China on global mean surface temperature. Nevertheless, the approach is useful for intercomparing the effects of different emitted species and scenarios.

Before discussing the temperature effects of the scenarios, we briefly demonstrate the difference in temporal behavior of different climate drivers and discuss consequent implications. This can also help guide the interpretation of results using our AGTPs in further work beyond the ChiNorBC project. Figure 5-13 illustrates this temporal behavior. Here we use the AGTP to quantify the temperature response to one year (2018) of emissions of aerosols and precursors in China – as a function of time after the that emission occurs. The focus here is not on the absolute temperature effects of individual emissions, but on the behavior and relative role of individual species. Central here is the well-known but important feature of the short atmospheric residence time of aerosols and other air pollutants compared to CO_2 and other long-lived greenhouse gases: While emissions of BC, OC, and SO_2 have strong, immediate temperature effects, the temperature response becomes dominated by CO_2 over time. This means, for instance, that reductions in BC (and OC) emissions will cause rapid reductions in surface temperature, but that also reductions in greenhouse gases are required to reduce temperature in the long term. Hence, one key message is that comprehensive assessments of the climate effects of policies targeting SLCFs should consider synergies and trade-offs also of the co-emitted greenhouse gases.

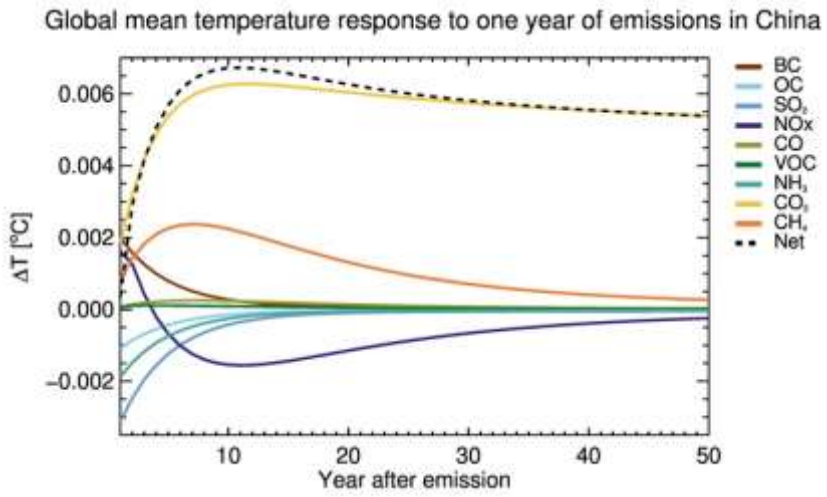

Figure 5-13 Global mean temperature effect of different species following one year (2018) of emissions in China. Emissions of CO_2 and methane (CH_4) are taken from the CEDS21 inventory, all other species from the ChiNorBC2018

In reality, emissions are of course not one-off, but continuous. Using the AGTP we can assess the temperature response to any given emission scenarios. Figure 5-14 shows the global mean temperature response to Chinese emissions under the three scenarios developed in ChiNorBC (described in Chapter 3). Here we show both the net temperature response to all scenario emissions provided (i.e. BC, OC, SO_2 and NOx, panel a) and the response to only BC and OC emissions, which is the primary focus on the project (panel b).

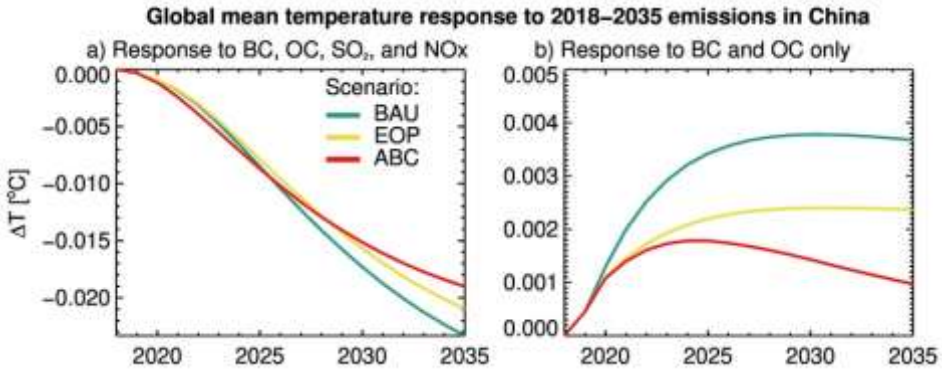

Figure 5-14 Global mean temperature response to emissions in China from 2018 to 2035 under the three scenarios: a) net response to BC, OC, SO_2 and NOx emissions and b) response to BC and OC emissions only

The objective here is to compare across scenarios and show how the different stringency of mitigation of these selected species play out in terms of differences in temperature response. In brief, the net impact on global temperature from emissions of BC, OC, SO_2, and NOx until 2035 is a cooling in all three scenarios, despite emission reductions over time. Here, SO_2, OC and NOx emissions cause cooling contributions which are partly offset by warming due to BC. Towards 2035, the cooling is strongest in the BAU scenario and weakens due to the removal of scattering aerosol in EOP and ABC. This weakening is partly offset by the concurrent removal of warming BC aerosols. The net effect of BC and OC on climate depends on their relative magnitude and can vary between sources. For sources that are rich in BC but lower in OC emissions, the net RF is positive. Hence, mitigating such sources yields a reduced warming effect. Our results show that this is the case for Chinese emissions under the three scenarios produced in the project. We note that the absolute temperature responses are small in magnitude and should be interpreted with care. This is because only the effect of selected emitted species is included, and only from 2018 onwards. Other species, such as NH_3 and co-emitted greenhouse gases, are not considered and neither is the full history of emissions. While scenarios for CO, VOC, NH_3 or greenhouse gases were not developed in the ChiNorBC project, we provide the full set of AGTPs in Annex 5.1 for future use with new or updated scenarios.

Another common application of emission metrics, for instance in emissions trading or national reporting, is to place the effects of different species on a common, CO_2-equivalent scale using the normalized metrics form. As discussed in Sect. 5.2, the radiative forcing efficiency, and hence emission metric values, of SLCFs such as aerosols can have a marked dependence on where emissions take place. For instance, Aamaas et al. (2016) and Collins et al. (2013) found lower GTP values for aerosol and precursors emissions in China than corresponding emissions in Europe. In this project, we have used the new model simulations to calculate an updated set of metrics specific for emissions occurring in China, building on the methodology in Lund et al. 2020. These are summarized in Tables 5.2 and 5.3 and can be applied e.g. in further assessments of mitigation strategies including additional species not studied in the ChiNorBC project. We emphasize that these metric values should be only multiplied with Chinese emissions and used to compare various scenarios for China. Metrics that are specific to other regions exist in the literature (e.g. Aamaas et al. 2016; Collins et al. 2013; Myhre et al. 2013; Lund et al. 2020). However, there may be differences in underlying assumptions and methodology that must be understood if these are used to contrast Chinese emissions with other sources. For CO_2, CH_4, and N_2O, the climate effect can be considered as largely independent on the location of emission. However, for methodological consistency, we also provide updated metrics for these three.

Table 5-2 Global Temperature change Potential (GTP) on four different time horizons. The values for CO_2, CH_4, and N_2O are applicable to any emission source, the remaining values are specific to emissions in China. Values are calculated based on radiative forcing estimates produced in the ChiNorBC project using a single model

GTP	**Time horizon**			
	10	**20**	**50**	**100**
CO_2	1	1	1	1

CH_4	127	79	17	8
N_2O	281	310	309	259
Values specific for emissions occurring in China:				
BC $_{China}$	518	110	54	43
OC $_{China}$	-143	-30	-15	-12
$SO_{2\ China}$	-119	-25	-12	-10
$NH_{3\ China}$	-55	-12	-6	-5
NOx $_{China}$	-161	-133	-32	-11
CO $_{China}$	5	3	1	0.3
VOC $_{China}$	9	5	1	0.5

Table 5-3 Global Warming Potential (GWP) by on four different time horizons. The values for CO_2, CH_4, and N_2O are applicable to any emission source, the remaining values are specific to emissions in China. Values are calculated based on radiative forcing estimates produced in the ChiNorBC project using a single model

GWP	**Time horizon**			
	10	**20**	**50**	**100**
CO_2	1	1	1	1
CH_4	136	110	63	37
N_2O	269	289	304	293
Values specific for emissions occurring in China:				
BC_{China}	1571	838	385	220
OC_{China}	-435	-232	-107	-61
$SO_{2\ China}$	-361	-193	-88	-51
$NH_{3\ China}$	-166	-89	-41	-23
NOx_{China}	-84	-113	-80	-48
CO_{China}	5	4	2	1
VOC $_{China}$	11	8	4	3

Importantly, using emissions metrics to aggregate short- and long-lived emissions comes with distinct challenges due to the different spatiotemporal behavior of the species. We note that many different types of metrics exist that can give different answers and there is no single correct metric – the metric choice depends on the question being addressed. Here we provide two metrics, GTP and GWP, and give values for four time horizons. We further note that substantial uncertainties are associated with the emissions and radiative forcing of many of species, which will translate to the metric values as well. For instance, the fifth Assessment Report (AR5) by the IPCC reported GTP20 and GWP100 for global BC emissions of 920 (95 to 2400) and 900 (100 to 1700), respectively (Myhre et al. 2013). While we have not performed a similar uncertainty assessment for the regional emission metric values within the ChiNorBC project, the overall scientific uncertainties of aerosol RF should be kept in mind in further applications and interpretations.

5.7 Summary

Here we document the findings from simulations performed with the global chemical transport model OsloCTM3 within the ChiNorBC project. We investigate the spatiotemporal pattern of aerosols over China using a novel inventory of national anthropogenic emissions, and how results with these emissions compare with those using one of the most recent global emission databases, the Community Emission Data System version 2021 (CEDSv21). Furthermore, we explore the evolution of regional aerosol abundances, and associated effects on the regional energy balance and global mean surface temperature, under three future scenarios.

Desert dust is another important source of aerosols, especially in Northern China. Periods of poorer air quality and higher AOD may hence occur in some regions even after strong reductions in anthropogenic emissions. While more the sources are more difficult to mitigate, understanding the role of dust and other natural aerosols, including possible responses of their emission sources to human activities and climate change, is important for comprehensive assessment of the role of aerosols on regional climate and environment.

Differences in estimates of anthropogenic emissions can cause substantial spread in the simulated distribution of aerosols, hence contributing to the existing uncertainty to estimates of aerosol-induced climate effects. Using the ChiNorBC-2018 emissions developed in the project (for BC, OC, SO_2, NOx, NH_3, CO, and VOC), we find approximately 10% lower regional total aerosol optical depth compared to using the CEDSv21. The main drivers are lower burdens of sulfate and ammonium nitrate aerosols where up to 20% lower burdens are found when using the new ChiNorBC-2018 emissions.

All three scenarios developed in the project show reductions in BC, OC, SO_2 and NOx to 2035. These reductions lead to associated reductions in the amount of BC, OA, sulfate, and nitrate over the region. The relative reductions are largest for BC and nitrate, and smallest for sulfate. When averaged over a region covering large parts of China, the combined reduction in total aerosol optical depth ranges from 4% in the BAU scenario to 7% in the most stringent ABC scenario.

For a more comprehensive assessment of the climate and environmental effects of emission changes in China, co-emitted greenhouse gases and other precursor species should also be considered. While such analyses are beyond the scope of the present project, we provide updated emission metrics to enable first order quantification and comparison of different species and scenarios in later work. Further studies are also required to quantify climate effects beyond global mean temperature, such as regional precipitation changes resulting from aerosol changes. Finally, we note that while a rigorous uncertainty assessment has not been conducted here, significant uncertainties – from emissions to temperature response – are associated with the emission metric values and should be kept in mind in future applications.

6 Health risk assessment

Authors: Yongjie Wei, Zhigang Li, Xiaojing Zhu (CRAES),Vegard Grytting, Marit Låg, Shilpa Rao, Per Schwarze(NIPH)

Air pollution is a leading environmental risk factor for premature mortality and loss of healthy life-years worldwide (IHME, 2020; Landrigan et al., 2018). The largest contributor to the disease burden due to air pollution is$PM_{2.5}$, which has been estimated to cause over 4 million premature deaths annually. While most of the disease burden occurs in low- and middle-income countries in Asia and Africa with high concentrations of PM2.5 (IHME, 2020; Landrigan et al., 2018), epidemiological studies have also shown associations with mortality at relatively low concentrations of PM in Europe and North America (Di et al., 2017; Pinault et al., 2016; Wolf et al., 2021). PM is not a single entity, but a mixture of particles originating from different sources that may vary considerably between areas and with time. A source apportionment study conducted in Beijing, China, identified soil dust, coal combustion, biomass burning, waste incineration emissions, traffic, industrial pollution, and secondary inorganic aerosol as the major sources contributing to ambient $PM_{2.5}$ mass and also observed large seasonal variation in PM composition (Zhang et al., 2013). Black carbon (BC) is an important constituent of atmospheric PM (Jacobson, 2001) and is formed by the incomplete combustion of diesel fuels, coal, biofuels, and outdoor biomass burning. Epidemiological evidence suggests an association between exposure to BC and adverse health effects, including mortality and morbidity due to cardiovascular diseases (Song et al., 2022; Yang et al., 2019).

Knowledge regarding the potential adverse effects of different types of particles from different sources is important for implementing effective mitigating measures. The purpose of the project was to:

1. Perform a health risk assessment of air pollution particles, including BC/OC.
2. Rank the emissions sectors and sources by the results of the health risk assessment.
3. Provide policymakers with a robust scientific basis for developing mitigation strategies for BC/OC.

The original intention was to compare PM/BC samples from various locations in China with contributions from different sources of PM. However, due to difficulties with Norway not receiving these samples, and the complexity of the Covid-19 pandemic, the health assessment part of the project was conducted with separate contributions from the Chinese and Norwegian project partners (See Figure 6-1 for outline). The Chinese contribution consists of in vivo studies in mice assessing the effects of ambient $PM_{2.5}$ on inflammation, epigenetic modifications, and imbalance of immune cell populations, as well as an in vitro study focusing on epigenetic changes induced by PM exposure and comparison of the pro-inflammatory effect of three different samples of $PM_{2.5}$. The Norwegian researchers compared the effects of a standard reference sample of urban PM with a traffic-derived $PM_{2.5}$ sample in advanced 3D cell culture models representing the human lung, using a state-of-the-art exposure system to simulate the inhalation of particles in the air. In this part of the report, the focus was on pro-inflammatory mediators, since inflammation is involved in the development of different respiratory and cardiovascular diseases.

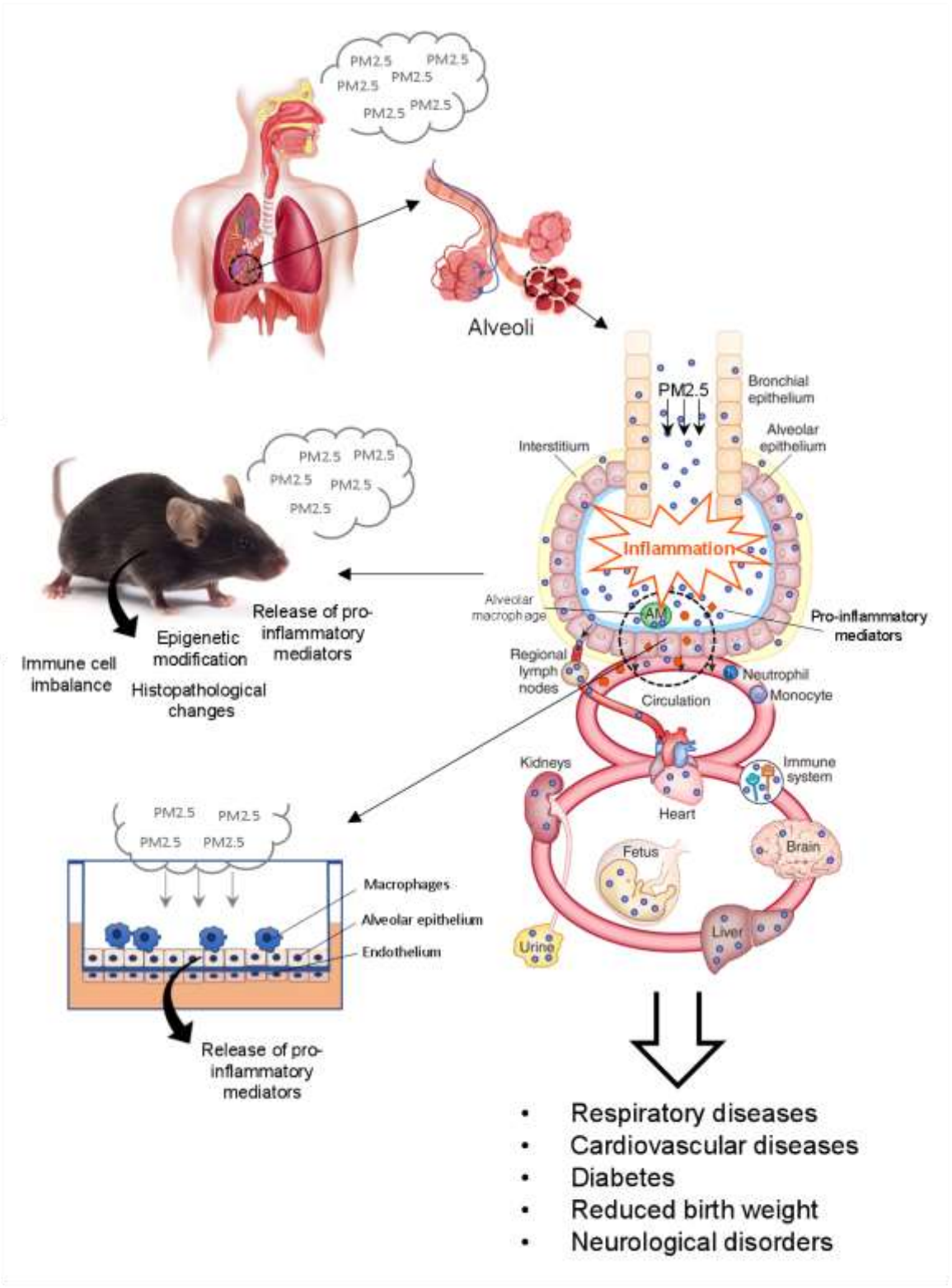

Figure 6-1 **Outline of the background and experimental approach of the project.** Inhaled fine particulate matter ($PM_{2.5}$) may deposit in the alveolar region of lungs and induce inflammation and oxidative stress, contributing to respiratory diseases. Alveolar epithelial cells and resident macrophages may contribute to the pro-inflammatory responses. Particles, soluble particle components and Inflammatory mediators released in the lungs may also cross over into circulation and cause adverse effects in distal tissues. Part of the figure is modified from Kreyling et al (2010).

6.1 Introduction

Ambient PM is composed of the element carbon (black carbon), metals, inorganic chemicals and organic hydrocarbons originating from various sources. The complexity of the physiochemical properties, chemical compositions or their synergism interactions of PM makes it highly toxic. It has been confirmed in previous studies that $PM_{2.5}$ can cause a range of metabolic diseases and is a major risk factor for them, such as asthma, bronchitis, pneumonia, high blood pressure, ischemia and myocardial infarction, etc. (Wei et al., 2016; Zhao et al., 2019). The chronic inflammatory response triggered by multiple inflammatory factors plays a key role in $PM_{2.5}$-induced inflammation. Inhaled $PM_{2.5}$ can produce free radicals in the lungs, breaking the fast oxidation and antioxidant balance (Zhou et al., 2020), which in turn provokes inflammatory responses resulting in the release of pro-inflammatory cytokines, including tumor necrosis factor-α (TNF-α) and interleukin-6 (IL- 6), leading lung injury (Azad et al., 2008; Rosanna and Salvatore, 2012). Researchers have shown that $PM_{2.5}$ can cause varying degrees of oxidative damage to lung and liver tissues in mice, resulting in significant toxic effects on the lungs and liver, leading to respiratory tract infections and inflammation (Deng et al., 2017; Du et al., 2016; Xing et al., 2016). Experimental studies showed that several signal transduction pathways have been proposed in relation to the mechanisms of toxic effects of $PM_{2.5}$ in the respiratory system, including oxidative stress, aberrant expression, cell proliferation, and DNA double-strand breaks (Li et al., 2015; Molina and Adjei, 2006). Although there are many theories on the pathogenesis of $PM_{2.5}$, the molecular mechanism and regularity of its specific harmful effects on the pulmonary still need to be further explored.

Different forms of PM vary in chemical composition, including their content of BC (EC) and organic carbon (OC), affecting their toxic properties. Experimental studies allow for high control of the exposure conditions and can provide valuable information regarding the toxicity of PM from different sources and the mechanisms behind the effects. Human cell lines, either derived from tumour cells or immortalized primary cells, are cost-effective and readily obtainable, have low variability, are easy to maintain and handle, and are stable in culture for extended periods of time (Hiemstra et al 2018). Although traditional cell culture experiments lack much of the complexity of *in vivo* models, making results difficult to extrapolate to human exposure, *in vitro* models are under continuous development. Recent advances include more complex 3-dimensional (3D) cell models that incorporate multiple cell types, as well as exposure at air-liquid interface (ALI), which provides a more realistic model system for particle exposure in the lungs (Klein et al 2013, Hiemstra et al 2018, Kletting et al 2018).

Inflammation is considered central to the adverse effects of inhaled particles. Although intrinsically a beneficial response, prolonged or excessive inflammation may lead to tissue damage and is involved in development of diseases, such as chronic obstructive pulmonary disease and atherosclerosis (Moldoveanu et al. 2009, Chen et al. 2018). Epithelial cells and macrophages express a range of cytosolic and cell-surface receptors that recognize specific molecular patterns associated with pathogens or cellular damage (Leiva-Juarez et al. 2018, Li and Wu 2021, Taban et al. 2022). Activation of these receptors initiates downstream signalling cascades culminating in activation of cellular effector functions and secretion of pro-inflammatory signalling mediators, such as cytokines and chemokines (Chen et al. 2018, Li and Wu 2021).

The aryl hydrocarbon receptor (AhR) pathway is important for the effects of PM and is highly expressed in lung tissue. AhR is activated by polycyclic aromatic hydrocarbons (PAH) and halogenated aromatic hydrocarbons, which are important organic compounds and prevalent in combustion particles (Esser and Rannug 2015, Vogel et al. 2020). AhR is known to be involved in the inflammatory response and may regulate cytokine expression (Podechard et al. 2008, Øvrevik et al. 2015, Weng et al. 2018). AhR activation also leads to expression of cytochrome P450 (CYP) monooxygenases that may metabolically activate PAH, forming electrophilic and redox-active metabolites that may damage cellular macromolecules and contribute to oxidative stress (Moorthy et al. 2015 Esser and Rannug 2015). Formation of reactive oxygen species (ROS) and induction of oxidative stress is regarded as an important molecular mechanism behind the adverse effects of PM (Møller et al. 2010).

RNA methylation regulates gene expression at the post-transcriptional level (Meyer, 2019). N^6-methyladenosine (m^6A) accounts for the largest proportion of RNA methylation (Yu et al., 2018), which is involved in cell apoptosis, cell proliferation and differentiation, and many other life activities (Lan et al., 2021). Many studies have revealed that the m6A modification is involved in the pathogenesis and development of some diseases, such as asthma,

chronic obstructive pulmonary disease (COPD), and cardiovascular diseases (Wu et al., 2020; Xu et al., 2022). $PM_{2.5}$ exposure induced an up-regulation of RNA m^6A levels, and increased expression of the RNA methyltransferase-like 3 (METTL3) and methyltransferase-like 14 (METTL14) in the lungs of mice and did not influence the expression of demethylase (Choe et al., 2019). In addition, activated phosphorylated Smad2/3 can enter the nucleus and bind to RNA methyltransferase complex, then induce m^6A RNA methylation in pluripotent stem cells. Given the above evidence, we speculate that TGFβ signal pathway could play the role in the regulation of RNA methylation induced by $PM_{2.5}$ exposure.

In this study, we investigated the health risk of ambient air $PM_{2.5}$ and black carbon from the following aspects. (1) By systemic review and meta-analysis, we summarized and assessed the risk of mortality of long-term and short-term exposure to ambient air BC in published papers worldwide to date; (2) From the perspective of epigenetic modification, we investigated the effect of $PM_{2.5}$ exposure on RNA methylation of the lung; (3) By performing transcriptome sequencing of the lung from exposed and control mice, we examined the possible mechanisms of $PM_{2.5}$-induced or BC-induced lung injury by examining the expression levels of relevant factors in lung tissues and tried to identify the new biomarkers of the effect of $PM_{2.5}$ exposure on health; (4) By in vitro study, we used BC and aged BC to assess the toxicity of BC by observing its effects on cell motility, viability and inflammatory factors; 5) We assessed the toxicity of PM samples by characterizing the pro-inflammatory potential of atmospheric PM in an advanced 3D cell culture model exposed under ALI conditions. 6) Then, to assess the hazards posed by different types and sources of particles, we characterized the adverse biological effects of different PM samples from three specific cities with representative pollution sources by co-culture.

6.2 Review of global studies on the effects of ambient air $PM_{2.5}$/black carbon on human health

Exposure to BC in the short or long term will have varying degrees of adverse effects, especially on the respiratory system, cardiovascular system, and even the nervous system. We identified the need for a systematic quantitative review of the evidence. Meta-analysis is an important systematic analysis method. It allows us to express quantitatively by summarizing the research results of scholars and using statistical methods. In this report, we mainly research all global articles related to ambient BC.

According to the Preferred Reporting Items for Systematic Review and Meta-Analyses (PRISMA) guide, four authoritative databases were searched for articles on epidemiology published from the establishment of the database to July 1, 2021. The databases were PubMed, Embase, The Cochrane Library, and Web of Science. Searching words were focused on BC, air pollution, mortality, and morbidity. The study design was based on an observational epidemiological study, including cohort, case-control, time-series, and case-crossover. We have included all studies on mortality or morbidity of heart and lung diseases, neurological diseases, and other diseases.

The search results were 82 eligibility articles. Among them, there were 43 articles about short-term exposure and 40 articles about long-term exposure. We only estimated the association between BC and mortality.

Pooled random effects relative risk (RR) estimates were calculated for mortality (such as total mortality, cardiovascular mortality, respiratory mortality, and lung cancer mortality) for which estimates from at least three different studies were available for the same age group and for different cities. To calculate pooled estimates and compare estimated effects for BC in each study, pooled effect estimates were expressed RR per 10 $\mu g/m^3$ and 95% confidence intervals (CIs). HR (hazard ratio) and OR (odds ratio) are usually equivalent to RR when the mortality is very low. The standardized effect estimates were pooled using the random-effect model for there was substantial heterogeneity between the included studies. Heterogeneity among the included studies was evaluated by a Chi-square-based Cochrane Q statistic test and I-squared statistic. The R Studio program package ‘meta’ was used to perform the meta-analysis.

6.2.1 Short-term health effects

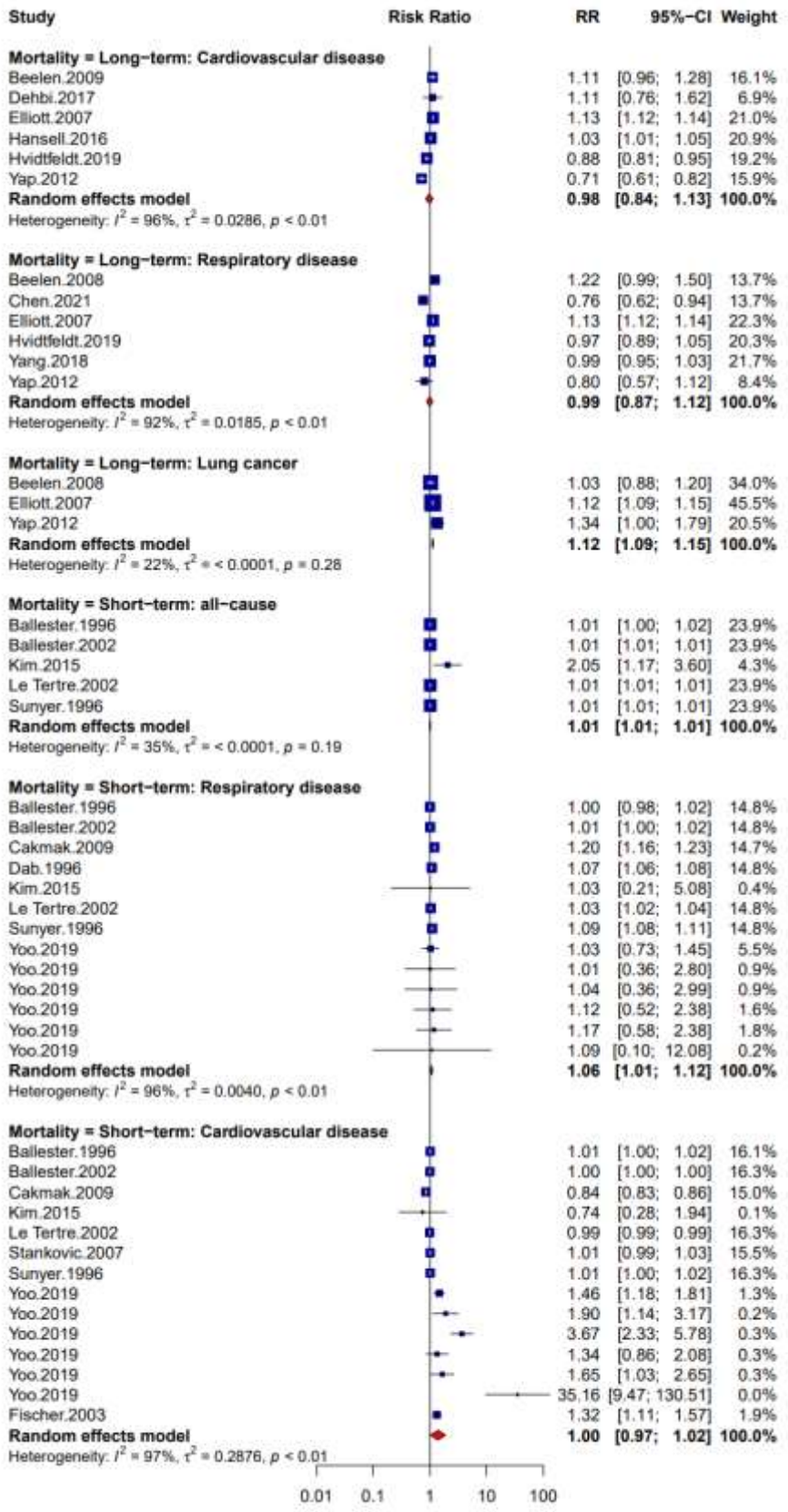

Figure 6-2 Forest plot for the association between BC and various mortalities in the general population. RR is for an increase of 10 μg/m3 of BC; 95%-CI means 95% confidence interval; I2 means the heterogeneity between effect estimates; τ2 means the variance I2 of between-study; the p-value is based on the Cochran's Q test.

The short-term relationships between air pollution and health effects are characterized by the time lag (in days) between exposure and health events and investigators vary in which lags they study and report. This means that the use of any particular lag would result in the exclusion of many other studies. Therefore, if more than one lag measure was presented, this review selected one for meta-analysis according to the following algorithm: 1) the lag that the author focused on or stated a priori; 2) the lag that was the most statistically significant (positive or negative) and 3) the lag with the largest effect estimate (positive or negative).

There were 5 studies on total mortality, 9 studies on cardiovascular disease mortality, and 8 studies on respiratory disease mortality, all of which had complete information and the effect size was RR. The overall pooled meta-estimates for total mortality, cardiovascular disease mortality, and respiratory mortality were 1.01 (95%CI: 1.00–1.01), 1.00 (95%CI: 0.97–1.02), and 1.06 (95%CI: 1.03–1.10) per 10 μg/m^3 increase in short-term BC exposure, respectively (Figure 6-2). The results of the meta-analysis showed a significant positive association of BC with both total mortality and respiratory disease mortality. The respiratory result had high heterogeneity.

6.2.2 Long-term health effects

For long-term exposure studies, the cohort study is one of the most commonly used study designs. And there was a meta-analysis about the cohort study of long-term exposure. Pooled random effect estimates were calculated for mortality (such as cardiovascular mortality, respiratory mortality, and lung cancer mortality).

There were 6 studies on cardiovascular disease mortality, 6 studies on respiratory disease mortality, and 3 studies on lung cancer mortality, all of which had complete information and the effect size was RR, HR or OR. The overall pooled meta-estimates for cardiovascular disease mortality, respiratory mortality, and lung cancer mortality were 0.98 (95%CI: 0.84–1.13), 0.99 (95%CI: 0.87–1.12), and 1.12 (95%CI: 1.09–1.15) per 10 μg/m3 increase in long-term BC exposure, respectively (see Figure 2). The results of the meta-analysis showed only a significant positive association between BC and lung cancer mortality with low heterogeneity. The reason for the lack of significant association of other outcomes with BC may be related to the small number of relevant studies.

6.3 In vivo study of the health effects of ambient $PM_{2.5}$/black carbon in China

6.3.1 Materials and methods

Exposure protocols

Inhalation exposure: The protocol for inhalation exposure to $PM_{2.5}$ has been described in detail in a previously published article (Li et al., 2019). Briefly, mice were exposed in stainless steel chambers to either HEPA-filtered clean air (control) or to real-world concentrations of ambient $PM_{2.5}$. The duration of exposure was either 24 h or 30 days, depending on the different experimental protocols. In some experiments, mice exposed to $PM_{2.5}$ for 24 h were transferred to the clean air chamber and exposed to HEPA-filtered air for another 120 hours.

Instillation exposure: mice were exposed to BC by instillation twice a week, for 4 weeks, and the dosage of BC for every instillation was 100μg, 200μg, 400μg.

BALF acquisition: Following exposure bronchoalveolar lavage fluid (BALF) was acquired by injecting 1 mL physiological saline into the lungs via a lagging needle inserted through a small hole in the trachea. In the process of injecting, the lung tied with a thin thread was massaged gently. Finally, the BALF was recycled by a syringe. All the BALFs were stored at -80 ℃.

ELISA

The release of IL-1β, IL-6, IFN-γ, IL-2, IL-4, IL-5, IL-10, IL-17, MEK, ERK and ICAM-1 in the BALF was measured by enzyme-linked immunosorbent assay (ELISA) using commercially available kits according to the manufacturer's instructions

Diff quick staining

The changes in macrophage number in BALF was detected using Diff Quik staining assay.

Lung morphometric analysis

A portion of the lung tissue was placed in a fixative solution, then dehydrated with ethanol. The wax was embedded in paraffin and sliced into thin slices. The slices were stained by hematoxylin-eosin (HE) staining. The histological and pathological features of the lung were detected using microscopy and immunohistochemistry.

Quantitative real-time PCR

The gene expression level of GATA-3 and T-bet were detected by real-time PCR. Total RNA was extracted by using an RNA isolation kit (Tiangen, China) following the manufacturer's instructions. The PrimeScript RT Master Mix (TaKaRa, Dalian, China) was used to synthesize cDNA. Real-time PCR validation was conducted using the Maxima® SYBR® Green qPCR Master Mix kit (CWBIOtech, China) according to the manufacturer's instruction. β-Actin as an internal reference gene. Each sample was repeated in triplicate and the fold change in gene expression was calculated according to the 2-ΔΔCt method.

RNA sequencing

Using second-generation RNA sequence of gene expression analysis, second-generation RNA sequence, RNA-seq, was used to analyze lung Gene expression profiling. We compared the altered gene pathways to the control group, $PM_{2.5}$ group, and reversal group by second-generation RNA sequence. The level of gene expression in all samples was evaluated to observe the gene changes in the lungs. The KEGG pathway was analyzed by using the database of DAVID.

Statistical analysis

Results are presented as means ± standard error of the mean (SEM). The pairwise comparison was performed by using Student's t-test or analysis of variance (ANOVA) after the analysis of homogeneity of variance and normal distribution. All statistics were calculated with GraphPad Prism 8.0 and p-values less than 0.05 were considered significant.

6.3.2 The effects of BC exposure on lung

BC exposure leads to pathological Injuries in the lungs

BC exposure impaired the morphology of the lung of mice. By BC exposure, we observed the fractured pulmonary alveolar wall and enlarged alveolar space and the tendency of the lung. The BC is also deposited in the lungs (Figure 6-3).

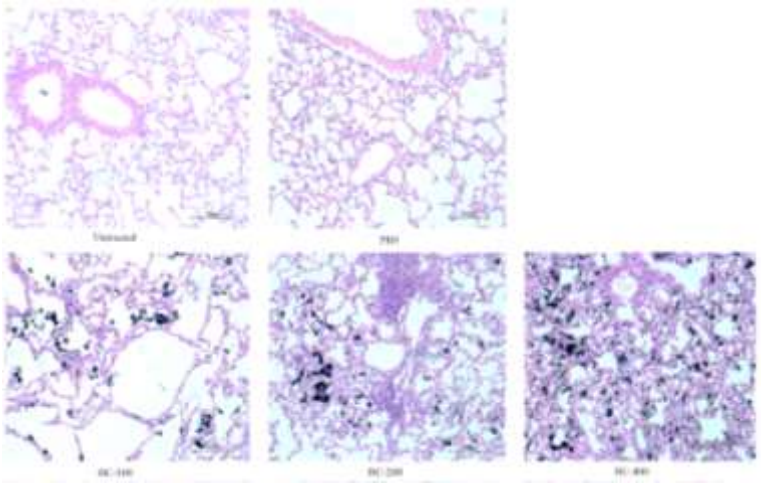

Figure 6-3 Histopathology of lung

BC exposure induced an increase in macrophage counts in the lung

By Diff Quik staining, we observed an increase in macrophage counts in the lung after BC exposure. Meanwhile, the counts of macrophages increased with the increase in BC concentration (Figure 6-4).

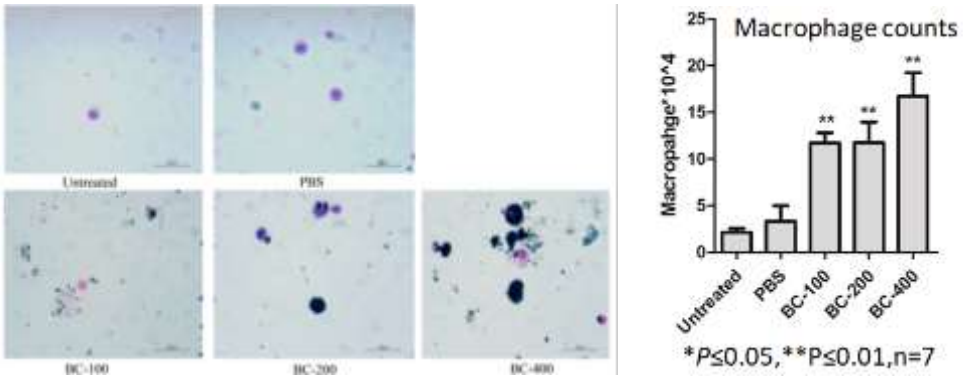

Figure 6-4 The macrophage counts of lungs after BC exposure

Effect of BC exposure on the expression of cytokines

By ELISA, we found that BC exposure elevated the expression of IL-1β and IL-6 (Figure 6-5).

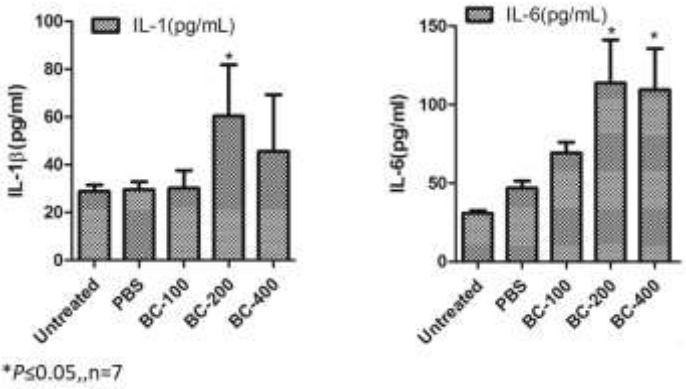

Figure 6-5 Levels of cytokines in BALF

Summary

BC is a key component of $PM_{2.5}$ and mainly exists in traffic-related particles. Our data showed that inhaled BC can be deposited in the lungs and produce significant lung inflammation. These results indicate that BC plays an important role in lung injury induced by $PM_{2.5}$ exposure.

6.3.3 The effects of air particle exposure on Th1/Th2 balance

$PM_{2.5}$ exposure leads to pathological Injuries in the lungs

After $PM_{2.5}$ exposure, microphotographs of the lung revealed that $PM_{2.5}$ exposure impaired the morphology of the lung of mice. After $PM_{2.5}$ exposure, a light microscopic examination showed a fractured pulmonary alveolar wall and enlarged alveolar space (Figure 6-6). Meanwhile, the alveolar wall also presented the tendency of lung consolidation. The interstitium of pulmonary alveoli is filled with inflammatory exudate (Figure 6-6).

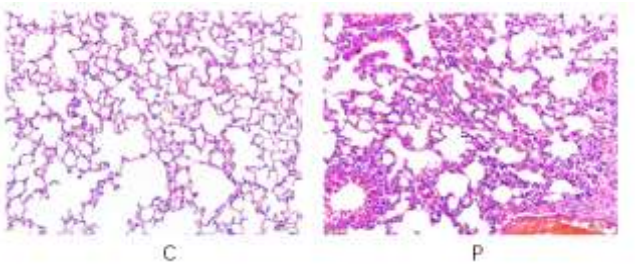

Figure 6-6 Lung histology (HE stain) of mice. C: ctrl; P:$PM_{2.5}$

$PM_{2.5}$ exposure significantly upregulated lung ECP levels

Eosinophil cationic protein (ECP) is a characteristic factor secreted by eosinophils, and it is a potential biomarker for the evaluation of asthma (Koh et,al). ECP expression levels in the lung were significantly upregulated ($P<0.01$) after $PM_{2.5}$ exposure (Figure 6-7).

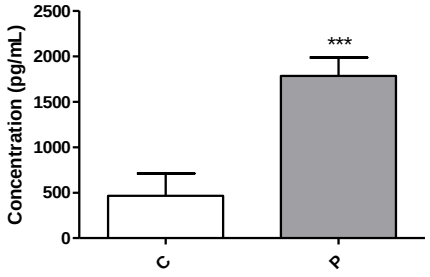

Figure 6-7 ECP protein expression level in BALF. (*P<0.05, **P<0.01, ***P<0.001). C: ctrl; P: $PM_{2.5}$

Effect of $PM_{2.5}$ on Th1/Th2 balance

To determine the effect of $PM_{2.5}$ on the Th1/Th2 balance, we measured the levels of inflammatory factors secreted by the helper T cells in BALF. IFN-γ and IL-2 were secreted by the Th1 cell; IL-4, IL-5, and IL-10 were secreted by the Th2 cell (Neurath et al., 2002). We found that $PM_{2.5}$ exposure induced the downregulation of IL-2 and up-regulation of IL-4, IL-5, and IL-10, but it did not influence the secretion of IFN-γ. (Figure 6-8)

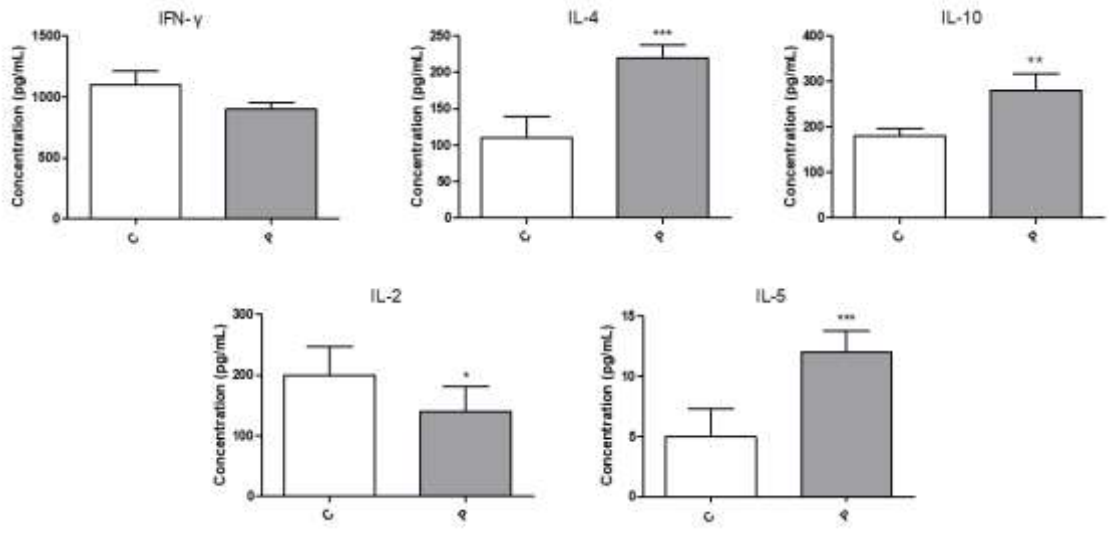

Figure 6-8 The protein expression level of inflammatory factors secreted by Th1 and Th2 cells in BLAF. IFN-γ and IL-2 were secreted by TH1 cell, IL-4, IL-5, IL-10 were secreted by TH2 cell (*P<0.05, **P<0.01, ***P<0.001). C: ctrl; P:$PM_{2.5}$

GATA-3 and T-bet gene expression level in the Th1/Th2 balance mechanism

Both GATA-3 and T-bet are key genes in the Th1/Th2 balance mechanism. GATA-3 controls the polarization of Th0 toward Th2 and T-bet controls the polarization of Th0 toward Th1 (Murphy and Reiner, 2002). Therefore, changes in the Th1/Th2 balance mechanism can be reflected by changes in T-bet and GATA-3 expression levels. The results showed (Figure 6-9) that $PM_{2.5}$ exposure induced the downregulation of T-bet and did not affect the expression of GATA-3.

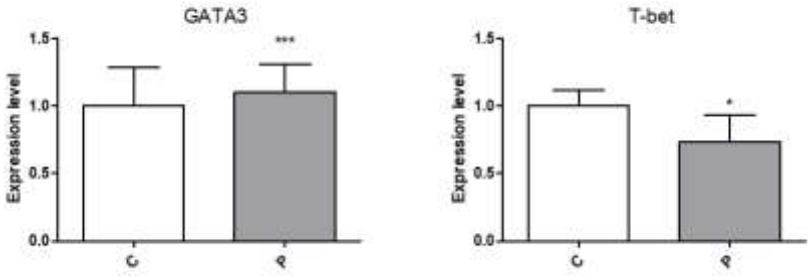

Figure 6-9 The levels of GATA-3 and T-bet were changed in wild group (*P<0.05, **P<0.01, ***P<0.001). C: ctrl; P:$PM_{2.5}$

Summary

The imbalanced Th1/Th2 cell function is the important pathogenesis of the development of asthma. Our results show that $PM_{2.5}$ exposure induced histopathological changes in the lungs, accompanied by upregulation of ECP, suggesting that $PM_{2.5}$ exposure could exacerbate eosinophilic asthma in mice. In addition, the expression of cytokines IL-4, IL-5, and IL-10 secreted by Th2 cells was upregulated and the expression of T-bet was significantly decreased after $PM_{2.5}$ exposure, indicating that $PM_{2.5}$ exposure induced the shifting of Th1/Th2 balance toward to Th2.

6.3.4 $PM_{2.5}$ exposure induces lung injury via Ras and Rap signaling pathways in mice

Pathological effects of $PM_{2.5}$ on lung morphology

Microphotographs of the lung revealed that $PM_{2.5}$ exposure impaired the morphology of lung of mice. As shown in Figure 10, the lung of $PM_{2.5}$ exposed animals showed obvious inflammatory infiltration, thickening of smooth muscle and rupture and fusion of alveolar septa compared with controls. Meanwhile, the alveolar wall also presented the tendency of lung consolidation (Figure 6-10a, b). When mice exposed to $PM_{2.5}$ was put into a clean chamber, after 120 h of air purification, the inflammatory infiltration and the damage to the Alveoli were reversed (Figure 6-10b, c).

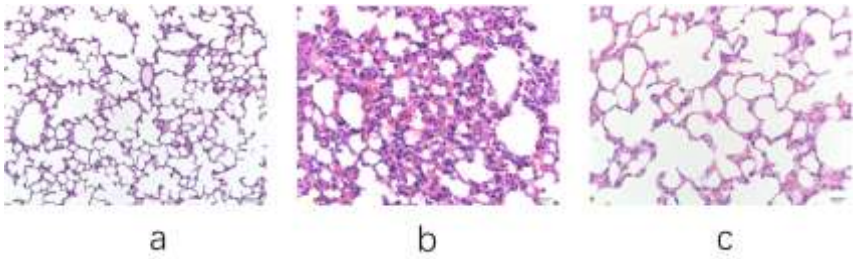

Figure 6-10 Lung histology (HE stain) of mice. (a) A representative HE image of the lung in the control group; (b) A representative HE image of the lung in the $PM_{2.5}$ exposure group; (c) A representative HE image of the lung in the reversal group.

Differentially expressed genes

A total of 19636 transcripts were detected by transcriptome sequencing analysis of lung tissues from exposed and control mice. Compared with the control group, 683 genes were significantly up-regulated and 1540 genes were significantly down-regulated in the exposed group, for a total of 2223 genes with significant differences (Figure 6-11)

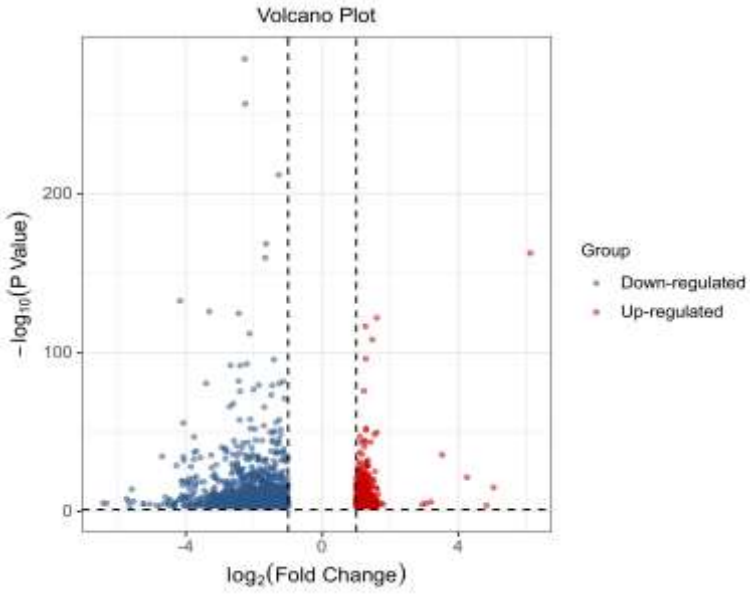

Figure 6-11 Volcano Plot of the genomic alterations in mice exposed to acute $PM_{2.5}$ exposure

$PM_{2.5}$ exposure leads to changes in signaling pathways

Compared with the control group, the Rap signal pathway in the $PM_{2.5}$ exposure group was up-regulated significantly ($p=0.037$) (Figure 6-12). The results showed that $PM_{2.5}$ could significantly induce changes in the Rap signal pathway. The effects were reversed when the animals were returned to filtered air. In the Rap pathway, the Ras / Raf/MEK/ERK was changed significantly by exposure to PM.

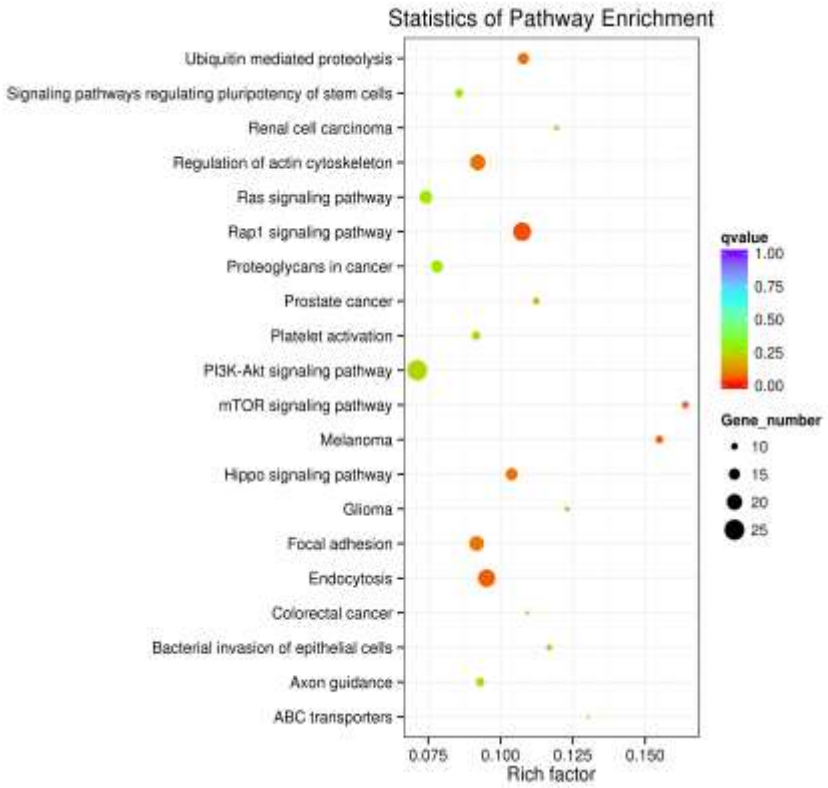

Figure 6-12 Top 20 KEGG pathway enrichment in the acute $PM_{2.5}$ exposure group.

Effects of $PM_{2.5}$ exposure on gene expression

We determined the expression levels of VEGF, Rap, Ras, and Raf typing (VEGFa, Rap1b, Kras, Braf) by PCR. The results showed that the expression levels of rap1b, Braf and VEGFa were significantly upregulated after $PM_{2.5}$ exposure and downregulated after air purification (Figure 6-13). While there was no significant change between the three groups of Kras (Figure 6-13).

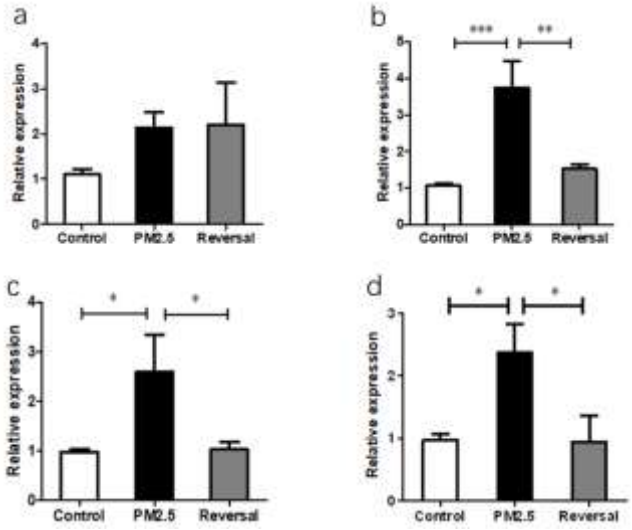

Figure 6-13 Rap1b, Braf, Kras and VEGFa mRNA expression levels in different lung tissue after $PM_{2.5}$ exposure. All data are mean ± S.E.M. *p<0.05, **p<0.01, ***p<0.001.

Effects of $PM_{2.5}$ exposure on inflammatory factors expression

We measured the levels of ICAM-1, MEK and ERK by ELISA. The results showed that the expression levels of ERK were significantly upregulated after $PM_{2.5}$ exposure. The expression levels of MEK and ICAM-1 were significantly upregulated after $PM_{2.5}$ exposure. All of these alterations by $PM_{2.5}$ exposure were reversed after air purification (Figure 6-14).

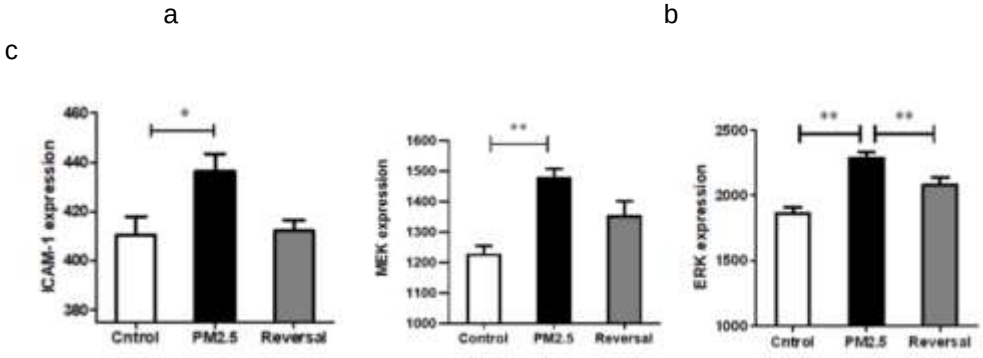

Figure 6-14 Enzyme-linked Immunosorbent Assay (ELISA) on ICAM-1, MEK and ERK expression levels in mice bronchoalveolar lavage fluid (BALF), All data are mean ± S.E.M. *p<0.05, **p<0.01, ***p<0.001.

Summary

In the study, $PM_{2.5}$ exposure induced inflammatory infiltration, and altered expression of genes related to the Ras/Rap signaling pathway. These changes were reversed after air purification. Based on these results, we speculate that lung injury induced by $PM_{2.5}$ exposure could involve in change of Ras/Raf/MEK/ERK signaling pathway.

6.3.5 Epigenetic modification of $PM_{2.5}$ /BC exposure

TGF-β1/Smad2/3 levels in lungs of mice after real-world $PM_{2.5}$ exposure in chambers

Our previous study showed that acute $PM_{2.5}$ exposure induced a reversible change of RNA m6A levels and METTL3 and METTL14 in the lungs of mice (Choe et al., 2019) Considering the change patterns of RNA m6A levels and METTL3 and METTL14, the expression of TGF-β1 and Smad2/3 were also analyzed to explore whether TGF-β-Smad pathway is involved in $PM_{2.5}$ exposure-induced m6A RNA methylation modification and to clarify its up and downstream relationships. We found that the expression of TGF-β1 gene was significantly increased in the lung tissues of mice in the $PM_{2.5}$ exposed group ($p < 0.05$) (Figure 6-15A). Meanwhile, the expression of Smad2 and Smad3 genes was also elevated significantly compared to the control group ($p < 0.05$) (Figure 6-15B, C). All these alterations returned to normal at 120 h after the mice were transferred to purified air.

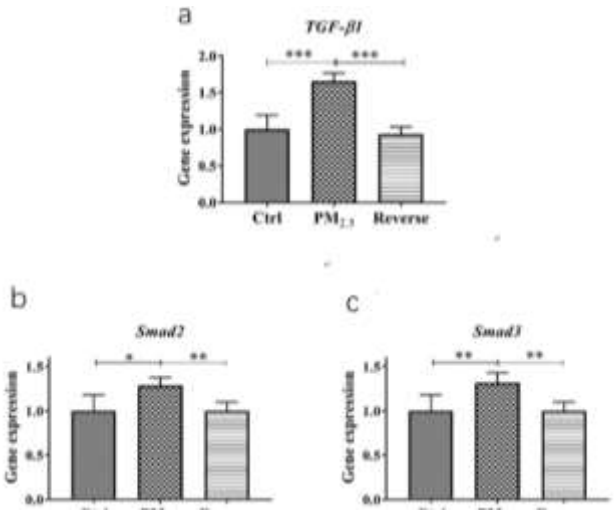

Figure 6-15 The expression of TGF-β1, Smad2/3 gene in lungs of mice after $PM_{2.5}$ exposure. (A) (B) (C) $PM_{2.5}$ exposure induced a significant up-regulation of TGF-β1, and Smad2/3 gene expression in the lung of mice， and their levels were back to normal after air purification. * $p < 0.05$. ** $p < 0.01$. *** $p < 0.001$.

Summary

$PM_{2.5}$ exposure induced the upregulation of m6A RNA methylation modification, and TGFβ signal pathway play the role in regulating m6A RNA methylation. In current study, we found the expression level of TGF-β1, Smad2/3 were upregulated. TGF-β1, Smad2/3 are the important factor of TGF-β signal pathway. Combined with the previous reports and the current results, we speculate the TGF-β signal pathway could involve in the m6A RNA methylation modification induced by $PM_{2.5}$ exposure.

6.4 In vitro study of the health effects of ambient $PM_{2.5}$/BC in China

6.4.1 Materials and methods

$PM_{2.5}$ and BC samples

Ambient air $PM_{2.5}$ was sampled in three specific cities with representative pollution sources in different seasons in the year 2019-2021 to assess the effects of $PM_{2.5}$ in vitro. The particles were collected on Teflon filters and extracted from the filters using freeze drying after ultrasonic elution with ultra-pure water. The BC samples we used in the present experiment consisted of BC (less than 1 μm in size) and aged BC, which was treated with ozone prior to the experiment. The chemical compositions of $PM_{2.5}$ samples were analyzed, including organic carbon (OC), element carbon (EC), sulfate, nitrate, ammonium, metals (28 species) and polycyclic aromatic hydrocarbons (PAHs) (EPA 16 species). The major chemical compositions of $PM_{2.5,}$ including OC/EC, sulfate, nitrate and ammonium in the 3 places in different seasons are shown in Figure 6-16. In summary, $PM_{2.5}$ concentrations were highest in 2019, and lowest in 2021. The concentrations of $PM_{2.5}$ were highest in winter and lowest in summer in all cities, with corresponding changes in the concentrations of various major components. The source of $PM_{2.5}$ of city 1was traffic; city 2 was heavy industry and coal combustion; city 3 was industries complex and vehicle. The City 2 with heavy industries and coal combustion sources had the highest $PM_{2.5}$ concentrations and the City 3with industry complex and vehicle source had the lowest $PM_{2.5}$ concentrations (Figure 6-16).

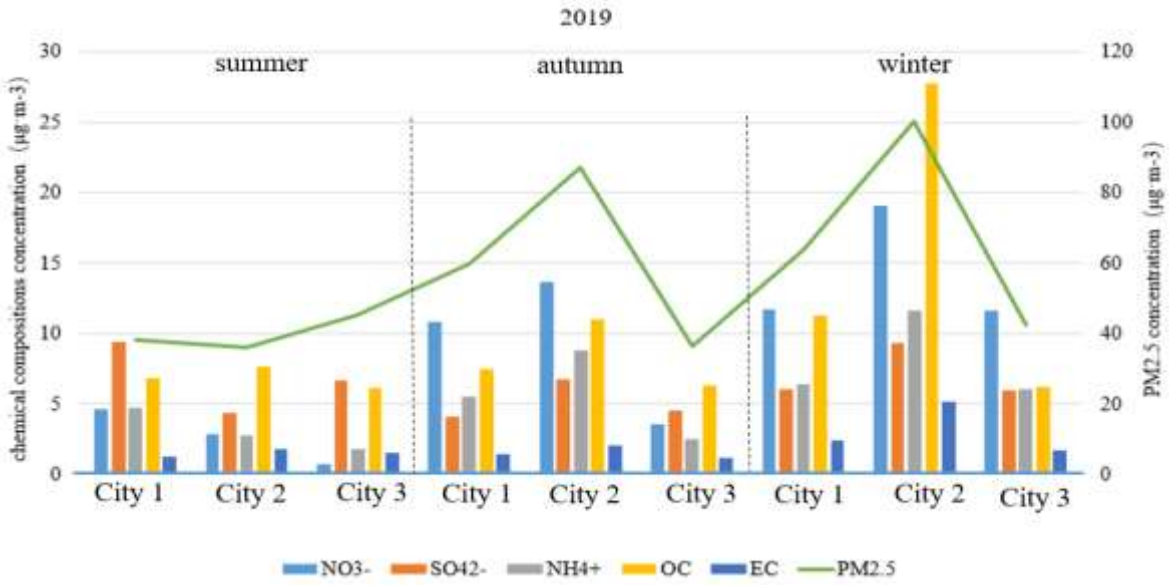

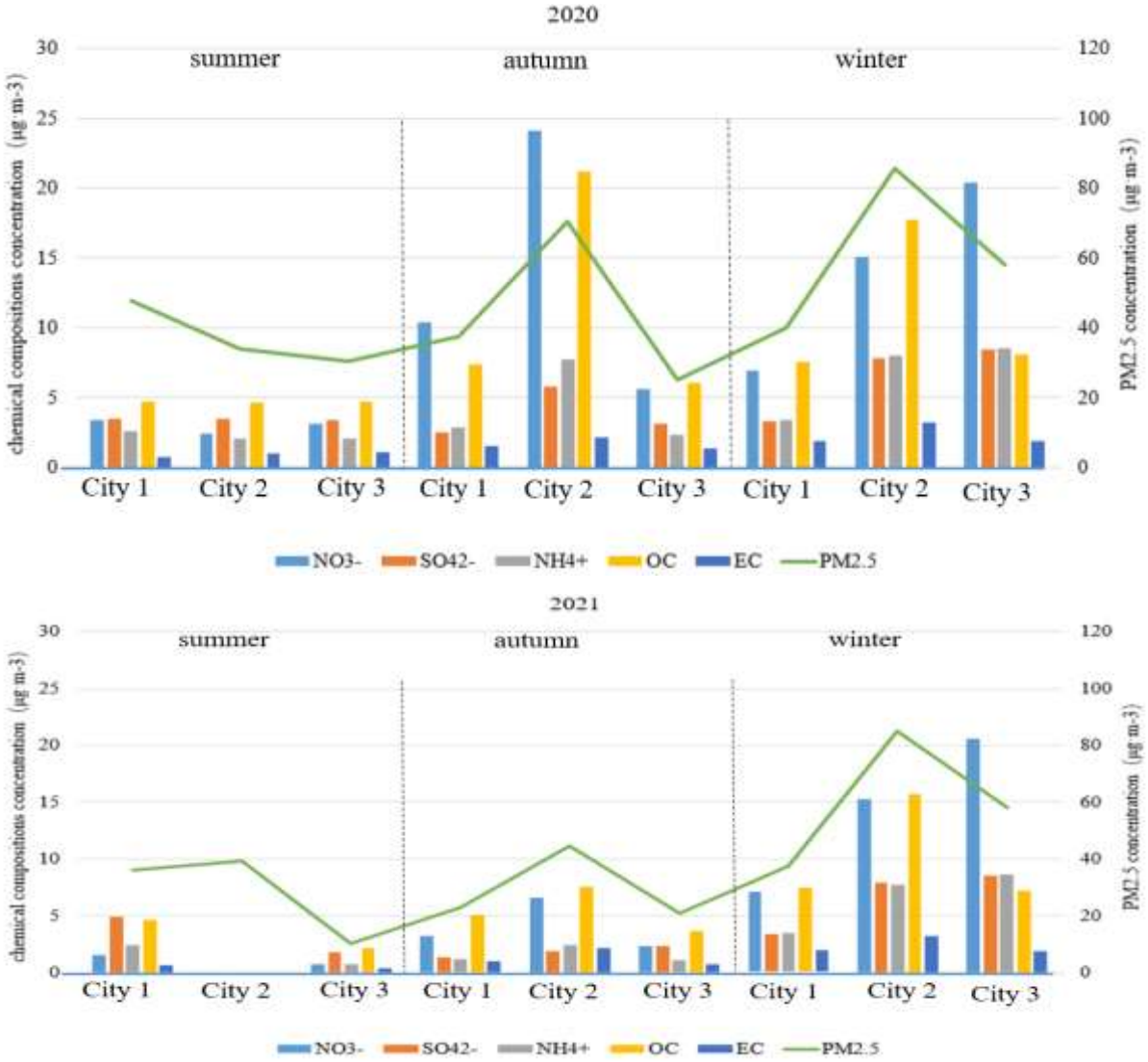

Figure 6-16 The concentrations of OC/EC, sulfate, nitrate and ammonium of $PM_{2.5}$ in the 3 cities

Moreover, two samples of PM were included in this study to characterize inflammatory responses in vitro and in vivo. Standard reference material (SRM) 2786 was purchased from National Institute of Standards and Technology (NIST). SRM2786 is a sample of ambient PM collected from the ventilation system of an exhibition center in Prague, Czech Republic, and is representative example of atmospheric PM from an urban area. The sample has been characterized for content of a range of organic and inorganic chemicals, including PAH, nitro-PAH and various metals. The mean particle diameter of the sample is 2.8 μm. A sample of traffic-related $PM_{2.5}$ (Traffic-$PM_{2.5}$, diameter below 2.5 μm) collected in a Norwegian road tunnel was also included in the study (Skuland et al. 2022). Sampling particles in a road tunnel limits contamination from other sources of particles, thus allowing study of the potential impact of PM from traffic-related sources. The sample has previously been characterized for particle size distribution, endotoxin levels, PAH content, and content of organic and elemental carbon, as described in a recent publication (Skuland et al. 2022). The content of PAH and metals is also provided in Appendix 6-1.

Cell cultures

Several cell lines were used in the present study to represent the cells of the human respiratory system. A549 is a human lung carcinoma cell line originally derived from ex-plant of human tissue (Giard et al. 1973), and represents an alveolar type epithelial cell. EA.hy 926 is an endothelial cell line that was originally established by fusing primary human umbilical vein cells with a clone of A549 (Edgell et al. 1983). THP-1 is a monocytic leukaemia cell line that can be differentiated into adherent macrophage-like cells (Daigneault et al. 2010, Lund et al. 2016). Differentiated THP-1 cells are referred to as THP-1 macrophages in the main body of the text. RAW264.7 is a

mouse macrophage cell line. The cell culture procedure is based on the protocol published in Skuland et al. (2017), with minor modifications. Some initial experiments were also performed to optimize the cell models and the results are presented in Appendix 2.

Cocultures of alveolar epithelial cells and macrophages, cells typical for the alveolar part of the respiratory system, were established by seeding differentiated THP-1 macrophages on confluent A549 monolayers and incubating the cultures overnight. The advanced 3D cell culture consisting of A549 cells, THP-1 macrophages and Ea.Hy cells (Figure 6-17) was grown on transwell inserts, with EA.hy 926 endothelial cells in the basolateral compartment and A549 epithelial cells in the apical compartment. Differentiated THP-1 macrophages were seeded in the apical compartment on a confluent A549 monolayer. The transwell inserts have pores that allows for translocation particle-associated chemical compounds and secreted mediators between the apical compartment and the basolateral compartment, which represents the alveolar space and circulation, respectively, allowing for intercellular communication that more closely recapitulates the in vivo situation. For experiments under air-liquid interface (ALI) conditions, the medium was removed after allowing the THP-1 macrophages to adhere to the A549 layer, and the 3D coculture incubated overnight. For experiments simulating effects of PM beyond the lung, human peripheral blood mononuclear cells (PBMC), isolated from the blood of healthy volunteers, were seeded in the basolateral compartment right before exposure to PM.

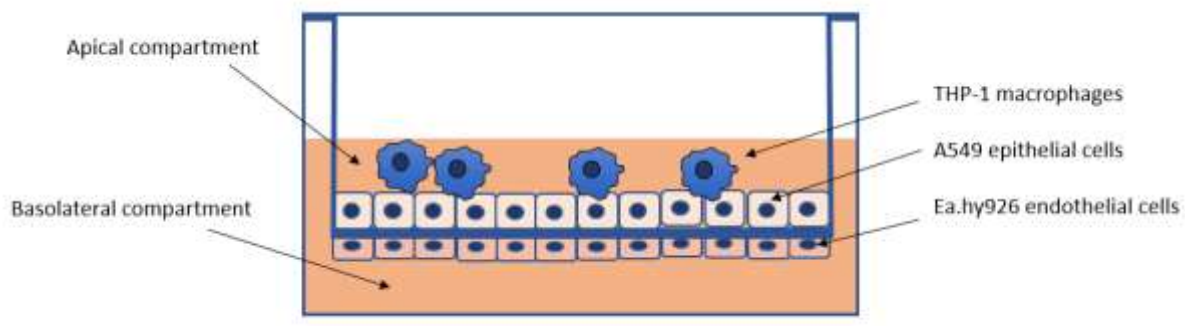

Figure 6-17 Schematic representation of the A549/THP-1/Ea.Hy926 3D cell culture

Exposure regime

BC exposure: When the cells were in logarithmic growth phase, cells were collected and seeded in 24-well plate at the concentration of 4 ×105 cell/mL (1 mL/well). After 24 h, the supernatant was replaced by new DMEM with different concentrations of BC and ozonized-BC exposure (1, 1.9,7.8 31.25, 125, and 500 μg/m), and then cells were incubated at 37 ℃ for 24 h.

$PM_{2.5}$ exposure: The A549 cells were seeded in a six-well plate at 1 $\times 10^6$ cells per well, and then were exposed to $PM_{2.5}$ suspension for 24 hours. The final concentration of $PM_{2.5}$ treatment was 0, 50, 100, 200 μg/mL.

Traffic-PM2.5 and SRM2786 exposure: Exposure of A549 and THP-1 monocultures, A549/THP-1 cocultures, and A549/THP-1/Ea.hy926 3D cell cultures under submerged conditions was performed in the same medium used to culture the cells. The final exposure concentrations were 12.5, 25, 50, 100 and 200 μg/mL, which corresponds to doses of 1.3, 2.6, 5.3, 10.5 and 21 μg/cm^2. Exposure of A549/THP-1/Ea.hy926 3D cell under ALI conditions was performed using a VITROCELL® Cloud Alpha 6 exposure system. As the cells are exposed to particles directly from air, this approach represents a more physiologically relevant exposure protocol. The particle sample is pipetted into the nebulizer unit which aerosolises the sample, creating a mist of fine droplet that deposits on the cell culture (Figure 6-18). The deposition efficiency of the system was initially determined using Na-fluorescein and was continually controlled during the experiments using the onboard quartz microbalance (QCM). However, the resulting exposure concentration in the experiments was somewhat lower than the estimated 10.5 μg/cm^2, at 5.71± 1.35 μg/cm^2. Following exposure to particle samples at either submerged or ALI conditions, the cells were incubated for 3-24 h at 37 ℃ depending on the experimental setup.

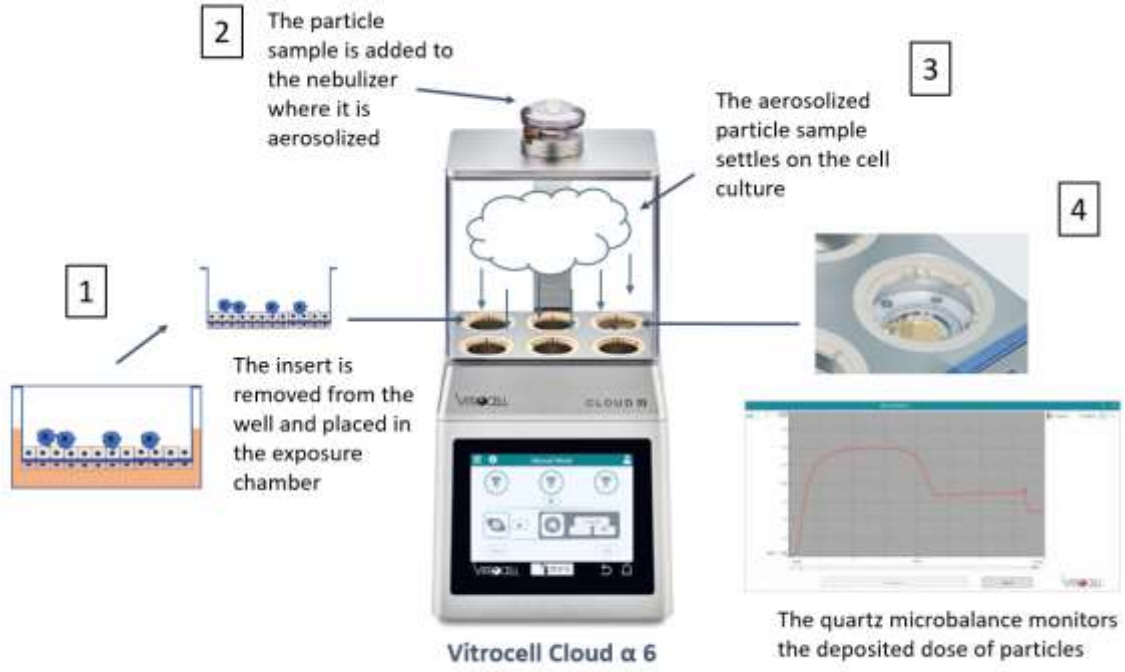

Figure 6-18 Exposure at air-liquid interface (ALI)

Cytotoxicity/ cell permeability

HCS LIVE/DEAD® Green Kit (Catalog no. H10290, Invitrogen, USA) with two-color nuclear fluorescence staining assay is used to evaluate the cell viability after $PM_{2.5}$ exposure (Moore et al., 2017). The kit includes Image-iT DEAD Green™ viability stain for discrimination of dead cells and HCS NuclearMask™ Deep Red stain for total cell demarcation. The Image-iT® DEAD Green™ viability stain in the kit is impermeable to healthy cells, whereas it can enter once the membrane integrity of the cells is compromised. High-content fluorescence imaging was performed using the SpectraMax i3 platform with MiniMax Imaging Cytometer (Molecular Devices, USA).

The viability of A549 and THP-1 monocultures, A549/THP-1 cocultures, and A549/THP-1/Ea.hy926 3D cell cultures after exposure to Traffic-$PM_{2.5}$ or SRM2786 was determined using the alamarBlue™ assay according to the manufacturers instructions.

Flow cytometry

The level of CD54 and CD86 were detected by flow cytometry.

Cytokine release

The levels of interleukin (IL)-1β, tumor necrosis factor alpha (TNFα), IL-6, and C-X-C motif chemokine ligand 8 (CXCL8) released in the cell culture supernatant was determined using enzyme-linked immunosorbent assay (ELISA), a highly specific and sensitive semi-quantitative assay for measuring proteins in a sample (Leng et al. 2008). All analyses were conducted using commercially available Cytoset (Invitrogen by Thermo Fischer Scientific, Waltham, MA, USA and Novex by Life Technologies Waltham, MA, USA) or Duoset (R&D systems, Minneapolis, MN, USA) kit according to the manufacturer's instructions, as detailed in a recent publication (Grytting et al. 2022).

QPCR

The PrimeScript RT Master Mix (TaKaRa, Dalian, China) was used to synthesize cDNA. Real-time PCR validation was conducted using the Maxima® SYBR® Green qPCR Master Mix kit (CWBIOtech, China) according to the manufacturer's instructions, in an ABI Prism 7500 Sequence Detection System 288 (Applied Biosystems Inc), with the following procedures: 95 ℃ for 10 minutes; 95 ℃ for 30s, 60 ℃ for 1 min, and 72 ℃ for 1 min; 40cycles. B-actin is used as a standardized internal control.

For detection of GAPDH, CXCL8, IL-1β, IL-6, TNFα, cytochrome p450 (CYP)1A1, heme oxygenase (HO)-1 and intercellular cell adhesion molecule (ICAM)-1 expression, RNA was first isolated using the NucleoSpin RNA Plus kit (Macherey-Nage, Düren, Germany) and reverse transcribed into cDNA using High Capacity cDNA Reverse Transcription Kit (Applied Biosystems by Thermofischer, Waltham, Ma, USA) and an S-100 thermal cycler (BioRad, Hercules, CA, USA). Gene expression was then determined using a CFX96 Touch Real-Time PCR Detection System (BioRad, Hercules, CA, USA) with pre-designed TaqMan Gene Expression Assays and TaqMan Universal PCR Master Mix, as detailed in a recent publication (Grytting et al. 2022).

Statistical analyses

The result is expressed as mean ± standard deviation. Statically significant differences between groups were determined by one or two-way analysis of variance (ANOVA) followed by Dunnett's, Tukey or Šídák's post-tests, depending on the experimental design. Log-transformation was used in cases where the data did not meet model assumptions of normality and homoscedasticity. All statistical analysis was performed in GraphPad Prism software (version 9.0.0) and p values less than 0.05 were considered as significant.

6.4.2 Cellular studies of BC exposure

The RAW264.7 (mouse mononuclear macrophages) cells were exposed to BC and aged-BC with different concentrations, 1, 1.9,7.8 31.25, 125, and 500 μg/ml. With increasing concentration of them, the viability of cells decreased gradually (Figure 6-19). The viability of cells induced by aged-BC exposure was lower than that in BC. Moreover, we examined the effect of BC and aged-BC exposure on the expression level of cell surface adhesion molecules, CD54 (ICAM-1) and CD86. BC exposure altered the expression level of CD54 and did not affect the expression level of CD86. ozonized-BC exposure did not induce the alteration of CD54 and CD86 (Figure 6-20).

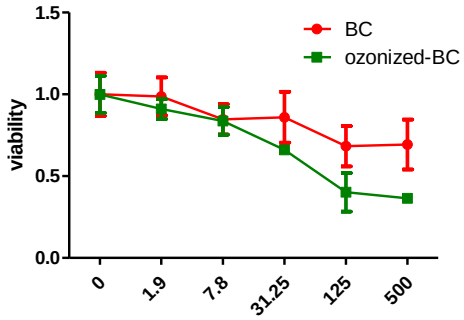

Figure 6-19 The viability of cells by different concentrations of BC exposure

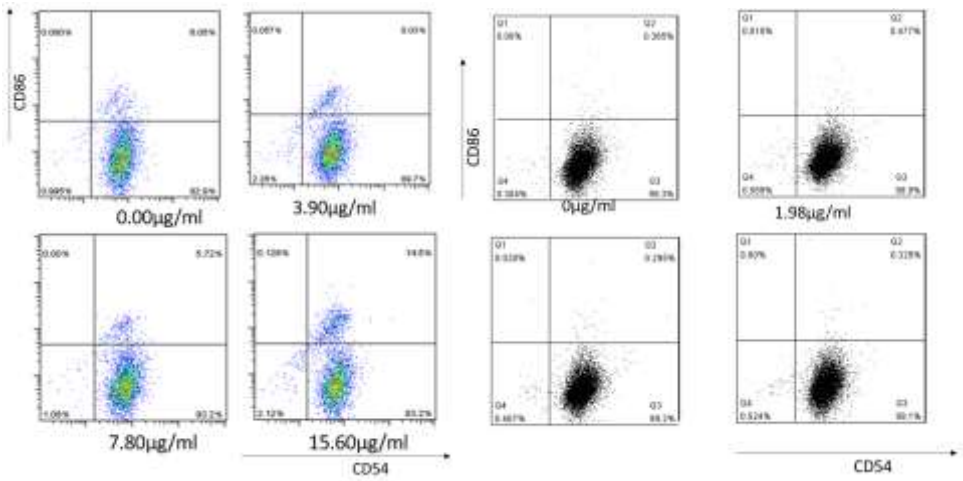

Figure 6-20 Effect of BC (left) and ozonized-BC (right) exposure on the expression level of cell surface adhesion molecules, CD54 and CD86

6.4.3 Cellular studies of sampled particles

6.4.3.1 RNA m6A modification of $PM_{2.5}$ exposure

In the present study, we collected the PM in the Chinese research academy of environmental sciences (CRAES). We found that the intensity of the green signal increased and the density of the cell decreased as we elevated the concentration of $PM_{2.5}$ (Figure 6-21). When the $PM_{2.5}$ concentration reached 200 ug/mL for 24 hours, the field of view was almost entirely filled with green signals, which meant that the cell membrane was completely permeated and cell survival was extremely low (Figure.6-21d). Therefore, the subsequent molecular biology analyses were performed at low to moderate concentrations of $PM_{2.5}$ (0, 50, 100 μg/mL).

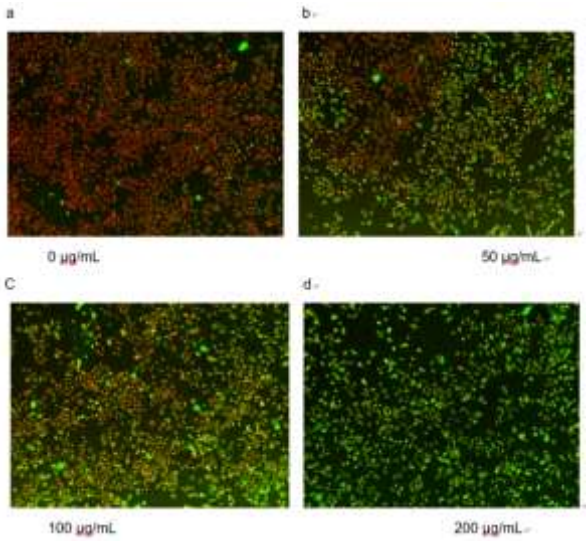

Figure 6-21 Fluorescence staining imaging results of A549 cells after $PM_{2.5}$ exposure for 24 hours. (a) There is almost no green fluorescence and the cells are impermeable without $PM_{2.5}$ treatment. (b) after exposure to 50 μg/mL $PM_{2.5}$, the green fluorescence signal is locally enhanced and the cells are locally permeable. (c) After exposure to 100 μg/mL $PM_{2.5}$, the green fluorescence signal is greatly enhanced, and the membrane was more permeable. (d) When the $PM_{2.5}$ exposure concentration reaches 200 μg/mL, the cell membrane is completely permeabilized and the cell survival rate is extremely low

We determined the concentration of m6A RNA methylation in cultured A549 cells after $PM_{2.5}$ treatment. The level of RNA m6A in A549 cells gradually increased with the increase of $PM_{2.5}$ concentration gradients (0, 50, 100 μg/mL) (Figure 6-22). When the concentration of $PM_{2.5}$ reached 100 μg/mL, the level of RNA m6A was significantly up-regulated ($p < 0.05$). Therefore, 100 μg/mL of $PM_{2.5}$ was selected as the representative exposure concentration for the subsequent study.

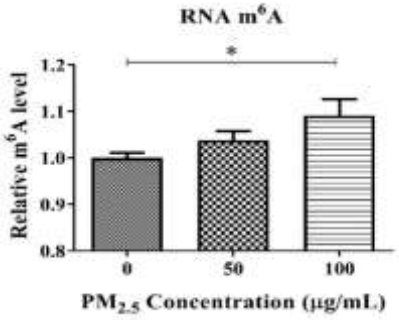

Figure 6-22 RNA m6A level in A549 cells after $PM_{2.5}$ exposure. $PM_{2.5}$ with the concentration of 100 μg/mL exposure induced a significant up-regulation of RNA m6A level in A549 cells. *: $p < 0.05$.

The expression level of the TGF-β1 gene and protein were detected. The results of qPCR and ELISA analysis showed that the expression of the TGF-β1 gene and protein in the A549 cell lysate treated with PM suspension was significantly higher than that in the absence of $PM_{2.5}$ ($p < 0.05$) (Figure 6-23).

a b

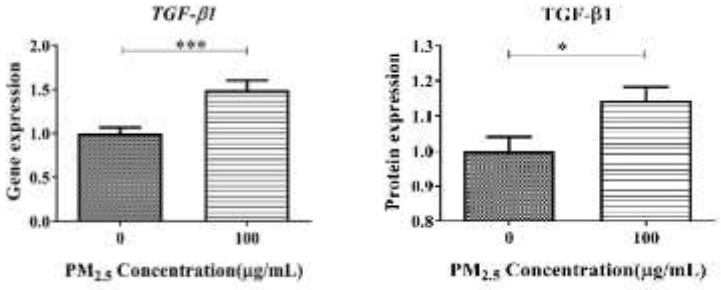

Figure 6-23 The expression of the TGF-β1 gene and protein in A549 cells after $PM_{2.5}$ exposure. (a) $PM_{2.5}$ exposure induced a significant up-regulation of TGF-β1 gene expression in A549. (b) $PM_{2.5}$ exposure induced a significant up-regulation of TGF-β1 protein expression in A549 cells. *: $p < 0.05$; ***: $p < 0.001$.

To further examine the role of TGF-β in $PM_{2.5}$-induced RNA m6A methylation, the TGF-β inhibitor fresolimumab (GC 1008) was added to the cell culture medium alone or together with $PM_{2.5}$. Fresolimumab is a high-affinity, fully human monoclonal antibody that neutralizes the active forms of human TGF-β1, β2, and β3 (Lacouture et al., 2015). The experimental group consisted of four groups: control group without any treatment (C); TGF-β inhibitor added group (G); $PM_{2.5}$ added group (P); $PM_{2.5}$ and TGF-β inhibitor simultaneously added group (PG). First, the TGF-β1 gene and protein expression levels of each experimental group were detected. The results showed that the $PM_{2.5}$-induced up-regulation of the TGF-β1 gene and protein expression was reversed after treatment with a TGF-β inhibitor ($p < 0.05$) (Figure 6-24), indicating that the inhibitor did suppress TGF-β1 expression. Going further, the RNA m6A levels of each experimental group were analyzed. The results showed that the $PM_{2.5}$-induced up-regulation of RNA m6A level was reversed after treatment with TGF-β inhibitor ($p < 0.05$) (Figure 6-25), which directly indicated that TGF-β1 was involved in $PM_{2.5}$-induced m6A RNA methylation.

a b

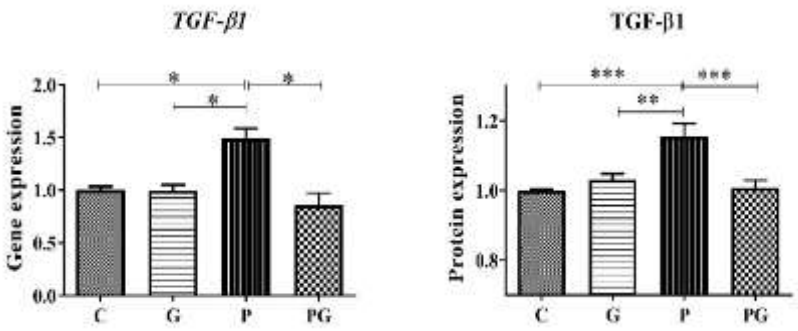

Figure 6-24 The expression of TGF-β1 gene and protein of A549 cells of all groups. C: control group without any treatment; G: TGF-β inhibitor added group; P: $PM_{2.5}$ added group; PG: $PM_{2.5}$ and TGF-β inhibitor simultaneously added group. (a) $PM_{2.5}$ induced up-regulation of TGF-β1 gene expression of A549 was inhibited after TGF-β inhibitor treatment. (b) $PM_{2.5}$ induced up-regulation of TGF-β1 protein expression of A549 was inhibited after TGF-β inhibitor treatment. *: $p < 0.05$; **: $p < 0.01$; ***: $p < 0.001$; No label means no statistically significant difference between groups (the same below).

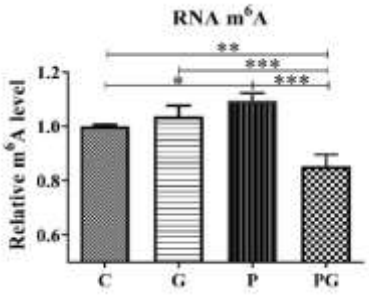

Figure 6-25 The RNA m6A levels of A549 cells of all groups. C: control group without any treatment; G: TGF-β inhibitor added group; P: $PM_{2.5}$ added group; PG: $PM_{2.5}$ and TGF-β inhibitor simultaneously added group. $PM_{2.5}$ induced up-regulation of RNA m6A level in A549 was reversed after TGF-β inhibitor treatment. *: $p < 0.05$; **: $p < 0.01$; ***: $p < 0.001$.

The result showed that there was no significant change in the Smad2 gene and protein expression in A549 after $PM_{2.5}$ exposure, while Smad2 expression was significantly downregulated in the group treated with both $PM_{2.5}$ and TGF-β inhibitors compared with the $PM_{2.5}$ added group (Figure 6-26a, b). Furthermore, $PM_{2.5}$ induced up-regulation of the Smad3 gene and protein expression in A549 was reversed after TGF-β inhibitor treatment ($p < 0.05$) (Figure 6-26c, d). These results indicated that TGF-β affected Smad3 expression in A549 after $PM_{2.5}$ exposure.

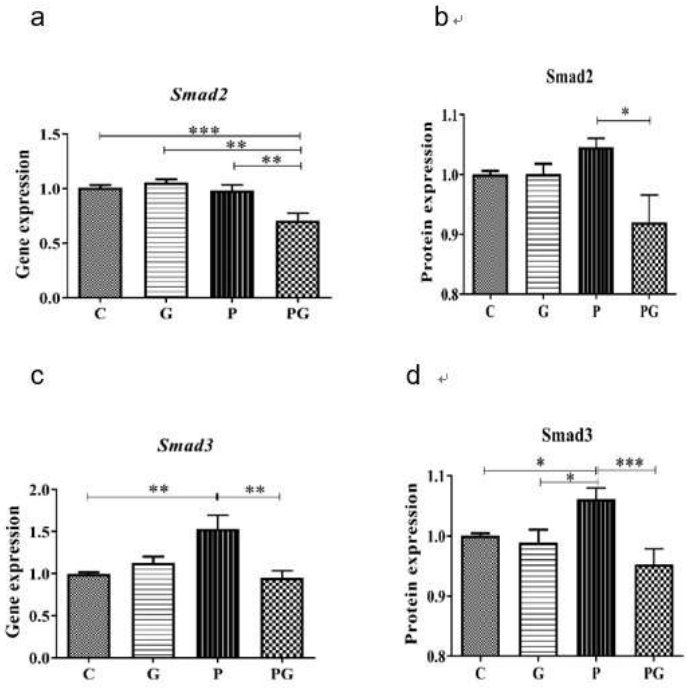

Figure 6-26 Smad2/3 level in A549 cells of all groups. C: control group without any treatment; G: TGF-β inhibitor added group; P: $PM_{2.5}$ added group; PG: $PM_{2.5}$ and TGF-β inhibitor simultaneously added group. (a) (b) Smad2 gene and protein expression did not change significantly after $PM_{2.5}$ exposure. (c) (d) $PM_{2.5}$ induced up-regulation of the Smad3 gene and protein expression was reversed after TGF-β inhibitor treatment. *: $p < 0.05$; **: $p < 0.01$; ***: $p < 0.001$.

The m6A RNA methylation is directly mediated by RNA methyltransferase and demethyltransferase. Therefore, we analyzed the expression of RNA methyltransferase like-3 (METTL3), methyltransferase like-14 (METTL14), wilms tumor 1 associated protein (WTAP), and demethyltransferase ALKB homolog 5 (ALKBH5), fat mass and obesity-associated protein (FTO). The results showed that $PM_{2.5}$ induced up-regulated gene and protein expression of METTL3 and METTL14 in A549 were reversed after TGF-β inhibitor treatment ($p < 0.05$) (Figure.6-27a, b, c, d). WTAP gene and protein expression did not change significantly after $PM_{2.5}$ exposure (Figure 6-27e, f).

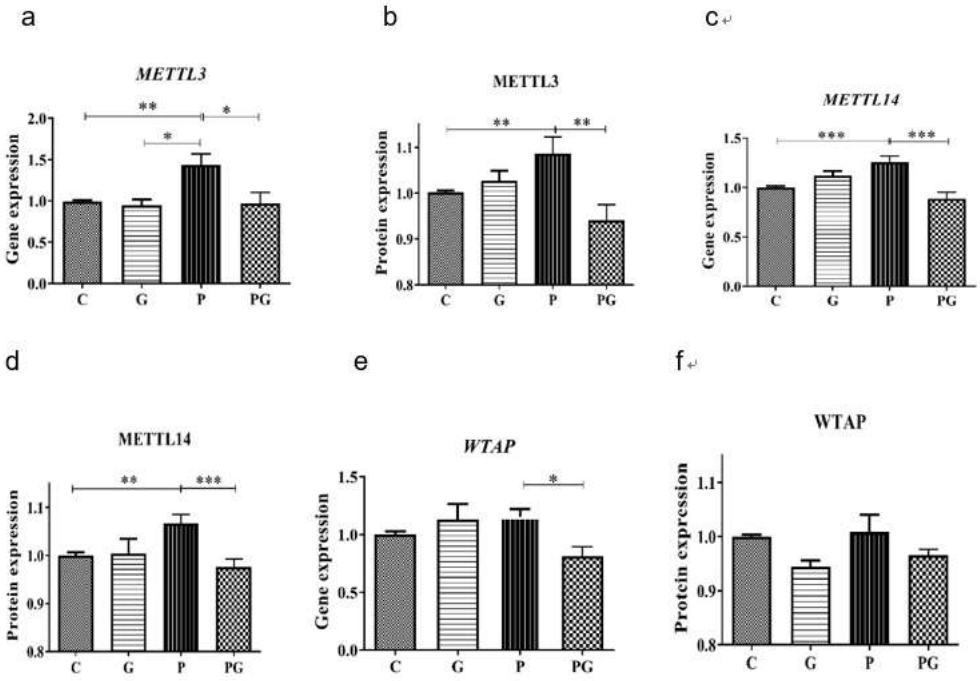

Figure 6-27 METTL3, METTL14 and WTAP level in A549 cells of all groups. C: control group without any treatment; G: TGF-β inhibitor added group; P: $PM_{2.5}$ added group; PG: $PM_{2.5}$ and TGF-β inhibitor simultaneously added group. (a) (b) $PM_{2.5}$ induced up-regulation of METTL3 gene and protein expression in A549 was reversed after TGF-β inhibitor treatment. (c) (d) $PM_{2.5}$ induced up-regulation of METTL14 gene and protein expression in A549 was reversed after TGF-β inhibitor treatment. (e) (f) WTAP gene and protein expression did not change significantly after $PM_{2.5}$ exposure. *: $p < 0.05$; **: $p < 0.01$; ***: $p < 0.001$.

In addition, at the gene level, $PM_{2.5}$-induced up-regulation of ALKBH5 expression in A549 was reversed after TGF-β inhibitor treatment (Figure 6-28a), while no significant changes were observed at the protein level (Figure 6-28b). Similarly, the FTO gene and protein expression did not change significantly after $PM_{2.5}$ exposure (Figure 6-28c, d).

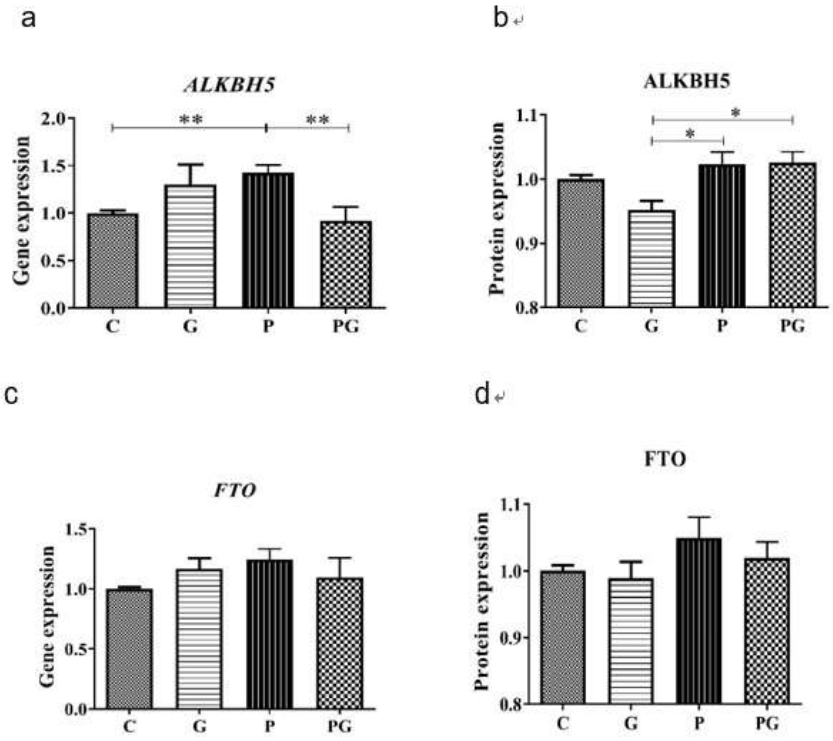

Figure 6-28 ALKBH5 and FTO levels in A549 cells of all groups. C: control group without any treatment; G: TGF-β inhibitor added group; P: $PM_{2.5}$ added group; PG: $PM_{2.5}$ and TGF-β inhibitor simultaneously added group. (a) $PM_{2.5}$ induced up-regulation of ALKBH5 gene expression in A549 was reversed after TGF-β inhibitor treatment. (b) ALKBH5 protein expression did not change significantly after $PM_{2.5}$ exposure. (c) (d) FTO gene and protein expression did not change significantly after $PM_{2.5}$ exposure. *: $p < 0.05$; **: $p < 0.01$.

In the present studies, we investigate the regulatory pathways and biomarkers of adverse health effects induced by $PM_{2.5}$/BC exposure through in vivo and in vitro studies. In vivo studies, we found many important pathways and biomarkers involved in Th1/Th2 balance, Ras and Rap signaling pathways. $PM_{2.5}$ exposure induced the shifting of Th1/Th2 balance toward to Th2. lung injury induced by $PM_{2.5}$ exposure could involve in change of Ras/Raf/MEK/ERK signaling pathway.

Furthermore, we explored the expression level of cytokines by the 3D co-culture model, which incorporates multiple cell types, as well as exposure at an air-liquid interface (ALI), which provides a more realistic model system for particle exposure in the lungs. Our study found a novel biomarker associated with the adverse health outcome induced by $PM_{2.5}$/BC exposure, which provides scientific evidence for preventing the diseases related to $PM_{2.5}$/BC exposure.

6.4.3.2 The pro-inflammatory effects of $PM_{2.5}$ exposure on the expression in an advanced 3D cell culture model

Pro-inflammatory responses were first assessed in a simple coculture of A549 cells and THP-1 macrophages. Exposure to SRM2786 induced a significant increase in the release of CXCL8 and IL-1β. However, the responses to the SRM2786 were qualitatively and quantitatively different between the two laboratories (Figure 6-29). As no solution was found to this issue, further comparison between the two laboratories was not attempted. The rest of this report will focus on assessing pro-inflammatory responses in the more complex 3D coculture model.

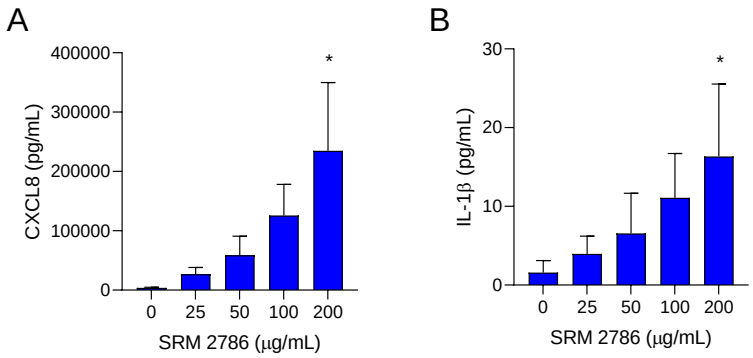

Figure 6-29 **Cytokine release in a A549/THP-1 coculture exposed to SRM2786.** Cocultures of A549 cell and THP-1 macrophages were exposed to 25, 50, 100 or 200 ug/mL SRM2786 for 24 h under submerged conditions. The release of CXCL8 (A) and IL-1β (B) (mean ± standard deviation, n=3) was measured in the cell culture medium by ELISA. * Statistically significant difference from control (0 ug/mL).

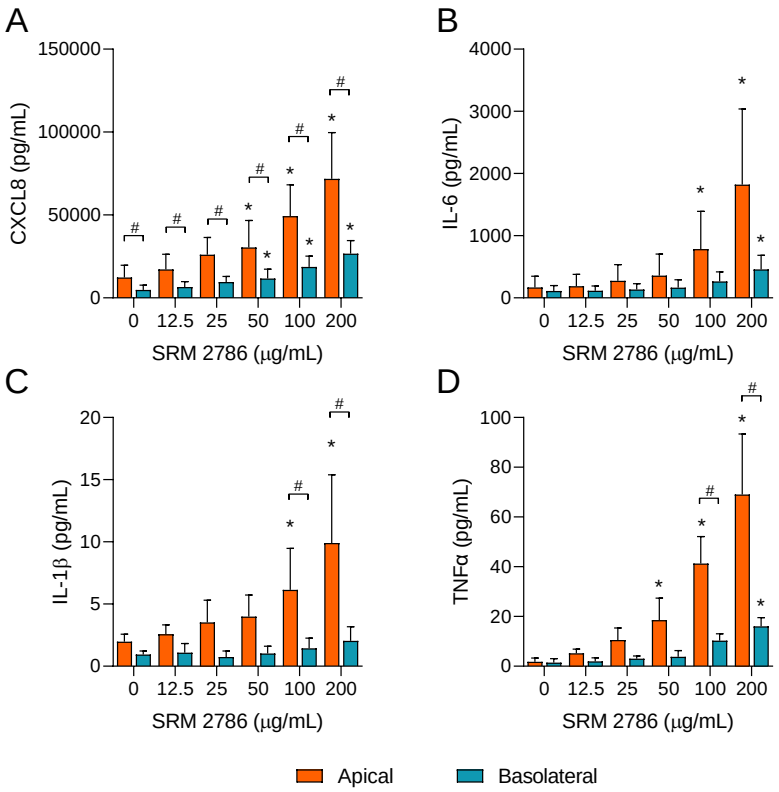

Figure 6-30 **Particle-induced cytokine release in the 3D cell culture under submerged conditions after exposure to SRM 2786.** 3D cocultures of A549 epithelial cells, Ea.Hy926 endothelial cells and THP-1-derived macrophages were exposed to 0-200 µg/mL SRM 2786 for 24 h under submerged conditions. The release of CXCL8 (A), IL-6 (B), IL-1β (C) and TNFα (D) (mean ± standard deviation, n=5) was measured in the cell culture medium from the apical (orange bars) and basolateral (blue bars) compartments by ELISA. * Statistically significant difference from control (0 µg/mL). # Statistically significant difference between insert and well at one concentration of SRM2786.

Exposure to SRM2786 particles induced a significant increase in the release of the pro-inflammatory cytokines CXCL8, IL-6 IL-1β and TNFα in the 3D cell cultures of A549 epithelial cells, Ea.Hy926 endothelial cells and THP-1-derived macrophages (Figure 6-30). Pro-inflammatory cytokines are signalling mediators that are involved in activating the inflammatory response in recipient cells and recruitment immune cells to the site of inflammation (Arango Duque and Descoteaux 2014, Turner et al. 2014). While the magnitude of the responses differed, all cytokines appeared to follow the same pattern. In the apical compartment (orange bars), exposure caused significant increases in CXCL8 (Figure 4A), IL-6 (Figure 6-30B), IL-1β (Figure 6-30C) and TNFα (Figure 6-30D) compared with controls, starting at 50-100 µg/mL (5.3-10.5 µg/cm^2) for all cytokines. By comparison, the levels of cytokines were lower in the basolateral compartment (blue bars) (Figure 6-30). However, a statistically significant release of CXCL8 compared to control was observed at 50 µg/mL (Figure 6-30A), while IL-6 and TNFα was significantly different from control at the highest concentration of 200 ug/mL (Figure 6-30C and D). This represents cytokines that have translocated through the transwell insert or that have been released from the endothelial cells in response to mediators from the apical compartment, or from particles or particle-associated chemical compounds. It should be kept in mind that the volume of medium is higher in the basolateral compartment than in the apical compartment, which will affect the resulting cytokine concentrations. Based on experiments where a THP-1/A549 coculture and monocultures of A549 cells and THP-1 macrophages were exposed in parallel, the responses in the apical compartment appeared to be mostly driven by the THP-1 macrophages, although evidence suggest that interaction between cells also contribute to the responses, especially for IL-6 release (Appendix 6-3: Additional figure 6- 3).

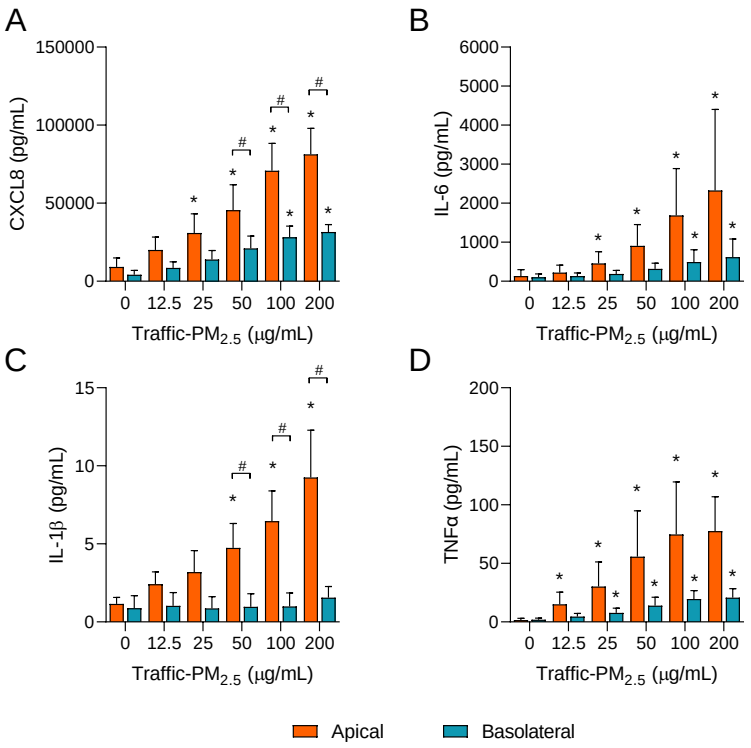

Figure 6-31 **Particle-induced cytokine release in the 3D cell culture under submerged conditions after exposure to fine particles from a road tunnel.** 3D cocultures of A549 epithelial cells, Ea.Hy926 endothelial cells and THP-1-derived macrophages were exposed to 0-200 µg/mL Traffic-PM$_{2.5}$ for 24 h under submerged conditions.

The release of CXCL8 (A), IL-6 (B), IL-1β (C) and TNFα (D) (mean ± standard deviation, n=5) was measured in the cell culture medium from the apical (orange bars) and basolateral (blue bars) compartments by ELISA. * Statistically significant difference from control (0 µg/mL). # Statistically significant difference between insert and well at one concentration of SRM2786.

The 3D cell culture was also exposed to Traffic-$PM_{2.5}$ sampled from a Norwegian road tunnel (Figure **6-31**). The cytokine responses induced by this particle sample was similar to what observed after exposure to the reference particles, SRM 2786, although the TNFα response appeared to level off at the highest concentrations. Higher levels of cytokines were detected in the apical compartment (orange bars) than the basolateral compartment (blue bars), reaching statistical significance for CXCL8 and IL-1β (Figure **6-31**A and C). Although the cytokine responses to SRM 2786 and Traffic-$PM_{2.5}$ were similar, cytokine levels were somewhat higher in both the apical and basolateral compartments after exposure to the traffic-derived particles with a significant increase in cytokines at a lower concentration of particles.

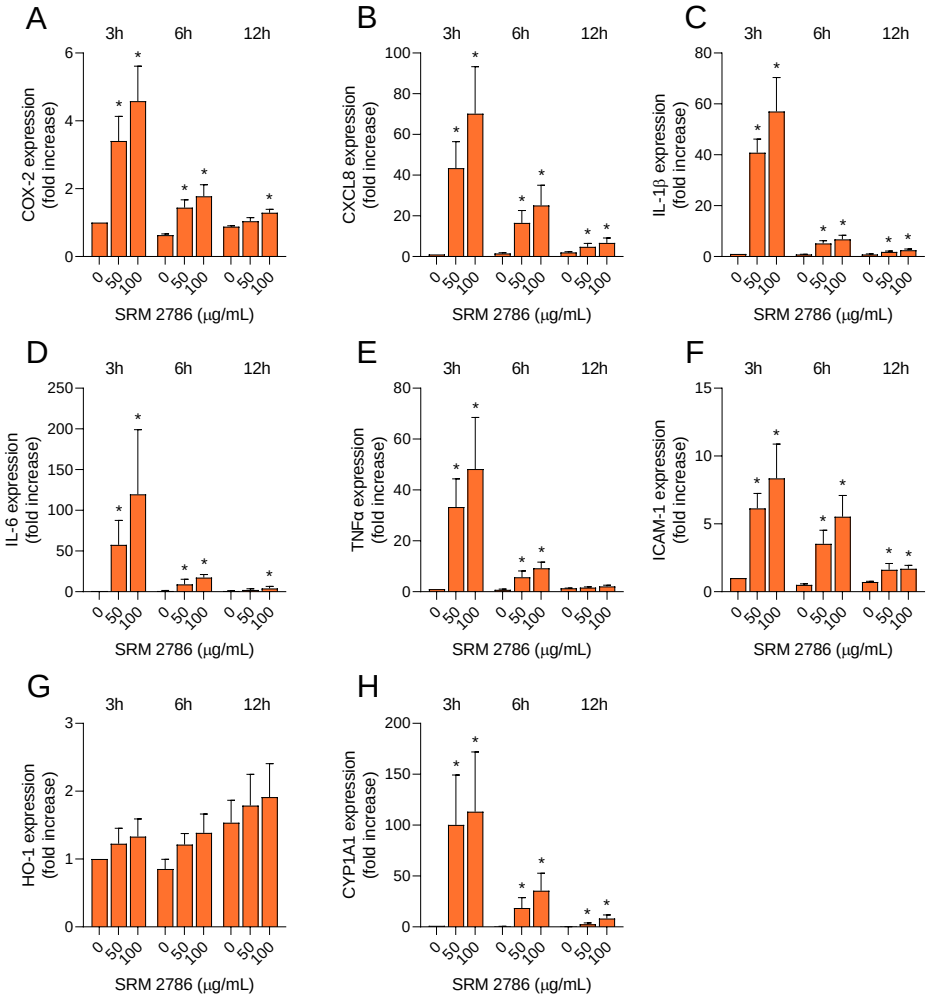

Figure 6-32 **Particle-induced changes in gene expression in the apical compartment after exposure to SRM 2786 under submerged conditions.** 3D cocultures of A549 epithelial cells, Ea.Hy926 endothelial cells and THP-1-derived macrophages were exposed to 50 or 100 µg/mL SRM 2786 for 3, 6 and 12 h under submerged conditions. The gene expression of COX-2 (A), CXCL8 (B), IL-1β (C), IL-6 (D), TNFα (E), ICAM-1 (F), HO-1 (G) and CYP1A1 (H) (mean ± standard deviation, n=3) in the apical compartment was measured using qPCR. * Statistically significant difference from control (0 µg/mL).

Next, the expression of genes related to the inflammatory responses, cell adhesion and recruitment, redox responses and xenobiotic metabolism was measured after 3h, 6h and 12h exposure to SRM2786 (Figure 6-32 and 6-33) and Traffic-$PM_{2.5}$ (Figure 6-34 and 6-35). In addition to the pro-inflammatory cytokines CXCL8, IL-1β, IL-6 and TNFα, the markers of inflammation included COX-2, an enzyme involved in the synthesis of inflammatory prostaglandins (Ricciotti and Fitzgerald 2011), and ICAM-1, a cell adhesion molecule induced by cytokines involved in recruitment of circulating immune cells (Ley et al. 2007, Harjunpaa et al. 2019). HO-1 is a commonly used marker for redox responses and is an enzyme under transcriptional control of the redox-sensitive nuclear factor erythroid 2-related factor 2 (Nrf2) pathway (Ahmed et al. 2017). CYP1A1 is an enzyme under transcriptional control of the AhR pathway and linked to metabolic activation of PAH (Moorthy et al. 2015 Esser and Rannug 2015).

All markers of inflammation followed a similar time-course after exposure to SRM 2786 with the highest increase after 3h and a decline with subsequent time-points. The strongest increase relative to control was observed for IL-6, followed by CXCL8, IL-1β and TNFα, although the IL-6 response was variable (Figure 6-32). The response for COX-2 expression was lower. Moreover, only low expression was seen for the cell adhesion molecule ICAM-1 (Figure 6-32A). CYP1A1 expression on the other hand, was highly expressed relative to control values. The expression followed the same time-course as the other genes, but expression was substantial even after 6h (Figure 6-32H). No substantial increase in HO-1 expression compared with control was observed, suggesting that ROS/oxidative stress was not important for the particle-induced responses (Figure 6-32G).

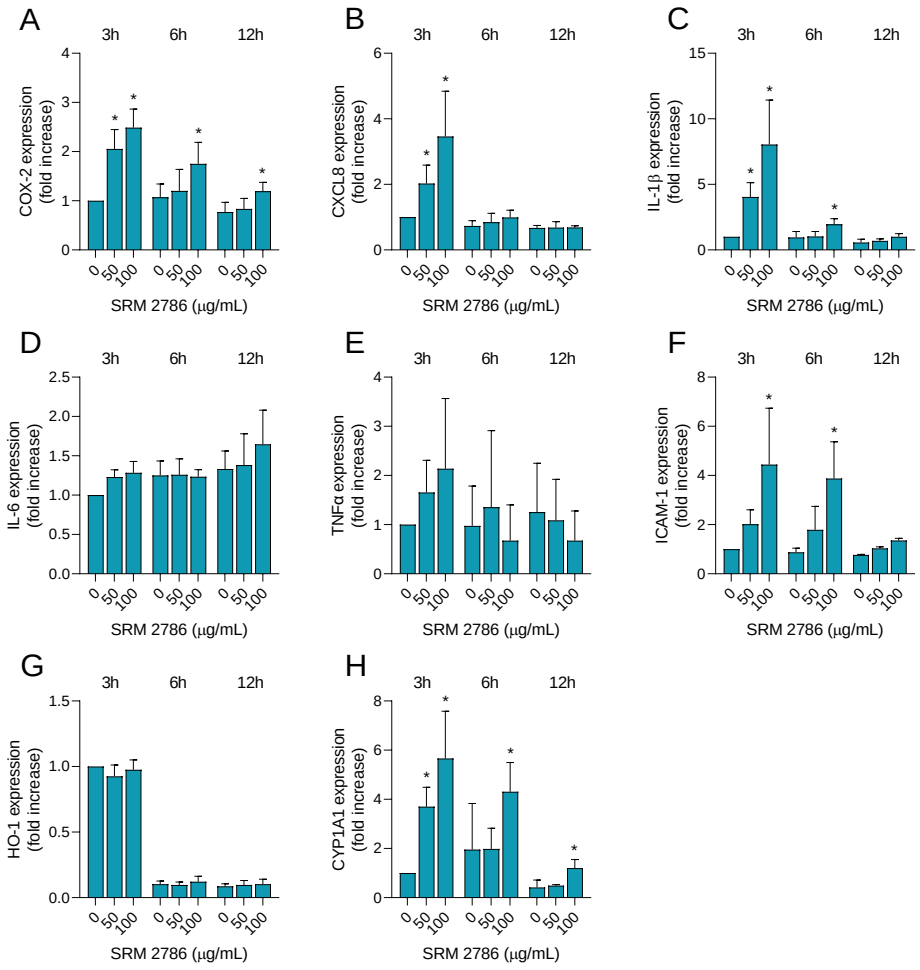

Figure 6-33 **Particle-induced changes in gene expression in the basolateral compartment after exposure to SRM 2786 under submerged conditions.** 3D cocultures of A549 epithelial cells, Ea.Hy926 endothelial cells and THP-1-derived macrophages were exposed to 50 or 100 µg/mL (5.3 and 10.5 µg/cm^2) SRM 2786 for 3, 6 and 12

h under submerged conditions. The gene expression of COX-2 (A), CXCL8 (B), IL-1β (C), IL-6 (D), TNFα (E), ICAM-1 (F), HO-1 (G) and CYP1A1 (H) (mean ± standard deviation, n=3) in the basolateral compartment was measured using qPCR. * Statistically significant difference from control (0 µg /mL).

All genetic markers were showed a lower relative expression in the basolateral compartment compared with the apical compartment (Figure 6-33). The pro-inflammatory markers followed a similar time-course as in the apical compartment with highest expression after 3 h (Figure 6-33). However, only low or no change in the expression of IL-6 and TNFα was observed (Figure 7D and E). In addition, several values at 6 and 12 h was below the limit of detection for TNFα. Consequently, the TNFα dataset was not analysed statistically. While the expression of HO-1 was not changed by exposure, a sharp decline in HO-1 expression was observed 6 h after exposure, possibly indicating cellular stress at early time-points caused by the exposure procedure (Figure 6-33G). Interestingly, an increase in CYP1A1 expression was observed in the basolateral compartment, possibly indicating that lipophilic organic chemicals like PAHs have translocated through the insert (Figure 6-33H).

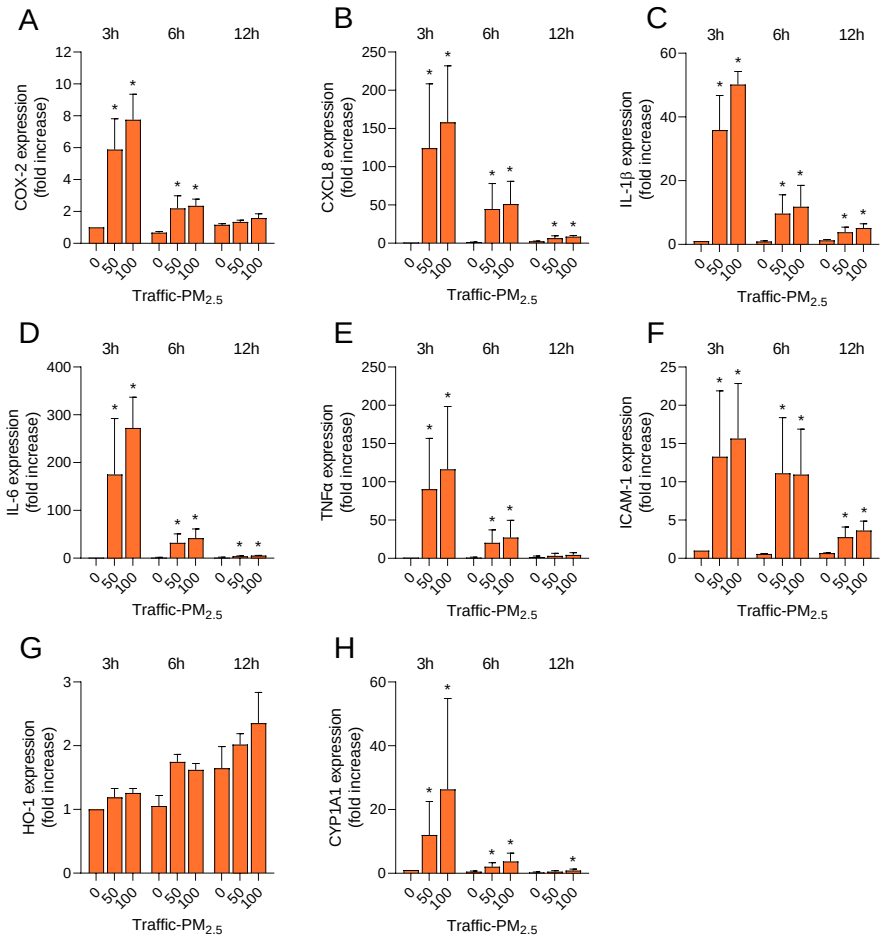

Figure 6-34 **Particle-induced changes in gene expression in the apical compartment after exposure to fine particles from a road tunnel under submerged conditions. 3D** cocultures of A549 epithelial cells, Ea.Hy926 endothelial cells and THP-1-derived macrophages were exposed to 50 or 100 µg/mL Traffic-$PM_{2.5}$ for 3, 6 and 12 h under submerged conditions. The gene expression of COX-2 (A), CXCL8 (B), IL-1β (C), IL-6 (D), TNFα (E), ICAM-1 (F), HO-1 (G) and CYP1A1 (H) (mean ± standard deviation, n=3) in the apical compartment was measured using qPCR. * Statistically significant difference from control (0 µg/mL).

All genes also followed a similar time-course after exposure to Traffic-$PM_{2.5}$ as observed after exposure to the SRM 2786, with the highest response after 3h followed by a decline in relative expression with subsequent time-points (Figure 6-34). The strongest relative expression was detected for IL-6, followed by CXCL8, IL-1β and TNFα (Figure 6-34B-E). Smaller responses were detected for COX-2, although the same pattern was observed (Figure 6-34A). With the exception of IL-1β, the expression of the pro-inflammatory markers was somewhat higher after exposure to the Traffic-$PM_{2.5}$ than after exposure to the SRM 2786 sample. However, the variation in response between experiments was quite high. An increase in the cell adhesion molecule ICAM-1 was also observed (Figure 6-34F). As with the pro-inflammatory markers, the expression of ICAM-1 was higher after exposure to Traffic-$PM_{2.5}$ compared with exposure to SRM2786. No substantial change in HO-1 was observed after exposure to Traffic-$PM_{2.5}$ (Figure 6-34G). CYP1A1 expression was markedly increased after 3h and declined with subsequent time-points (Figure 6-34H). Unlike the inflammatory genetic markers, the relative increase in CYP1A1 expression was lower for Traffic-$PM_{2.5}$ than after exposure to SRM 2786, possibly reflecting lower content or bioavailability of organic chemicals like PAHs in the Traffic-$PM_{2.5}$.

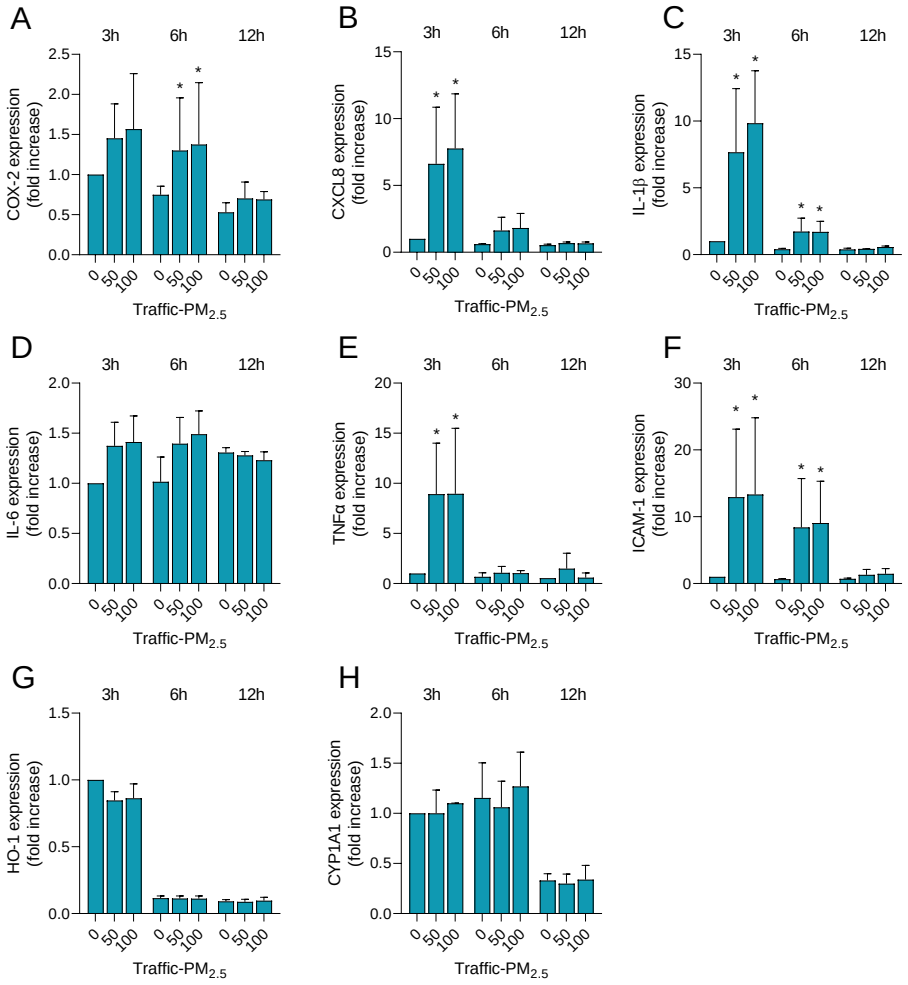

Figure 6-35 **Particle-induced changes in gene expression in the basolateral compartment after exposure to fine particles from a road tunnel under submerged conditions.** 3D cocultures of A549 epithelial cells, Ea.Hy926 endothelial cells and THP-1-derived macrophages were exposed to 50 or 100 µg/mL Traffic-$PM_{2.5}$ for 3, 6 and 12h under submerged conditions. The gene expression of COX-2 (A), CXCL8 (B), IL-1β (C), IL-6 (D), TNFα (E), ICAM-1 (F), HO-1 (G) and CYP1A1 (H) (mean ± standard deviation, n=3) in the basolateral compartment was measured using qPCR. * Statistically significant difference from control (0 µg/mL).

Lower relative expression of all the genes was observed in the basolateral compartment, as also observed for SRM2786 exposure. Most of the genes followed a similar time-course as in the apical compartment (Figure 6-35). For the pro-inflammatory markers, the highest expression was observed for IL-1β and TNFα, followed by CXCL8, while no substantial increase in IL-6 and COX-2 expression was observed (Figure 6-35A-E). The expression of COX-2 was also lower than observed after exposure to SRM2786. ICAM-1 was the only with similar expression in the basolateral and apical compartments and expression was higher than after exposure to SRM 2786 (Figure 6-35F). Exposure to Traffic-$PM_{2.5}$ did not change the expression of HO-1 showing limited capacity to induce increased ROS and oxidative stress in this model system. However, as also shown in figure 6-33, overall HO-1 expression decreased with time, possibly indicating cellular stress during the exposure procedure (Figure 6-35G). This was also observed in the experiments with SRM 2786. Furthermore, in contrast to the effects of SRM2786, no increase in CYP1A1 expression was observed after exposure to Traffic-$PM_{2.5}$ (Figure 6-35H).

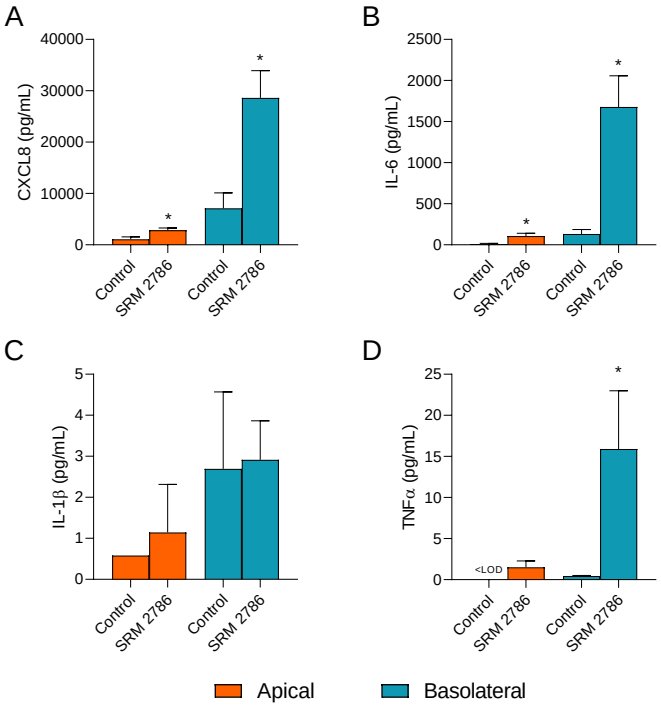

Figure 6-36 **Particle-induced cytokine release a 3D cell culture exposed to SRM 2786 at air-liquid interface (ALI).** 3D cocultures of A549 epithelial cells, Ea.Hy926 endothelial cells and THP-1-derived macrophages were exposed to SRM 2786 at ALI. Exposure dose was 4.75 ± 1.34 (mean ± SD). After 24 h the release of CXCL8 (A), IL-6 (B), IL-1β (C) and TNFα (D) (mean ± standard deviation, n=3) was measured in the cell culture medium from the apical (orange bars) and basolateral (blue bars) compartments using ELISA. * Statistically significant difference from respective control (0 µg/mL).

The 3D cell model was also exposed to SRM 2786 under ALI conditions for comparison with the submerged cell cultures presented in figures 6-30, 6-32 and 6-34. In ALI exposure, the medium is removed from the insert so that the cells can be exposed directly to aerosolized particle samples in air, thus offering a more realistic simulation of real-world exposure. The cultures exposed under ALI displayed relatively higher levels of cytokines in the basolateral compartment compared with cell cultures exposed under submerged conditions (Figure 4 and 10). Exposure to SRM2786 (4.75 ± 1.34 µg/cm^2) significantly increased the release of CXCL8 and IL-6 in both the apical and basolateral compartments compared with control (Figure 6-36A and B), while the level of TNFα was significantly increased only in the basolateral compartment (Figure 6-36D). TNFα secretion in the apical compartment was around or below the limit of detection (Figure 6-36D). Similarly, only very low levels of IL-1β were detected in both compartments and several values were at or below the limit of detection (Figure 6-36C).

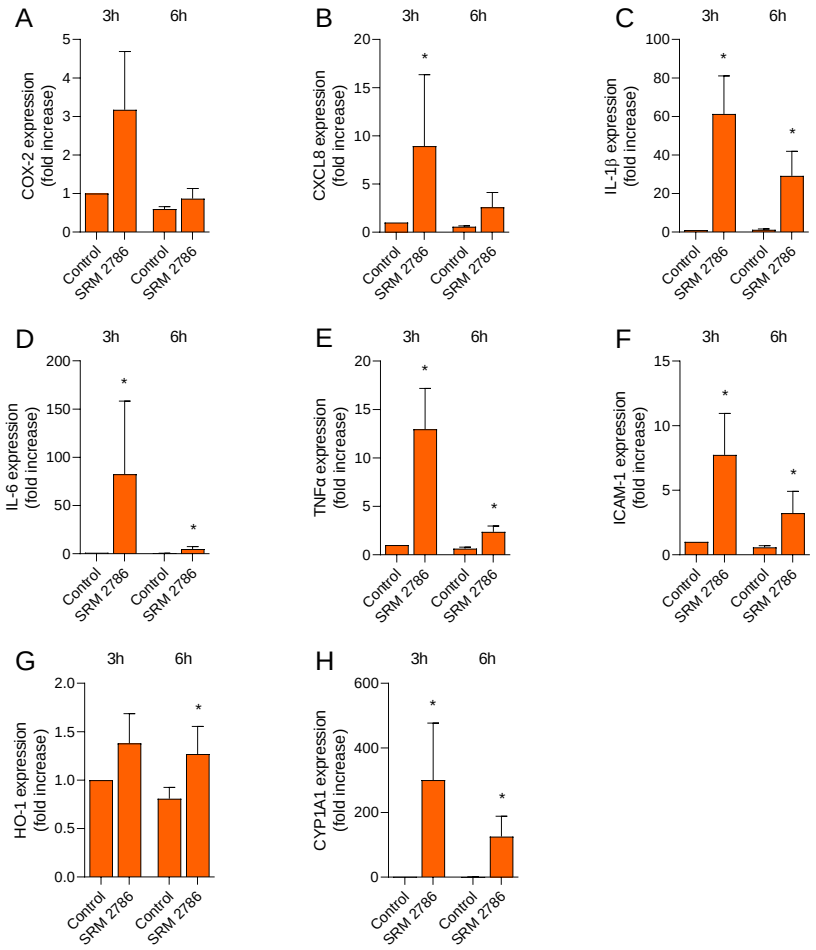

Figure 6-37 **Gene expression of inflammatory markers, cell adhesion molecules and enzymes linked to xenobiotic metabolism and redox responses in the apical compartment after exposure to SRM 2786 at air-liquid interface (ALI).** 3D cocultures of A549 epithelial cells, Ea.Hy926 endothelial cells and THP-1-derived macrophages were exposed to SRM 2786 at ALI. Exposure dose was 4.75 ± 1.34 (mean ± SD). Gene expression of COX-2 (A), CXCL8 (B), IL-1β (C), IL-6 (D), TNFα (E), ICAM-1 (F) HO-1 (G) and CYP1A1 (H) (mean ± standard deviation, n=3) was measured in the apical compartment after 3 h and 6 h using qPCR. * Statistically significant difference from respective control (0 µg/mL).

Expression of genes related to the inflammatory response, cell adhesion and recruitment, redox responses, and xenobiotic metabolism was measured 3 h and 6 h after exposure to SRM2786 (4.75 ± 1.34 µg/mL) at ALI (Figure 6-37). All assessed genes appeared to follow a similar time course with an increase in expression at 3 h exposure that decreased after 6 h, although the magnitude of the response relative to controls differed substantially for the different genes (Figure 6-37). Statically significant differences in expression compared with controls were observed for CXCL8 (Figure 6-37B), IL-1β (Figure 6-37C), IL-6 (Figure 6-37D), TNFα (Figure 6-37E), ICAM-1 (Figure 6-37F) and CYP1A1 (Figure 6-37H). HO-1 expression was negligible at both time points, although the small increase from control reached statistical significance after 6 h exposure (Figure 6-37G). Compared with exposure under submerged conditions (Figure 6-32), the fold increase in CXCL8 and TNFα appeared to be lower after ALI exposure (Figure 6-37). CYP1A1 expression on the other hand, was somewhat higher expressed in cell exposed under ALI conditions (Figure 6-32 and 6-37). However, it should be noted that the exposure concentrations are not directly comparable between the two exposure conditions, and that the variation between experiments under both conditions was rather high.

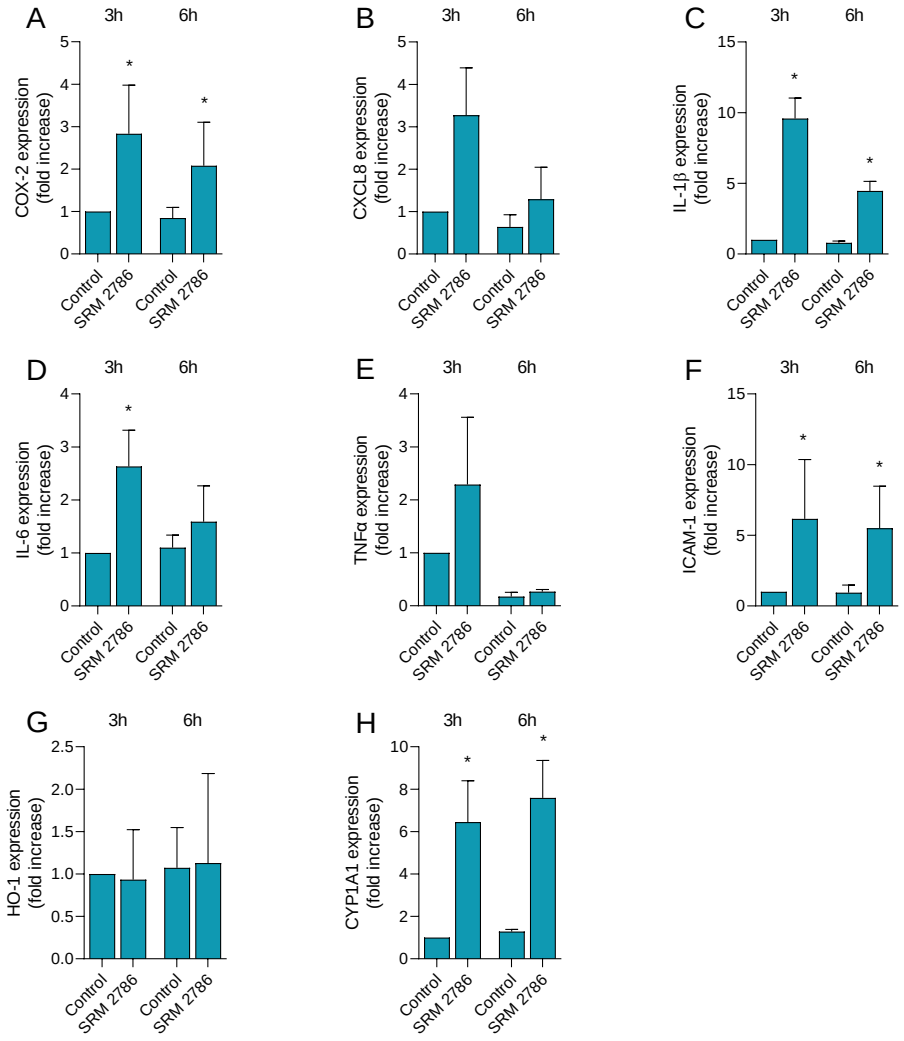

Figure 6-38 **Gene expression of inflammatory markers, cell adhesion molecules and enzymes linked to xenobiotic metabolism and redox responses in the basolateral compartment after exposure to SRM 2786 at air-liquid interface (ALI). 3D** cocultures of A549 epithelial cells, Ea.Hy926 endothelial cells and THP-1-derived macrophages were exposed to SRM 2786 at ALI. Exposure dose was 4.75 ± 1.34 (mean ± SD). Gene expression of COX-2 (A), CXCL8 (B), IL-1β (C), IL-6 (D), TNFα (E), ICAM-1 (F) HO-1 (G) and CYP1A1 (H) (mean ± standard deviation, n=3) was measured in the basolateral compartment after 3 h and 6 h using qPCR. * Statistically significant difference from respective control (0 μg/mL).

Similar results were observed in the well/basolateral compartment, although the fold increase in most of the genes were lower compared with the insert/apical compartment (Figure 6-38). Significant increases in gene expression were observed for COX-2 (Figure 6-38A), IL-1β (Figure 6-38C), IL-6 (Figure 6-38D), ICAM-1 (Figure 6-38F), and CYP1A1 (Figure 6-38H). The increase in gene expression was greatest after 3h exposure for most genes. However, the decrease observed after 6 h was not as pronounced as in the apical compartment and the expression of ICAM-1 and CYP1A1 was similar at the two time points (Figure 6-38F and H). As CYP1A1 expression is regulated by activation of AhR, a pathway activated by chemicals present in combustion PM, expression of this gene in the basolateral compartment may indicate translocation of organic chemicals through the insert. Unlike what was observed for gene expression in the apical compartment, IL-1β and IL-6 expression appeared to be somewhat higher in the basolateral compartment when cells were exposed under ALI conditions than submerged (Figure 6-33 and 6-38). CYP1A1 and ICAM-1 also appeared somewhat higher after ALI exposure, although the variation between experiments were quite high for both conditions. Although no increase in HO-1 expression was

observed in either exposure condition, the decrease in HO-1 expression compared with control observed under submerged condition was not observed when cells were exposed at ALI (Figure 6-33 and 6-38).

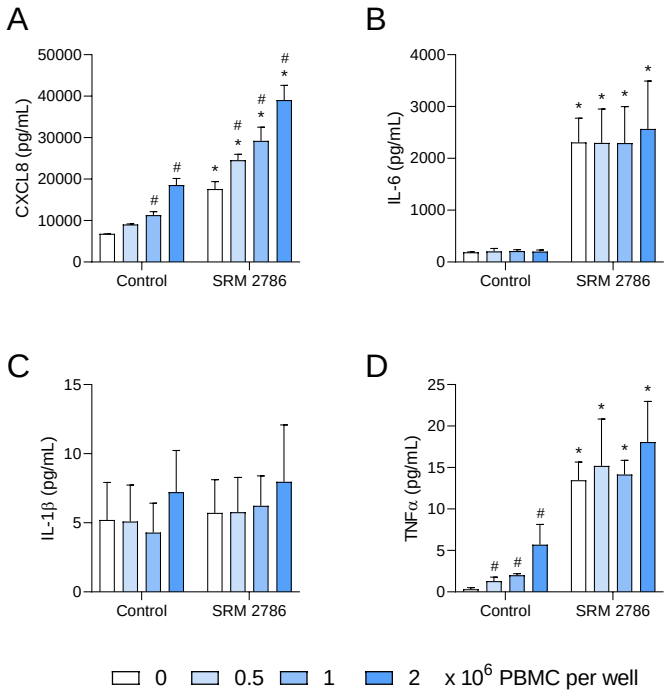

Figure 6-39 **Cytokine responses in peripheral blood mononuclear cells exposed in a lung 3D cell culture model at air-liquid interface (ALI). 3D** cocultures of A549 epithelial cells, Ea.Hy926 endothelial cells and THP-1-derived macrophages with either 0, 0.5, 1 or 2 million PBMC in the basolateral compartment were exposed to SRM 2786 under ALI conditions. The exposure concentration was 6.66 ± 0.09 µg/mL. The release of CXCL8 (A), IL-6 (B), IL-1β (C) and TNFα (D) (mean ± standard deviation, n=3) was measured after 24h using ELISA. * significantly different from control. # significantly different from 0 PBMC.

To test the ability of the particles to induce systemic inflammatory responses, different concentrations of peripheral blood mononuclear cells (PBMC) were added to the well/basolateral compartment of the A549/Ea.HY926/THP-1 3D coculture and the cytokine levels measured after exposure to SRM2786 at ALI (Figure 6-39). Exposure to SRM2786 (6.66 ± 0.09 µg/mL) induced a statistically significant increase in all cytokines except IL-1β in the basolateral compartment of the 3D coculture (Figure 6-39). Basal secretion of CXCL8 and TNFα increased by increasing the concentration of PBMC in the basolateral compartment (Figure 13A and D). An increase in CXCL8 secretion was also observed with increasing concentrations of PBMC after exposure to SRM2786 (Figure 6-39A). However, the relative increase was similar between control and particle-exposed cocultures, suggesting that the increase is due to basal secretion of cytokines from the PBMC rather than activation of these cells by particles or by inflammatory mediators. No change in TNFα release was observed between the different concentrations of PBMC after exposure to SRM2786 (Figure 6-39D).

Summary

The induction of a pulmonary inflammatory response is considered to be important component of the health effects of particulate matter. In this part of the report, particle-induced pro-inflammatory responses were assessed in advanced coculture models representing the human airways. The cells were exposed under submerged and air-liquid interface (ALI) conditions to a standard reference sample of urban particulate matter (SRM2786) and a sample of traffic-related $PM_{2.5}$ sampled in a Norwegian road tunnel. Endpoints included the release of pro-

inflammatory cytokines, signaling molecules central to the inflammatory response, and the expression genes linked to inflammation and pathways important for the adverse effects of inhaled particles.

- Exposure to SRM2786 and a sample of traffic-related $PM_{2.5}$ induced marked pro-inflammatory responses in an advanced 3D cell culture of epithelial cells, macrophages and endothelial cells.
- The pro-inflammatory responses were somewhat higher after exposure to the traffic-related PM than SRM2786, both in terms of cytokine release and gene expression, although some variability was observed between experiments.
- Exposure to SRM2786 under submerged conditions induced the highest levels of cytokines in the apical compartment of the 3D model, while higher levels were detected in the basolateral compartment following exposure at air-liquid interface (ALI). However, the results for gene expression after ALI exposure was more similar to those observed under submerged conditions.
- Particle exposure increased the expression of CYP1A1, indicating activation of the aryl hydrocarbon receptor (AhR) pathway. CYP1A1 expression was also detected in the endothelial cells, which indicate that mediators from the apical compartment or particle-associated chemicals have translocated through epithelial layer. CYP1A1 expression in both compartments was higher after exposure to SRM2786 than the traffic-$PM_{2.5}$ sample.
- Oxidative stress is likely not the main contributor to the observed effects, as particle exposure did not change the expression of HO-1 an enzyme induced in response to increased production of reactive oxygen species (ROS).
- No change in cytokine release attributable to the particle exposure was observed in human peripheral blood mononuclear cells when the cells were grown in the basolateral compartment of the 3D model. More specific markers may be needed to delineate the contribution from these cells.

6.5 Toxicity ranking of $PM_{2.5}$ from different cities and sources

To assess the hazards posed by different types and sources of particles, we characterized the adverse biological effects of different PM samples in specific cities with representative pollution sources. The results shown in Figure 6-40 are from the experiments conducted with PM collected in the autumn of 2019 and 2020 and mixed the particles (the detailed chemical compositions are shown in Figures 6-16). We examined the expression level of cytokines (IL-1β and IL-8) with A549 & THP-1 co-culture model by the different PM-samples exposure. Although the level of IL-1β and IL-8 were elevated by the three PM-samples exposure, the level of elevation was different. The results may suggest a higher contribution of industrial emissions and coal burning to PM toxicity than traffic emissions (Figure 6-40).

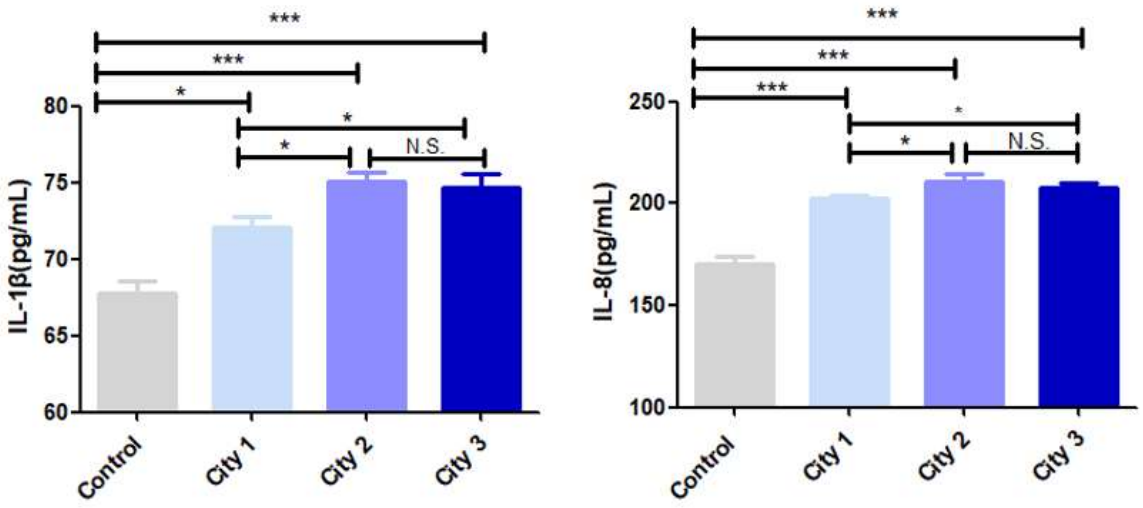

Figure 6-40 The expression level of IL-1β and IL-8 in A549 & THP-1 co-culture of different PM samples in specific cities with representative pollution sources

The main function of the city determines the chemical compositions of the atmospheric PM. A summary of the total source apportionment results for the 3 specific cities for 2019-2021 is shown in Figure 6-41, which confirms our judgment of the main functions of each city. These 3 cities have distinctive source emission characteristics. Due to the prevalence of covid-2019 and quarantine measures, we did not have the opportunity to collect samples from various emission sources, thus, $PM_{2.5}$ sampled from different cities was used to represent the emissions of the main sources. In the present study, we combined the toxic composition, the results of cellular experiments and source apportionment of $PM_{2.5}$ from different cities to rank the toxicity of $PM_{2.5}$ from different cities/sources.

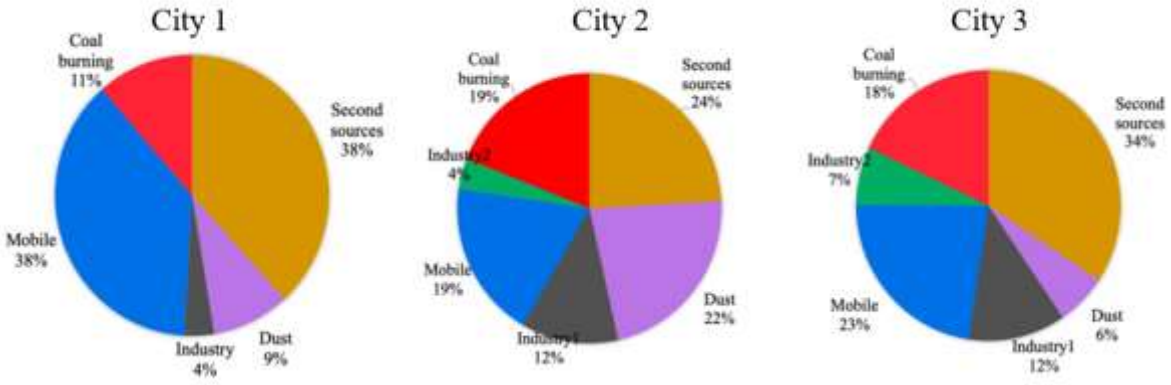

Figure 6-41 Source apportionment of $PM_{2.5}$ of the 3 cities in 2019-2021

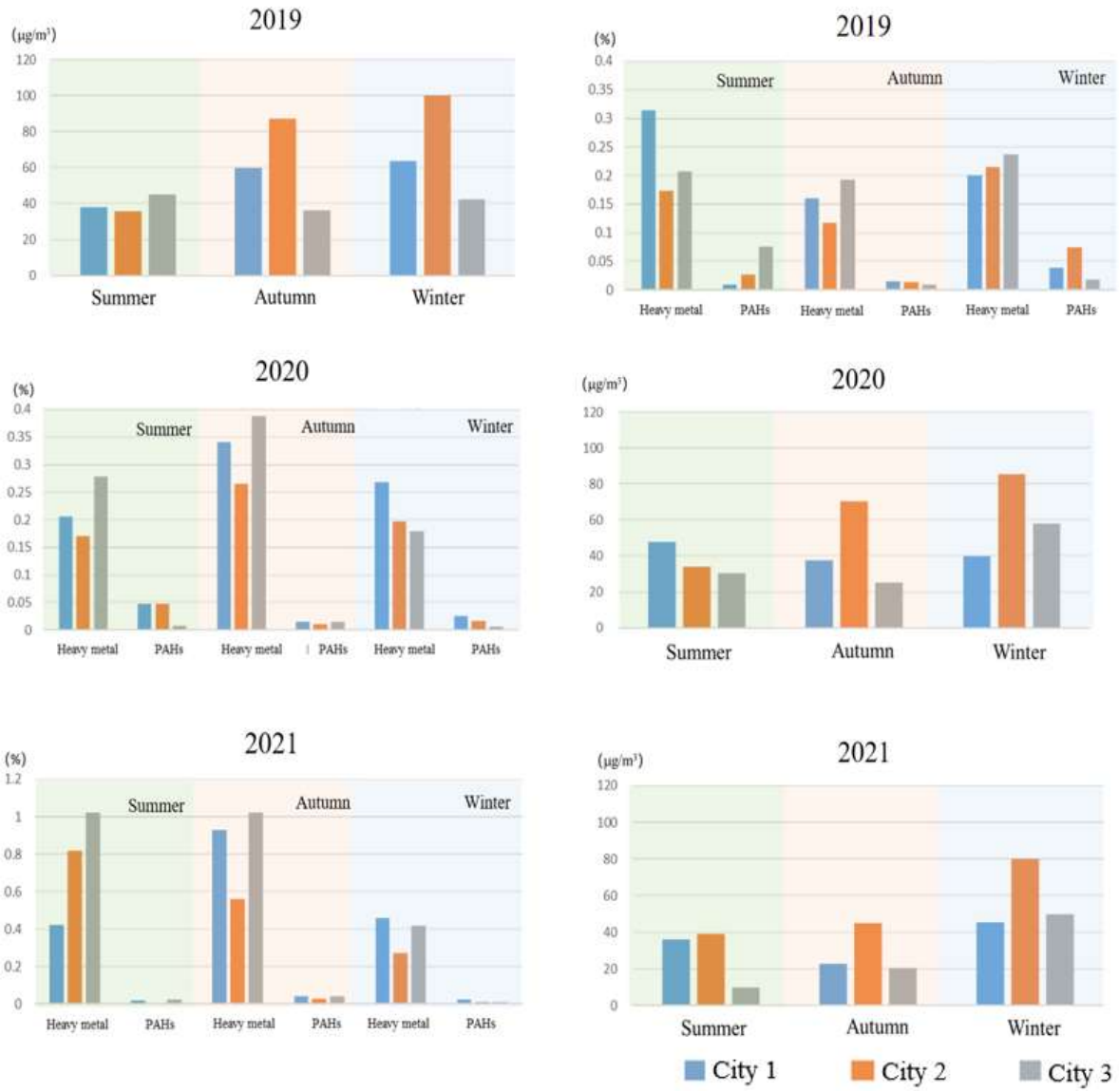

Figure 6-42 The concentrations of $PM_{2.5}$ and heavy metals and PAHs of $PM_{2.5}$ in the 3 cities

1) Ranking the toxicities of different sources by the chemical compositions of $PM_{2.5}$ in the 3 cities in 2019-2021

Figure 6-42 shows the concentrations of heavy metals and PAHs of $PM_{2.5}$ in the 3 specific cities in the year 2019-2021. Here, we take heavy metals and PAHs as toxic components in $PM_{2.5}$. We may find that although most of the time the concentrations of $PM_{2.5}$ in the city with heavy industries and coal combustion source were the highest, its toxic components were not the highest. Meanwhile, the city with industries complex and vehicle source had the lowest $PM_{2.5}$ in many seasons, but its toxic components were often the highest. The concentration and toxicity of $PM_{2.5}$ in the city with traffic source were largely in second place in the 3 cities in many seasons. These results implicated the toxicities of industry emissions could be the highest in all the sources.

2)Ranking the toxicities of different sources by the level of cytokines after PM2.5 exposure in the 3 cities in 2019 and 2020

Figure 6-40 shows the levels of cytokines after $PM_{2.5}$ exposure in the 3 specific cities in autumn in the years 2019 and 2020. Because in autumn, there is no heating-use coal burning, thus most of the $PM_{2.5}$ was emitted by industries and vehicles. Meanwhile, the city with traffic source has almost no industry; thus, we can assume that the $PM_{2.5}$ in the city in autumn comes mainly from motor vehicles, while the $PM_{2.5}$ in the city with heavy industries and coal

combustion source and the city with industries complex and vehicle source comes mainly from industries and motor vehicles. The levels of cytokines show clearly that the PM sourced from industries and coal combustion is more toxic than PM where traffic is the main source of pollution.

Combining the above results of toxicological experiments, toxic chemical compositions and the source apportionment, we determined that industrial emissions and coal combustion made a higher contribution to PM toxicity than motor vehicles.

6.6 Discussion and conclusions

Knowledge regarding the potential adverse effects of different types of particles from different sources is important for implementing effective mitigating measures. Several endpoints linked to the adverse effects of inhaled particles were included by both the Chinese and Norwegian research groups. Studies performed in China showed that inhalation exposure to real-world concentrations of ambient $PM_{2.5}$ caused a transient increase in RNA methylation in the lungs of mice. Moreover, there was histopathological evidence of pulmonary inflammation in the lung tissue and an altered cytokine profile indicating an imbalance of the T cell population towards Th2 after exposure to $PM_{2.5}$. RNA methylation is important for regulating gene expression, both in normal physiology and in various disease states (Komal et al. 2021, He and He 2021), while increased Th2-type inflammation is a hallmark of allergic asthma (Leon and Blesteros-Tato et al. 2021). The findings in mice on RNA methylation were also confirmed in a human lung epithelial cell line exposed to collected $PM_{2.5}$. Inflammation is regarded to have an important role in the adverse effects of inhaled particles (Sayjan and Mossman 2017). Further in vitro studies compared the pro-inflammatory responses to three different samples of $PM_{2.5}$ in a coculture of lung epithelial cells and macrophage-like cells. The results show that increased release of the pro-inflammatory cytokines CXCL8 and IL-1β, which are responsible for initiating the inflammatory response and recruitment of immune cells (Turner et al. 2014). $PM_{2.5}$-induced pro-inflammatory responses were also the focus of the Norwegian contribution. The responses to urban $PM_{2.5}$ (SRM2786) and traffic-related $PM_{2.5}$ sampled in a road tunnel in Norway were assessed using a more advanced 3 dimensional (3D)-coculture model representing the alveolar compartment in the lungs. In addition, the same co-culture model used in the experiments conducted in China was used by the Norwegian group. The results using the advanced 3D cell culture show that exposure to PM induced increased release of the pro-inflammatory cytokines CXCL8, IL-6, IL-1β and TNFα, and increased expression of genes related to inflammation and xenobiotic metabolism.

The intention of this part of the project was to perform a health risk assessment of different PM/BC samples from various locations in China with contributions from different emission sources and to use the results to rank the emissions sectors to aid policymakers in developing mitigation strategies. The Chinese study compared the responses to $PM_{2.5}$ sampled in three specific cities with representative pollution sources. While the source profile was similar for the different samples, PM with traffic source had a higher contribution from traffic and secondary sources, while PM with heavy industries/coal combustion source and industries complex/vehicle source had a higher contribution from coal burning and industrial emissions. Moreover, PM with heavy industries/coal combustion source had the highest content of heavy metals and PAH of the three samples. While the results may indicate a larger contribution from coal burning and industrial emissions, the differences in cytokine responses between the exposed and the unexposed cells, as well as between cells exposed to the different $PM_{2.5}$ samples, were rather marginal. Likely the magnitude of these differences might be within the uncertainty of the experiments and does not necessarily reflect contribution from any particular source. Moreover, comparison of the cell culture studies in Norway and China shows that the CXCL8 response is several orders of magnitude higher in the Norwegian studies, while the IL-1β response was higher in the Chinese experiments. As the Chinese group has not included the standard reference sample in their experiments, inter-laboratory comparison of the results is unfortunately not possible. Likely the marginal effects on cytokine release detected in the Chinese experiments reflect some issue with the cell culture conditions or experimental setup. However, due to difficulties in exchanging personnel because of the Corona pandemic, challenges in cell culture procedure were not avoided and the reason for the different responses was not found. In the experiments conducted in Norway, the traffic-$PM_{2.5}$ sample induced potent pro-inflammatory responses in the advanced 3D-coculture models, suggesting that particles from traffic (including both exhaust and non-exhaust particles) could be an important contributor to the adverse effects

of ambient PM. The total carbon content of the Traffic-$PM_{2.5}$ used in this study was dominated by organic carbon (OC) with little contribution from elemental carbon (EC) (Skuland et al. 2022). Moreover, analysis of several samples of size-fractioned PM, including the traffic-$PM_{2.5}$ sample used in this report, showed a correlation between pro-inflammatory responses and the content of organic carbon (OC) in the particles (Skuland et al. 2022), suggesting that organic particle constituents are important for the effects of traffic-related particles.

Taken together, the results presented in this report show that exposure to $PM_{2.5}$ induce effects in mice and in advanced cell culture models that are linked to adverse health effects. However, due to the low number of particle samples, and inconsistencies in the results, examined endpoints and experimental procedures, no firm conclusions can be drawn regarding which sources of PM contributes most to these adverse effects.

7 Policy recommendations

Authors: Yixuan Zheng, Xuying Wang, Wenxin Cao (CAEP),Xiaohui Du, Yongjie Wei, Miaomiao Cheng (CRAES),Marianne T. Lund (CICERO), VigdisVestreng (NEA)

7.1 Multi-aspect benefits of BC/OC emission control

7.1.1 Potential emission abatements

Reducing air pollutant emissions is the fundamental to improve air quality. Hence, reduced air pollutant emissions could be expected as China continues pursuing clean air. As shown in Chapter 3, three scenarios are designed in this study, including the business as usual scenario (BAU), strengthened end of pipe control scenario (EOP) and ambitious control scenario (ABC). In the three emission reduction scenarios designed in this study, the ABC, which considers stringent end-of-pipe control measures and stricter structural adjustments applied in the key regions, is probably the most likely scenario based on the logic of environmental policymaking in China.

7.1.1.1 Reductions in BC and OC emissions

Based on the assessment of different black carbon and organic carbon (BC/OC) emission control scenarios, the emissions of BC and OC could be reduced significantly with appropriate structural adjustments and end-of-pipe control measures implemented in Northern China. In the ABC scenario, structure adjustment, end-of-pipe control measures, as well as industrial layout adjustment would together reduce the emissions of BC and OC in Northern China by around 43% and 35% respectively by 2035, compared with 2018 (as shown in Fig. 7-1). Compared with the EOP scenario, additional emission reductions indicate that the strengthened layout adjustments will have a considerable emission reduction effect. The largest reductions occur between 2018 and 2020, because in the ABC scenario, strong end-of-pipe control measures were applied in years after 2018.

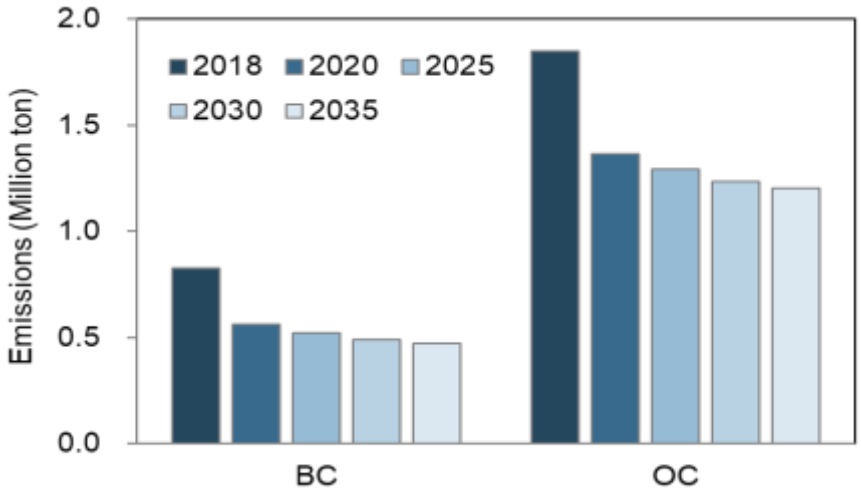

Figure 7-1 Changes in BC and OC emissions in Northern China in the ABC scenario

Figures 7-2 and 7-3 show the spatial distribution of percent changes in BC and OC emissions in Northern China in the ABC scenario. Considerable spatial disparities could be seen in the reduction rates of both BC and OC, which could be attributable to the differences in the structure of emissions sources, such as varying industrial and energy structures, as well as the levels of control applied in 2018. Based on the analysis, BC and OC emission reduction potentials are the greatest in the Shanxi province, which may be explained by coal-dominated energy consumption and a >80% reduction in industrial and heating coal consumption by 2035 in this province.

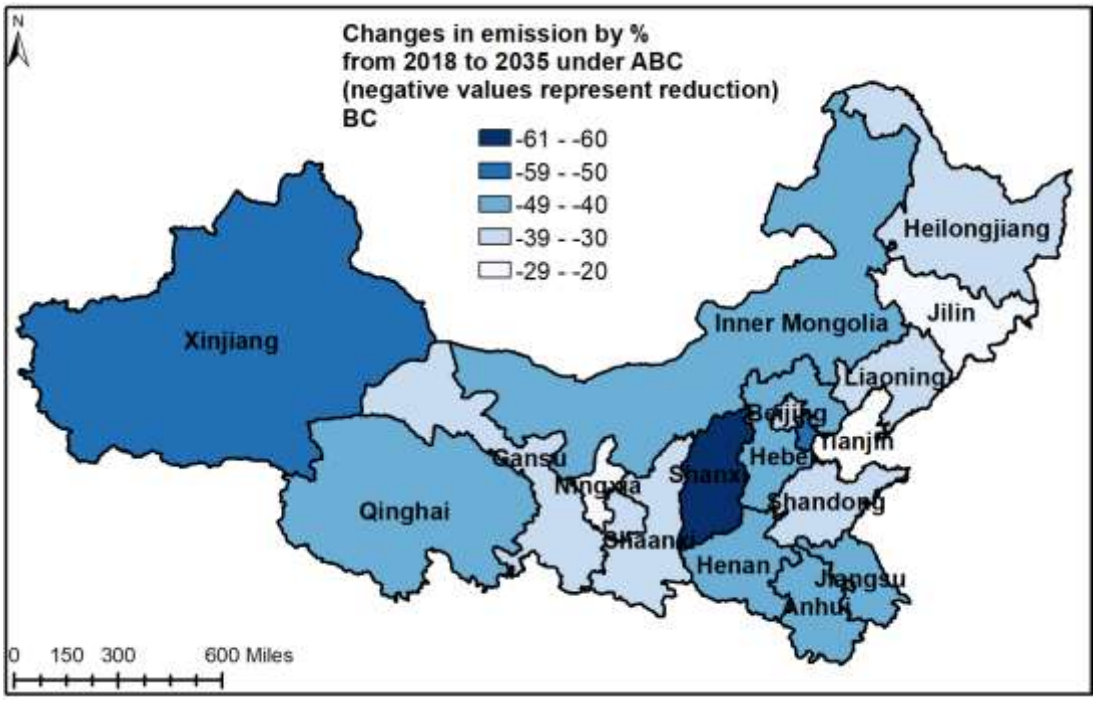

Figure 7-2 Distribution of changes in BC emission from 2018 to 2035 in the ABC scenario

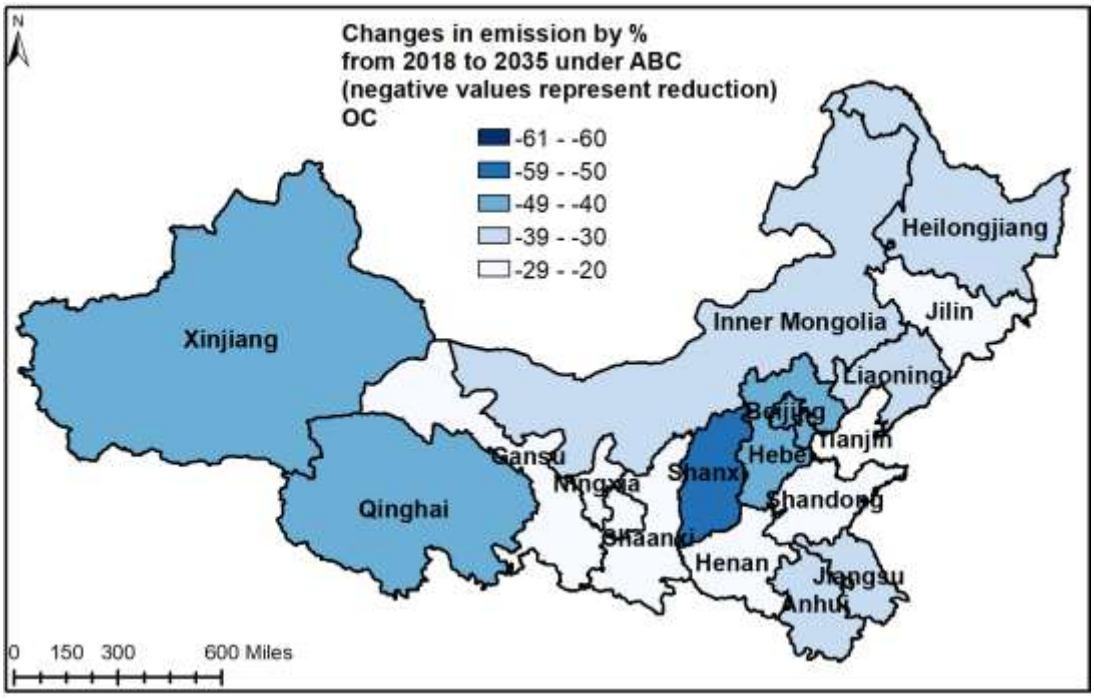

Figure 7-3 Distribution of changes in OC emission from 2018 to 2035 in ABC scenario

7.1.1.2 Reductions in emissions of other air pollutants

Based on the scenario analysis, in addition to BC and OC, there are also considerable emission abatements for other air pollutants such as SO_2, NO_X, and $PM_{2.5}$ in Northern China during the period 2018-2035, with the implementation of structure adjustments, end of pipe control measures and industrial layout adjustment. In the ABC scenario, emissions of SO_2, NO_X, and $PM_{2.5}$ in Northern China are reduced by 35%, 57%, and 53% respectively by 2035, compared with 2018 (as shown in Fig. 7-4). Reductions in $PM_{2.5}$ emissions also vary greatly across regions. Based on our analysis, provincial reduction in the ABC scenario is estimated to range from 37%

to 72%, with the largest reduction occurring in Shanxi province, which is consistent with the BC and OC emission reductions.

Figure 7-5 shows the spatial distribution of percent changes in $PM_{2.5}$ emissions in Northern China in the ABC scenario. Considerable spatial disparities could be seen between reductions in BC, and the total primary $PM_{2.5,}$ which could be mainly explained by the different sources of BC and $PM_{2.5}$ components other than BC. For example, BC emissions mainly originated from incomplete combustion, and hence, limited BC would be emitted from sources such as coal-fired power plants. Yet, a certain amount of primary $PM_{2.5}$ (i.e., species other than BC) could still be found in the exhaust gas of coal-fired power plants. Therefore, a switch from the coal-fired power plant to natural gas power plant or renewable energy infrastructure would contribute notably to reducing primary $PM_{2.5}$ but not to reducing BC emissions.

It should be noted that emission reductions of SO_2 and NO_X need to be reduced to improve air quality, but the reductions are likely to contribute to warming the atmosphere. To compensate for this climate effect, larger efforts may be needed to abate the warming components. This is further elaborated below in Chapter 7.1.3.

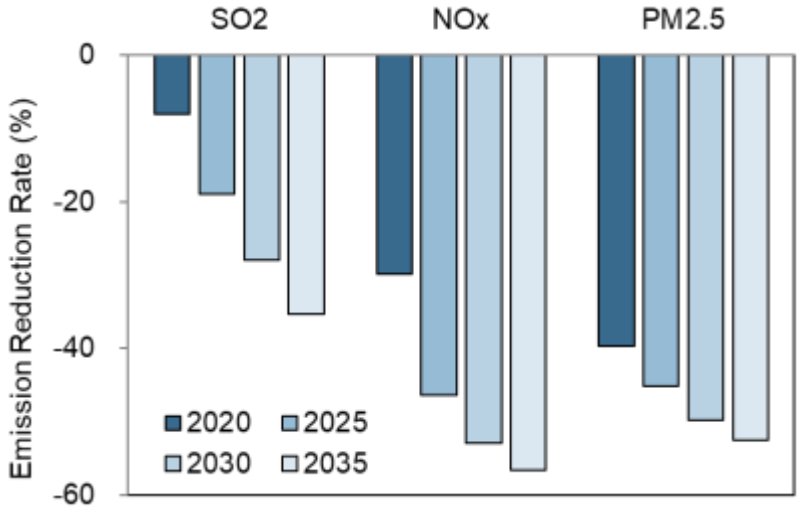

Figure 7-4 Reduction rates of SO_2, NO_X, and $PM_{2.5}$ emissions in northern China in the ABC scenario in 2020, 2025, 2030 and 2035 compared with 2018

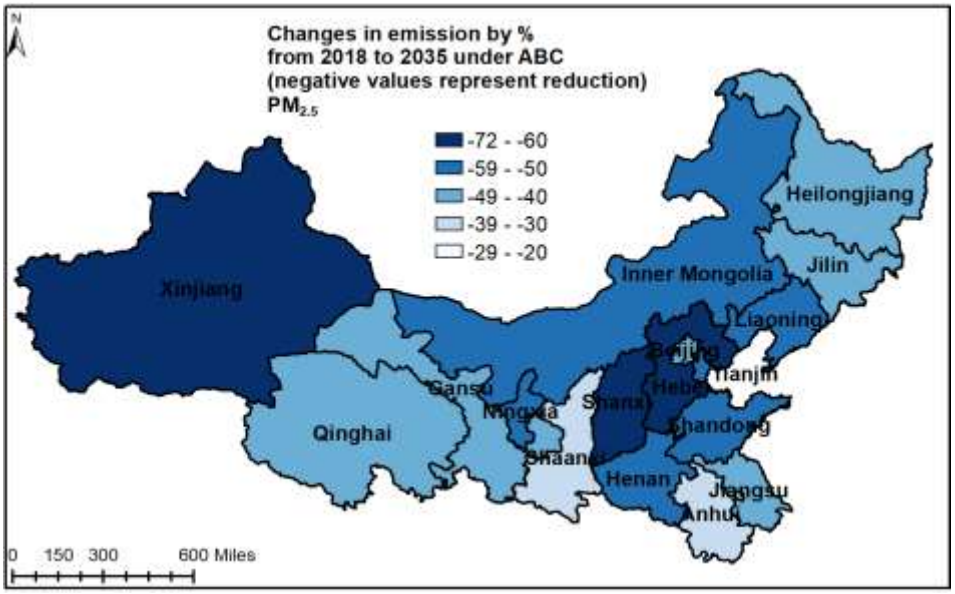

Figure 7-5 Changes in emission for $PM_{2.5}$ by % from 2018 to 2035 under ABC

7.1.2 Air quality benefits

Considerable air quality improvement could be expected based on the reductions in air pollutant emissions. Based on the updated anthropogenic emission inventories developed in this study and the estimated emission reductions in the ABC scenario, gridded anthropogenic emissions in the ABC scenario are compiled. Changes in air quality concentrations are then simulated based on the gridded emission in the ABC scenario in the year 2035, as driven by the 2018 meteorology conditions. We then analyze and summarize the changes in $PM_{2.5}$, BC, and OC concentrations simulated in Northern China in the ABC scenario, considering the spatial distribution of BC, OC, and $PM_{2.5}$ emission reduction trends. It should be noted that we focus on the changes in concentration of particles, rather than SO_2 and NO_2, because the Chinese government focuses more on particle pollution, as the SO_2 and NO_2 pollution has been greatly reduced and most of the Chinese cities have successfully attained the current national standard for SO_2 and NO_2.

7.1.2.1 Changes in $PM_{2.5}$ concentrations

The spatial distribution of the percentage decrease in $PM_{2.5}$ emissions for the ABC abatement scenario shows that the largest decreases in $PM_{2.5}$ emissions were seen in the provinces of Xinjiang, Hebei, and Shanxi. The $PM_{2.5}$ concentrations simulated under the ABC emission reduction scenario show a decreasing trend across the region, with the average percentage decrease in $PM_{2.5}$ concentrations simulated being below -20% (Table 7-1).

Like the spatial distribution of $PM_{2.5}$ emission decreases (Figure 7-5), the largest decrease in simulated concentrations of $PM_{2.5}$ is also found in Shanxi Province, with a grid-level maximum percentage decrease of about -61%. In Shanxi, the mean value of $PM_{2.5}$ reduction is estimated as about -54%, and the grid-level minimum value is about -46% (Table 7-1). Other regions with relatively large decreases in concentrations were mainly Xinjiang and Beijing-Tianjin-Hebei and surrounding areas, with most regions showing decreases of ratios between 40% and 50%.

The areas with smaller simulated decreases in $PM_{2.5}$ concentrations, such as Gansu, Shaanxi, Heilongjiang and Jilin, also had similarly small percentage decreases in emissions, with these provinces experiencing $PM_{2.5}$ concentration decreases in the range of -30% to -40%. In addition, although the percentage decrease in $PM_{2.5}$ emissions in Qinghai Province was -46.5%, close to -50%, the simulated percentage decrease in $PM_{2.5}$ concentrations was smaller due to the smaller baseline $PM_{2.5}$ emissions in Qinghai Province, with an average percentage decrease in concentrations of -21%. A table with absolute values can be found in Appendix 7-1.

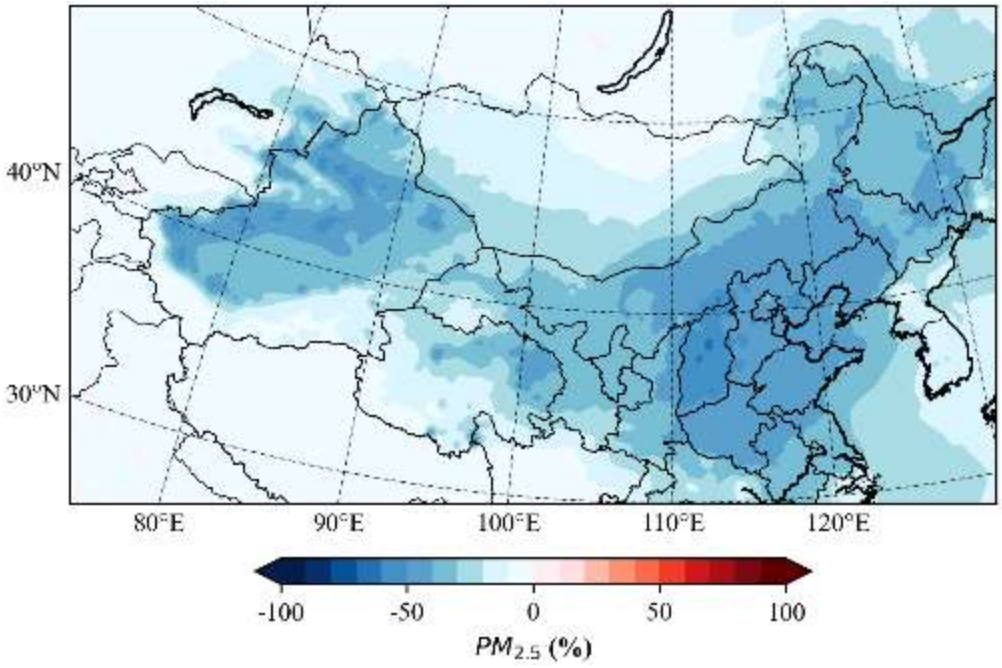

Figure 7-6 Spatial distribution of percentage change in $PM_{2.5}$ concentration in the ABC scenario

Table 7-1 Grid-level maximum, minimum, and average percentage reductions in $PM_{2.5}$, BC and OC concentrations by province in Northern China in the ABC scenario

	Average Reduction			Maximum Reduction			Minimum Reduction		
	BC	OC	$PM_{2.5}$	BC	OC	$PM_{2.5}$	BC	OC	$PM_{2.5}$
Hebei	-47%	-40%	-48%	-52%	-45%	-53%	-43%	-35%	-42%
Heilongjiang	-34%	-29%	-35%	-39%	-34%	-42%	-22%	-16%	-13%
Inner Mongolia	-40%	-34%	-35%	-47%	-41%	-49%	-18%	-15%	-13%
Xinjiang	-44%	-37%	-30%	-51%	-45%	-52%	-4%	-2%	-1%
Jilin	-31%	-27%	-39%	-37%	-32%	-42%	-27%	-25%	-34%
Liaoning	-37%	-33%	-42%	-43%	-37%	-46%	-30%	-29%	-34%
Gansu	-36%	-30%	-30%	-47%	-39%	-39%	-19%	-15%	-14%
Beijing	-43%	-40%	-43%	-46%	-41%	-46%	-40%	-40%	-40%
Shanxi	-56%	-49%	-54%	-60%	-54%	-61%	-47%	-42%	-46%
Tianjin	-49%	-41%	-47%	-51%	-42%	-48%	-49%	-40%	-46%
Shaanxi	-34%	-26%	-37%	-43%	-36%	-47%	-24%	-18%	-22%
Ningxia	-28%	-24%	-33%	-30%	-26%	-37%	-24%	-23%	-31%
Qinghai	-39%	-33%	-21%	-49%	-46%	-46%	-15%	-8%	-3%
Shandong	-39%	-31%	-44%	-42%	-33%	-46%	-37%	-30%	-38%
Henan	-44%	-30%	-44%	-52%	-41%	-51%	-35%	-23%	-38%
Jiangsu	-42%	-31%	-37%	-46%	-33%	-43%	-35%	-26%	-27%
Anhui	-41%	-31%	-37%	-46%	-33%	-43%	-27%	-21%	-24%

A table with absolute values can be found in Appendix 7-1.

7.1.2.2 Changes in BC and OC concentrations

Like $PM_{2.5}$, the spatial distribution of the percentage decrease in simulated BC/OC concentrations under the ABC emission reduction scenario remained consistent with the spatial distribution of the percentage decrease in emissions. The simulated BC/OC concentrations show a decreasing trend across Northern China, with the lowest average percentage decrease in BC/OC concentrations -28% and -24%, respectively in Ningxia (Table 7-1). For simulated BC concentrations, the percentage decrease was greater in Xinjiang, Beijing-Tianjin-Hebei and surrounding areas, Inner Mongolia and parts of Qinghai, with the largest decrease in simulated BC concentrations in Shanxi Province, with a maximum percentage decrease of approximately -60%, a mean of approximately -56% and a minimum of approximately -47% (Table 7-1). The maximum and average percentage decreases were below -30% for most areas. For simulated OC concentrations, the overall percentage decrease was less than BC, with larger percentage decreases mainly in Xinjiang, Shanxi, and parts of Hebei and Qinghai, with the largest percentage decrease of approximately -54% in Shanxi Province, with an average value of approximately -49% and a minimum value of approximately -42%. Most areas had percentage decreases in simulated OC concentrations of at least -25%.

The areas with smaller decreases in simulated BC/OC concentrations had similarly small percentage decreases in emissions, with overall smaller percentage decreases in simulated BC/OC concentrations in the provinces of Ningxia, Gansu, Shaanxi, Jilin in the Northeast and Heilongjiang. The average decreases in BC/OC concentrations in these provinces ranged from -30% to -40% and 20% to 30% respectively. The reason why we see the difference

in the percentage reductions of BC and OC concentration across Northern China is that sources of BC and OC emissions are not necessarily consistent.

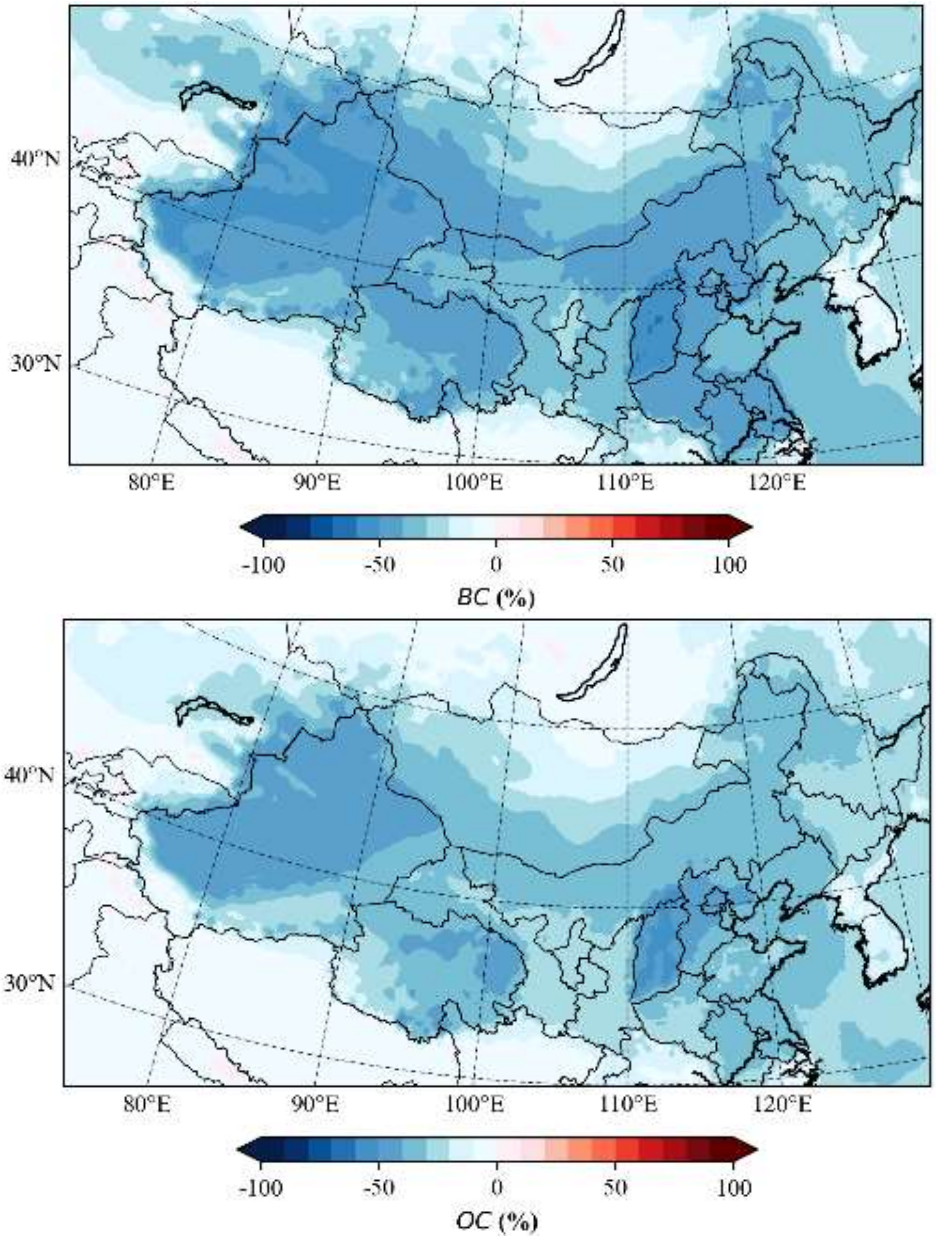

Figure 7-7 Spatial distribution of percentage change in BC and OC concentrations under ABC emission scenario

7.1.3 Climate effects of BC and OC emissions

In addition to their detrimental impact on air quality, BC and OC aerosols can play an important role in shaping local climate, as well as in anthropogenic climate change, due to their interactions with solar radiation and clouds. Using the gridded ChiNorBC-2018 emissions and the three scenarios described in Chapter 3 as input to a global chemistry-transport model with subsequent offline radiative transfer calculations, the effect of the projected emission reductions on abundances of BC and organic aerosol (OA) over China is explored. We also estimate impact of BC and OC emissions in China from 2018 to 2035 on global mean surface temperature, comparing the three scenarios developed in the project.

Figure 7-6a shows the total abundance, measured in terms of optical depth, of BC and OA over China as simulated for the year 2018. The optical depth is a measure of the total amount of aerosols present from the surface to the top of the atmosphere and their optical properties, which is of relevance for the aerosol-induced effect on the

Earth's energy balance and climate. Here, the highest optical depth can be found in Eastern China, in the Beijing-Tianjin-Hebei and surrounding areas (region B).

In this region, the projected emission reductions result in markedly lower mean optical depth of BC and OA by 2035 under all three scenarios, as seen in Figure 7-6b. As expected, the reduction from 2018 is strongest in the ABC scenario, however, the largest changes take place between the BAU and EOP scenario. Reductions up 40% for BC and 30% for OA are found over region B in the ABC scenario. For the broader region A, corresponding mean reductions are 20 and 12% for BC and OA, respectively.

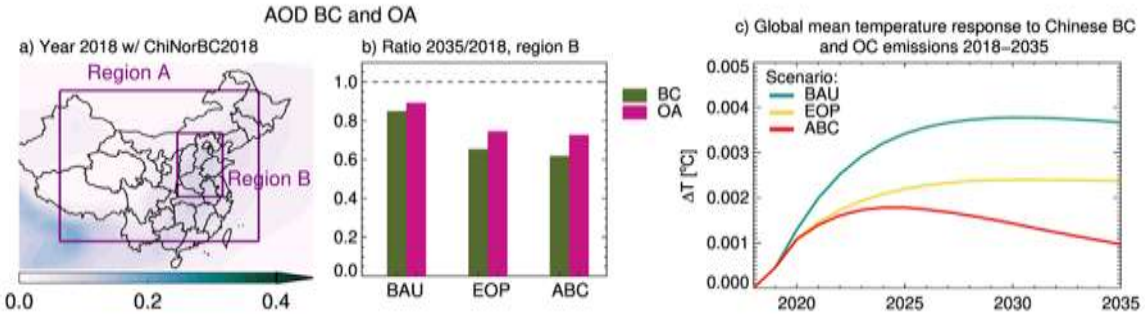

Figure 7-8: a) The optical depth of BC and OA simulated for 2018 with the ChiNorBC emissions. The boxes show focus regions. b) The relative change in BC and OA optical depth over focus region B in the three scenarios compared to 2018 levels. c) the global mean surface temperature effect resulting from Chinese emissions of BC and OC under the three scenarios developed in the project, calculated using a simple, analytical climate model.

Aerosols can both scatter and absorb radiation, causing a negative RF (cooling climate effect) and positive RF (warming climate effect), respectively. The net effect of the combined change in all anthropogenic aerosol species from pre-industrial to present-day is estimated to be a negative RF, dominated by the increase in aerosols that scatter radiation. Hence, combined reductions in emissions of anthropogenic aerosols and their precursors can be expected to give a positive RF. For a given source, for example sector or region, the net of effect of BC (an absorbing aerosol) and OC (a primarily scattering aerosol) depends on their relative contributions to the total emission. In the case of BC and OC emissions in China from 2018 to 2035, we find a net warming contribution to global surface temperature change in all three scenarios, that is, warming by BC dominates. This warming weakens in the EOP and ABC scenarios compared to BAU due to the more stringent mitigation measures implemented. In 2035, the global mean surface temperature impact due to Chinese BC and OC emissions is 70% smaller in ABC and under BAU.

Changes in BC and OC emissions may induce further effects on regional and local climate, including on extreme weather, through interactions with the hydrological cycle and climate dynamics. Such effects have not been quantified in the ChiNorBC project but would be important to consider in more comprehensive assessments of climate impacts following aerosol emission reductions as China improves its air quality. Furthermore, any concurrent changes in other emissions will be important for the net temperature impact. Through the ChiNorBC project, we provide a tool that can be applied in further studies.

7.1.4 Health effects

Mitigations of both air pollution and global warming would help reducing associated adverse health effects[6,7]. This project focuses on air pollution while the health effects of global warming is not investigated. According to IPCC (2023) every region in the world is projected to face further increases in climate hazards, increasing multiple risks to ecosystems and humans. Hazards and associated risks expected in the near-term include an increase in heat-related human mortality and morbidity, food-borne, water-borne, and vector-borne diseases, and mental health challenges[8].

When it comes to air pollution, the meta-analysis conducted in the ChiNorBC project suggests that the risks of short-term exposure to BC on total mortality, respiratory mortality, and long-term exposure to BC on lung cancer mortality are 1.01 (95%CI: 1.00–1.01), 1.06 (95%CI: 1.03–1.10) and 1.12 (95%CI: 1.09–1.15) per 10 μg/m3 increase, respectively[16]. We speculate that BC has a higher adverse health effect on the respiratory system than on the cardiovascular system. This is different from the effect of $PM_{2.5}$. Therefore, more studies are needed to consider BC as a separate pollutant, and not just as a component of $PM_{2.5}$. The emission reduction measures of BC can effectively reduce the health risk of air pollutants. The toxicology experiments of $PM_{2.5}$ from different sources show that industrial emissions and coal burning seem more toxic to human health than emissions from traffic (exhaust and non-exhaust). In order to better protect the public health of Chinese citizens, future air pollution control policies are suggested to focus more on emissions from industrial processes and coal burning. These activities occur in regions with a lot of people that will be exposed to pollution.

The emission reductions contributed by the ultra-low emission standard applied to the thermal power plants in China during the past years imply a great potential for other non-electricity industries to cut their emissions by installing advanced end-of-pipe control devices[9]. For example, China is now promoting the ultra-low emission standard in some energy-intensive industries, with various, but all strict requirements apply to different key industries. More than 600 million tons of production capacity of crude steel has already met the ultra-low emission standard or is undergoing the emission control retrofit to meet the ultra-low emission standard. Future actions to deploy advanced end-of-pipe technologies in other heavily polluting industries would further cut air pollutant emissions from industrial processes, thus protecting public health.

During the past ten years, China has made marked progress in optimizing its energy structure. From 2012 to 2021, the contribution of coal to the country's total energy consumption has dropped from 68.5% to 56%, with clean energy resolving 2/3 of the increased energy demand. These substantial changes are achieved by the large-scale deployment of renewable energy infrastructures such as wind turbines and solar PVs, as well as a large-scale phase-out of coal-powered boilers and kilns. These efforts would help reduce air pollutant emissions and greenhouse gases from coal. China's new carbon peaking and carbon neutrality pledge would further lead to fundamental changes in the country's energy structure, with coal substituted by renewable energy and hence protect people from coal-sourced air pollution.

7.2 Maximizing the co-benefits of different policy strategies

With the pledge of carbon peaking and carbon neutrality and the missions of building a "Beautiful China" and a "Healthy China", tailored policies that can simultaneously provide better air quality, climate mitigation, and public health benefits should be prioritized. From the perspective of air quality protection, which is one of the main topics of the ChiNorBC project, measures and actions targeted at improving air quality would to a large extent contribute to meet China's updated Nationally Determined Contribution (NDC) goals[10]. These goals are set out in China's Achievements, New Goals and New Measures for Nationally Determined Contributions[11]. China's updated NDC goals are as follows: aims to have CO_2 emissions peak before 2030 and achieve carbon neutrality before 2060; to lower CO_2 emissions per unit of GDP by over 65% from the 2005 level, to increase the share of non-fossil fuels in primary energy consumption to around 25%, to increase the forest stock volume by 6 billion cubic meters from the 2005 level, and to bring its total installed capacity of wind and solar power to over 1.2 billion kilowatts by 2030. The various actions that could be applied to improve air quality, such as increasing the share of non-fossil fuels by reducing coal and expanding the construction of renewable infrastructures will result synergies between environmental protection and climate mitigation[12].

7.2.1 Recommendations for abatement measures

[16] Risk value of 1 means no risk. CI represents confidence interval, and if the 95% CI interval crosses 1, or is less than 1, e.g. 0.9-1.1 or 0.8-0.9, it means that the confidence interval for the result is too large and the result is not credible and there would be no risk. If the 95% CI is greater than 1, it indicates a risk, e.g. 1.01-1.03, meaning that for every 10 μg/m3 increase, the risk increases by 1-3%.

The results of the scenario analysis have identified key sectors to focus on to reduce BC and OC emissions and obtain co-benefits. As an important climate forcer that warms the Earth, BC in the atmosphere also deteriorates air quality together with other $PM_{2.5}$ species, and further harms human health by penetrating the respiratory system. Therefore, measures that could effectively reduce BC emission would also result in co-benefits between air quality, climate, and public health. It is noteworthy that we do not mean solely abating BC and OC emissions are enough to achieving China's air quality target as sulphate and nitrate still contribute substantially to total aerosol abundance, and thus reducing SO_2 and NO_X emissions also play key roles in improving China's air quality.

The measures that reduce BC and OC most in all scenarios are those related to the residential sector followed by measures to reduce emissions from the industry. A shift from coal use for heating and cooking in households to renewable energy, industrial waste heat, cogeneration, electricity, and gas will, according to the scenarios, be particularly beneficial to reduce air pollution and will also contribute to reducing CO_2-emissions. It should also be noted that these efforts may also result in trade-offs in climate effects such as warming induced by declines in sulphate aerosols due to less coal consumption.

The meta-analysis conducted by this project (see more in Chapter 6) shows that industrial emissions are the most dangerous to human health, followed by coal burning, vehicle exhaust emissions. This ranking of the toxicity of emissions needs to be taken into account when designing policy recommendations.

To keep improving air quality and mitigating with climate change, based on the results from the ChiNorBC project, it is recommended to strengthen the control of BC and OC emissions in Northern China by promoting the adjustment of energy, industry and transportation structures and further strengthening the potential of end-of-pipe treatment. Specific focus should be on key sectors such as industrial, rural residential, and transportation sectors. The actions to be taken in order to achieve reductions in BC/OC and obtain substantial co-benefits for air quality, health and climate are:

i. Optimize energy structure toward a low-carbon society

- Scaling up the deployment of clean power generation
  Coal consumption is one of the most important emission sources of BC/OC and greenhouse gases. Measures such as coal control, coal reduction and clean energy substitution can effectively reduce air pollutants and greenhouse gas emissions. Therefore, it is suggested, as the most important measure, to control the country's coal consumption, with a focus on key coal industries, such as phasing down unabated coal power plants. Meanwhile, it is suggested to scale up the deployment of clean power generation by promoting the large-scale development and high-quality development of wind power and solar power, as well as promoting the construction of hydropower bases.
- Reducing residential coal use
  Particles emitted from coal burning have been identified as the second most toxic to human health. In addition, as suggested by the scenario analysis, substantial BC and OC abatements could be expected from the residential sector. We therefore suggest continue promoting clean energy in the residential sector. Specifically, promoting clean heating should be the most important part of the residential energy transformation project. Clean heating is not only an important people's livelihood project, but also a key measure to effectively control BC/OC and other air pollutant emissions. It is therefore suggested to adopt renewable energy, industrial waste heat, cogeneration, electricity, gas and other applicable ways to substitute coal-fired heating boilers and bulk coal use in Northern China. The substitution approach should be selected carefully according to local conditions.
- Elimination coal-fired boilers
  In order to reducing coal burning, it is also suggested to continue eliminating coal-fired boilers in polluting cities and key regions, to improve air quality and reduce GHGs emissions together. Coal-fired boilers and small coal-fired thermoelectricity plants can be shut down when residential and industrial heating demand is satisfied by nearby cogeneration power plants.
- Promote clean energy substitution of industrial furnaces
  Safely and steadily promote the conversion of industrial furnaces using highly polluting fuels to industrial waste heat, electric energy, natural gas, etc. Promote the use of clean energy instead of fuel gas generators.

ii. Optimize industrial structure by phasing out heavy-polluting energy-intensive industries

- Limit the development of energy-intensive projects with high emissions and backward production capacity

  Projects with high emissions and backward production capacity are generally potential large emitters of BC and OC, as most of these projects would rely on coal as a key energy source. It is therefore suggested to comprehensively check the projects under construction, planned and in stock, and implement inventory management, classified disposal and dynamic monitoring; Stop the projects under construction that do not meet the requirements, seriously investigate, and deal with the stock projects that are approved and constructed in violation of laws and regulations, and scientifically and steadily promote the proposed projects that meet the requirements.
- Accelerate the elimination of backward production capacity in key industries

  Promote the gradual elimination of backward processes and equipment in industries related to BC/OC emission, and orderly adjust the space layout of steel, coking, electrolytic aluminum and other BC/OC-related key industrial sectors.

iii. Promote transportation structure adjustment

- Adjust the freight transportation mode

  Trucks are now an important source of BC in China and globally. Reducing the use of internal combustion engine trucks, especially those powered by diesel is vital for controlling BC emissions from transport. It is therefore suggested to promote railway and waterway transportation for the medium and long-distance transportation of bulk commodities, such as coal and ore, and the use of closed belt corridors or electric vehicles for short-distance transportation.
- Strengthen the comprehensive treatment of non-road mobile sources

  Diesel-power off-road machines are another important source of BC. It is therefore suggested to accelerate the new energy utilization of new or updated operating vehicles and machinery in railway freight yards, logistics parks, ports, airports, and thermal power, steel, coal, coking, building materials, mines and other industrial and mining enterprises. Accelerate the elimination of old ships with high energy consumption and high emissions, and promote the adoption of measures such as replacing engines or installing pollution control devices for in-depth treatment if applicable.

iv. Promote in-depth end-of-pipe control for key industries

- Promote ultra-low emission transformation of key industries

  At present, the country has introduced ultra-low emission transformation plans for the power industry and steel industries. In the next step, in addition to continuing to promote ultra-low emission transformation in the iron and steel industry in accordance with national requirements, it is suggested to orderly carry out ultra-low emission transformation of other important industries such as cement, coking etc. with the consideration of impletion factors such as technology maturity in Northern China.
- Accelerate the upgrading and transformation of key industries and boilers

  China has made great efforts in upgrading and transforming key industries and boilers in the past decade, and notable air quality and climate benefits have been obtained. Yet, previous measures primarily focus on the power sector and the iron and steel and cement industries. With the clean air actions continuing, in addition to accelerating ultra-low emission transformation for applicable industries, it is now suggested to strengthen the implementation of in-depth control of pollutant emissions in other high-polluting industries such as glass, casting, lime, mineral wool, non-ferrous metal smelting etc, whose share in BC/OC emissions are increasing due to the clean air measures applied in other key sectors.

7.2.2 Recommendations for public participation

i. Strengthen dissemination and guidance

Use traditional media and new media to timely publish air quality, pollution control policies and other related information, and widely publicize and interpret relevant policies, and measures. Vigorously popularize the basic concepts, knowledge and co-benefits of air quality, health and climate change in order to improve citizens' awareness. The ChiNorBC project contributes to developing dissemination material through a website (chinorbc.net), a brochure for the public, and a cartoon movie. All products are in both Chinese and English. In

addition, a hard copy book reviewing the status of emission control, air quality, health, and Chinese policies are published.

ii. Promote public participation

Advocate for public participation for improving air quality and mitigating climate change. This includes strengthen citizens' environmental awareness, advocating for voluntary public service, and lifestyle changes. In addition, the government should set an example by implementing circular economy principles.

7.2.3 Future recommendations

i. Regularly updating BC and OC emission inventory and reduce uncertainty

The emission inventory of BC and OC serves as a basis for formulating BC and OC control policies as it provides spatial-temporal and sectorial distribution of BC and OC emissions. In addition, the uncertainty of BC emission inventory is generally believed to be higher than species such as SO_2 and NO_X. It is therefore highly recommended to keep updating BC and OC emissions, and reducing the uncertainty of key parameters, therefore providing timely and accurate information on the variations in BC/OC emissions for scientists and policymakers. Observations are essential in order to validate modelling tools and track effectiveness of mitigation strategies. Sustained and broad observational capacity, including species specific surface measurements should be ensured.

ii. Conduct cost-benefit analysis

A better understanding of the cost and multi-aspect benefits of all potential measures would help the policymakers to identify measures that should be prioritized. Therefore, it is highly recommended to conduct systematic cost-benefit analysis on the abovementioned BC and OC control measures, with the measure-specific air quality improvement, climate mitigation, and health benefits evaluated.

iii. Further work related to air pollution assessments

Accurately evaluating the impacts of clean air policies and measures is the basis for formulating effective control measures. It is therefore recommended to applying various method including satellite remote sensing, numeric simulation, ground-based observation to conduct multi-aspect analysis on the effects of historical air pollution control policies. In addition, pre-assessment of proposed clean air measures are also necessary.

iv. Further work related to climate assessments

While achieving the most stringent mitigation scenarios is estimated to result in marked reductions in the abundances of anthropogenic aerosol species over the most polluted region of China, the largest relative reduction achieved is -40% for BC. This suggests additional mitigation options and/or mitigation implemented in sectors not considered in our project is required for further reducing the amounts of atmospheric BC concentrations. If also sulfate, nitrate, and OC aerosols are reduced, the net effect may be a net warming contribution to temperature, as estimated for the ChiNorBC scenarios. While not negating the importance of reductions of these aerosol species for air quality improvements, this additional warming must be considered in comprehensive assessments of the climate co-benefits and trade-offs of mitigation strategies. Rapid/strong changes in aerosol and precursor emissions can also have significant impacts on regional climate beyond radiative effects, but these remain insufficiently quantified. Support for and assessment of research on local-to-regional scale impacts of aerosols on precipitation, dynamics, and extremes is required for more comprehensive understanding of potential near-term climate risk.

v. Further investigations on the health impacts of BC and OC pollution

The understanding of health impacts of BC and OC exposure is still not adequate for supporting precise decision-making. It is therefore suggested to further investigate the health impacts of BC and OC pollution by experiments as well as in-depth meta-analysis.

References

[1]Aamaas, B., Berntsen, T. K., Fuglestvedt, J. S., Shine, K. P., and Bellouin, N.: Regional emission metrics for short-lived climate forcers from multiple models, Atmos. Chem. Phys., 16, 7451–7468, https://doi.org/10.5194/acp-16-7451-2016, 2016.

[2]Aamaas, B., Peters, G. P., and Fuglestvedt, J. S.: Simple emission metrics for climate impacts, Earth Syst. Dynam., 4, 145–170, https://doi.org/10.5194/esd-4-145-2013, 2013.

[3]Agency, U.S.E.P. 2012. Report to Congress on Black Carbon.

[4]Aiken A. C., DeCarlo P. F., Kroll J. H., Worsnop D. R., Huffman J. A., Docherty K. S., Ulbrich I. M., Mohr C., Kimmel J. R., Sueper D., Sun Y., Zhang Q., Trimborn A., Northway M., Ziemann P. J., Canagaratna M. R., Onasch T. B., Alfarra M. R., Prevot A. S. H., Dommen J., Duplissy J., Metzger A., Baltensperger U. & Jimenez J. L. O/C and OM/OC Ratios of Primary, Secondary, and Ambient Organic Aerosols with High-Resolution Time-of-Flight Aerosol Mass Spectrometry, *Environmental Science & Technology.* 42(12), 4478-4485, 10.1021/es703009q, 2008.

[5]Anthes R A. A cumulus parameterization scheme utilizing a one-dimensional cloud model[J]. Monthly Weather Review, 1977, 105(3): 270-286.

[6]Appel K W, Napelenok S L, Foley K M, et al. Description and evaluation of the Community Multiscale Air Quality (CMAQ) modeling system version 5.1[J]. Geoscientific model development, 2017, 10(4): 1703-1732.

[7]Azad, N., Rojanasakul, Y., and Vallyathan, V. (2008). Inflammation and lung cancer: roles of reactive oxygen/nitrogen species. J Toxicol Environ Health B Crit Rev 11, 1-15.

[8]Begum B A, Biswas S K, Pandit G G, et al. Long–range transport of soil dust and smoke pollution in the South Asian region[J]. Atmospheric Pollution Research, 2011, 2(2): 151-157.

[9]Berglen T. F., Berntsen T. K., Isaksen I. S. A. & Sundet J. K. A global model of the coupled sulfur/oxidant chemistry in the troposphere: The sulfur cycle, *Journal of Geophysical Research-Atmospheres.* 109(D19), D19310, 10.1029/2003jd003948, 2004.

[10]Berntsen T., Fuglestvedt J., Myhre G., Stordal F. & Berglen T. F. Abatement of greenhouse gases: Does location matter?, *Climatic Change.* 74(4), 377-411, 10.1007/s10584-006-0433-4, 2006.

[11]Bond T.C, Doherty SJ, Fahey DW et al., 2013. Bounding the role of black carbon in the climate system: A scientific assessment. Journal of Geophysical Research: Atmospheres. 118:5380-552. DOI: 10.1002/jgrd.50171.

[12]Borge R, Lumbreras J, Vardoulakis S, et al. Analysis of long-range transport influences on urban PM10 using two-stage atmospheric trajectory clusters[J]. Atmospheric Environment, 2007, 41(21): 4434-4450.

[13]Carter W P L. Implementation of the SAPRC-99 chemical mechanism into the Models-3 framework[J]. Report to the United States Environmental Protection Agency, January, 2000, 29.

[14]Center on Emissions Inventories and Projections (CEIP). 2020. https://www.ceip.at/the-emep-grid/grid-definiton

[15]Chen L, Deng H, Cui H, Fang J, Zuo Z, Deng J, et al. 2018. Inflammatory responses and inflammation-associated diseases in organs. Oncotarget 9:7204.

[16]Chen, C., Park, T., Wang, X. et al. 2019. China and India lead in greening of the world through land-use management. Nat Sustain 2, 122–129. https://doi.org/10.1038/s41893-019-0220-7.

[17]Cheng Miaomiao, Scott Randall, Ingeborg Rønning, Vigdis Vestreng, and Fan Meng. 2022. Review of BC/OC emissions and control measures in China and Norway. http://chinorbc.net/publications/.

[18]Cheng, J. et al. Pathways of China's PM2.5 air quality 2015-2060 in the context of carbon neutrality. Natl Sci Rev 8, nwab078, doi:10.1093/nsr/nwab078 (2021).

[19]Chi Z, Guan J, Zhong L, et al. Using Numerical Simulation Technology to Assess the Contribution of Key Polluters to Air Pollution in the Huancui District, Weihai, China[J]. International Journal of Environmental Science and Development, 2017, 8(4): 264.

[20]China Association of Agricultural Machinery Manufactures. China Agricultural Machinery Industry Yearbook [M]. Beijing, 2019.

[21]China Association of Automobile Manufactures. China Automotive Industry Yearbook [M]. Beijing, 2019.

[22]China Construction Machinery Association. China Construction Machinery Industry Yearbook [M]. Beijing, 2019.

[23]Chinanews. 2021. "MEE: Winning the Blue Sky Battle." from https://www.sohu.com/a/452745029_270669.
[24]China's updated NDC, <https://unfccc.int/sites/default/files/NDC/2022-06/China%E2%80%99s%20Achievements%2C%20New%20Goals%20and%20New%20Measures%20for%20Nationally%20Determined%20Contributions.pdf>
[25]Choe, S.A., Eliot, M.N., Savitz, D.A., and Wellenius, G.A. (2019). Ambient air pollution during pregnancy and risk of gestational diabetes in New York City. Environ Res 175, 414-420.
[26]Collins, W. J., Fry, M. M., Yu, H., Fuglestvedt, J. S., Shindell, D. T., and West, J. J.: Global and regional temperature-change potentials for near-term climate forcers, Atmos. Chem. Phys., 13, 2471–2485, https://doi.org/10.5194/acp-13-2471-2013, 2013.
[27]Daigneault M, Preston JA, Marriott HM, Whyte MK, Dockrell DH. 2010. The identification of markers of macrophage differentiation in pma-stimulated thp-1 cells and monocyte-derived macrophages. PloS one 5:e8668. doi:8610.1371/journal.pone.0008668.
[28]Deng, H., Eckel, S.P., Liu, L., Lurmann, F.W., Cockburn, M.G., and Gilliland, F.D. (2017). Particulate matter air pollution and liver cancer survival. Int J Cancer 141, 744-749.
[29]Department of Energy Statistics, National Bureau of Statistics. 2020. China energy statistical yearbook. Beijing: China Statistics Press.
[30]Di Q, Wang Y, Zanobetti A, Wang Y, Koutrakis P, Choirat C, et al. 2017. Air pollution and mortality in the medicare population. N Engl J Med 376:2513-2522.
[31]Di, Q., Wang, Y., Zanobetti, A., Wang, Y., Koutrakis, P., Choirat, C., Dominici, F., and Schwartz, J.D. (2017). Air Pollution and Mortality in the Medicare Population. N Engl J Med 376, 2513-2522.
[32]Du, Y., Xu, X., Chu, M., Guo, Y., and Wang, J. (2016). Air particulate matter and cardiovascular disease: the epidemiological, biomedical and clinical evidence. J Thorac Dis 8, E8-E19.
[33]Edgell C-J, McDonald CC, Graham JB. 1983. Permanent cell line expressing human factor viii-related antigen established by hybridization. Proceedings of the National Academy of Sciences 80:3734-3737.
[34]Emery C, Liu Z, Russell A G, et al. Recommendations on statistics and benchmarks to assess photochemical model performance[J]. Journal of the Air & Waste Management Association, 2017, 67(5): 582-598.
[35]Esser C, Rannug A. 2015. The aryl hydrocarbon receptor in barrier organ physiology, immunology, and toxicology. Pharmacol Rev 67:259-279.
[36]Etminan M., Myhre G., Highwood E. J. & Shine K. P.: Radiative forcing of carbon dioxide, methane, and nitrous oxide: A significant revision of the methane radiative forcing, Geophysical Research Letters. 43(24), 12,614-612,623, 10.1002/2016gl071930, 2016.
[37]Feng, L., Smith, S. J., Braun, C., Crippa, M., Gidden, M. J., Hoesly, R., Klimont, Z., van Marle, M., van den Berg, M., and van der Werf, G. R.: The generation of gridded emissions data for CMIP6, Geosci. Model Dev., 13, 461–482, https://doi.org/10.5194/gmd-13-461-2020, 2020.
[38]Forster, P., T. Storelvmo, K. Armour, W. Collins, J.-L. Dufresne, D. Frame, D.J. Lunt, T. Mauritsen, M.D. Palmer, M. Watanabe, M. Wild, and H. Zhang: The Earth's Energy Budget, Climate Feedbacks, and Climate Sensitivity. In Climate Change 2021: The Physical Science Basis. Contribution of Working Group I to the Sixth Assessment Report of the Intergovernmental Panel on Climate Change [Masson-Delmotte, V., P. Zhai, A. Pirani, S.L. Connors, C. Péan, S. Berger, N. Caud, Y. Chen, L. Goldfarb, M.I. Gomis, M. Huang, K. Leitzell, E. Lonnoy, J.B.R. Matthews, T.K. Maycock, T. Waterfield, O. Yelekçi, R. Yu, and B. Zhou (eds.)]. Cambridge University Press, Cambridge, United Kingdom and New York, NY, USA, pp. 923–1054, doi:10.1017/9781009157896.009, 2021
[39]Fuglestvedt J. S., Shine K. P., Berntsen T., Cook J., Lee D. S., Stenke A., Skeie R. B., Velders G. J. M. & Waitz I. A.: Transport impacts on atmosphere and climate: Metrics, Atmospheric Environment. 44(37), 4648-4677, https://doi.org/10.1016/j.atmosenv.2009.04.044, 2010.
[40]Gauss, M.: Impact of aircraft emissions and ozone changes in the 21st century: 3-D model studies, Ph.D. thesis, University of Oslo, Department of Geophysics, Section of Meteorology and Oceanography, PB. 1022 Blindern, 0315 Oslo, Norway, ISSN 1501–7710, No. 304, 2003.
[41]Geoffroy O., Saint-Martin D., Olivié D. J. L., Voldoire A., Bellon G. & Tytéca S.: Transient Climate Response in a Two-Layer Energy-Balance Model. Part I: Analytical Solution and Parameter Calibration Using CMIP5 AOGCM Experiments, Journal of Climate. 26(6), 1841-1857, 10.1175/jcli-d-12-00195.1, 2013

[42]Giard DJ, Aaronson SA, Todaro GJ, Arnstein P, Kersey JH, Dosik H, et al. 1973. In vitro cultivation of human tumors: Establishment of cell lines derived from a series of solid tumors. Journal of the National Cancer Institute 51:1417-1423.

[43]Grytting VS, Chand P, Lag M, Ovrevik J, Refsnes M. 2022. The pro-inflammatory effects of combined exposure to diesel exhaust particles and mineral particles in human bronchial epithelial cells. Part Fibre Toxicol 19:14.

[44]Guenther A, Jiang X, Shah T, et al. Model of emissions of gases and aerosol from nature version 3 (MEGAN3) for estimating biogenic emissions[C]//International Technical Meeting on Air Pollution Modelling and its Application. Springer, Cham, 2018: 187-192.

[45]He PC, He C. 2021. M(6) a rna methylation: From mechanisms to therapeutic potential. EMBO J 40:e105977.

[46]HEI, IHME. 2020. State of global air 2020. (Special Report). Boston, MA:Health effects Institue.

[47]Hiemstra PS, Grootaers G, van der Does AM, Krul CAM, Kooter IM. 2018. Human lung epithelial cell cultures for analysis of inhaled toxicants: Lessons learned and future directions. Toxicol In Vitro 47:137-146.

[48]Hoffmann, T., Odum, J. R., Bowman, F., D.Collins, Klockow, D., Flagan, R. C., and Seinfeld, J. H.: Formation of Organic Aerosols from the Oxidation of Biogenic Hydrocarbons, J. Atmos. Chem., 26, 189–222, 1997.

[49]Holben B. N., Eck T. F., Slutsker I., Tanré D., Buis J. P., Setzer A., Vermote E., Reagan J. A., Kaufman Y. J., Nakajima T., Lavenu F., Jankowiak I. & Smirnov A.: AERONET—A Federated Instrument Network and Data Archive for Aerosol Characterization, Remote Sensing of Environment. 66(1), 1-16, https://doi.org/10.1016/S0034-4257(98)00031-5, 1998.

[50]Houyoux M, Vukovich J, Brandmeyer J E. Sparse Matrix Operator Kernel Emissions (SMOKE) modeling system user manual[J]. University of North Carolina at Chapel Hill, online available at: http://www. Smoke-model. Org, last access, 2009, 2005.

[51]Hoyle C. R., Berntsen T., Myhre G. & Isaksen I. S. A. Secondary organic aerosol in the global aerosol-chemical transport model Oslo CTM2, *Atmos. Chem. Phys.* 7(5675-5694), 2007.

[52]IHME, H. (2020). State of Global Air 2020：A Special Report on Globle Exposure to Air Pollution and Its Health Impacts. IHME.

[53]IPCC,2013. Myhre, G., D. Shindell, F.-M. Bréon, W. Collins, J. Fuglestvedt, J. Huang, D. Koch, J.-F. Lamarque, D. Lee, B. Mendoza, T. Nakajima, A. Robock, G. Stephens, T. Takemura and H. Zhang, 2013: Anthropogenic and Natural Radiative Forcing. In: Climate Change 2013: The Physical Science Basis. Contribution of Working Group I to the Fifth Assessment Report of the Intergovernmental Panel on Climate Change [Stocker, T.F., D. Qin, G.-K. Plattner, M. Tignor, S.K. Allen, J. Boschung, A. Nauels, Y. Xia, V. Bex and P.M. Midgley (eds.)]. Cambridge University Press, Cambridge, United Kingdom and New York, NY, USA.

[54]IPCC,2023: AR6 Synthesis Report Climate Change 2023. Summary for Policy makers, <https://www.ipcc.ch/report/ar6/syr/>

[55]IPCC,2021. Climate change 2021: The physical science basis. Contribution of Working Group I to the Sixth Assessment Report of the Intergovernmental Panel on Climate Change (AR6), [Masson-Delmotte, V., et al. eds]. Cambridge University Press, In Press.

[56]IPCC: Report prepared for Intergovernmental Panel on Climate Change by Working Group I. J.T. Houghton, G.J. Jenkins and J.J. Ephraums (eds.). Cambridge University Press, Cambridge, Great Britain, New York, NY, USA and Melbourne, Australia 410 pp., 1990

[57]Jacobson, M.Z. (2001). Strong radiative heating due to the mixing state of black carbon in atmospheric aerosols. Nature 409, 695-697.

[58]Ji D, Gao M, Maenhaut W, et al. The carbonaceous aerosol levels still remain a challenge in the Beijing-Tianjin-Hebei region of China: Insights from continuous high temporal resolution measurements in multiple cities[J]. Environment international, 2019, 126: 171-183.

[59]Klein SG, Serchi T, Hoffmann L, Blömeke B, Gutleb AC. 2013. An improved 3d tetraculture system mimicking the cellular organisation at the alveolar barrier to study the potential toxic effects of particles on the lung. Particle and fibre toxicology 10:1-18.

[60]Kletting S, Barthold S, Repnik U, Griffiths G, Loretz B, Schneider-Daum N, et al. 2018. Co-culture of human alveolar epithelial (haelvi) and macrophage (thp-1) cell lines. ALTEX 35:211-222.

[61]Komal S, Zhang LR, Han SN. 2021. Potential regulatory role of epigenetic rna methylation in cardiovascular diseases. Biomed Pharmacother 137:111376.
[62]Kupiainen, K. J., Aamaas, B., Savolahti, M., Karvosenoja, N., and Paunu, V.-V.: Climate impact of Finnish air pollutants and greenhouse gases using multiple emission metrics, Atmos. Chem. Phys., 19, 7743–7757, https://doi.org/10.5194/acp-19-7743-2019, 2019.
[63]Kurokawa J, Ohara T, Morikawa T, et al. Emissions of air pollutants and greenhouse gases over Asian regions during 2000–2008: Regional Emission inventory in Asia (REAS) version 2[J]. Atmospheric Chemistry and Physics, 2013, 13(21): 11019-11058.
[64]Lacouture, M.E., Morris, J.C., Lawrence, D.P., Tan, A.R., Olencki, T.E., Shapiro, G.I., Dezube, B.J., Berzofsky, J.A., Hsu, F.J., and Guitart, J. (2015). Cutaneous keratoacanthomas/squamous cell carcinomas associated with neutralization of transforming growth factor β by the monoclonal antibody fresolimumab (GC1008). Cancer Immunology, Immunotherapy 64, 437-446.
[65]Lan, Q., Liu, P.Y., Bell, J.L., Wang, J.Y., Huttelmaier, S., Zhang, X.D., Zhang, L., and Liu, T. (2021). The Emerging Roles of RNA m(6)A Methylation and Demethylation as Critical Regulators of Tumorigenesis, Drug Sensitivity, and Resistance. Cancer Res 81, 3431-3440.
[66]Landrigan PJ, Fuller R, Acosta NJR, Adeyi O, Arnold R, Basu N, et al. 2018. The lancet commission on pollution and health. The Lancet 391:462-512.
[67]Landrigan, P.J., Fuller, R., Acosta, N.J.R., Adeyi, O., Arnold, R., Basu, N.N., Balde, A.B., Bertollini, R., Bose-O'Reilly, S., Boufford, J.I., et al. (2018). The Lancet Commission on pollution and health. Lancet 391, 462-512.
[68]Laskin, A., Laskin, J., & Nizkorodov, S. A. 2015. Chemistry of atmospheric brown carbon. Chemical reviews, 115(10), 4335–4382. https://doi.org/10.1021/cr5006167.
[69]Lei Y, Zhang Q, He K B, et al. Primary anthropogenic aerosol emission trends for China, 1990–2005 [J]. Atmos Chem Phys, 2011, 11(3): 931-54.
[70]Leiva-Juarez MM, Kolls JK, Evans SE. 2018. Lung epithelial cells: Therapeutically inducible effectors of antimicrobial defense. Mucosal Immunol 11:21-34.
[71]Leng SX, McElhaney JE, Walston JD, Xie D, Fedarko NS, Kuchel GA. 2008. Elisa and multiplex technologies for cytokine measurement in inflammation and aging research. The Journals of Gerontology Series A: Biological Sciences and Medical Sciences 63:879-884.
[72]Leon B, Ballesteros-Tato A. 2021. Modulating th2 cell immunity for the treatment of asthma. Front Immunol 12:637948.
[73]Li D, Wu M. 2021. Pattern recognition receptors in health and diseases. Signal Transduct Target Ther 6:291.
[74]Li J, Wang Z, Zhuang G, et al. Mixing of Asian mineral dust with anthropogenic pollutants over East Asia: a model case study of a super-duststorm in March 2010[J]. Atmospheric Chemistry and Physics, 2012, 12(16): 7591-7607.
[75]Li M, Zhang Q, Kurokawa J, et al. MIX: a mosaic Asian anthropogenic emission inventory under the international collaboration framework of the MICS-Asia and HTAP[J]. Atmospheric Chemistry and Physics, 2017, 17(2): 935-963.
[76]Li X, Hussain S A, Sobri S, et al. Overviewing the air quality models on air pollution in Sichuan Basin, China[J]. Chemosphere, 2021, 271: 129502.
[77]Li, R., Kou, X., Xie, L., Cheng, F., and Geng, H. (2015). Effects of ambient PM2.5 on pathological injury, inflammation, oxidative stress, metabolic enzyme activity, and expression of c-fos and c-jun in lungs of rats. Environ Sci Pollut Res Int 22, 20167-20176.
[78]Li, Z., Li, N., Guo, C., Li, X., Qian, Y., Wu, J., Yang, Y., and Wei, Y. (2019). Genomic DNA methylation signatures in different tissues after ambient air particulate matter exposure. Ecotoxicology and Environmental Safety 179, 175-181.
[79]Liu Y., Liu J. & Tao S.: Interannual variability of summertime aerosol optical depth over East Asia during 2000–2011: a potential influence from El Niño Southern Oscillation, Environmental Research Letters. 8(4), 044034, 10.1088/1748-9326/8/4/044034, 2013.
[80]Liu, Y. et al. Role of climate goals and clean-air policies on reducing future air pollution deaths in China: a modelling study. The Lancet Planetary Health 6, e92-e99, doi:10.1016/s2542-5196(21)00326-0 (2022).
[81]Lu, Z., Zhang, Q., Streets, D.G., 2011. Sulfur dioxide and primary carbonaceous aerosol emissions in China and India, 1996–2010. Atmos. Chem. Phys. 11, 9839-9864.

[82]Lund M. T., Myhre G., Haslerud A. S., Skeie R. B., Griesfeller J., Platt S. M., Kumar R., Myhre C. L. & Schulz M. Concentrations and radiative forcing of anthropogenic aerosols from 1750 to 2014 simulated with the Oslo CTM3 and CEDS emission inventory, *Geosci. Model Dev.* 11(12), 4909-4931, 10.5194/gmd-11-4909-2018, 2018.

[83]Lund M. T., Myhre G., Haslerud A. S., Skeie R. B., Griesfeller J., Platt S. M., Kumar R., Myhre C. L. & Schulz M.: Concentrations and radiative forcing of anthropogenic aerosols from 1750 to 2014 simulated with the Oslo CTM3 and CEDS emission inventory, Geosci. Model Dev. 11(12), 4909-4931, 10.5194/gmd-11-4909-2018, 2018.

[84]Lund ME, To J, O'Brien BA, Donnelly S. 2016. The choice of phorbol 12-myristate 13-acetate differentiation protocol influences the response of thp-1 macrophages to a pro-inflammatory stimulus. J Immunol Methods 430:64-70.

[85]Lund, M. T., Aamaas, B., Berntsen, T., Bock, L., Burkhardt, U., Fuglestvedt, J. S., and Shine, K. P.: Emission metrics for quantifying regional climate impacts of aviation, Earth Syst. Dynam., 8, 547–563, https://doi.org/10.5194/esd-8-547-2017, 2017.

[86]Lund, M. T., Aamaas, B., Stjern, C. W., Klimont, Z., Berntsen, T. K., and Samset, B. H.: A continued role of short-lived climate forcers under the Shared Socioeconomic Pathways, Earth Syst. Dynam., 11, 977–993, https://doi.org/10.5194/esd-11-977-2020, 2020.

[87]Lund, M. T., Myhre, G., Skeie, R. B., Samset, B. H., and Klimont, Z.: Differences between recent emission inventories strongly affect anthropogenic aerosol evolution from 1990 to 2019, Atmos. Chem. Phys. Discuss. [preprint], https://doi.org/10.5194/acp-2022-639, in review, 2022.

[88]Lund, M. T., Myhre, G., Skeie, R. B., Samset, B. H., and Klimont, Z.: Differences between recent emission inventories strongly affect anthropogenic aerosol evolution from 1990 to 2019, Atmos. Chem. Phys. Discuss. [preprint], https://doi.org/10.5194/acp-2022-639, in review, 2022

[89]Ma S, Xiao Z, Zhang Y, et al. Assessment of meteorological impact and emergency plan for a heavy haze pollution episode in a core city of the North China Plain[J]. Aerosol and Air Quality Research, 2020, 20(1): 26-42.

[90]Metzger, S., Dentener, F., Krol, M., Jeuken, A., and Lelieveld, J.: Gas/aerosol partitioning – 2. Global modeling results, J. Geophys. Res.-Atmos., 107(D16), 4313, doi:10.1029/2001JD001103, 2002a.

[91]Metzger, S., Dentener, F., Pandis, S., and Lelieveld, J.: Gas/aerosol partitioning: 1. A computationally efficient model, J. Geophys. Res.-Atmos., 107(D16), 4312, doi:10.1029/2001JD001102, 2002b.

[92]Meyer, K.D. (2019). m(6)A-mediated translation regulation. Biochim Biophys Acta Gene Regul Mech 1862, 301-309.

[93]Ministry of Ecology and Environment of People's Republic of China. Road Motor Vehicle Air Pollutant Emission Inventory Development Technical Guidelines (Trial) [M]. Beijing, 2014.

[94]Ministry of Ecology and Environment of People's Republic of China. Technical Guidelines for the Air Pollutant Emission Inventories of Residential Coal (Trial) [M]. Beijing. 2016.

[95]Ministry of Ecology and Environment of People's Republic of China. Technical Guidelines for the Development of Inventories of Atmospheric Pollutants from Non-road Mobile Sources (Trial) [M]. Beijing, 2014.

[96]Ministry of Transportation of People's Republic of China. China Statistical Yearbook of China Traffic Yearbook [M]. Beijing, 2019.

[97]MOD08 MODIS Level 3 Atmosphere Products (MOD 08), Data Products Handbook Volume 2. https://modis.gsfc.nasa.gov/data/dataprod/dataproducts.php?MOD_NUMBER=08 (accessed 572 04/26/2018), 2018

[98]Moldoveanu B, Otmishi P, Jani P, Walker J, Sarmiento X, Guardiola J, et al. 2009. Inflammatory mechanisms in the lung. Journal of inflammation research 2:1.

[99]Molina, J.R., and Adjei, A.A. (2006). The Ras/Raf/MAPK Pathway. Journal of Thoracic Oncology 1, 7-9.

[100]Moller P, Jacobsen NR, Folkmann JK, Danielsen PH, Mikkelsen L, Hemmingsen JG, et al. 2010. Role of oxidative damage in toxicity of particulates. Free Radic Res 44:1-46.

[101]Monahan, E., D. Spiel, and K. Spiel, 1986: *Oceanic Whitecaps.* Reidel.

[102]Moorthy B, Chu C, Carlin DJ. 2015. Polycyclic aromatic hydrocarbons: From metabolism to lung cancer. Toxicol Sci 145:5-15.

[103]Moosmüller, H., Chakrabarty, R.K., and Arnott, W.P. 2009. Aerosol light absorption and its measurement: A review. JOURNAL OF QUANTITATIVE SPECTROSCOPY AND RADIATIVE TRANSFER 110, 844-878.

[104]Murphy, K.M., and Reiner, S.L. (2002). The lineage decisions of helper T cells. Nat Rev Immunol 2, 933-944.

[105]Myhre G., Samset B. H., Schulz M., Balkanski Y., Bauer S., Berntsen T. K., Bian H., Bellouin N., Chin M., Diehl T., Easter R. C., Feichter J., Ghan S. J., Hauglustaine D., Iversen T., Kinne S., Kirkevåg A., Lamarque J. F., Lin G., Liu X., Lund M. T., Luo G., Ma X., van Noije T., Penner J. E., Rasch P. J., Ruiz A., Seland Ø., Skeie R. B., Stier P., Takemura T., Tsigaridis K., Wang P., Wang Z., Xu L., Yu H., Yu F., Yoon J. H., Zhang K., Zhang H. & Zhou C. Radiative forcing of the direct aerosol effect from AeroCom Phase II simulations, Atmos. Chem. Phys. 13(4), 1853-1877, 10.5194/acp-13-1853-2013, 2013a.

[106]Myhre G., Shindell D., Bréon F.-M., Collins W., Fuglestvedt J., Huang J., Koch D., Lamarque J.-F., Lee D., Mendoza B., Nakajima T., Robock A., Stephens G., Takemura T. & Zhang H.: Anthropogenic and natural radiative forcing. In: Climate Change 2013: The Physical Science Basis. Contribution of Working Group I to the Fifth Assessment Report of the Intergovernmental Panel on Climate Change [Stocker, T.F., D., Qin, G.-K. Plattner, M. Tignor, S.K. Allen, J. Boschung, A. Nauels, Y. Xia, V. Bex and P.M. Midgley (eds). Cambridge University Press, Cambridge, United Kingdom and New York, NY, USA 2013b.

[107]National Bureau of Statistics of China. China Energy Statistical Yearbook 2018.

[108]National Bureau of Statistics of China. China Statistical Yearbook 2018.

[109]Neu J. L. & Prather M. J. Toward a more physical representation of precipitation scavenging in global chemistry models: cloud overlap and ice physics and their impact on tropospheric ozone, *Atmos. Chem. Phys.* 12(7), 3289-3310, 10.5194/acp-12-3289-2012, 2012.

[110]Neurath, M.F., Finotto, S., and Glimcher, L.H. (2002). The role of Th1/Th2 polarization in mucosal immunity. Nat Med 8, 567-573.

[111]O'Rourke P. R., Smith S. J., Mott A., Ahsan H., McDuffie E. E., Crippa M., Klimont S., McDonald B., Wang Z., Nicholson M. B., Feng L. & Hoesly R. M. (2021), CEDS v-2021-02-05 Emission Data 1975-2019 (Version Feb-05-2021), edited, Zenodo.

[112]Otte T L, Pleim J E. The Meteorology-Chemistry Interface Processor (MCIP) for the CMAQ modeling system: updates through MCIPv3. 4.1[J]. Geoscientific Model Development, 2010, 3(1): 243-256.

[113]Øvrevik J, Refsnes M, Låg M, Holme JA, Schwarze PE. 2015. Activation of proinflammatory responses in cells of the airway mucosa by particulate matter: Oxidant- and non-oxidant-mediated triggering mechanisms. Biomolecules 5:1399-1440.

[114]Pinault L, Tjepkema M, Crouse DL, Weichenthal S, van Donkelaar A, Martin RV, et al. 2016. Risk estimates of mortality attributed to low concentrations of ambient fine particulate matter in the canadian community health survey cohort. Environ Health 15:18.

[115]Pinault, L., Tjepkema, M., Crouse, D.L., Weichenthal, S., van Donkelaar, A., Martin, R.V., Brauer, M., Chen, H., and Burnett, R.T. (2016). Risk estimates of mortality attributed to low concentrations of ambient fine particulate matter in the Canadian community health survey cohort. Environ Health 15, 18.

[116]Podechard N, Lecureur V, Le Ferrec E, Guenon I, Sparfel L, Gilot D, et al. 2008. Interleukin-8 induction by the environmental contaminant benzo(a)pyrene is aryl hydrocarbon receptor-dependent and leads to lung inflammation. Toxicol Lett 177:130-137.

[117]Qin SG, T.J., Wen Yp 2001. Black carbon and its importance in climate change studies. Meteorological Monthly 27(11), 3-7.

[118]Quaas J., Boucher O. & Lohmann U.: Constraining the total aerosol indirect effect in the LMDZ and ECHAM4 GCMs using MODIS satellite data, Atmos. Chem. Phys. 6(4), 947-955, 10.5194/acp-6-947-2006, 2006.

[119]Ramboll U S. Corporation, User's Guide Comprehensive air quality model with extensions version 6.50[J]. 2018.

[120]Randerson J. T., van der Werf G. R., Giglio L., Collatz G. J. & Kasibhatla P. S. Global Fire Emissions Database, Version 4.1 (GFEDv4). ORNL DAAC, Oak Ridge, Tennessee, USA. , https://doi.org/10.3334/ORNLDAAC/1293, 2017.

[121]Rauner, S., Hilaire, J., Klein, D., Strefler, J. & Luderer, G. Air quality co-benefits of ratcheting up the NDCs. Climatic Change 163, 1481-1500, doi:10.1007/s10584-020-02699-1 (2020).

[122]Rosanna, D.P., and Salvatore, C. (2012). Reactive oxygen species, inflammation, and lung diseases. Curr Pharm Des 18, 3889-3900.
[123]Samset B. H., Lund M. T., Bollasina M., Wilcox L. & Myhre G.: Rapidly emerging patterns of Asian aerosol forcing, Nature Geosience 12, 582-584, 2019.
[124]Sayan M, Mossman BT. 2015. The nlrp3 inflammasome in pathogenic particle and fibre-associated lung inflammation and diseases. Particle and fibre toxicology 13:1-15.
[125]Schutgens, N. A. J., Partridge, D. G., and Stier, P.: The importance of temporal collocation for the evaluation of aerosol models with observations, Atmos. Chem. Phys., 16, 1065–1079, https://doi.org/10.5194/acp-16-1065-2016, 2016.
[126]Scovronick, N. et al. The impact of human health co-benefits on evaluations of global climate policy. Nat Commun 10, 2095, doi:10.1038/s41467-019-09499-x (2019).
[127]SCPRC. 2013. Notice of the General Office of the State Council on Issuing the Air Pollution Prevention and Control Action Plan. State Council of the People's Republic of China website. http://www.jingbian.gov.cn/gk/zfwj/gwywj/41211.htm [Chinese] (accessed 29 August 2019).
[128]SCPRC. 2018. Notice of the State Council on Issuing the Three-Year Action Plan for Winning the Blue Sky Defense Battle. State Council of the People's Republic of China website. http://www.gov.cn/zhengce/content/2018-07/03/content_5303158.htm [Chinese] (accessed 29. August 2019).
[129]Shindell, D. & Smith, C. J. Climate and air-quality benefits of a realistic phase-out of fossil fuels. Nature 573, 408-411, doi:10.1038/s41586-019-1554-z (2019).
[130]Shine K. P., Fuglestvedt J. S., Hailemariam K. & Stuber N.: Alternatives to the Global Warming Potential for Comparing Climate Impacts of Emissions of Greenhouse Gases, Climatic Change. 68(3), 281-302, 10.1007/s10584-005-1146-9, 2005.
[131]Shrestha, G., Traina, S., and Swanston, C. 2010. Black Carbon's Properties and Role in the Environment: A Comprehensive Review. Sustainability 2, 294-320.
[132]Sindelarova K., Granier C., Bouarar I., Guenther A., Tilmes S., Stavrakou T., Müller J. F., Kuhn U., Stefani P. & Knorr W. Global data set of biogenic VOC emissions calculated by the MEGAN model over the last 30 years, *Atmos. Chem. Phys.* 14(17), 9317-9341, 10.5194/acp-14-9317-2014, 2014.
[133]Skuland T, Grytting VS, Lag M, Jorgensen RB, Snilsberg B, Leseman D, et al. 2022. Road tunnel-derived coarse, fine and ultrafine particulate matter: Physical and chemical characterization and pro-inflammatory responses in human bronchial epithelial cells. Part Fibre Toxicol 19:45.
[134]Skuland T, Lag M, Gutleb AC, Brinchmann BC, Serchi T, Ovrevik J, et al. 2020. Pro-inflammatory effects of crystalline- and nano-sized non-crystalline silica particles in a 3d alveolar model. Part Fibre Toxicol 17:13.
[135]Smith, M. H., P. M. Park, and I. E. Consterdine, 1993: Marine aerosol concentration and estimated fluxes over sea. *Quart. J. Roy. Meteor. Soc.,* **119,** 809–824.
[136]Song X, Hu Y, Ma Y, Jiang L, Wang X, Shi A, et al. 2022. Is short-term and long-term exposure to black carbon associated with cardiovascular and respiratory diseases? A systematic review and meta-analysis based on evidence reliability. BMJ Open 12:e049516.
[137]Song, X., Hu, Y., Ma, Y., Jiang, L., Wang, X., Shi, A., Zhao, J., Liu, Y., Liu, Y., Tang, J., et al. (2022). Is short-term and long-term exposure to black carbon associated with cardiovascular and respiratory diseases? A systematic review and meta-analysis based on evidence reliability. BMJ Open 12.
[138]Søvde O. A., Prather M. J., Isaksen I. S. A., Berntsen T. K., Stordal F., Zhu X., Holmes C. D. & Hsu J. The chemical transport model Oslo CTM3, *Geosci. Model Dev.* 5(6), 1441-1469, 10.5194/gmd-5-1441-2012, 2012.
[139]Søvde, O. A., Gauss, M., Smyshlyaev, S. P., and Isaksen, I. S. A.: Evaluation of the chemical transport model Oslo CTM2 with focus on Arctic winter ozone depletion, J. Geophys. Res., 113, D09304, doi:10.1029/2007jd009240, 2008.
[140]Stamnes K., Tsay S. C., Wiscombe W. & Jayaweera K.: Numerically stable algorithm for discrete-ordinate-method radiative transfer in multiple scattering and emitting layered media, Appl. Opt. 27(12), 2502-2509, 10.1364/AO.27.002502, 1988.
[141]Stjern C. W., Samset B. H., Myhre G., Forster P. M., Hodnebrog Ø., Andrews T., Boucher O., Faluvegi G., Iversen T., Kasoar M., Kharin V., Kirkevåg A., Lamarque J.-F., Olivié D., Richardson T., Shawki D., Shindell D., Smith C. J., Takemura T. & Voulgarakis A.: Rapid Adjustments Cause Weak Surface Temperature

Response to Increased Black Carbon Concentrations, Journal of Geophysical Research: Atmospheres. 122(21), 11,462-411,481, 10.1002/2017JD027326, 2017.

[142]Stjern, C. W., Samset, B. H., Myhre, G., Bian, H., Chin, M., Davila, Y., Dentener, F., Emmons, L., Flemming, J., Haslerud, A. S., Henze, D., Jonson, J. E., Kucsera, T., Lund, M. T., Schulz, M., Sudo, K., Takemura, T., and Tilmes, S.: Global and regional radiative forcing from 20 % reductions in BC, OC and SO_4 – an HTAP2 multi-model study, Atmos. Chem. Phys., 16, 13579–13599, https://doi.org/10.5194/acp-16-13579-2016, 2016.

[143]Sun W, Shao M, Granier C, et al. Long-term trends of Anthropogenic SO2, NOx, CO, and NMVOCs emissions in China[J]. Earth's Future, 2018, 6(8): 1112-1133.

[144]Szopa, S., V. Naik, B. Adhikary, P. Artaxo, T. Berntsen, W.D. Collins, S. Fuzzi, L. Gallardo, A. Kiendler-Scharr, Z. Klimont, H. Liao, N. Unger, and P. Zanis, 2021: Short-Lived Climate Forcers. In Climate Change 2021: The Physical Science Basis. Contribution of Working Group I to the Sixth Assessment Report of the Intergovernmental Panel on Climate Change [Masson-Delmotte, V., P. Zhai, A. Pirani, S.L. Connors, C. Péan, S. Berger, N. Caud, Y. Chen, L. Goldfarb, M.I. Gomis, M. Huang, K. Leitzell, E. Lonnoy, J.B.R. Matthews, T.K. Maycock, T. Waterfield, O. Yelekçi, R. Yu, and B. Zhou (eds.)]. Cambridge University Press, Cambridge, United Kingdom and New York, NY, USA, pp. 817–922, doi:10.1017/9781009157896.008.

[145]Taban Q, Mumtaz PT, Masoodi KZ, Haq E, Ahmad SM. 2022. Scavenger receptors in host defense: From functional aspects to mode of action. Cell Commun Signal 20:2.

[146]Tiedtke, M.: A comprehensive mass flux scheme for cumulus parameterisation on large scale models, Mon. Weather Rev., 17, 1779–1800, doi:10.1175/1520-0493(1989)117<1779:ACMFSF>2.0.CO;2, 1989.

[147]Tong, D. et al. Health co-benefits of climate change mitigation depend on strategic power plant retirements and pollution controls. Nature Climate Change 11, 1077-1083, doi:10.1038/s41558-021-01216-1 (2021).

[148]Turner MD, Nedjai B, Hurst T, Pennington DJ. 2014. Cytokines and chemokines: At the crossroads of cell signalling and inflammatory disease. Biochim Biophys Acta-Mol Cell Res 1843:2563-2582.

[149]Turpin B. J. & Lim H.-J. Species Contributions to PM2.5 Mass Concentrations: Revisiting Common Assumptions for Estimating Organic Mass, *Aerosol Science and Technology*. 35(1), 602-610, 10.1080/02786820119445, 2001.

[150]UNEP (2011). United Nations Environment Programme (2011). Integrated assessment of black carbon and tropospheric ozone: summary for decision makers. https://wedocs.unep.org/20.500.11822/8028.

[151]Vogel A., Alessa G., Scheele R., Weber L., Dubovik O., North P. & Fiedler S.: Uncertainty in Aerosol Optical Depth From Modern Aerosol-Climate Models, Reanalyses, and Satellite Products, Journal of Geophysical Research: Atmospheres. 127(2), e2021JD035483, https://doi.org/10.1029/2021JD035483, 2022.

[152]Vogel CFA, Van Winkle LS, Esser C, Haarmann-Stemmann T. 2020. The aryl hydrocarbon receptor as a target of environmental stressors - implications for pollution mediated stress and inflammatory responses. Redox Biol 34:101530.

[153]Wang R, Andrews E, Balkanski Y, Boucher O, Myhre G, Samset BH, Schulz M, Schuster GL, Valari M, Tao S. Spatial Representativeness Error in the Ground-Level Observation Networks for Black Carbon Radiation Absorption. Geophys Res Lett. 2018 Feb 28;45(4):2106-2114. doi: 10.1002/2017GL076817. PMID: 29937603; PMCID: PMC5993241.

[154]Wang Xuying and Zheng Yixuan. 2022. Review of Policies of China for the Control of Black and Organic Carbon. http://chinorbc.net/wp-content/uploads/2022/08/Output-5-Review-of-Policies-of-China-for-the-Control-of-Black-and-Organic-Carbon-FINAL.pdf

[155]Wang, Baoqing, Yinuo Li, Zhenzhen Tang, and Ningning Cai. 2021. The carbon components in indoor and outdoor PM2. 5 in winter of Tianjin. Scientific reports 11.1 (2021): 1-10.

[156]Wei, Y., Zhang, J., Li, Z., Gow, A., Chung, K.F., Hu, M., Sun, Z., Zeng, L., Zhu, T., Jia, G., et al. (2016). Chronic exposure to air pollution particles increases the risk of obesity and metabolic syndrome: findings from a natural experiment in Beijing. The FASEB Journal 30, 2115-2122.

[157]Weng CM, Wang CH, Lee MJ, He JR, Huang HY, Chao MW, et al. 2018. Aryl hydrocarbon receptor activation by diesel exhaust particles mediates epithelium-derived cytokines expression in severe allergic asthma. Allergy 73:2192-2204.

[158]Witek, M. L., Diner, D. J., and Garay, M. J. (2016), Satellite assessment of sea spray aerosol productivity: Southern Ocean case study, *J. Geophys. Res. Atmos.*, 121, 872– 894, doi:10.1002/2015JD023726.

[159]Wolf K, Hoffmann B, Andersen ZJ, Atkinson RW, Bauwelinck M, Bellander T, et al. 2021. Long-term exposure to low-level ambient air pollution and incidence of stroke and coronary heart disease: A pooled analysis of six european cohorts within the elapse project. The Lancet Planetary Health 5:e620-e632.

[160]Wolf, K., Hoffmann, B., Andersen, Z.J., Atkinson, R.W., Bauwelinck, M., Bellander, T., Brandt, J., Brunekreef, B., Cesaroni, G., Chen, J., et al. (2021). Long-term exposure to low-level ambient air pollution and incidence of stroke and coronary heart disease: a pooled analysis of six European cohorts within the ELAPSE project. Lancet Planet Health 5, e620-e632.

[161]Wu, S., Zhang, S., Wu, X., and Zhou, X. (2020). m(6)A RNA Methylation in Cardiovascular Diseases. Mol Ther 28, 2111-2119.

[162]Xing, J. et al. The quest for improved air quality may push China to continue its CO2 reduction beyond the Paris Commitment. Proc Natl Acad Sci U S A 117, 29535-29542, doi:10.1073/pnas.2013297117 (2020).

[163]Xing, Y.F., Xu, Y.H., Shi, M.H., and Lian, Y.X. (2016). The impact of PM2.5 on the human respiratory system. J Thorac Dis 8, E69-74.

[164]Xu, L., Zhou, L., Yan, C., and Li, L. (2022). Emerging role of N6-methyladenosine RNA methylation in lung diseases. Exp Biol Med (Maywood) 247, 1862-1872.

[165]Yang Y, Ruan Z, Wang X, Yang Y, Mason TG, Lin H, et al. 2019. Short-term and long-term exposures to fine particulate matter constituents and health: A systematic review and meta-analysis. Environ Pollut 247:874-882.

[166]Yang, Y., Ruan, Z., Wang, X., Yang, Y., Mason, T.G., Lin, H., and Tian, L. (2019). Short-term and long-term exposures to fine particulate matter constituents and health: A systematic review and meta-analysis. Environ Pollut 247, 874-882.

[167]Yerramilli A, Venkata B R D, Sudha Y. Air pollution, modeling and GIS based decision support systems for air quality risk assessment[J]. Advance air pollution, 2011: 295-324.

[168]Yu, J., Chen, M., Huang, H., Zhu, J., Song, H., Zhu, J., Park, J., and Ji, S.J. (2018). Dynamic m6A modification regulates local translation of mRNA in axons. Nucleic Acids Res 46, 1412-1423.

[169]Zaidi S M, Gisen J I A. Evaluation of Weather Research and Forecasting (WRF) Microphysics single moment class-3 and class-6 in Precipitation Forecast[C]//MATEC Web of Conferences. EDP Sciences, 2018, 150: 03007.

[170]Zender C. S., Bian H. & Newman D. Mineral Dust Entrainment and Deposition (DEAD) model: Description and 1990s dust climatology, *Journal of Geophysical Research: Atmospheres.* 108(D14), doi:10.1029/2002JD002775, 2003.

[171]Zeng Y, Cao Y, Qiao X, et al. Air pollution reduction in China: Recent success but great challenge for the future[J]. Science of the Total Environment, 2019, 663: 329-337.

[172]Zhang R, Jing J, Tao J, Hsu SC, Wang G, Cao J, et al. 2013. Chemical characterization and source apportionment of pm<2.5 in Beijing: Seasonal perspective. Atmospheric Chemistry and Physics 13:7053-7074.

[173]Zhang Y, Zhi G, Guo S, et al. Algorithm developed for dynamic quantification of coal consumption for and emission from rural winter heating [J]. Science of The Total Environment, 2020, 737(2020): 139762.

[174]Zhang, F., Wang, Y., Peng, J., Chen, L., Sun, Y., Duan, L., Ge, X., Li, Y., Zhao, J., Liu, C., Zhang, X., Zhang, G., Pan, Y., Wang, Y., Zhang, A. L., Ji, Y., Wang, G., Hu, M., Molina, M. J., & Zhang, R. 2020. An unexpected catalyst dominates formation and radiative forcing of regional haze. Proceedings of the National Academy of Sciences of the United States of America, 117(8), 3960–3966. https://doi.org/10.1073/pnas.1919343117

[175]Zhang, Q. et al. Drivers of improved PM2.5 air quality in China from 2013 to 2017. Proc Natl Acad Sci U S A 116, 24463-24469, doi:10.1073/pnas.1907956116 (2019).

[176]Zhang, R., Jing, J., Tao, J., Hsu, S.C., Wang, G., Cao, J., Lee, C.S.L., Zhu, L., Chen, Z., Zhao, Y., et al. (2013). Chemical characterization and source apportionment of PM_{2.5} in Beijing: seasonal perspective. Atmospheric Chemistry and Physics 13, 7053-7074.

[177]Zhao, J., Li, M., Wang, Z., Chen, J., Zhao, J., Xu, Y., Wei, X., Wang, J., and Xie, J. (2019). Role of PM2.5 in the development and progression of COPD and its mechanisms. Respiratory Research 20.

[178]Zhi G, Chen Y, Sun J, et al. Harmonizing Aerosol Carbon Measurements between Two Conventional Thermal/Optical Analysis Methods [J]. Environmental Science & Technology, 2011, 45(45): 2902-8.

[179]Zhou, Y., Ma, J., Wang, B., Liu, Y., Xiao, L., Ye, Z., Fan, L., Wang, D., Mu, G., and Chen, W. (2020). Long-term effect of personal PM(2.5) exposure on lung function: A panel study in China. J Hazard Mater 393, 122457.

[180]Ahmed, S. M., L. Luo, A. Namani, X. J. Wang and X. Tang (2017). "Nrf2 signaling pathway: Pivotal roles in inflammation." Biochim Biophys Acta Mol Basis Dis 1863(2): 585-597.

[181]Arango Duque, G. and A. Descoteaux (2014). "Macrophage cytokines: involvement in immunity and infectious diseases." Front Immunol 5: 491.

[182]Grytting, V. S., M. Refsnes, J. Øvrevik, M. S. Halle, J. Schönenberger, R. van der Lelij, B. Snilsberg, T. Skuland, R. Blom and M. Låg (2021). "Respirable stone particles differ in their ability to induce cytotoxicity and pro-inflammatory responses in cell models of the human airways." Particle and Fibre Toxicology 18(1): 18.

[183]Harjunpaa, H., M. Llort Asens, C. Guenther and S. C. Fagerholm (2019). "Cell Adhesion Molecules and Their Roles and Regulation in the Immune and Tumor Microenvironment." Front Immunol 10: 1078.

[184]Holme, J. A., M. Låg, T. Skuland, M. Parenicová, M. Ciganek, K. Pencíková, V. S. Grytting, J. Neca, J. Øvrevik and E. Mariussen (2023). "Characterization of elements, PAHs, AhR-activity and pro-inflammatory responses of road tunnel-derived particulate matter in human hepatocyte-like and bronchial epithelial cells." Toxicology in Vitro 90: 105611.

[185]Kocbach, A., A. Totlandsdal, M. Låg, M. Refsnes and P. Schwarze (2008). "Differential binding of cytokines to environmentally relevant particles: a possible source for misinterpretation of in vitro results?" Toxicology letters 176(2): 131-137.

[186]Ley, K., C. Laudanna, M. I. Cybulsky and S. Nourshargh (2007). "Getting to the site of inflammation: the leukocyte adhesion cascade updated." Nat Rev Immunol 7(9): 678-689.

[187]Ricciotti, E. and G. A. FitzGerald (2011). "Prostaglandins and inflammation." Arterioscler Thromb Vasc Biol 31(5): 986-1000.

Appendices

A1. Chemical transport model configuration

The configuration of CMAQ model is shown in **Table A1**. In the vertical direction, the top air pressure of the model is the same as that of WRF model, which is 50hPa, but the vertical stratification is divided into 20 layers with unequal distance. Sigma height layer is set to 1.0000, 0.9975, 0.9950, 0.9900, 0.9800, 0.9700, 0.9600, 0.9400, 0.9200, 0.9000, 0.8750, 0.8500, 0.8200, 0.7550, 0.6850, 0.5800, 0.5100, 0.4400, 0.3200, 0.2000,0.0000, the height from the ground to the top of the first layer (about 20m) was mainly considered in the study. The number of horizontal 36km resolution grids was set as 200 rows×160 columns. The number of horizontal 12km resolution grids was set as 234 rows × 418 columns (**Fig. A3 a**). **Figure A3** b shows the geographical coverage by province. The selection of chemical mechanism is one of the important parameters for CMAQ simulation. In this paper, SAPRC99 gas phase chemical mechanism, Aero5 aerosol mechanism and Cloud_acm_ae5 cloud chemical mechanism are selected to simulate the concentration field, and the list file of corresponding chemical mechanism is used to provide emission source information for CMAQ simulation.

Table A1 CAMQ model parameter configuration

CMAQ mode input option	36km parameter Settings	12km parameter setting
Simulation grid	Lambert projection coordinates (25 °N~46 °N, 110 °E), 200×160	Lambert projection coordinates (25 °N~46 °N, 110 °E), 120×102
Vertical layer	20	
The boundary conditions	The preset value	Provided by 36 kilometers
Gas phase chemistry	SAPRC99	
Chemical mechanism of aerosol	Aero5	
Cloud chemical mechanism	Cloud_acm_ae5	
Horizontal advection scheme	Yamo	
Vertical diffusion scheme	ACM2	

In this study, two concentration field simulations with different nesting scales were carried out, and the corresponding flow diagrams are shown in **Figure A1** and **Figure A2**. For the simulation of 36km resolution grid area, the default file is used to provide boundary field conditions and initial field conditions of the first day, and the subsequent initial field conditions are provided by CONC-36km concentration file of the previous day. Aiming at the simulation of 12km resolution grid area, the daily boundary field of fine grid is cut out from the daily concentration simulation results of master grid, and boundary field conditions are provided to reduce the influence of boundary field conditions on simulation results. The first day's initial field file is provided by CONC-36km on the same day, and then the first day's initial field file is provided by CONC-12km file on the previous day. The simulation is advanced by 10 days to reduce the influence of initial field conditions on the simulation results. The impact of dust emission inventory is not considered in the simulation because the MEIC inventory does not include dust emission.

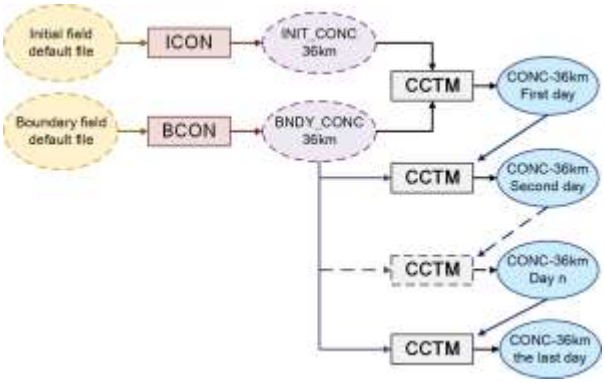

Figure A1 Simulation diagram of initial field and boundary field of master grid of CMAQ model

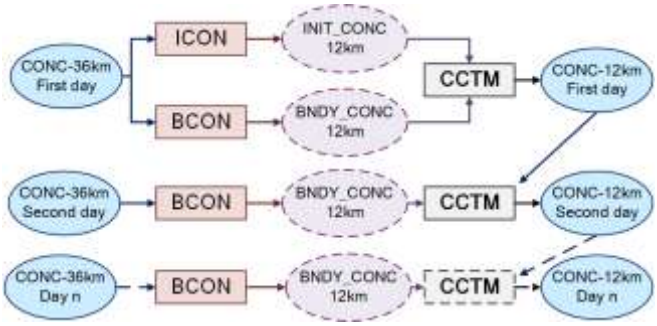

Figure A2 Simulation diagram of initial field and boundary field of nested grid of CMAQ model

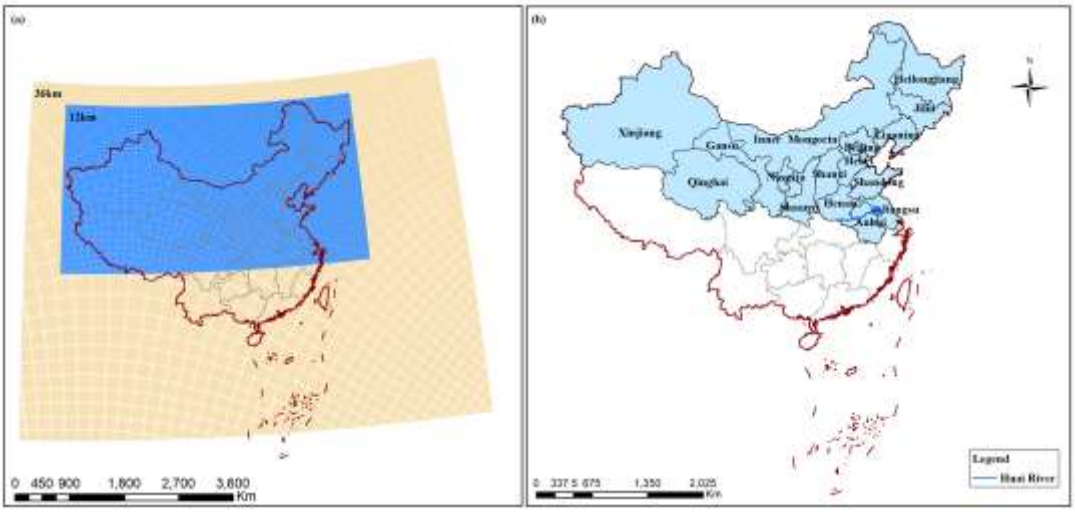

Figure A3 (a) CMAQ simulation master and nested grid area setting and (b) Provincial city distribution in Northern China

A2. Meteorological model configuration

The configuration information of the meteorological parameters of the WRF model is shown in **Table A2**. In the vertical direction, the pressure height of the top layer of the model was set as 50hPa, and vertical stratification is divided into 35 layers with unequal distance. In the horizontal direction, the resolution of the master grid is 36km×36km; the resolution of the nested grid is 12km×12km. The external initial data used were United States Geological Survey (USGS) 30S global topographic data and Moderate-Resolution Imaging Spectroradiometer (MODIS) subsurface data. In WRF model, two kinds of reanalysis data are used to provide meteorological initial field and boundary conditions, which are Final Reanalysis Data (FNL) global analysis data (horizontal resolution 1 °×1 °, 6-hour interval) published by National Centers for Environmental Prediction (NCEP) of the United States and ERA5 reanalysis data (horizontal resolution 1 °×1 °, 6-hour interval) published by Medium-Range Weather Forecasts (ECMWF) of European Meteorological Center.

For the selection of internal parameterization schemes, Kain-Fritsch (New Eta) cumulus cloud parameterization scheme, WSM3 simple ice microphysics parameterization scheme, Noah land surface process scheme and RRTM (Rapid Transfer Model) long wave scheme and Dudhia short wave scheme, Meanwhile, two boundary layer schemes, Yonsei University Scheme(YSU) scheme and Asymmetric Convective Model scheme (ACM2)scheme, are also selected. Under the condition that other Settings remain unchanged, two kinds of reanalysis data and two kinds of boundary layer schemes are combined to form four kinds of WRF meteorological parameterization schemes. Finally, the optimal scheme is selected by comparing the meteorological simulation results with the real meteorological observation data to provide the meteorological field.

Table A2 Configuration of Meteorological Parameters of WRF Model

WRF input options	36km parameter Settings	12km parameter setting

Vertical coordinates	Terrain following coordinate system	
Nested grid scheme	A heavy one-way	
Projection coordinate type	Lambert projection coordinates	
Horizontal resolution	the number of grids is 210×200	the number of grids is 130×112
Vertical hierarchy	The model top pressure is 50hPa, and the vertical resolution is higher near the stratum	
Land use type	USGS 30	
Large-scale meteorological background field and boundary conditions	1°×1°NCEP data FNL(6 h interval)/1°×1°ECMWF data ERA5(6 h interval)	
Microphysical parameterization scheme	WSM3 Simple ice solution	
Boundary layer parameterization scheme	YSU	
Atmospheric radiation scheme	RRTM long wave and Cloud (Dudhia) short-wave radiation schemes	

The regional air quality model system composed of WRF, Model of Emissions of Gases and Aerosols from Nature (MEGAN), SMOKE and CMAQ was used to establish a numerical simulation system for simulated areas, which was composed of a terrestrial ecosystem gas estimation model MEGAN, an emission source treatment model SMOKE, and the latest generation of mesoscale forecasting models WRF and CMAQ models.

A3. Simulation results under future emission scenarios

Table A3 Absolute difference in annual, regional mean surface concentrations [μg/m^3] of aerosols in 2035 compared to 2018 under each of the three emission scenarios developed in the project

	CHN			BTH		
	BAU	**EOP**	**ABC**	**BAU**	**EOP**	**ABC**
BC	-0.30	-0.70	-0.72	-0.49	-1.18	-1.32
OC	-0.57	-1.29	-1.34	-1.00	-2.17	-2.40
$PM_{2.5}$	-3.99	-8.30	-9.54	-6.28	-14.63	-17.55
NO_2	-3.48	-4.33	-5.26	-4.97	-7.25	-8.76
SO_2	-0.99	-1.72	-1.80	-0.95	-2.25	-2.89
O_3	-1.35	-1.66	-0.03	1.87	2.20	-0.01

B1. Tabulated values of AGTP(t)

Absolute global temperature change potential (AGTP) [K/kg] for the first 100 years

Year	CO_2	CH_4	N_2O	BC_{China}	OC_{China}	$SO_{2\ China}$	$NH_{3\ China}$	NOx_{China}	CO_{China}	VOC_{China}
0	0	0	0	0	0	0	0	0	0	0
1	1.82E-16	2.78E-14	4.21E-14	1.89E-12	-5.23E-13	-4.34E-13	-2.00E-13	1.06E-13	7.39E-16	4.02E-15
2	3.14E-16	4.75E-14	7.50E-14	1.49E-12	-4.12E-13	-3.42E-13	-1.58E-13	8.29E-14	1.59E-15	5.70E-15
3	4.09E-16	6.11E-14	1.01E-13	1.18E-12	-3.26E-13	-2.71E-13	-1.25E-13	2.75E-14	2.12E-15	5.92E-15
4	4.78E-16	7.01E-14	1.21E-13	9.36E-13	-2.59E-13	-2.15E-13	-9.91E-14	-1.42E-14	2.47E-15	5.98E-15
5	5.26E-16	7.56E-14	1.36E-13	7.45E-13	-2.06E-13	-1.71E-13	-7.90E-14	-4.47E-14	2.69E-15	5.92E-15
6	5.59E-16	7.84E-14	1.48E-13	5.96E-13	-1.65E-13	-1.37E-13	-6.32E-14	-6.65E-14	2.81E-15	5.80E-15
7	5.82E-16	7.94E-14	1.58E-13	4.79E-13	-1.33E-13	-1.10E-13	-5.07E-14	-8.16E-14	2.85E-15	5.62E-15
8	5.97E-16	7.88E-14	1.65E-13	3.87E-13	-1.07E-13	-8.89E-14	-4.10E-14	-9.17E-14	2.84E-15	5.40E-15
9	6.06E-16	7.73E-14	1.70E-13	3.14E-13	-8.69E-14	-7.22E-14	-3.32E-14	-9.79E-14	2.79E-15	5.16E-15

10	6.11E-16	7.50E-14	1.75E-13	2.56E-13	-7.10E-14	-5.90E-14	-2.72E-14	-1.01E-13	2.71E-15	4.91E-15
11	6.13E-16	7.22E-14	1.78E-13	2.11E-13	-5.85E-14	-4.86E-14	-2.24E-14	-1.02E-13	2.61E-15	4.65E-15
12	6.13E-16	6.91E-14	1.80E-13	1.75E-13	-4.86E-14	-4.03E-14	-1.86E-14	-1.02E-13	2.50E-15	4.40E-15
13	6.12E-16	6.59E-14	1.82E-13	1.47E-13	-4.07E-14	-3.38E-14	-1.56E-14	-1.00E-13	2.39E-15	4.15E-15
14	6.10E-16	6.25E-14	1.83E-13	1.25E-13	-3.45E-14	-2.87E-14	-1.32E-14	-9.74E-14	2.27E-15	3.90E-15
15	6.07E-16	5.92E-14	1.84E-13	1.07E-13	-2.96E-14	-2.46E-14	-1.13E-14	-9.43E-14	2.15E-15	3.67E-15
16	6.04E-16	5.59E-14	1.84E-13	9.26E-14	-2.57E-14	-2.13E-14	-9.81E-15	-9.07E-14	2.03E-15	3.45E-15
17	6.01E-16	5.27E-14	1.84E-13	8.13E-14	-2.25E-14	-1.87E-14	-8.62E-15	-8.70E-14	1.91E-15	3.23E-15
18	5.97E-16	4.96E-14	1.84E-13	7.23E-14	-2.00E-14	-1.66E-14	-7.67E-15	-8.31E-14	1.80E-15	3.03E-15
19	5.94E-16	4.67E-14	1.84E-13	6.51E-14	-1.80E-14	-1.50E-14	-6.90E-15	-7.92E-14	1.69E-15	2.84E-15
20	5.91E-16	4.39E-14	1.84E-13	5.93E-14	-1.64E-14	-1.36E-14	-6.29E-15	-7.53E-14	1.59E-15	2.67E-15
21	5.87E-16	4.12E-14	1.84E-13	5.47E-14	-1.51E-14	-1.26E-14	-5.79E-15	-7.15E-14	1.49E-15	2.50E-15
22	5.84E-16	3.87E-14	1.83E-13	5.09E-14	-1.41E-14	-1.17E-14	-5.39E-15	-6.78E-14	1.40E-15	2.34E-15
23	5.81E-16	3.64E-14	1.83E-13	4.78E-14	-1.32E-14	-1.10E-14	-5.06E-15	-6.42E-14	1.31E-15	2.20E-15
24	5.78E-16	3.42E-14	1.82E-13	4.52E-14	-1.25E-14	-1.04E-14	-4.79E-15	-6.08E-14	1.23E-15	2.06E-15
25	5.75E-16	3.21E-14	1.81E-13	4.31E-14	-1.20E-14	-9.92E-15	-4.57E-15	-5.75E-14	1.16E-15	1.94E-15
26	5.72E-16	3.02E-14	1.81E-13	4.14E-14	-1.15E-14	-9.52E-15	-4.39E-15	-5.44E-14	1.09E-15	1.82E-15
27	5.69E-16	2.84E-14	1.80E-13	3.99E-14	-1.11E-14	-9.18E-15	-4.23E-15	-5.14E-14	1.02E-15	1.71E-15
28	5.67E-16	2.67E-14	1.79E-13	3.87E-14	-1.07E-14	-8.90E-15	-4.10E-15	-4.86E-14	9.61E-16	1.61E-15
29	5.64E-16	2.51E-14	1.79E-13	3.76E-14	-1.04E-14	-8.65E-15	-3.98E-15	-4.60E-14	9.04E-16	1.52E-15
30	5.62E-16	2.36E-14	1.78E-13	3.67E-14	-1.02E-14	-8.44E-15	-3.89E-15	-4.35E-14	8.51E-16	1.43E-15
31	5.60E-16	2.23E-14	1.77E-13	3.59E-14	-9.93E-15	-8.25E-15	-3.80E-15	-4.12E-14	8.02E-16	1.35E-15
32	5.57E-16	2.10E-14	1.76E-13	3.51E-14	-9.73E-15	-8.08E-15	-3.72E-15	-3.90E-14	7.56E-16	1.27E-15
33	5.55E-16	1.99E-14	1.76E-13	3.45E-14	-9.55E-15	-7.94E-15	-3.66E-15	-3.69E-14	7.14E-16	1.20E-15
34	5.53E-16	1.88E-14	1.75E-13	3.39E-14	-9.39E-15	-7.80E-15	-3.59E-15	-3.49E-14	6.74E-16	1.14E-15
35	5.51E-16	1.78E-14	1.74E-13	3.34E-14	-9.24E-15	-7.68E-15	-3.54E-15	-3.31E-14	6.38E-16	1.08E-15
36	5.49E-16	1.68E-14	1.73E-13	3.29E-14	-9.11E-15	-7.56E-15	-3.48E-15	-3.14E-14	6.03E-16	1.02E-15
37	5.47E-16	1.59E-14	1.73E-13	3.24E-14	-8.98E-15	-7.46E-15	-3.44E-15	-2.98E-14	5.72E-16	9.71E-16
38	5.45E-16	1.51E-14	1.72E-13	3.20E-14	-8.86E-15	-7.36E-15	-3.39E-15	-2.83E-14	5.42E-16	9.23E-16
39	5.43E-16	1.44E-14	1.71E-13	3.16E-14	-8.75E-15	-7.27E-15	-3.35E-15	-2.69E-14	5.15E-16	8.79E-16
40	5.42E-16	1.37E-14	1.70E-13	3.12E-14	-8.65E-15	-7.18E-15	-3.31E-15	-2.56E-14	4.90E-16	8.38E-16
41	5.40E-16	1.30E-14	1.69E-13	3.09E-14	-8.55E-15	-7.10E-15	-3.27E-15	-2.43E-14	4.66E-16	7.99E-16
42	5.38E-16	1.24E-14	1.69E-13	3.05E-14	-8.45E-15	-7.02E-15	-3.23E-15	-2.31E-14	4.44E-16	7.64E-16
43	5.37E-16	1.18E-14	1.68E-13	3.02E-14	-8.36E-15	-6.94E-15	-3.20E-15	-2.21E-14	4.24E-16	7.30E-16
44	5.35E-16	1.13E-14	1.67E-13	2.99E-14	-8.27E-15	-6.87E-15	-3.17E-15	-2.10E-14	4.05E-16	7.00E-16
45	5.34E-16	1.08E-14	1.66E-13	2.96E-14	-8.19E-15	-6.80E-15	-3.13E-15	-2.01E-14	3.88E-16	6.71E-16
46	5.32E-16	1.04E-14	1.66E-13	2.93E-14	-8.11E-15	-6.73E-15	-3.10E-15	-1.92E-14	3.71E-16	6.44E-16
47	5.31E-16	9.96E-15	1.65E-13	2.90E-14	-8.03E-15	-6.67E-15	-3.07E-15	-1.83E-14	3.56E-16	6.20E-16
48	5.29E-16	9.57E-15	1.64E-13	2.87E-14	-7.96E-15	-6.61E-15	-3.04E-15	-1.75E-14	3.42E-16	5.97E-16
49	5.28E-16	9.20E-15	1.63E-13	2.85E-14	-7.88E-15	-6.55E-15	-3.02E-15	-1.68E-14	3.29E-16	5.75E-16
50	5.27E-16	8.86E-15	1.62E-13	2.82E-14	-7.81E-15	-6.49E-15	-2.99E-15	-1.61E-14	3.16E-16	5.55E-16
51	5.25E-16	8.54E-15	1.62E-13	2.80E-14	-7.74E-15	-6.43E-15	-2.96E-15	-1.54E-14	3.05E-16	5.36E-16
52	5.24E-16	8.24E-15	1.61E-13	2.77E-14	-7.68E-15	-6.38E-15	-2.94E-15	-1.48E-14	2.94E-16	5.19E-16
53	5.23E-16	7.97E-15	1.60E-13	2.75E-14	-7.61E-15	-6.32E-15	-2.91E-15	-1.42E-14	2.84E-16	5.03E-16
54	5.22E-16	7.71E-15	1.59E-13	2.73E-14	-7.55E-15	-6.27E-15	-2.89E-15	-1.37E-14	2.75E-16	4.88E-16
55	5.20E-16	7.47E-15	1.59E-13	2.70E-14	-7.49E-15	-6.22E-15	-2.86E-15	-1.32E-14	2.67E-16	4.74E-16
56	5.19E-16	7.24E-15	1.58E-13	2.68E-14	-7.43E-15	-6.17E-15	-2.84E-15	-1.27E-14	2.58E-16	4.60E-16
57	5.18E-16	7.03E-15	1.57E-13	2.66E-14	-7.37E-15	-6.12E-15	-2.82E-15	-1.23E-14	2.51E-16	4.48E-16
58	5.17E-16	6.83E-15	1.56E-13	2.64E-14	-7.32E-15	-6.08E-15	-2.80E-15	-1.19E-14	2.44E-16	4.36E-16
59	5.16E-16	6.65E-15	1.55E-13	2.62E-14	-7.26E-15	-6.03E-15	-2.78E-15	-1.15E-14	2.37E-16	4.26E-16
60	5.15E-16	6.48E-15	1.55E-13	2.60E-14	-7.21E-15	-5.99E-15	-2.76E-15	-1.11E-14	2.31E-16	4.15E-16
61	5.14E-16	6.32E-15	1.54E-13	2.58E-14	-7.16E-15	-5.94E-15	-2.74E-15	-1.07E-14	2.25E-16	4.06E-16
62	5.13E-16	6.16E-15	1.53E-13	2.56E-14	-7.10E-15	-5.90E-15	-2.72E-15	-1.04E-14	2.20E-16	3.97E-16
63	5.12E-16	6.02E-15	1.52E-13	2.55E-14	-7.06E-15	-5.86E-15	-2.70E-15	-1.01E-14	2.15E-16	3.89E-16
64	5.11E-16	5.89E-15	1.52E-13	2.53E-14	-7.01E-15	-5.82E-15	-2.68E-15	-9.80E-15	2.10E-16	3.81E-16

65	5.10E-16	5.76E-15	1.51E-13	2.51E-14	-6.96E-15	-5.78E-15	-2.66E-15	-9.53E-15	2.06E-16	3.73E-16
66	5.10E-16	5.64E-15	1.50E-13	2.50E-14	-6.91E-15	-5.74E-15	-2.65E-15	-9.27E-15	2.01E-16	3.66E-16
67	5.09E-16	5.53E-15	1.49E-13	2.48E-14	-6.87E-15	-5.70E-15	-2.63E-15	-9.02E-15	1.97E-16	3.60E-16
68	5.08E-16	5.43E-15	1.49E-13	2.46E-14	-6.83E-15	-5.67E-15	-2.61E-15	-8.79E-15	1.94E-16	3.54E-16
69	5.07E-16	5.33E-15	1.48E-13	2.45E-14	-6.78E-15	-5.63E-15	-2.59E-15	-8.57E-15	1.90E-16	3.48E-16
70	5.07E-16	5.24E-15	1.47E-13	2.43E-14	-6.74E-15	-5.60E-15	-2.58E-15	-8.37E-15	1.87E-16	3.42E-16
71	5.06E-16	5.15E-15	1.47E-13	2.42E-14	-6.70E-15	-5.56E-15	-2.56E-15	-8.17E-15	1.84E-16	3.37E-16
72	5.05E-16	5.07E-15	1.46E-13	2.40E-14	-6.66E-15	-5.53E-15	-2.55E-15	-7.99E-15	1.81E-16	3.32E-16
73	5.04E-16	4.99E-15	1.45E-13	2.39E-14	-6.62E-15	-5.50E-15	-2.53E-15	-7.82E-15	1.78E-16	3.28E-16
74	5.04E-16	4.92E-15	1.44E-13	2.38E-14	-6.58E-15	-5.47E-15	-2.52E-15	-7.65E-15	1.75E-16	3.23E-16
75	5.03E-16	4.85E-15	1.44E-13	2.36E-14	-6.54E-15	-5.43E-15	-2.50E-15	-7.50E-15	1.73E-16	3.19E-16
76	5.02E-16	4.78E-15	1.43E-13	2.35E-14	-6.51E-15	-5.40E-15	-2.49E-15	-7.35E-15	1.71E-16	3.15E-16
77	5.02E-16	4.72E-15	1.42E-13	2.34E-14	-6.47E-15	-5.37E-15	-2.48E-15	-7.21E-15	1.68E-16	3.11E-16
78	5.01E-16	4.66E-15	1.41E-13	2.32E-14	-6.44E-15	-5.34E-15	-2.46E-15	-7.08E-15	1.66E-16	3.08E-16
79	5.01E-16	4.60E-15	1.41E-13	2.31E-14	-6.40E-15	-5.32E-15	-2.45E-15	-6.96E-15	1.64E-16	3.04E-16
80	5.00E-16	4.55E-15	1.40E-13	2.30E-14	-6.37E-15	-5.29E-15	-2.44E-15	-6.84E-15	1.62E-16	3.01E-16
81	5.00E-16	4.49E-15	1.39E-13	2.29E-14	-6.33E-15	-5.26E-15	-2.42E-15	-6.73E-15	1.60E-16	2.98E-16
82	4.99E-16	4.44E-15	1.39E-13	2.27E-14	-6.30E-15	-5.23E-15	-2.41E-15	-6.62E-15	1.59E-16	2.95E-16
83	4.99E-16	4.40E-15	1.38E-13	2.26E-14	-6.27E-15	-5.21E-15	-2.40E-15	-6.52E-15	1.57E-16	2.92E-16
84	4.98E-16	4.35E-15	1.37E-13	2.25E-14	-6.24E-15	-5.18E-15	-2.39E-15	-6.42E-15	1.55E-16	2.89E-16
85	4.98E-16	4.31E-15	1.37E-13	2.24E-14	-6.20E-15	-5.15E-15	-2.37E-15	-6.33E-15	1.54E-16	2.87E-16
86	4.97E-16	4.27E-15	1.36E-13	2.23E-14	-6.17E-15	-5.13E-15	-2.36E-15	-6.24E-15	1.52E-16	2.84E-16
87	4.97E-16	4.23E-15	1.35E-13	2.22E-14	-6.14E-15	-5.10E-15	-2.35E-15	-6.16E-15	1.51E-16	2.82E-16
88	4.96E-16	4.19E-15	1.35E-13	2.21E-14	-6.11E-15	-5.08E-15	-2.34E-15	-6.08E-15	1.50E-16	2.79E-16
89	4.96E-16	4.16E-15	1.34E-13	2.20E-14	-6.08E-15	-5.05E-15	-2.33E-15	-6.00E-15	1.48E-16	2.77E-16
90	4.96E-16	4.12E-15	1.33E-13	2.19E-14	-6.06E-15	-5.03E-15	-2.32E-15	-5.93E-15	1.47E-16	2.75E-16
91	4.95E-16	4.09E-15	1.33E-13	2.18E-14	-6.03E-15	-5.01E-15	-2.31E-15	-5.86E-15	1.46E-16	2.73E-16
92	4.95E-16	4.06E-15	1.32E-13	2.17E-14	-6.00E-15	-4.98E-15	-2.29E-15	-5.80E-15	1.45E-16	2.71E-16
93	4.94E-16	4.03E-15	1.31E-13	2.16E-14	-5.97E-15	-4.96E-15	-2.28E-15	-5.73E-15	1.44E-16	2.69E-16
94	4.94E-16	4.00E-15	1.31E-13	2.15E-14	-5.94E-15	-4.94E-15	-2.27E-15	-5.67E-15	1.43E-16	2.67E-16
95	4.94E-16	3.97E-15	1.30E-13	2.14E-14	-5.92E-15	-4.91E-15	-2.26E-15	-5.62E-15	1.42E-16	2.65E-16
96	4.94E-16	3.94E-15	1.29E-13	2.13E-14	-5.89E-15	-4.89E-15	-2.25E-15	-5.56E-15	1.41E-16	2.64E-16
97	4.93E-16	3.91E-15	1.29E-13	2.12E-14	-5.86E-15	-4.87E-15	-2.24E-15	-5.51E-15	1.40E-16	2.62E-16
98	4.93E-16	3.89E-15	1.28E-13	2.11E-14	-5.84E-15	-4.85E-15	-2.23E-15	-5.46E-15	1.39E-16	2.60E-16
99	4.93E-16	3.86E-15	1.27E-13	2.10E-14	-5.81E-15	-4.83E-15	-2.22E-15	-5.41E-15	1.38E-16	2.59E-16
100	4.92E-16	3.84E-15	1.27E-13	2.09E-14	-5.79E-15	-4.81E-15	-2.21E-15	-5.36E-15	1.37E-16	2.57E-16

C1. Characterization of the traffic-$PM_{2.5}$ sample

Supplementary Table 6-1 Content of elements in $PM_{2.5}$ sampled in a road tunnel (ng/mg PM) measured by inductively coupled plasma mass spectrometry (ICP-MS). The results are published in Holme et al. (2023).

Element	ng/mg PM
Be	0.32
Mg	8084
Al	17101
Si	108843
Ca	12932
Ti	1886
V	68.6

Cr	81.5
Mn	397
Fe	26847
Co	17.2
Cu	378
Zn	412
As	2.71
Sr	79.3
Mo	15.59
Cd	0.09
Sn	92.4
Sb	97.8
Cs	1.04
Ba	329
W	83.0
Pb	8.20
U	0.77

SupplementaryTable 6-2 Content of US EPA priority PAH in $PM_{2.5}$ sampled in a road tunnel (ng/mg PM) measured by high-performance liquid chromatography (HPLC). The results are published in Holme et al. (2023).

US EPA PAH	**Coarse PM**	**Fine PM**	**Ultrafine PM**
Fluorene	<0.05	0.23	0.28
Phenanthrene	3.4	7.4	9.1
Anthracene	0.05	0.33	0.37
Fluoranthene	1.3	3.8	4.9
Pyrene	1.7	4.9	7.0
Benz[*a*]anthracene	0.08	0.52	0.29
Chrysene	0.07	0.78	0.45
Benzo[*b*]fluoranthene	0.05	0.09	0.17
Benzo[*k*]fluoranthene	0.09	0.15	0.11
Benzo[*a*]pyrene	0.38	0.62	0.45
Dibenz[*a,h*]anthracene	0.04	0.04	0.03
Benzo[*ghi*]perylene	0.84	0.29	0.18
Indeno[1,2,3-*cd*]pyrene	0.34	0.27	0.19
Sum:	8.3	19.5	23.5

Supplementary Table 6-3 Characterization of in $PM_{2.5}$ sampled in a road tunnel (Holme et al., 2023)

Characteristics	**Coarse PM**	**Fine PM**	**Ultrafine PM**
Hydrodynamic size (by mass) (µm)	3.01	1.56	2.22/0.07
Hydrodynamic size (by number) (µm)	0.05	0.06	0.07
Organic carbon (OC, mg/mg PM)	28 ±10	94 ±37	131 ±29
Elementary carbon (EC, mg/mg PM)	0	0	0
Endotoxin content (EU/mg PM)	0.61 ±0.29	0.25 ±0.13	0.09 ±0.09
ROS (OP^{DDT}(nmol DTT/ng*min))	0.038	0.043	0.013

C2. Optimalization of the cell culture models

Choice of serum concentration in exposure medium:

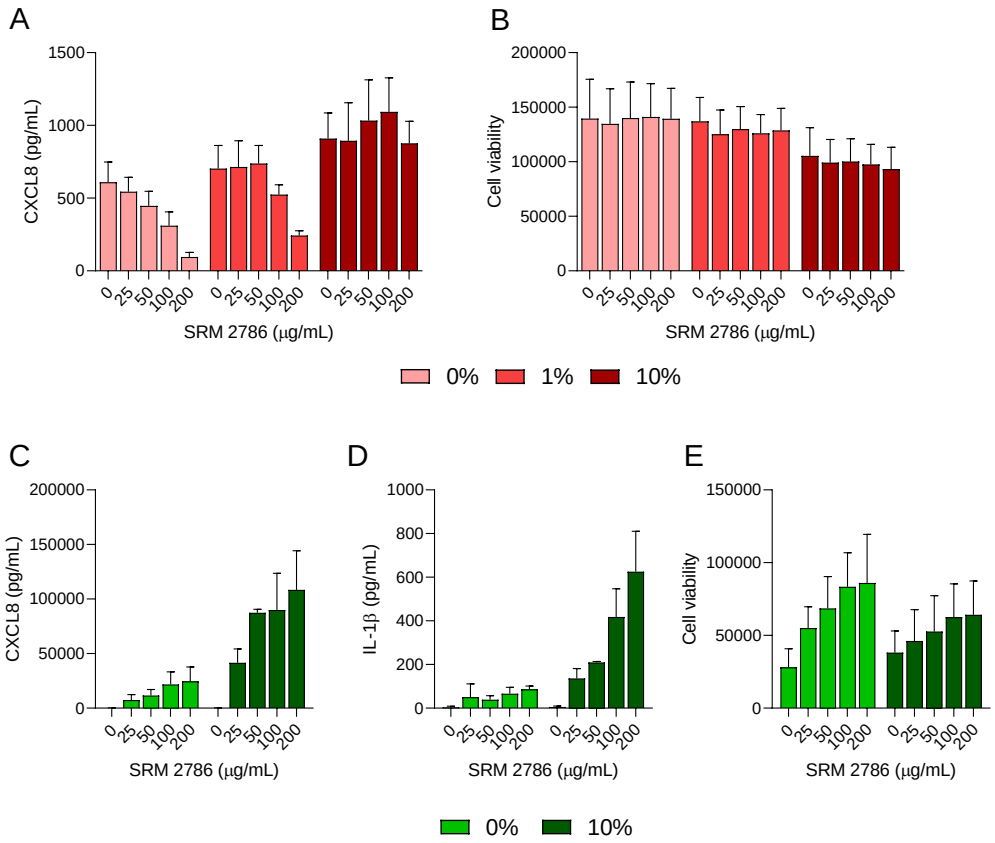

Additional figure 6-1. **Effect of serum supplementation for particle-induced responses.** A549 epithelial cells (A and B) or THP-1-derived macrophages (C-D) were exposed to 0, 25, 50, 100 or 200 µg/mL (2.6, 5.3, 10.5 and 21 µg/cm^2) SRM2786. After 24 h the concentration of CXCL8 (A and C) and IL-1β (D) was measured in the cell culture supernatant using ELISA. Cell viability (B and E) was also determined after 24h using AlamarBlue assay. Results are presented as mean ± SD for n=2-4 independent experiments.

To test the effects of serum supplementation for the particle-induced responses in the A549 and THP-1 cells, the cell culture media was replaced with medium containing different concentrations of serum prior to exposure.
In the A549 cells, an apparent dose-dependent decrease in the secretion of CXCL8 compared with control was observed after exposure to the particles, which was diminished by adding increasing concentrations of serum during exposure (Additional figure 6-1A). The levels of IL-1β were below the limits of detection in this cell model. The decrease in cytokine levels likely stems from non-specific binding of cytokines to the particles, which is known to occur for particles derived from both combustion and non-combustion sources (Kocbach et al. 2008, Grytting et al. 2020). The ability of serum to block this effect has also been documented (Kocbach et al. 2008). The viability of the cells was not substantially affected by exposure to the particles or by the serum concentration. In contrast to the A549 cells, a clear dose-dependent increase in the secretion of CXCL8 (Additional figure 6-1C) and IL-1β (Additional figure 6-1D). The levels of cytokines were higher in the cells exposed to particles in serum supplemented with 10% serum, causing a steep increase in both cytokines already at the lowest concentration. The viability of the THP-1 cells appeared to increase with increasing particles concentration, likely from metabolic activation of the cells, but was not substantially altered by addition of serum.

Based on these results, medium supplemented with 10% serum was used for all experiments in the main body of the text.

Number of THP-1 macrophages added to the cocultures:

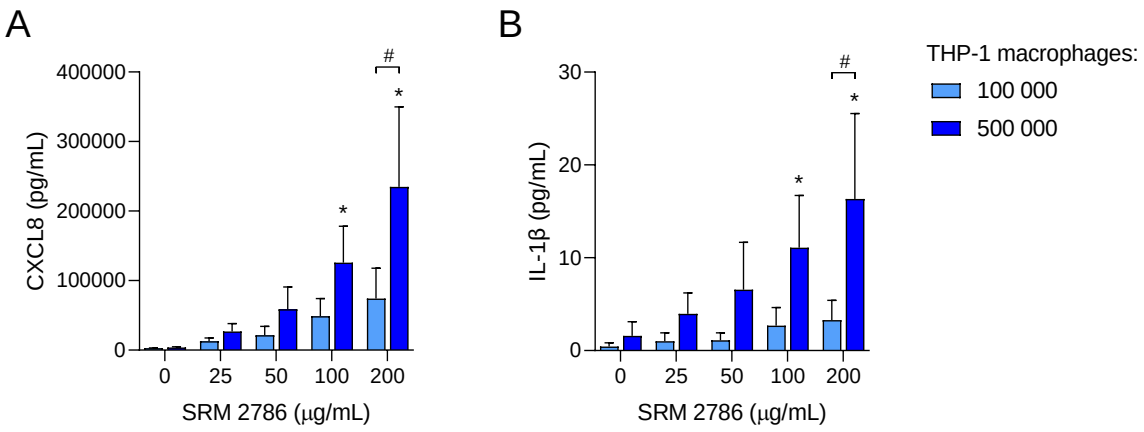

Additional figure 6-1. **Effect of different macrophage concentrations for particle-induced responses in a coculture**. Cocultures A549 epithelial cells and 100 000 (light blue columns) or 500 000 (dark blue columns) THP-1-derived macrophages were exposed to 0, 25, 50, 100 or 200 μg/mL SRM2786. After 24 h the concentration of CXCL8 (A) and IL-1β (B) was measured in the cell culture supernatant using ELISA. Results are presented as mean ± SD for n=3 independent experiments. Statistically significant differences between groups were determined using two-way ANOVA followed by Dunnet's or Sidak's post-tests. * Significant difference from respective control (0 μg/mL SRM2786). # Significant difference between groups within one concentration of SRM2786.

In the initial experiments, different concentrations of THP-1 macrophages were tested in the A549/THP-1 coculture to assess the sensitivity of the cell models for particle exposure. A dose-dependent increases in the release CXCL8 (Additional figure 6-2A) and IL-1β (Additional figure 6-2B) were observed in cocultures containing both 100 000 and 500 000 THP-1-derived macrophages. The responses were higher for the coculture containing the 500 000 THP-1-derived macrophages and were significantly higher than control at 100-200 μg/mL and significantly higher than the coculture containing the least macrophages at the highest concentration.
Based on these results, 500 000 THP-1-derived macrophages were used in the coculture experiments presented in the main body of the text.

C3. Contribution of the different cell types to the coculture

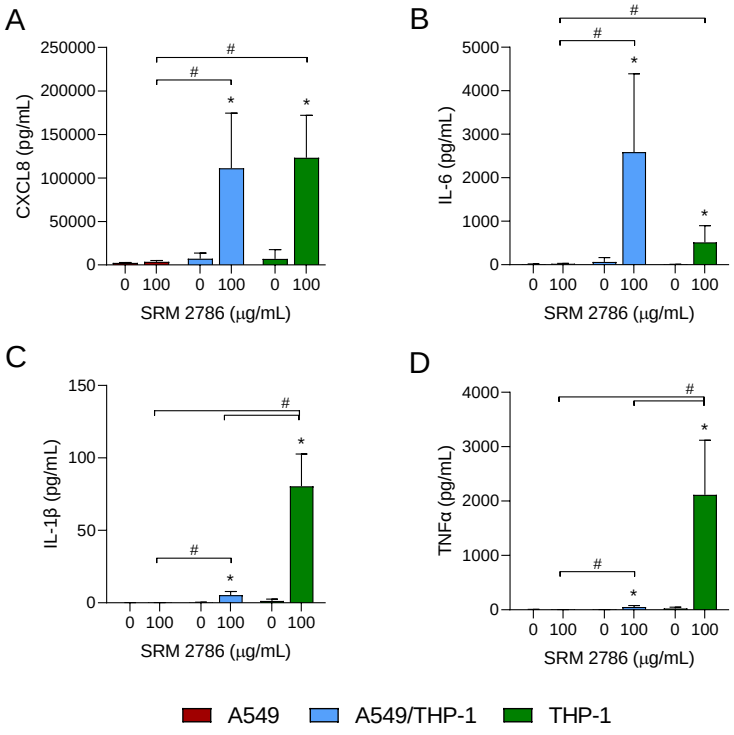

Additional figure 6-2. **The contribution of the different cell types to the responses in the coculture.** A540 cell (red bars), THP-1-derived macrophages (Green bars) and A549/THP-1 cocultures (Blue bars) were exposed to 100 µg/mL (10.5 µg/cm^2). After 24h the concentration of CXCL8 (A), IL-6 (B), IL-1β (C) and TNFα (D) was measures in the cell culture supernatant using ELISA. Statistically significant differences between groups were determined using two-way ANOVA with Tukey and Šídák's post-tests. All datasets were log-transformed prior to statistical analyses due to violation of model assumptions. * Significantly different from the respective control (0 µg/mL). # Significantly different from the response in a different cell type at the same concentration of SRM2786.

To determine the contribution of each cell type to the particle-induced cytokine responses, a coculture of A549 epithelial cells and THP-1-derived macrophages, or monocultures of A549 cells and THP-1-derived macrophage monocultures cultured under the same conditions as the coculture, were exposed to SRM2786 in parallel. Although experimental design allows for an approximation of each cell type's contribution to the responses in the coculture, it should be considered that there still are more THP-1 cells in the monoculture as the cells tend to attach more readily bare plastic wells than the epithelial monolayer. Significant increases in CXCL8, IL-6, IL-1β and TNFα compared with controls was detected for both the coculture and the THP-1 monoculture (Additional figure 6-3). By comparison, only very small levels of cytokines were released by the A549 cells, suggesting that the THP-1-derived macrophages are the main contributor to the particle-induced responses in the coculture (Additional figure 6-3). Interestingly, the level of CXCL8 was similar between the coculture and the THP-1 monoculture (Additional figure 6-3A). Similarly, the mean level of IL-6 was higher in the coculture, although non-significantly (Additional figure 6-3B). These results may indicate that interactions between the epithelial cells and macrophages contribute to the responses in the coculture. The levels of IL-1β and TNFα was substantially higher in the THP-1 monoculture compared with the coculture, which is likely due to the THP-1 macrophages detaching from the coculture.

D1. The reductions in the ABC scenario

Table A 7-1 Grid-level maximum, minimum and average reductions in $PM_{2.5}$, BC and OC concentrations by province in Northern China in the ABC scenario (Unit: μg/m^3)

	Average Reduction			Maximum Reduction			Minimum Reduction		
	BC	OC	$PM_{2.5}$	BC	OC	$PM_{2.5}$	BC	OC	$PM_{2.5}$
Hebei	-1.47	-2.61	-17.79	-6.46	-10.48	-81.96	-0.14	-0.24	-2.48
Heilongjiang	-0.52	-1.06	-4.66	-5.36	-7.35	-28.38	-0.02	-0.03	-0.19
Inner Mongolia	-0.19	-0.34	-1.87	-2.80	-3.92	-14.30	-0.01	-0.02	-0.16
Xinjiang	-0.18	-0.33	-1.30	-9.66	-11.13	-37.69	0.00	0.00	-0.01
Jilin	-0.72	-1.37	-7.30	-2.87	-4.07	-20.07	-0.12	-0.22	-2.09
Liaoning	-1.03	-1.92	-11.41	-5.03	-6.73	-36.16	-0.27	-0.50	-4.33
Gansu	-0.12	-0.21	-1.60	-1.19	-1.35	-7.36	-0.01	-0.02	-0.10
Beijing	-0.86	-1.73	-12.06	-1.86	-4.05	-22.89	-0.36	-0.69	-6.42
Shanxi	-1.51	-2.54	-14.65	-9.32	-13.77	-51.36	-0.42	-0.68	-5.59
Tianjin	-1.64	-2.88	-22.82	-2.26	-4.14	-34.32	-1.25	-2.07	-18.12
Shaanxi	-0.39	-0.59	-5.75	-3.07	-3.75	-20.02	-0.10	-0.16	-2.14
Ningxia	-0.30	-0.53	-3.76	-1.19	-1.78	-9.48	-0.14	-0.28	-2.49
Qinghai	-0.04	-0.07	-0.34	-2.63	-3.65	-12.82	0.00	0.00	-0.01
Shandong	-1.01	-1.90	-17.89	-1.76	-3.66	-29.76	-0.27	-0.48	-5.15
Henan	-1.19	-2.04	-18.99	-2.73	-3.65	-28.96	-0.38	-0.64	-8.10
Jiangsu	-0.84	-1.88	-13.90	-2.34	-5.01	-29.03	-0.19	-0.38	-3.34
Anhui	-0.90	-2.08	-15.38	-3.49	-6.18	-33.66	-0.23	-0.48	-4.14